ISBN 978-82-326-1944-3 (printed version)
ISBN 978-82-326-1945-0 (electronic version)
ISSN 1503-8181

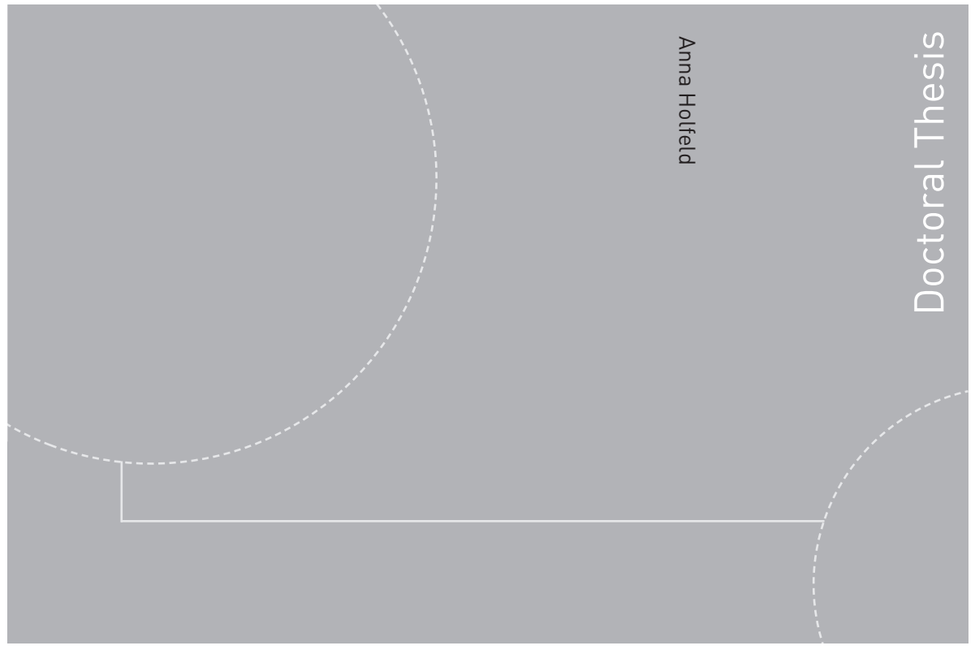

Doctoral theses at NTNU, 2016:303

Anna Holfeld

Experimental investigation of heat transfer and pressure drop in compact waste heat recovery units

NTNU
Norwegian University of Science and Technology

Doctoral theses at NTNU, 2016:303

NTNU

NTNU
Norwegian University of Science and Technology
Faculty of Engineering Science and Technology
Department of Energy and Process Engineering

NTNU
Norwegian University of Science and Technology

Anna Holfeld

Experimental investigation of heat transfer and pressure drop in compact waste heat recovery units

Thesis for the degree of Philosophiae Doctor

Trondheim, June 2016

Norwegian University of Science and Technology
Faculty of Engineering Science and Technology
Department of Energy and Process Engineering

NTNU
Norwegian University of
Science and Technology

NTNU
Norwegian University of Science and Technology

Thesis for the degree of Philosophiae Doctor

Faculty of Engineering Science and Technology
Department of Energy and Process Engineering

ISBN 978-82-326-1944-3 (printed version)
ISBN 978-82-326-1945-0 (electronic version)
ISSN 1503-8181

Doctoral theses at NTNU, 2016:303

Printed by Skipnes Kommunikasjon as

ABSTRACT

The objective of this thesis is to assess the optimal design of a compact and efficient waste heat recovery.

In order to investigate the heat transfer and pressure drop of compact heat exchangers an experimental rig was build. Eight different finned tube bundles were tested, all in a staggered 30° arrangement. The tube bundles varied in fin type, fin height, fin pitch, fin tip clearance and tube diameter. The Reynolds number was varied in the range between 3500 and 54000, based on the tube outside diameter and the velocity in the minimum free-flow area. The experimental results were compared to literature correlations, showing some agreements but also pointing out a large spread between the prediction results of the correlations. The row-to-row-variation of the heat transfer coefficient was examined as well.

In addition to the experimental data, published data from the literature was collected and used for the development of new correlations for the prediction of heat transfer and pressure drop in finned tube bundles. Therefore a linear regression analysis was carried out. The new correlations predict 95% of the experimental and published heat transfer data within 21% (for serrated-fin tubes) respectively 26% (for solid-fin tubes). The pressure drop data is to 95% predicted within 34%.

The implication for the design of compact and efficient waste heat recover units varies, depending on the main objective. This could be efficiency (small pumping power), small volume and/or low weight. The best fitting design of the waste heat recovery unit needs to be evaluated for each application separately. The results from the experiments and the correlations point towards high fins and a wide tube arrangement for a small pumping power. Small volume waste heat recovery units should tend towards serrated-fin tubes with a large number of low fins and a closely spaced tube bundle arrangement. This is also the case for weight optimised waste heat recovery units.

ACKNOWLEDGMENT

Firstly, I would like to express my sincere thanks to my supervisors Erling Næss and Geir Skaugen for their continuous support of my PhD study and related research, for their open doors, motivation and discussions.

Thanks to all the people working in the lab, for their help during the build-up of the test rig.

I thank my fellow office mates Christian, Henrik, Kolbeinne as well as Maria and Alexis for the lunch time discussions and for all the good times we have had together in the last years.

I would like to thank my beloved family, my parents and my siblings, for accompanying me through my life.

Finally, I thank my dear husband Sven for his continuous motivation and support throughout all ups and downs during the writing of this thesis. This will be a time we won't forget.

TABLE OF CONTENTS

NOTATION

Roman symbols

Symbol	Unit	Description
A_f	m^2	Flow area
$A_{f,fin}$	m^2	Flow area between the fins $A_{f,fin} = (d_f - d_o) \cdot (1 - N_f \cdot t_f) =$ $= 2 \cdot h_f \cdot (1 - N_f \cdot t_f)$
$A_{f,min}$	m^2	Minimum free-flow area $A_{f,min} = P_t - d_o - 2 \cdot h_f \cdot N_f \cdot t_f$
$A_{0,f}$	m^2	Fin heat transfer surface
$A_{0,i}$	m^2	Tube internal heat transfer surface
$A_{0,t}$	m^2	Tube heat transfer surface (between the fins)
A_{ht}	m^2	External heat transfer surface $A_{ht} = A_{0,t} + A_{0,f}$
Ar	-	Overall extended-surface-area ratio
B	m	Thickness
c_f	m	Fin-tip clearance
c_p	J/kg·K	Specific heat capacity
D	m	Diameter
d_f	m	Fin outside diameter $d_f = d_o + 2 \cdot h_f$
d_h	m	Hydraulic diameter $dh = 4 \cdot A_{f,min} / (2 \cdot N_f \cdot (s_f + 2 \cdot h_f))$
d_o	m	Base tube external diameter
d_v	m	Volumetric diameter $d_v = d_o + 2 \cdot h_f \cdot t_f \cdot N_f$
E	-	Elasticity factor
F	-	Correction factor
g_f	m	Fin gap $g_f = p_f - t_f$
H	$W/m^2 \cdot K$	Heat transfer coefficient
H	m	Height
h_f	m	Fin height
h_s	m	Height of the segmented section of the fin
H	-	Heat capacity ratio
I	-	Bessel function of the first kind
J	$kg/s \cdot m^2$	Mass flux (mass velocity)
K	W/m·K	Thermal conductivity

Symbol	Unit	Description
K	-	Bessel function of the second kind
l	m	Length
l_t	m	Tube length
l_w	m	Welding length
l_{wi}	m	Welding interruption length
LMTD	K	Logarithmic mean temperature difference
$\dot{m}$	kg/s	Mass flow rate
m	-	Fin parameter (Eq. 2-5)
m	-	Reynolds number exponent
N_f	1/m	Number of fins per unit tube length
N_l	-	Number of longitudinal tube rows
N_t	-	Number of transversal tube rows
NTU	-	Number of transfer units
p	Pa	Pressure
Δp	Pa	Pressure drop
P_d	m	Diagonal tube pitch
P_l	m	Longitudinal tube pitch
P_t	m	Transversal tube pitch
P	-	Temperature ratio
Q	W	Heat duty
R	m^2·K/W	Thermal resistance
R^2	-	Coefficient of determination
s_f	m	Fin pitch
t	-	Student t multiplier
t	°C	Temperature
T	K	Temperature
w	m	Width
W	J/s·K	Heat capacity
U	W/m^2·K	Overall heat transfer coefficient
u	m/s	Velocity
$\dot{V}$	m^3/s	Volume flow rate

Greek symbols

Symbol	Unit	Description
β	°	Tube angle
η_f	-	Fin efficiency
ν	m²/s	Kinematic viscosity
μ	kg/m·s	Dynamic viscosity
ρ	kg/m^3	Density

Subscript

air	air (hot side)	o	outside
bt	bare tube	out	outlet
d	diagonal	s	segment
f	fin	ser	serrated
fb	fin base	sol	solid
ft	fin tip	t	tube
H	Hashizume correction	t	transversal
i	inside	ts	test section
in	inlet	th	theoretical
l	longitudinal	wg	water-glycol mixture (cold side)
m	mean	W	Weierman correction
max	maximum		

Dimensionless numbers

Eu Euler number $$Eu = \frac{2 \cdot \Delta p}{\rho \cdot u_{max}^2 \cdot N_l}$$

Nu Nusselt number $$Nu = \frac{h \cdot d_o}{k}$$

Pr Prandtl number $$Pr = \frac{c_p \cdot \mu}{k}$$

Re Reynolds number $$Re = \frac{\rho \cdot u_{max} \cdot d_o}{\mu} = \frac{\dot{m} \cdot d_o}{A_{f,min} \cdot \mu}$$

1 INTRODUCTION

Background

Climate change is becoming more obvious. Severe weather phenomena such as floods, storms or drought happen more often, as well as the melting of the ice on the poles. In order to mitigate the climate change, measures are needed to reduce the emission of greenhouse gases such as CO_2 from fossil fuel combustion and industrial processes, which contribute to a large extent to the global greenhouse emissions (Edenhofer et al. (2014)). Efficiency enhancement is one of the key mitigation strategies described by Edenhofer et al. (2014) in the Report of the Intergovernmental Panel on Climate Change (IPCC).

Increased energy efficiency can lead to a conservation of resources and reduction of CO_2 emissions. In the case of fossil fuel combustion, as e.g. in gas turbines, energy efficiency improvement can also lead to reduced operational cost due to savings in the gas consumption and partially implemented emission taxes.

One way to increase energy efficiency is to reuse the heat in the exhaust gases from gas turbines. As they have a high energy content it is desirable to recover this energy and use it for further applications. This approach is used in combined cycle power plants, where a gas turbine is combined with a bottoming cycle which uses the heat recovered from the exhaust gas of the gas turbine.

Combined cycles are used widely onshore; however this approach is not common offshore. As Skaugen et al. (2014) describe, the hot exhaust gas from offshore gas turbines is often released to the ambient or only partially recovered. By implementing a bottoming cycle more heat could be recovered and further used for electrical power production. However, an offshore application of waste heat recovery units demands specific requirements as space is limited and weight restrictions exist. Therefor compact solutions are required which are small and have a low weight.

Objective and scope

The objective of this thesis is to assess the optimal design of a waste heat recovery unit for offshore applications. Due to weight and space limitations, a compact power cycle is needed, containing a compact waste heat recovery unit. The successful design of the compact waste heat recovery unit requires knowledge of thermal-hydraulic characteristics which implies knowing the heat transfer coefficient and the pressure drop behavior of a heat exchanger.

In order to investigate the thermal-hydraulic characteristic of compact heat exchangers an experimental rig was build and measurements were carried out. The measurements were used to develop a correlation for the prediction of the thermal-hydraulic behavior of a waste heat recovery unit. Recommendations for the design of a compact waste heat recovery unit for an offshore application were defined.

Structure of the thesis

Chapter 2 LITERATURE REVIEW, presents different methods to enhance gas side heat transfer. Finned tubes is the main focus. The influence of different parameters of finned tube bundles (fluid flow rate, bundle layout and tube geometry) on the heat transfer and pressure drop performance is presented. In addition the calculation of the fin efficiency for finned tubes is presented as well as methods to extend the theoretical calculation to account for the actual non-uniform heat transfer behaviour. Available correlations for the prediction of the heat transfer and pressure of finned tube bundles are presented. Modelling and simulation attempts of finned tube bundles are reported. The gaps in the literature are defined, such as the extension of the experimental data for small tube diameters. The chapter is concluded with a summary and the definition of the scope of this work.

Chapter 3 EXPERIMENTAL FACILITY describes the test rig that was constructed for providing experimental heat transfer and pressure drop data. Components and instrumentation are described, as well as the details of the finned tube bundles tested.

Chapter 4 DATA REDUCTION describes how the measured data were used to calculate the heat transfer and pressure drop of the tested bundles. It includes the uncertainty analysis for the calculations.

Chapter 5 EXPERIMENTAL RESULTS contains the presentation of the experimental results and the comparison to the correlations gathered from the literature and published experimental data. In addition the row to row variation in the tube bundle of the heat transfer is shown including the influences of turbulences on it.

Chapter 6 CORRELATION DEVELOPMENT introduces a holistic database of published experimental data on heat transfer and pressure drop of finned tube bundles. The data from the database and the new experimental data are used to develop new correlations for the prediction of heat transfer and pressure drop for finned tube bundles.

Chapter 7 IMPLEMENTATION OF THE DESIGN OF COMPACT WHRU shows the comparison of the tested geometries in terms of heat transferred per unit pressure drop, volume and weight. Results from the optimization of a compact WHRU performed using the developed correlations is presented.

Chapter 8 SUMMARY, CONCLUSION AND RECOMMENDATIONS sums up the findings and proposes fields for further studies.

The appendix provides additional information on the collected published heat transfer and pressure drop correlations, the experimental data and publications.

2 LITERATURE REVIEW

This chapter provides an overview of the possibilities for enhancing gas side heat transfer. The focus is on finned tubes. The influence of different geometric parameters of finned tube bundles is presented, together with published correlations for the estimation of heat transfer coefficient and pressure drop. An overview of current progress in the numerical modelling of the performance of finned tube bundles is given at the end of the chapter.

2.1 Types of gas side enhancements

Typically, thermal resistance in heat transfer ($R = \frac{1}{h \cdot A_{ht}}$) is usually higher on the gas side than on the liquid side. There are two ways to decrease this resistance: the first is to increase the heat transfer surface A_{ht} and the second is to increase the heat transfer coefficient h.

Extending the heat transfer surface A_{ht}, can be achieved by using fins.

Increasing the heat transfer coefficient, h, can be achieved by either boundary layer manipulation or flow manipulation. Boundary layer manipulation involves a breakup or thinning of the boundary layer forming on the heat transfer surface. A breakup of the boundary layer can be achieved by applying dents, serrations or cuts. Flow manipulation is performed by influencing the flow through the heat exchanger. One possibility is the application of vortex generators, which introduce vortices and a more turbulent flow. The design of the heat exchanger itself can also lead to a more turbulent flow by introducing flow obstacles, e.g. using a staggered layout.

A combination of both methods (increasing the heat transfer coefficient and extending the surface) is realised by using serrated fins. When such fins are applied to a tube, the heat transfer area is increased and the cuts in the fins lead to a breakup of the boundary layer.

Finned tubes

Fin types

Different fin geometries are available for finned tubes. The basic fin type is solid fin (Figure 2-1 a). Alternatives having interrupted or serrated fins to introduce a breakup of the boundary layer and thereby increase the heat transfer coefficient have also been proposed (Figure 2-1 b-e).

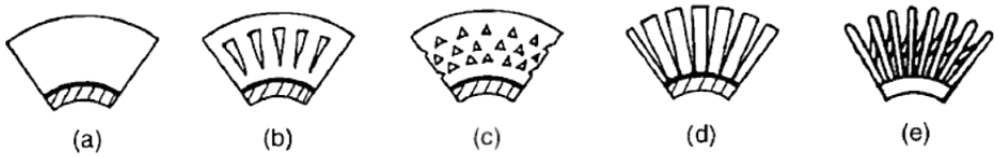

Figure 2-1 Enhanced circular fin geometries. (a) plain circular fin, (b) slotted fin, (c) punches and bent triangular projections, (d) serrated fin and (e) wire loop extended surface [Webb and Kim (2005)]

Ma et al. (2012) stated that limitations during manufacturing, as well as heat transfer behaviour, resulted in a trend away from the use of mainly solid-fin tubes to serrated-fin tubes in the 1960s.

Assessing the heat transfer and pressure drop of different fin types is difficult because the availability of such data varies for the different fin types. For solid and serrated-fin tubes, some data is available. For other fin types, there is less information; although, PFR (1976) reports some data on slotted fins, wire loop extended surfaces and helical integral fins.

Fin attachment

Different methods of attaching fins to the base tube exist. Figure 2-2 shows grooved and extruded fins. The advantage of extruded fins is the perfect thermal contact between the tube and the fins. However, the material needs to be soft for the production (e.g. aluminium or copper), which makes it difficult to use them for high temperature applications. Grooved fin attachment is prone to imperfect thermal contact and mechanically weak. They are mainly used in air-cooler and heating, ventilation and air conditioning (HVAC) systems.

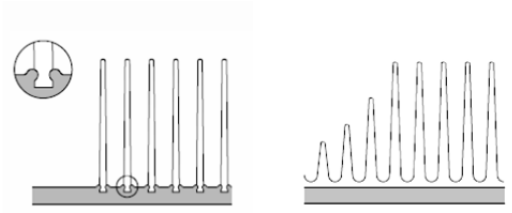

Figure 2-2: Types of fin attachment. Left: G-foot fins (grooved fins), right: extruded fins [Spiro-Gills (2012)]

For high operating temperatures, it is necessary to weld the fins to the tube. Steel is the preferred tube and fin material. Stainless steel can be used in a corrosive environment; otherwise, carbon steel is a better choice as it has a higher thermal conductivity compared to stainless steel.

For helically welded tubes, a metal strip is wrapped around and welded to the tube. In the early days of welded finned tube use, L-Foot fins were used. The metal strip was bent so that a larger contact area could be welded to the tube. With an improved welding technique, I-foot fins became more common (Ma et al. (2012)). In the case of I-foot fins, only the short side is welded to the tube. The advantage of I-foot fins compared to L-foot fins is that the metal strip does not need to be bent; thus, it requires less material for the same fin height and is therefore not as heavy. Normally, I-foot fins are high frequency resistance welded, and L-foot and U-foot fins are low frequency resistance welded, to the base tube.

Figure 2-3 shows the different types of welded fin attachments. In order to weld serrated I-foot and U-foot fins to the tube, these fins are not serrated all the way down to the tube base; there remains a solid region, typically of 5mm in length. For small tube diameters, for example d_o = 10mm, only solid fins would be possible in the case of an I-foot attachment because the serrated region would be very small. However, this is not the case for L-foot fins as serration is possible down to the tube base.

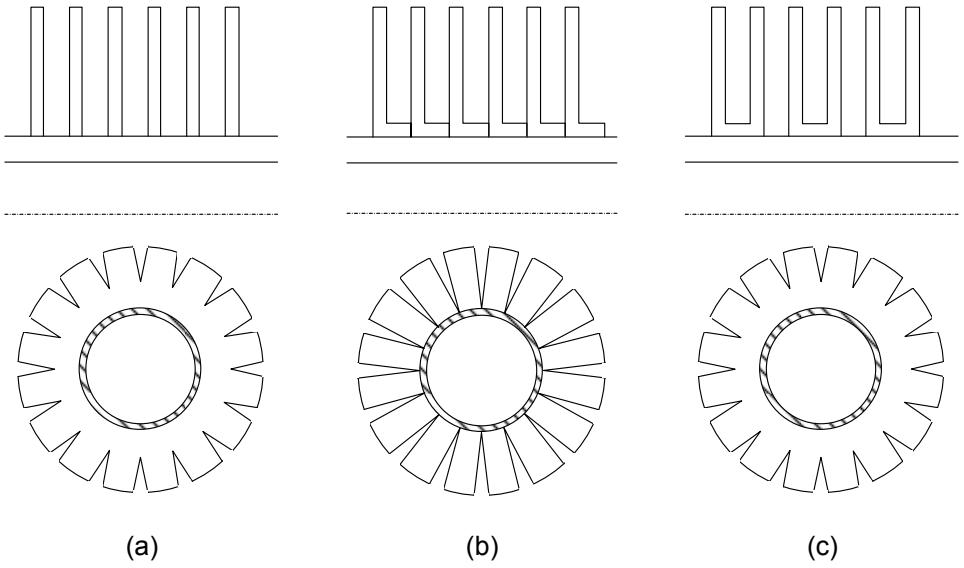

Figure 2-3: Types of welded fin attachments and the possible degrees of fin serration. (a) I-foot fin, (b) L-foot fin and (c) U-foot fin as reported by Hofmann (2009)

Oval finned tubes

Brauer (1964) compared circular and oval finned tubes in a staggered layout. He found that the heat transfer coefficient was higher and the pressure drop lower for oval finned tubes than for circular finned tubes. The reduction in pressure drop was explained by the smaller wake region behind the tubes. Brauer also stated that the use of oval tubes could lead to a reduction in the heat exchanger size, making it more compact.

However, oval tubes must be designed to withstand the internal fluid pressure. If the tube side pressure gets too high, the tube deforms. This results not only in an increase of pressure drop but also in the probable separation of the fins from the tubes. Without contact between fin and tube, heat transfer decreases significantly.

Semicircular fins

Hashizume (1981) carried out measurements with semicircular fin tubes (Figure 2-4, left), where the downstream side of the fins was cut off. The advantage of these tubes is that they can be arranged in a more compact manner than common fin tubes (Figure 2-4, right). In addition to heat transfer and pressure drop measurements, Hashizume carried out flow visualizations. For solid-fin tubes, he found a vortex pair forming a recirculation zone, with a lower heat transfer, downstream of the fin. For semicircular fin tubes, he found the same vortices; however, they were observed to be unstable. Semicircular fin tubes showed a higher heat transfer coefficient and a lower pressure drop compared to solid-fin tubes. However, the heat transfer coefficient was not increased sufficiently to compensate for the reduced heat transfer surface. This means that the transferred heat for tubes of the same length would be lower for a semicircular finned tube. In order to transfer the same heat more tubes need to be added. Comparing the different fin types tested by Hashizume (1981) in terms of transferred heat per unit volume, whatever fin type is chosen, the transferred heat per unit volume is the same. Another disadvantage of semicircular fin tubes is that they are difficult to manufacture.

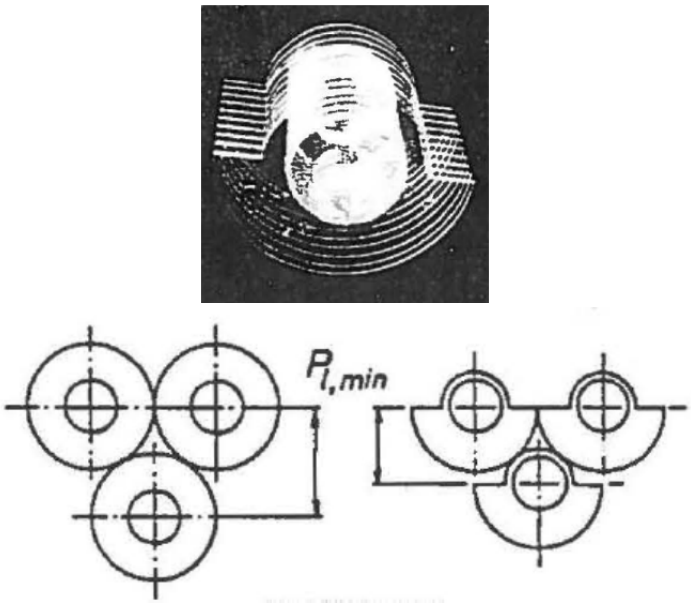

Figure 2-4: Left: semicircular finned tube, middle: staggered arrangement of a solid-fin tube, right: staggered arrangement of a semicircular fin tube [Hashizume (1981)]

Vortex Generators

Vortex generators are used to decrease the wake region behind the tubes and thus improve the heat transfer. Webb and Kim (2005) stated that this improvement on circular fins is not as significant as the improvement induced by the vortices, which form at the front of the fins and cause longitudinal vortices along the fin surface, which already improve the heat transfer.

Fiebig et al. (1993) studied the effect of vortex generators on solid finned tubes. He found the optimum location for the vortex generators behind the tube. In a staggered layout, heat transfer was increased by 9% and the pressure drop decreased by 3% by placing vortex generators on plain fins. Fiebig concluded that the increase in heat transfer and pressure drop is small for finned circular tubes.

O'Brien et al. (2003) tested the effect of different vortex generator configurations on circular finned tubes (see Figure 2-5). He obtained a 28%–40% increase in heat transfer coefficient, but the pressure drop coefficient also increased by 9%–24%. These contrasting results of Fiebig and O'Brien on the influence of vortex generators, especially on the pressure drop, seem to be related to the height of the vortex generator being tested. O'Brien used relatively high vortex generators compared to Fiebig (100% of the fin gap vs. 35% of the fin gap, respectively).

Even though vortex generators enhance the heat transfer, they are difficult to apply to the fins during manufacturing.

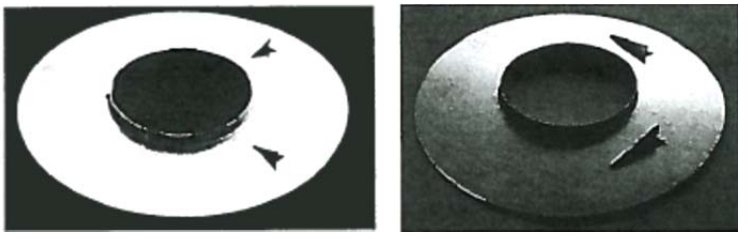

Figure 2-5: Individual fins having a pair of vortex generators. Left: common flow down configuration, right: common flow up configuration [O'Brien et al. (2003)]

2.2 Influence of different parameters on the heat transfer and pressure drop performance of finned tube bundles

The heat transfer and pressure drop of finned tube bundles are influenced by various parameters, which are flow, bundle and tube specific. Tube bundle parameters are the tube bundle layout, including the tube spacing, tube layout angle and the number of tube rows in the flow direction. Tube parameters influencing the heat transfer and pressure drop of a finned tube bundle are the fin type, tube diameter, fin height and fin pitch.

In the evaluation of the influence of the different parameters, only one parameter was varied at the time.

2.2.1 Influence of flow rate

In the literature (e.g. PFR (1976), Stasiulevičius et al. (1988), Kawaguchi et al. (2005) and (2006b), Næss (2010)), it is shown that for the same tube bundle an increasing flow rate results in an increase in the heat transfer coefficient. This is because of the increase in flow turbulence with increasing velocity and the thinning of the boundary layer, which enhance heat transfer.

The behaviour of the pressure drop is similar, i.e. with an increasing flow rate the pressure drop is roughly proportional to the square of the flow velocity u.

$$dp \approx Eu \cdot \frac{\rho}{2} \cdot u^2 \qquad \textit{Eq. 2-1}$$

However, the Euler number Eu decreases with increasing velocity until it becomes constant. At this point a fully turbulent flow regime has developed. For each tube bundle, this transition depends on the bundle layout as well as the tube geometry (Stasiulevičius et al. (1988)).

2.2.2 Influence of tube bundle layout

Three factors determine the bundle layout: the tube arrangement (basically staggered vs. inline), the number of longitudinal tube rows and the tube layout angle.

Tube arrangement

Figure 2-6 shows the principally two ways of arranging tubes in a tube bundle, a staggered arrangement (left of figure) and an inline arrangement (right of figure).

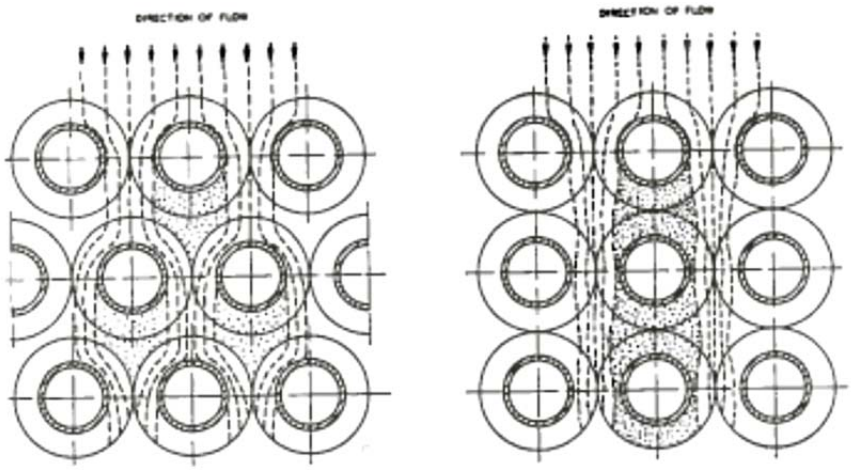

Figure 2-6: Schematic diagram of flow through staggered (left) and inline (right) finned tube banks [Brauer (1964)]

Staggered tube arrangements generally lead to a more compact packing of the tube bundle. Brauer (1964) carried out measurements on staggered and inline tube arrangements and observed the flow patterns. He observed that low heat transfer zones for a staggered layout were smaller than for an inline layout. Measurements confirmed these observations. The flow through a staggered tube bundle is interrupted after each tube row by the following tube row, creating turbulence and mixing, which increase the heat transfer. Weierman et al. (1978) compared different serrated-fin tubes in both inline and staggered layouts. The measured heat transfer coefficients for the staggered layout were higher than for the inline layout, but the pressure drop was also higher. In accordance with the above investigations, PFR (1976) concluded that both the heat transfer coefficients and pressure drop for a staggered tube arrangement were higher than for an inline layout.

Number of tube rows

In a staggered finned tube bundle the heat transfer coefficient increases in the first few tube rows and stabilizes from approximately the fourth tube row. This is because of an increasing level of turbulence in the tube bank (Neal and Hitchcock (1967)).

PFR (1976) described two methods that were used by investigators to measure this effect:

1. The number of tube rows in a bundle is varied and an average heat transfer coefficient is calculated.
2. The number of tube rows in a bundle is constant and the heat flux and temperature of each tube row is measured.

Jameson (1945), Brauer (1961), Kawaguchi et al. (2005) and Hofmann (2009) used the first method and all observed a lower heat transfer coefficient in the first tube rows. Jameson (1945) and Brauer (1961) stated that the heat transfer coefficient is constant from the fourth row.

The second method was used by Ward and Young (1959), Mirkovic (1974), Zozulya et al. (1973) and Stasiulevičius et al. (1988). Their results are similar to those from the investigators who changed the number of tube rows, observing a constant heat transfer coefficient from the fourth row. However, Zozulya et al. (1973) claimed that the extent of heat transfer coefficient reduction in the first tube rows depends on the turbulence level of the flow approaching the tube bundle. The higher the turbulence levels, the smaller the difference in the heat transfer coefficient between the tube rows.

According to Jameson (1945), Weierman (1977), Kawaguchi et al. (2004) and Hofmann (2009), the number of tube rows does not have an influence on the Euler number Eu.

Tube layout angle

The transversal tube pitch P_t, the longitudinal tube pitch P_l and the resulting tube layout angle β (Eq. 2-2) define the tube layout.

$$\tan \beta = \frac{P_t/2}{P_l} \qquad \textit{Eq. 2-2}$$

The most compact tube layout is a 30° (and 60°) layout. The larger the tube layout angle β becomes, the more the tube layout changes from a staggered arrangement to an inline arrangement.

Increasing the tube layout angle β to more than ca. 45° results in a shift of the narrowest flow passage from the transversal plane to the diagonal plane.

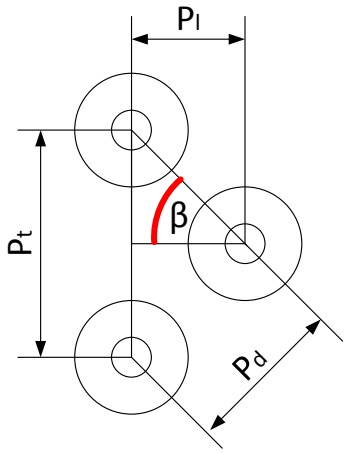

Figure 2-7: Schematic sketch of the tube layout

The tube layout can be changed in three ways:

1. Changing the transversal tube pitch P_t and keeping the longitudinal tube pitch P_l constant, which also results in a change of the tube layout angle β.
2. Keeping the transversal tube pitch P_t constant and changing the longitudinal tube pitch P_l, this also results in a change of the tube layout angle β.
3. Changing the transversal tube pitch P_t and the longitudinal tube pitch P_l proportionally, keeping the tube layout angle β constant.

In the literature, the effect of tube layout on the heat transfer and pressure drop in finned–tube bundles was studied by either changing the transversal tube pitch P_t or the longitudinal tube pitch P_l. A change in transversal tube pitch P_t

has no effect on heat transfer according to Ma et al. (2012), Kawaguchi et al. (2005) and Stasiulevičius et al. (1988), and only a small effect was observed by Worley and Ross (1960). The longitudinal tube pitch P_l was found not to influence heat transfer by Kawaguchi et al. (2005) and Worley and Ross (1960), and to have only a small effect by Ma et al. (2012) and Stasiulevičius et al. (1988).

Tube layout does not significantly influence heat transfer; however, this is not the case for pressure drop. Moving to a more compact tube layout by decreasing either of the tube pitches leads to a higher pressure drop; as observed by Stasiulevičius et al. (1988), Ma et al. (2012) and Robinson and Briggs (1966). In contrast, Kawaguchi et al. (2004) and Næss (2010) reported no tube layout effect on the pressure drop coefficient (Euler number).

Næss (2010) also investigated heat transfer and pressure drop in finned tube bundles where the diagonal plane was the narrowest flow passage. For such layouts, Næss found that the heat transfer coefficient and the Euler number decrease with an increasing tube layout angle (increasing P_t/P_l).

2.2.3 Influence of tube geometry

The finned tube parameters influencing heat transfer and pressure drop are the tube and fin characteristics. The tube diameter and shape can vary, together with fin type, size and arrangement.

Tube diameter

The influence of the tube diameter d_o has not been the specific focus of previous research. Worley and Ross (1960) compared three different tube sizes. The non-dimensional heat transfer coefficient (Nusselt number, Nu) correlates well with the non-dimensional velocity (Reynolds number, Re). The unique correlation between the Nusselt number and Reynolds number, both having d_o as the specific length scale, come together in one line for different tube diameters.

The tube diameter d_o as a specific length scale, used in the calculation of the Nusselt and Reynolds numbers, is chosen by many authors (Weierman (1976),

Stasiulevičius et al. (1988), Ma et al. (2012)). However, some authors use the fin diameter d_f (Næss (2007)), the hydraulic diameter d_{hy} (PFR (1976), Kawaguchi (2004, 2006a)) or volumetric diameter d_v (Kawaguchi (2005, 2006b)) as length scale. Næss (2007) reported from a Webb and Kim (2005) study, which found out that there is no clear choice for a specific characteristic length in the literature. Using the tube diameter as the length scale for the non-dimensional numbers is therefore considered sufficient.

Fin type

As shown in Figure 2-8, two main fin types are commonly used in waste heat recovery units: solid and serrated fins. For the same fin height, solid fins provide a larger heat transfer surface than serrated fins; however, serrated fins improve the heat transfer by breaking up the boundary layer, which develops on the fin surface. Along with these two main fin types, others have been presented and discussed in Chapter 2.1 Types of gas side enhancement.

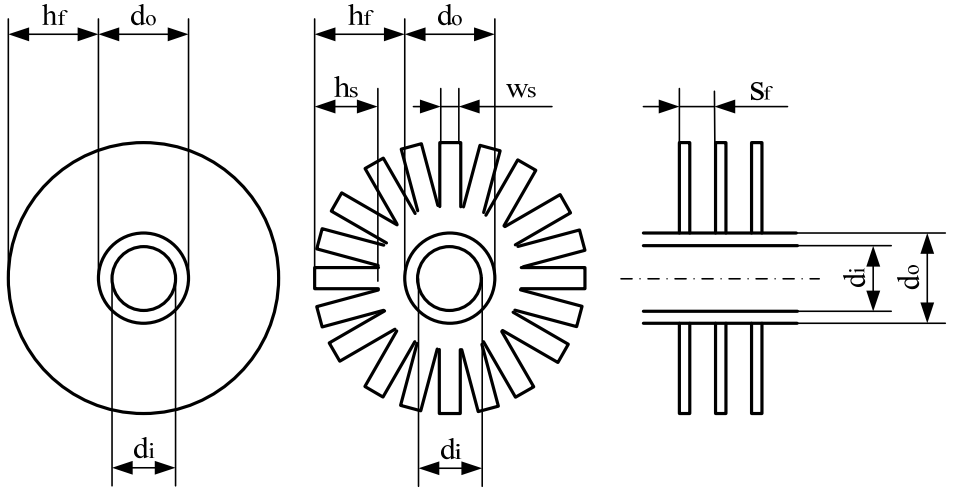

Figure 2-8: Schematic overview of the fin types and geometry parameters. Left: solid-fin tubes, middle: serrated-fin tubes, right: view from the side

Weierman (1977), Kawaguchi et al. (2004, 2005) and Hofmann (2009) compared solid and serrated finned tubes. All three authors found that

serrated-fin tubes have a higher heat transfer coefficient and a higher Euler number than solid-fin tubes. Kawaguchi et al. (2005) claimed that the heat transfer coefficient advantage of serrated fins is even more obvious for larger fin pitches. The segment width w_s was found by Weierman (1977) to have an influence on the Euler number: the smaller the segment width, the larger the Euler number.

The literature does not clearly state which fin type is more efficient when comparing heat duty per unit pumping power of a finned tube bundle. For solid fins, the heat transfer coefficient is not as high as for serrated fins; on the other hand, the heat transfer surface area is larger and the pressure drop is smaller. Taking into account these two parameters, no clear performance advantage can be distinguished for either type; therefore, the performance optimum must be evaluated from case to case.

Fin height

Increasing fin height h_f leads not only to an increase in the heat transfer surface area but also to a decrease in the fin efficiency. Stasiulevičius et al. (1988) and Næss (2010) measured higher heat transfer coefficients for higher fins. This is in accordance with observations for serrated finned tubes by Kawaguchi et al. (2006b). However, Kawaguchi et al. (2006b) also measured a lower heat transfer coefficient for solid fins with an increased fin height. Worley and Ross (1960) did not observe an influence of fin height on the heat transfer coefficient.

Different observations have been reported regarding the influence of fin height on pressure drop. Kawaguchi et al. (2006a) and Næss (2010) reported a larger pressure drop for higher finned tubes. This is contradictory to Stasiulevičius et al. (1988) who observed a smaller pressure drop. Again, Worley and Ross (1960) did not observe an influence of fin height on pressure drop performance.

Fin pitch

Decreasing the fin pitch s_f leads to a higher fin density and an increase in the heat transfer surface area. No clear picture on the influence of fin pitch on heat transfer is given in the literature. The reported comparisons were based on the same Reynolds number. An increase in the heat transfer coefficient for a decreased fin pitch was observed by Kawaguchi et al. (2005) and Næss (2010). Contrary to this, Žukauskas et al. (1966) and Ma et al. (2012) reported a decrease in the heat transfer coefficient for denser fins. Worley and Ross (1960) did not observe an influence of fin pitch on the heat transfer coefficient.

For the pressure drop, all investigations have shown that a decreased fin pitch results in a larger pressure drop (Worley and Ross (1960), Kawaguchi et al. (2004), Næss (2010), Ma et al. (2012)), presumably because of the increased friction surface.

2.2.4 Summary

From the observations reported in the literature, it can be concluded that flow velocity has the largest impact on heat transfer and pressure drop of finned tube bundles. Table 2-1 and Table 2-2 give an overview of the findings on the influence of different geometric parameters on the heat transfer coefficient and pressure drop. Changing the bundle layout to a more compact packing by decreasing the tube pitches was reported to either have no influence on the tube bundle performance or to have a negative effect on the heat transfer coefficient and pressure drop.

Increasing the heat transfer surface per unit tube length is possible by increasing the tube diameter, increasing the fin height or decreasing the fin pitch. The influence of tube diameter has not been studied extensively. A larger fin height seems to increase the heat transfer coefficient but also yields a larger pressure drop. For a decrease in fin pitch, no clear answer can be given for its influence on heat transfer; however, the pressure drop of the tube bundle is larger for denser fins.

Table 2-1: Overview of findings on the influence of different geometric parameters on the heat transfer coefficient

Parameter	**Heat transfer coefficient increased**	**Heat transfer coefficient decreased**	**No effect**
P_t decreased		Worley and Ross (1960); Ackerman and Brunsvold (1970)	Kawaguchi et al. (2005) ; Ma et al. (2012)
P_l decreased		Ma et al. (2012)	Worley and Ross (1960); Ackerman and Brunsvold (1970); Kawaguchi et al. (2005)
Serrated fins vs. solid fins	Weierman (1977); Kawaguchi et al. (2005); Hofmann (2009)		
d_o increased			Worley and Ross (1960)
h_f increased	Stasiulevičius et al. (1988); Kawaguchi et al. (2006b) *for serrated fins;* Næss (2010)	Kawaguchi et al. (2006b) *for solid fins*	Worley and Ross (1960)
s_f decreased	Kawaguchi et al. (2005; Næss (2010)	Žukauskas et al. (1966); Ma et al. (2012)	Worley and Ross (1960)

Table 2-2: Overview of findings on the influence of different geometric parameters on the pressure drop

Parameter	**Pressure drop larger**	**Pressure drop smaller**	**No effect**
P_t decreased	Ma et al. (2012)		Kawaguchi et al. (2004); Næss (2010)
P_l decreased	Robinson and Briggs (1966); Ma et al. (2012)		Kawaguchi et al. (2004); Næss (2010)
Serrated fins vs. solid fins	Weierman (1977); Kawaguchi et al. (2005) *for a high fin pitch;* Hofmann (2009)	Kawaguchi et al. (2005) *for a low fin pitch*	
d_o increased			Worley and Ross (1960)
h_f increased	Kawaguchi et al. (2006a) Næss (2010)	Stasiulevičius et al. (1988)	Worley and Ross (1960)
s_f decreased	Worley and Ross (1960); Kawaguchi et al. (2004); Næss (2010); Ma et al. (2012)		

2.3 Fin efficiency

Fin efficiency is an important parameter when dealing with extended surfaces. Because of the finite thermal conductivity in a fin, a temperature gradient is established in the radial direction, resulting in less heat transfer compared to a fin having infinite conductance.

2.3.1 Uniform distribution of the heat transfer coefficient

Gardner (1945) was the first to solve the differential conduction equation representing the heat transfer in a fin. He used the following assumptions:

1. steady state conditions
2. homogeneous fin material
3. constant thermal conductivity of the fin
4. uniform distribution of the heat-transfer coefficient over the entire fin surface
5. no additional heat sources in the fin
6. uniform temperature of the surrounding fluid T_∞
7. uniform temperature at the base of the fin T_{tb}
8. the fin thickness is small compared the fin height
9. the heat transferred through the fin tip is negligible

The differential conduction equation for a straight fin having a constant thickness b_f is

$$0 = \frac{d^2 T_f}{dx^2} - \frac{2 \cdot h_f}{k_f \cdot b_f} \cdot \left(T_f - T_\infty\right) \qquad \textit{Eq. 2-3}$$

with the boundary conditions

$$T_f = T_{tb} \text{ for } x = 0$$

$$\frac{d}{dx} \cdot \left(\frac{T_f - T_\infty}{T_{tb} - T_\infty} \right) = 0 \text{ for } x = h_f$$

The fin efficiency is defined as the ratio of actual transferred heat to the heat transferred in a fin having infinite conductance, i.e. for a straight, rectangular fin, (Baehr and Stephan (2006))

$$\eta_f = \frac{T_f - T_\infty}{T_{tb} - T_\infty} = \frac{\tanh(m \cdot h_f)}{m \cdot h_f} \qquad \textit{Eq. 2-4}$$

with

$$m = \sqrt{\frac{2 \cdot h_{air}}{k_f \cdot b_f}} \qquad \textit{Eq. 2-5}$$

Based on his assumptions, Gardner (1945) published Bessel–function solutions of the fin efficiency for various fin shapes. The solution for an annular solid fin with constant thickness is calculated according to Eq. 2-6. The geometric parameters are shown in Figure 2-9.

$$\eta_{th,sol} = \frac{2 \cdot r_0}{m \cdot (r_2^{\,2} - r_0^{\,2})} \cdot \frac{I_1(m \cdot r_2) \cdot K_1(m \cdot r_0) - I_1(m \cdot r_0) \cdot K_1(m \cdot r_2)}{I_0(m \cdot r_0) \cdot K_1(m \cdot r_2) + I_1(m \cdot r_2) \cdot K_0(m \cdot r_0)} \qquad \textit{Eq. 2-6}$$

where I and K are modified Bessel functions of the first and second kind.

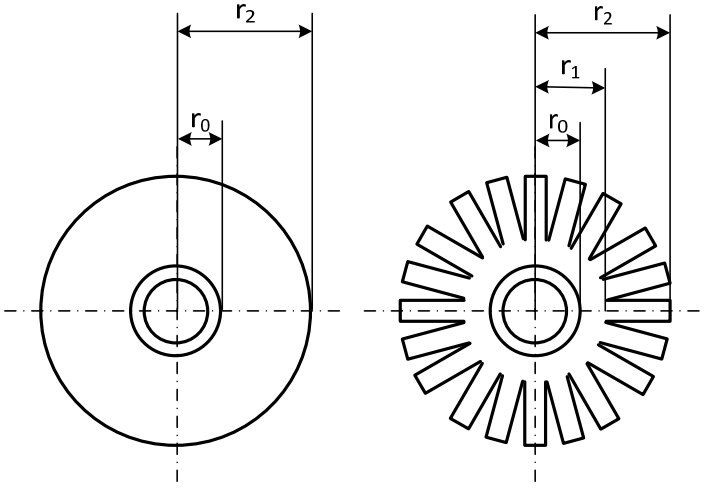

Figure 2-9: Geometric parameters for the fin efficiency calculation. Left: solid-fin; right: serrated-fin

Hashizume et al. (2002) investigated the fin efficiency of serrated I-foot fin tubes consisting of a solid region and a serrated region (see Figure 2-9, right). He presented a theoretical fin efficiency based on the assumptions of a uniform heat transfer coefficient and an insulated fin tip. The fin efficiency of the serrated-fin is calculated according to Eq. 2-7.

$$\eta_{th,ser} = \frac{2 \cdot r_0}{m \cdot (r_0^2 + r_1^2 - 2 \cdot r_1 \cdot r_2)} \cdot \frac{X}{Y} \qquad \textit{Eq. 2-7}$$

with

$$X = \left[I_0(m \cdot r_1) \cdot K_1(m \cdot r_0) + I_1(m \cdot r_0) \cdot K_0(m \cdot r_1) \right] \cdot \sinh\left[m \cdot (r_1 - r_2) \right] - \left[I_1(m \cdot r_1) \cdot K_1(m \cdot r_0) - I_1(m \cdot r_0) \cdot K_1(m \cdot r_1) \right] \cdot \cosh\left[m \cdot (r_1 - r_2) \right]$$

and

$$Y = \left[I_0(m \cdot r_0) \cdot K_0(m \cdot r_1) - I_0(m \cdot r_1) \cdot K_0(m \cdot r_0) \right] \cdot \sinh\left[m \cdot (r_1 - r_2) \right] + \left[I_0(m \cdot r_0) \cdot K_1(m \cdot r_1) + I_1(m \cdot r_1) \cdot K_0(m \cdot r_0) \right] \cdot \cosh\left[m \cdot (r_1 - r_2) \right]$$

2.3.2 Non-uniform distribution of the heat transfer coefficient

A uniform heat transfer coefficient distribution from the fin base to the fin tip is a common assumption in the calculation of fin efficiency and heat transfer. However, as shown by various authors, this assumption is incorrect.

Lymer and Ridal (1961), Žukauskas et al. (1966) and Neal and Hitchcock (1967) used heated fins to investigate the temperature and heat transfer coefficient distribution on a fin. Later investigations were conducted by Krückels and Kottke (1970) and Hu and Jacobi (1993). These researchers used a naphthalene layer on the fin, measuring the change in the layer thickness and using the similarity between heat and mass transfer. They all found that the heat transfer coefficient of the fin is higher upstream, in the stagnation point and on the sides. However, the heat transfer coefficient was decreased downstream, in the wake region behind the tube. Figure 2-10 shows the distribution of the mass transfer coefficient on a fin. It can be seen that with a higher velocity (lower part of the figure), the vortex structure is more visible.

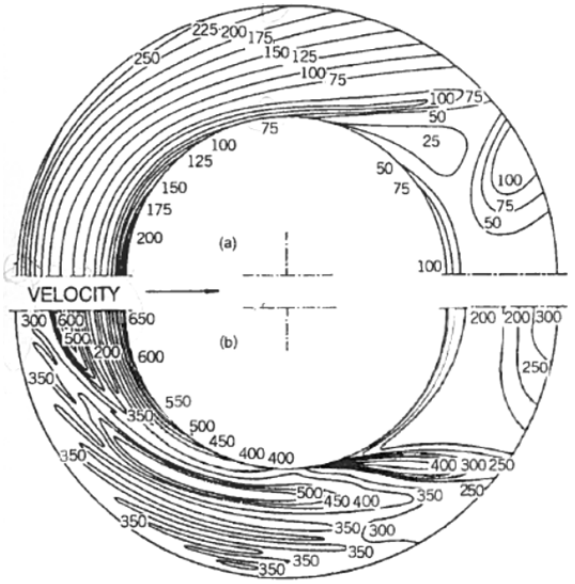

Figure 2-10: Distribution of mass transfer coefficient (m3/m2 h) on a single circular finned tube: (a) Red=1940, (b) Red=9700 [Krückels and Kottke (1970)]

Acknowledging the non-uniform heat transfer distribution on the fin surface, some corrections for fin efficiency have been published and are presented below.

Weierman correction

Weierman (1976) based his correction on data from Lymer and Ridal (1961), Žukauskas et al. (1966) and Yudin and Tokhtorova (1973). He introduced a rather simple correction for fin efficiency, of the form

$$\eta_f = \eta_{th} \cdot \left(A + B \cdot \eta_{th}\right) \qquad \textit{Eq. 2-8}$$

where A and B are given in Table 2-3.

Table 2-3: Factors for the Weierman (1976) fin efficiency correction for an uneven heat transfer distribution

Fin type	A	B
Serrated	0.9	0.1
Solid	0.7	0.3

Hashizume correction

Hashizume et al. (2002) based their correction correlations on their own experiments using fins of different material (copper, carbon steel and stainless steel). They placed an electrically heated tube in a tube bundle and measured the tube base temperature t_{tb}. The effective Nusselt number, obtained from the experiments, was plotted against the reciprocal of the thermal conductivity of the fin in a semi-logarithmic graph. The intersection of the curve with the Y-axis gave the actual average heat transfer coefficient. From the effective and actual Nusselt number, they calculated the actual fin efficiency. They reported a correction factor which depends on the Reynolds number Re, the segment-height-to-segment-width ratio h_s/w_s, the fin-diameter-to-tube-diameter ratio d_f/d_o and the product of the fin parameter and fin height $m \cdot h_f$.

Eq. 2-9 shows the correction for the fin efficiency for solid finned tubes, and Eq. 2-10 shows the same for serrated finned tubes.

$$\eta_{sol} = \eta_{th,sol} \cdot \left\{ 1 - \left(m_{sol} \cdot h_f \right) \cdot \left[0.14 \cdot \left(\frac{d_f}{d_o} \right)^{2.7} \cdot \left(1 - 0.097 \cdot \ln\left(Re_{d_o} \right) \right) \right] \right\} \qquad \textit{Eq. 2-9}$$

$$\eta_{ser} = \eta_{th,ser,H} \cdot \left\{ 1 - \left(m_{sol} \cdot h_f \right) \cdot \left[0.016 \cdot \left(\frac{h_s}{w_s} \right) + 0.14 \cdot \left(\frac{d_f}{d_o} \right)^{2.7} \cdot \left(1 - 0.097 \cdot \ln\left(Re_{d_o} \right) \right) \right] \right\} \qquad \textit{Eq. 2-10}$$

Using Eq. 2-11 for the theoretical fin efficiency of serrated I-foot fins

$$\eta_{th,ser,H} = \eta_{th,H} - a \cdot \left(\eta_{th,H} - \eta_{th,sol} \right) \qquad \textit{Eq. 2-11}$$

with

$$\eta_{th,H} = \frac{\tanh\left(m \cdot h_f \right)}{m \cdot h_f} \qquad \textit{Eq. 2-12}$$

and

$$a = \left\{ \cos\left[\left(\frac{\pi}{2} \right) \cdot \left(\frac{h_s}{h_f} \right) \right] \right\}^{1.6 - 0.094 \cdot m \cdot h_f \cdot \frac{d_f}{d_o}} \qquad \textit{Eq. 2-13}$$

The fin efficiency correction of Hashizume et al. is valid for

- a staggered tube arrangement,
- a fin-diameter ratio of $1.80 \leq (d_f/d_o) \leq 2.15$,
- a segment-height ratio of $0 \leq (h_s/h_f) \leq 0.86$,
- an aspect ratio of the segmented section of $0 \leq (h_s/w_s) \leq 2.60$,
- a Reynolds number of $5 \cdot 10^3 \leq Re \leq 3 \cdot 10^4$ and
- the non-dimensional characteristic $0 < m \cdot h_f < 2.0$.

Žukauskas correction

Žukauskas et al. (1966) placed heating elements on a trapezoidal fin and heated the fin with an electric current. Thermocouple measured the temperatures in different areas of the fin.

As suggested by Žukauskas et al., the correction for fin efficiency for a non-uniform heat transfer distribution on solid-fin tubes is

$$\eta_f = \eta_{th,sol} \cdot \left[0.97 - 0.056 \cdot (m \cdot h_f) \right] \qquad \text{Eq. 2-14}$$

Eq. 2-14 is valid for solid-fin tubes and $0.3 < m \cdot h_f < 3.0$.

Yudin correction

Yudin and Tokhtorova (1973) analysed their own set of experimental data for solid-fin tubes and proposed a correction to the fin efficiency for a non-uniform heat transfer distribution, as shown in Eq. 2-15.

$$\eta_f = \eta_{th,sol} \cdot \left[1 - 0.058 \cdot (m \cdot h_f) \right] \qquad \text{Eq. 2-15}$$

Eq. 2-15 is valid for solid-fin tubes and $0.1 < m \cdot h_f < 3.7$.

Comparison of the corrections for non-uniform heat transfer coefficient distribution

A comparison of the different fin efficiency corrections and their influence on the heat transfer coefficient is shown in Figure 2-11 and Figure 2-12. The experimental data of geometries 1 and 2 were used for the comparison as these geometries differ only in fin type.

In Figure 2-11, the influence of the corrections for serrated-fin tube Geometry 1 is shown based on the fin parameter m_{th} calculated with the theoretical fin efficiency. The influence of the fin efficiency using the corrections proposed by Weierman (1976) and Hashizume et al. (2002) can be seen on the left. It can be seen that these two corrections show opposite trends. The Weierman correction increases with an increasing $m_{th} \cdot h_f$, whereas the Hashizume correction decreases. The resulting influence on the heat transfer coefficient (see Figure 2-11) is 3%–7% for the correction of Weierman and 14%–33% for the correction of Hashizume.

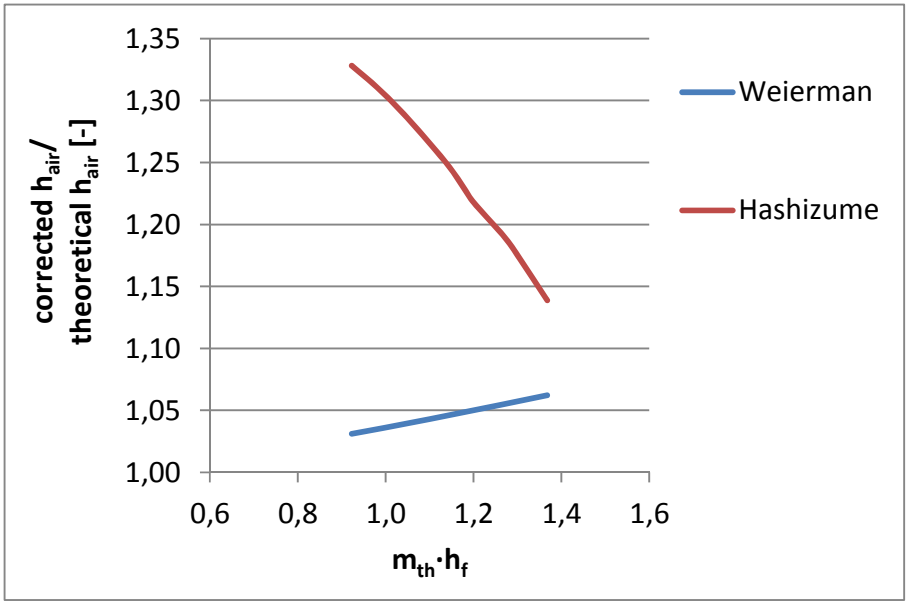

Figure 2-11: Comparison of the different fin efficiency corrections for a non-uniform heat transfer distribution for serrated-fin tubes (Geometry 1). Left: effect on the fin efficiency; right: effect on the heat transfer coefficient

Figure 2-12 shows the corrections of Weierman (1976), Hashizume et al. (2002), Žukauskas et al. (1966) and Yudin and Tokhtorova (1973) for the fin efficiency on solid-fin tube Geometry 2. As observed for serrated-fin tubes, the corrections for solid-fin tubes also show three opposing trends. The Weierman correction increases with an increasing $m_{th} \cdot h_f$, but to a larger degree than for serrated-fin tubes. The Hashizume correction decreases with an increasing $m_{th} \cdot h_f$. In addition, the corrections proposed by Žukauskas and Yudin seem to yield a rather small and almost constant correction. The resulting effect of the fin efficiency correction on the heat transfer coefficient differs markedly. Using the correction of Weierman gives 11–33% higher heat transfer coefficient; with the Hashizume correction the heat transfer coefficient is 1%–18% higher, and is 6%–7% higher for the Žukauskas correction and 2%–3% higher using the Yudin correction.

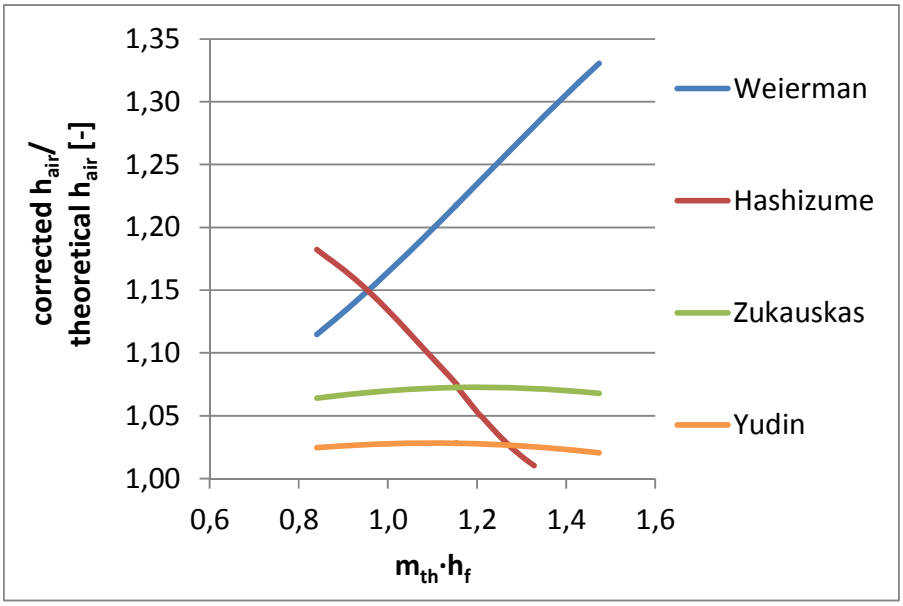

Figure 2-12: Comparison of the different fin efficiency corrections for a non-uniform heat transfer distribution for solid-fin tubes (Geometry 2). Left: effect on the fin efficiency; right: effect on the heat transfer coefficient

2.4 Published heat transfer and pressure drop correlations

A variety of correlations have been published for the prediction of the heat transfer and pressure drop behaviour of finned tube bundles. Most of these correlations are based on a limited number of experiments carried out by a single author. As a consequence, the validity range of the proposed correlations is in general limited to the parameter range of the experiments carried out. Nir (1991) and PFR (1976) collected data from several sources and used these to generate more general correlations with a wider validity range. Mon (2003) used her own numerical simulations to establish heat transfer and pressure drop prediction correlations

Heat transfer correlations are presented in the literature in terms of Nusselt number Nu or Colburn j-factor j. The correspondence between Nu and j is given by Eq. 2-16

$$j = \frac{Nu}{Re \cdot Pr^{1/3}} \qquad \text{Eq. 2-16}$$

The pressure drop correlations are presented in terms of the Euler number Eu.

The presented correlations (see Appendix I) are limited to staggered tube arrangements with a transversal free-flow area that is smaller than the diagonal free-flow area (tube layout angles below 45°).

The published correlations use either dimensionless groups or area ratios.

Dimensionless groups

The dimensionless groups can be divided into those that represent the bundle layout (Figure 2-13) and those that represent the tube geometry (Figure 2-14). According to the Buckingham Π-Theorem, a set of parameters can be grouped in dimensionless numbers. The number of independent dimensionless numbers is defined as the number of original dimensional parameters minus the number of independent base parameter, which is 1 in this case. Several dimensionless groups will be possible; but they can be shown to be combinations of one another.

Bundle arrangement:
Parameters:
P_t, P_l, P_d, d_o

Dimensionless groups:
$\left(\frac{P_l}{P_t}\right), \left(\frac{P_t}{P_d}\right), \left(\frac{P_t}{d_o}\right)$

Tube geometry:
Parameters:
d_o, h_f, s_f, g_f, b_f, h_s, w_s

Dimensionless groups
$\left(\frac{h_f}{d_o}\right), \left(\frac{s_f}{d_o}\right), \left(\frac{g_f}{d_o}\right), \left(\frac{g_f}{b_f}\right),$
$\left(\frac{h_s}{h_f}\right), \left(\frac{w_s}{h_f}\right)$

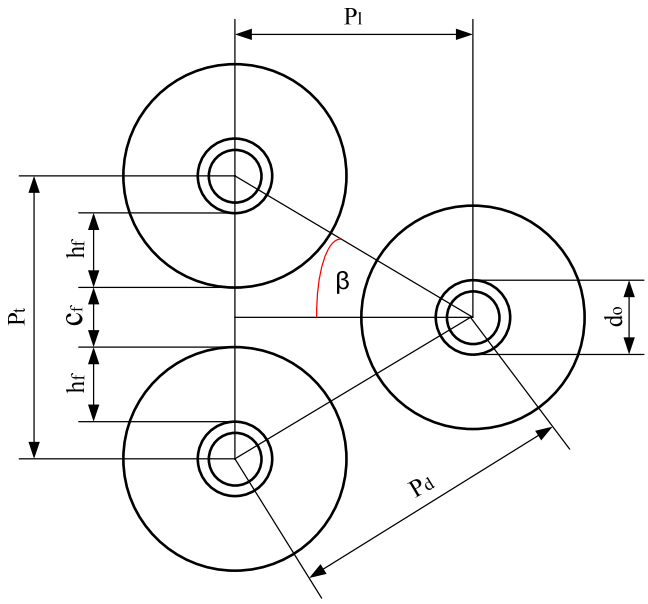

Figure 2-13: Tube bundle layout

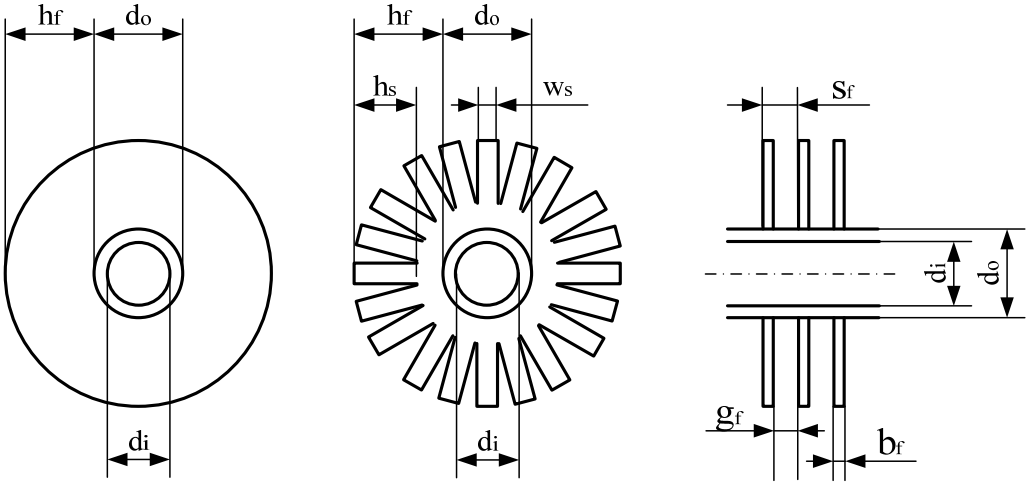

Figure 2-14: Tube geometry parameters. Left: solid-fin, middle: serrated-fin, right: view in flow direction (solid and serrated-fins)

For heat transfer prediction, ratios representing tube geometry are more commonly used in the literature. This is because heat transfer is influenced by

the heat transfer surface, which is represented by the tube geometry, i.e. tube diameter d_o, fin height h_f, fin pitch s_f, fin gap g_f and fin thickness b_f. For the pressure drop prediction, the groups representing the bundle arrangement are more commonly used and these contain the tube pitches P_t, P_l or P_d. They define the flow distribution and how the flow is led through the tube bundle. This is a main influence on the pressure drop as it is proportional to the square of the flow velocity

Area ratios

PFR (1976) introduced the extended-surface-area ratio. The extended-surface-area ratio is the ratio of the heat transfer surface of the finned tube to the surface of the bare tube without fins (see Eq. 2-17). PFR claimed that this ratio contains all the tube variables in one dimensionless number. It is calculated for solid-fin tubes according to Eq. 2-18, for serrated I-foot tubes according to Eq. 2-19 and for serrated L-foot tubes according to Eq. 2-20.

$$Ar = \frac{A_{ht}}{A_{bt}} = \frac{A_{0,f} + A_{0,t}}{A_{bt}} \qquad \textit{Eq. 2-17}$$

$$Ar_{sol} = 1 + N_f \cdot 2 \cdot h_f \cdot \left(1 + \frac{h_f + b_f}{d_o}\right) \qquad \textit{Eq. 2-18}$$

$$Ar_{ser,I-foot} = 1 + N_f \cdot 2 \cdot \left(h_f - h_s\right) \cdot \left(1 + \frac{\left(h_f - h_s\right) + 2 \cdot h_s + \frac{2 \cdot h_s \cdot b_f}{w_s} + b_f}{d_o} + \frac{h_s + \frac{h_s \cdot b_f}{w_s}}{\left(h_f - h_s\right)}\right) \qquad \textit{Eq. 2-19}$$

$$Ar_{ser,L-foot} = 1 + N_f \cdot 2 \cdot h_f \cdot \left(1 + \frac{b_f}{w_s}\right) \qquad \textit{Eq. 2-20}$$

Nir (1991) used the flow distribution in a tube bundle to define dimensionless area ratios. He defined three important flow distributions:

1. flow that passes between the fins (taking part in the heat transfer)
2. flow that bypasses the fins in the fin-tip-to-fin-tip clearance
3. flow after passing a tube row, where the temperature and velocity field are irregular

He further defined three main area ratios that he used in his correlations:

a. heat-transfer-surface-area-to-minimum-free-flow-area $A_{ht}/A_{f,min}$
b. minimum-free-flow-area-to-free-flow-area-between-the-fins $A_{f,min}/A_{f,fin}$
c. diagonal-to-transversal-free-flow-area $A_{f,d}/A_{f,t}$

Nir included the first two ratios in his heat transfer correlation. For his pressure drop correlation, he used only the heat transfer surface area to minimum free-flow area.

Mon (2003) used a mixture of both area ratios presented by PFR (1976) and Nir (1991). Her correlations included the extended-surface-area ratio Ar and the heat transfer surface area to minimum free-flow area $A_{ht}/A_{f,min}$.

Reynolds number dependency

Flow velocity is the main parameter influencing heat transfer and pressure drop in finned tube bundles. The Reynolds number is the dimensionless measure for flow velocity. The correlations collected in Appendix I were compared in terms of their Reynolds number dependency.

Heat transfer

A comparison of the Reynolds number exponent for the heat transfer correlations is shown in Figure 2-15. It can be seen that the range of the Reynolds number exponent m is from 0.59 (Mieth (1970)) to 0.88 (Kawaguchi et al. (2006b)). No difference can be seen between solid and serrated-fin tubes: the Weierman (1976), Nir (1991) and Kawaguchi et al. (2005) correlations have equal exponent for solid and serrated-fin tubes. This is not

the case for Kawaguchi et al. (2006b) who published correlations for solid and serrated-fin tubes. Most authors' correlations show a Reynolds number exponent in the range of 0.6–0.7; exceptions are Kawaguchi et al. (2005 and 2006b) and Stasiulevičius et al. (1988). Their exponents are in the range of 0.77–0.88. Stasiulevičius et al. (1988) also tested high Reynolds numbers (20 000 – 200 000) and found that for numbers above Re = 200 000, the Reynolds number exponent was further increased to m = 0.95.

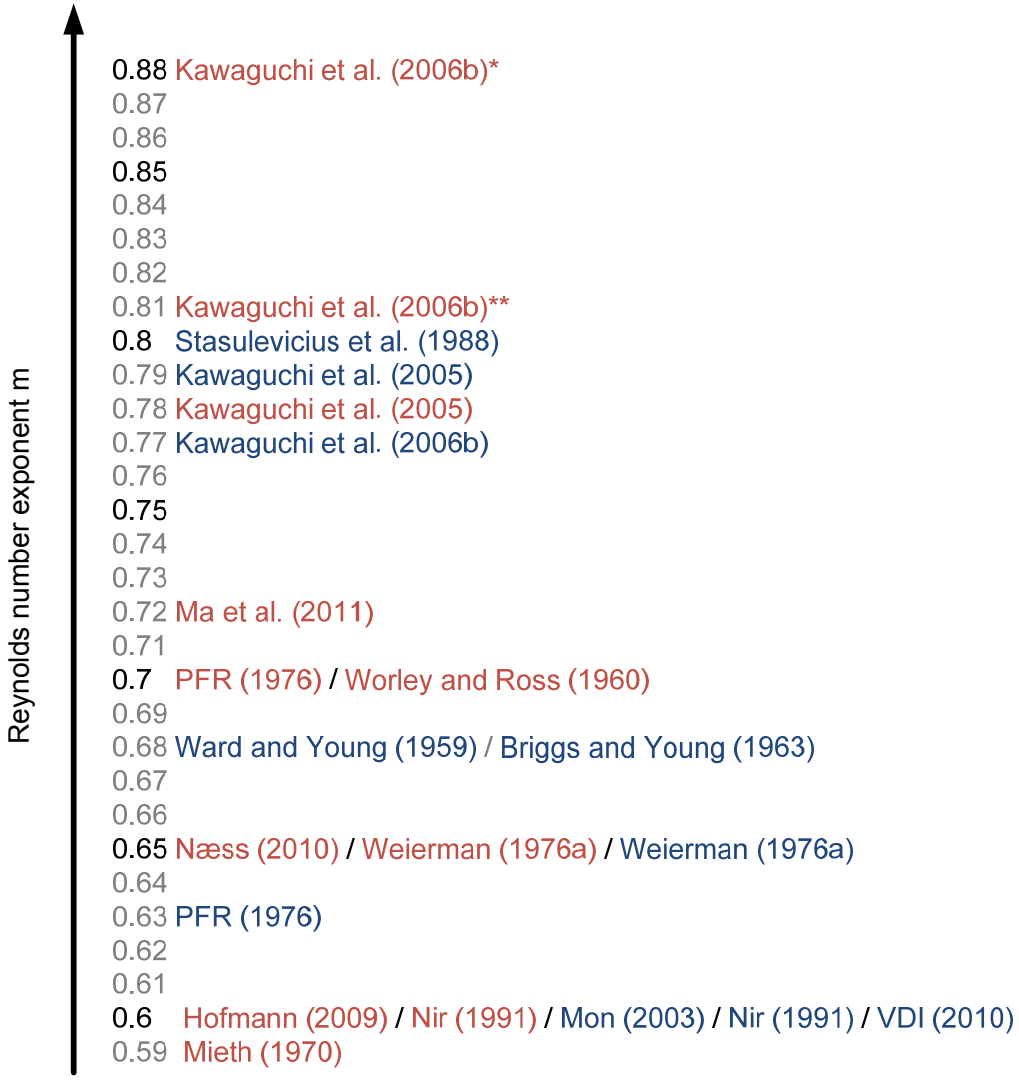

* Re_{dv} > 30 000
** Re_{dv} < 30 000

Serrated-fin correlation
Solid-fin correlation

Figure 2-15: Comparison of the Reynolds number exponent m for heat transfer correlations

Pressure Drop

In Figure 2-16 a comparison of the Reynolds number exponents for pressure drop correlations are shown.

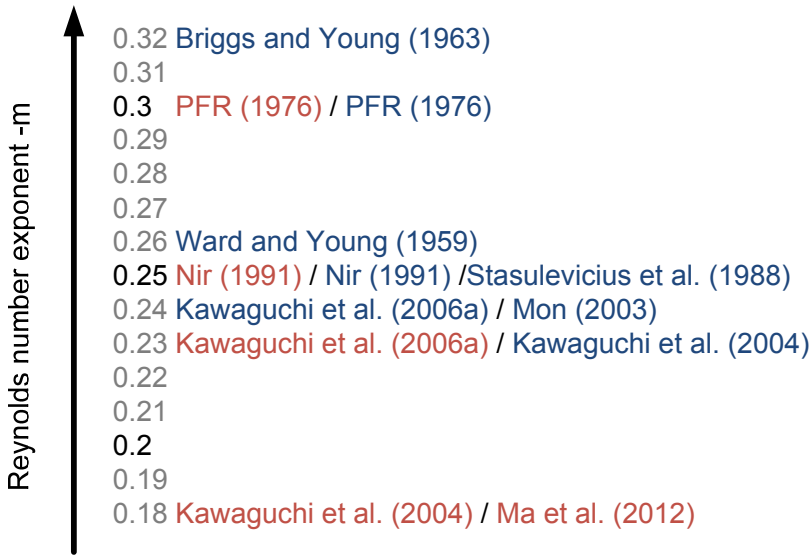

Figure 2-16: Comparison of the Reynolds number exponent m for pressure drop correlations

The range of the Reynolds number exponent in pressure drop correlations is −0.18 (Kawaguchi et al. (2004) and Ma et al. (2012)) to −0.32 (Briggs and Young (1963)). As for the heat transfer, there is no noticeable difference between solid and serrated-fin tubes: the correlations of PFR (1976), Nir (1991) and Kawaguchi et al. (2006a) have the same exponent for solid and serrated-fin tubes. The correlations from Kawaguchi et al. (2004) show a different Reynolds number dependency for solid and serrated-fin tubes. Most authors' correlations have a Reynolds number exponent in the range of −0.23 to −0.32; Ma et al. (2012) also reported a lower Reynolds number dependency. It can be seen from Chapter 5.1 that the correlation of Ma predicts the lowest Euler numbers of all correlations and has the largest under-prediction of the measured data.

In addition to the listed correlations, others tend towards an asymptotic value, like Weierman (1976) and Næss (2010).

2.5 Progress on numerical modelling

Mon (2003) used CFD to calculate the air flow distribution, temperature distribution, heat transfer and pressure drop within solid-fin tube bundles. The RNG[1] k - ϵ turbulence model was used with the assumption of laminar flow between the fins and turbulent bulk flow. Twenty-nine tube bundles were modelled: 18 with an equilateral staggered tube layout and 11 with an inline tube layout. Besides the bundle arrangement (staggered or inline), the tube diameter d_o, fin height h_f, fin thickness t_f, fin pitch s_f and the number of tube rows were varied. From the data gained through modelling, Mon developed heat transfer and pressure drop correlations for staggered and inline tube arrangements. Mon found that for the same Reynolds numbers a decreased tube diameter led to an increase in the pressure drop, heat transfer coefficient and transferred heat. However, this was because of the influence of the velocity in the minimum flow area. For the same Reynolds number, the velocity is higher for smaller tube diameters, and therefore causes higher heat transfer and pressure drop. She further found that an increased fin height h_f lead to a higher pressure drop and lower heat transfer coefficient. However, because of the increased heat transfer surface per tube (resulting also in an increased bundle volume), the overall transferred heat increased. Increasing the fin pitch s_f caused a lower pressure drop but did not influence the heat transfer coefficient. No influence on the heat transfer and pressure drop was found for fin thickness.

McIlwain (2003) simulated solid fin staggered and inline tube bundles. He used a Realizable k - ϵ turbulence model, which seemed to improve the heat transfer prediction compared to a standard RNG k - ϵ. His model was based on the experimental work of Henry (1994) who had examined tube bundles with touching fins. For touching fins, the pressure loss is highest, consisting only of the skin friction and form drag of the fins and the tube. Ralston et al. (1997) continued the work of Henry and introduced fin, tube and gap loss coefficients for the prediction of the flow distribution and heat transfer and pressure drop

[1] Re-Normalization Group

predictions. Chu and Ralston (1998) revised the first model and obtained an improved prediction for existing experimental data. However, the prediction for deep bundles was not satisfactory. Through his models, McIlwain (2003) found that the faster gap velocity penetrates between the fins. He corrected and improved the existing model by adding coefficients. This improved the prediction for deep tube bundles having more than 10 longitudinal tube rows.

Hofmann (2009) investigated fluid flow, heat transfer and pressure drop behaviour on an I-foot solid-fin tube and I-foot and U-foot serrated-fin tubes. He carried out simulations as well as experiments, and these were found to match. For the simulation, a RNG k - ϵ turbulence model was used. Based on the data Hofmann obtained, he developed heat transfer and pressure drop correlations.

Lemouedda et al. (2011) investigated one solid fin and two serrated-fin tube bundles in a staggered tube layout with three tube rows. They assumed laminar flow as they claimed that the boundary layer remains laminar for flow across a cylinder, and the investigated Reynolds number range was rather low (in the range from $600 < Re < 2600$), so no turbulence model was used. In their study, they investigated the effect of the twisting of fin segments, which occurs during the production process, and the influence of the number of segments and the segment width. They found that small and moderate twisting angles (5° and 10°) showed an improved heat transfer performance compared to fins without twisting. Higher twisting (20° and 25°) had a lower heat transfer performance compared to fins without twisting. The pressure drop was higher in all cases. Serrated-fin tubes with a higher number of segments (slimmer segments) showed an increased heat transfer performance. However, they did not compare their results with experimental data or correlations from the literature.

Cléirigh and Smith (2014) studied one solid-fin and two serrated-fin tube bundles. For the simulation, CFX was used together with a SST[2] k - ω turbulence model. The serrated-fin tubes differed in their degree of serration (46.8% vs. 97.5%). The modelled range of the Reynolds number was $5000 \leq Re \leq 30000$. They found that a higher degree of serration showed a higher heat transfer performance. A comparison with correlations from the literature showed good agreement with their results. However, they claimed that the

[2] Shear Stress Transport

effect of the degree of serration was not represented by most of the correlations.

Table 2-4 gives an overview of the fin types and bundle arrangements simulated and the simulation software and turbulence models used.

Table 2-4: Overview of the simulations

Author	Fin type	Bundle arrangement	Simulation Software	Turbulence model
Mon (2003)	Solid	Staggered Inline	FLUENT	RNG k - ϵ
McIlwain (2003)	Solid	Staggered Inline	FLUENT	Realizable k - ϵ
Hofmann (2009)	Solid Serrated	Staggered Inline	FLUENT	RNG k - ϵ
Lemouedda et al. (2011)	Solid Serrated	Staggered	FLUENT	-
Cléirigh and Smith (2014)	Solid Serrated	Staggered	CFX	SST k - ω

2.6 Summary

The literature review showed that there are contradictory findings and gaps in the experimental data.

Experimental data

Table 2-1 and Table 2-2 in chapter 2.2.4 showed the contradictory findings in the literature. Especially on the influence of the fin height h_f and the fin pitch s_f showed the disagreement in the published experimental data.

Topics that have not been studied extensively are the influence of the fin type on the heat transfer and pressure drop of finned tube bundles as well as on their compactness.

So far, finned tubes having outer tube diameter less than ca. 19.05mm (3/4") have not been explored sufficiently, and only few experimental data are available, within limited parameter ranges. If, for example, high pressure

supercritical CO_2 would be the choice of fluid in a bottoming cycle, then smaller tube diameters would be desirable.

The question whether solid or serrated fins would lead to a more compact and less heavy heat exchanger cannot be answered instantly. Both fin types seems to have the potential to be the optimal choice. Solid fins have a larger heat transfer surface while serrated fins yield the higher effective heat transfer coefficient. The question might need to be addressed by means of an optimization taking into account heat duty, pressure drop, the heat exchanger size and weight.

Correlations

Several correlations for the prediction of the heat transfer and pressure drop of finned tube bundles are published and presented in chapter 2.4 and Appendix I. A comparison of different correlation is shown in Figure 2-17 for heat transfer and Figure 2-18 for pressure drop. The selected geometry for the comparison had a tube diameter of d_o = 31.75mm, fin height h_f = 18mm; number of fins N_f = 276 1/m, fin thickness b_f = 1mm, fin-tip clearance c_f= 2mm and was arranged in a staggered, 30° tube bundle layout. The serrated-fin tube had in addition a segment height h_s = 11mm and segment width w_s = 4.5mm.

It can be seen in Figure 2-17 and Figure 2-18 that, depending on the choice of the correlation, different results are predicted. The spread between the correlations is smaller for the heat transfer coefficient prediction (27% for solid finned tubes and 65% for serrated finned tubes) than for the Euler number prediction (359% for solid finned tubes and 219% for serrated finned tubes). As both heat transfer and pressure drop play an important role in the design of efficient and compact waste heat recovery units, a further improvement of the correlations is desired.

Compactness of WHRU

The compactness of the waste heat recovery unit (WHRU) is important in offshore applications. A small and lightweight design is necessary due to space and weight limitations. Most WHRUs are installed onshore where compactness might be only a desire with the goal of installation cost savings due to material savings. However, usually there are no limitations on the size and weight. Therefore no studies have been carried out to define criteria for a compact, lightweight WHRU design.

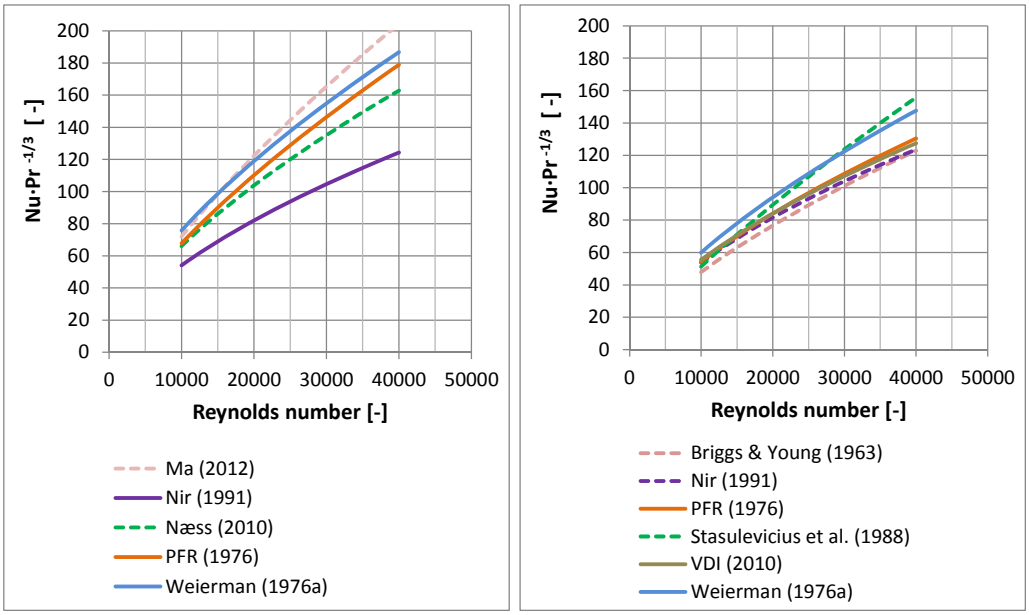

Figure 2-17: Heat transfer coefficient prediction of different correlations; left: serrated-finned tubes; right: solid-finned tubes

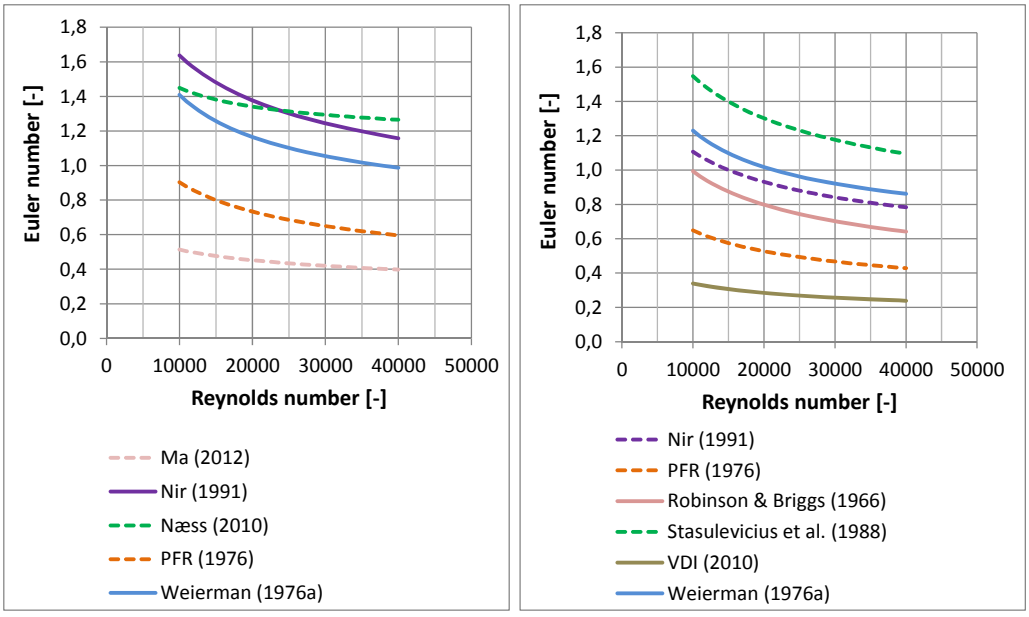

Figure 2-18: Euler number prediction of different correlations; left: serrated-finned tubes; right: solid-finned tubes

3 EXPERIMENTAL FACILITY

This chapter describes the experimental facility used for the investigation of the heat transfer and pressure drop of finned tube bundle geometries. First, an overview of the test rig is given, as well as detailed design criteria, dimensions and specifications of the components used. The chapter concludes by presenting the parameters of the tested fin tube bundles.

3.1 Test rig overview

A test rig was built to measure the influence of different geometric parameters on the fin tube bundle heat transfer and pressure drop performance. Figure 3-1 shows the schematic flow diagram of the test rig.

In the air circuit, air is sucked from outside of the laboratory through two fans and passed through a heating battery where it is heated to ca. 150°C in order to keep the air inlet temperature in the test section at 125°C. After passing the orifice, which measures the flow rate, it passes the diffuser, which leads to the settling chamber. In the diffusor and settling chamber, the flow is slowed down and the installed honeycomb and screens in the settling chamber decrease the turbulence level and establishes a uniform flow. Next, the flow passes the contraction section to the test section. Downstream of the test section, the air is sucked by means of an additional fan and ejected to the outside of the building.

In the cooling circuit, a water-glycol mixture is used in order to prevent corrosion of the tubes. The water-glycol mixture is pumped through the test section by means of a circulation pump having a variable speed drive to control the coolant flow rate, which is measured by an electromagnetic flow meter. A plate heat exchanger cools the water-glycol mixture to a pre-set temperature of 25°C (which is above the air side vapour dew point temperature), by means of cold city water. In addition, the water-glycol circuit contains an expansion tank and instrumentation. The supply of cold water from the city water circuit is controlled by a valve regulated by the water-glycol inlet temperature into the test section.

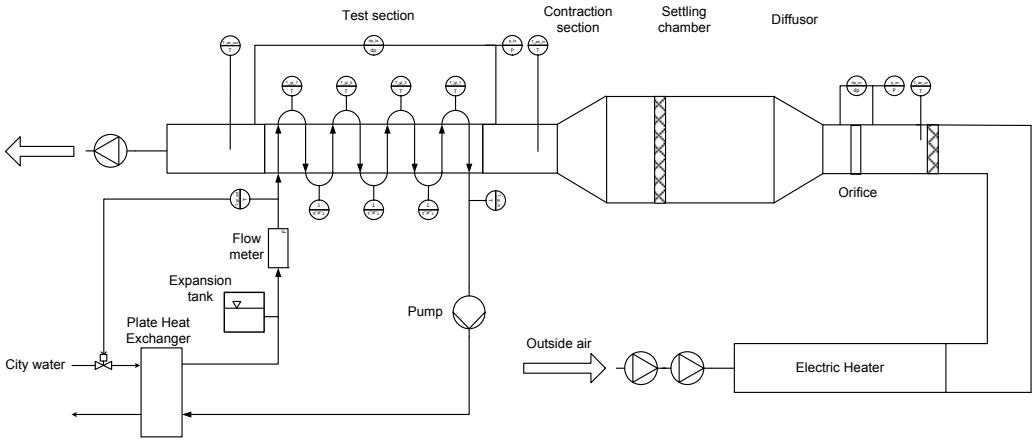

Figure 3-1: Flow diagram

3.2 Component design and dimensions

Fans

In the basement of the laboratory, two fans operating in series are installed. They can provide up to 2.5m^3/s (Rygvold (2010)). A third fan downstream of the heat exchanger controls the air pressure in the test section to ensure a constant pressure (close to atmospheric pressure) independent of the air flow rate.

Heating Battery

The heating battery had an installed power capacity of 400kW. The heat duty was adjusted to an air temperature into the test section of 125°C.

Diffusor

The diffusor enlarges the flow area and thereby decreases the gas velocity. It also changes the shape of the flow area from a circular geometry to a square geometry. The diffusor is designed according to the principles outlined by Mehta and Bradshaw (1979). The angle of the diffusor opening was chosen by

considering the area enlargement and the number of screens placed in the diffusor for an operation without flow separation and a uniform outlet flow velocity profile. The screens were positioned where the diffusor wall changes, as these are the locations where flow separation is most likely. Screens, made of 0.3mm thick wires with a mesh opening of 1mm, were placed at the entrance and middle of the diffusor. The porosity of the screens was 58%. A perforated plate was placed at the outlet of the diffusor and had a porosity of 51%.

Figure 3-2 shows the overall dimensions of the diffusor and the position of the screens and the perforated plate.

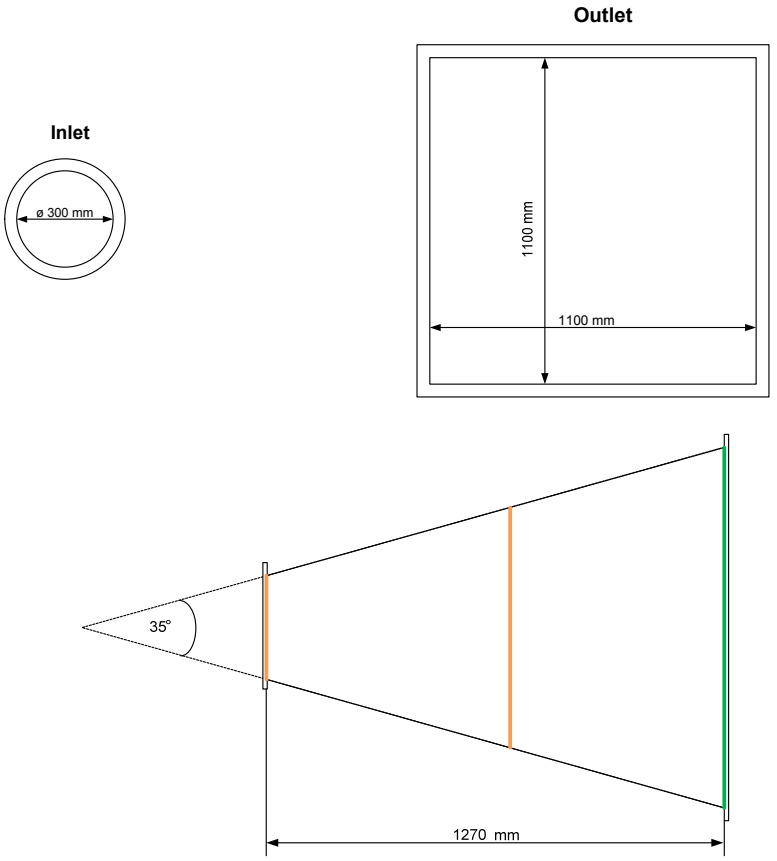

Figure 3-2: Diffusor dimensions. Top left: diffusor inlet; top right: diffusor outlet; bottom: diffusor view from the side (the positions of the screens are marked in orange and the position of the perforated plate is marked in green)

Settling chamber

The purpose of the settling chamber is to decrease turbulence and create a uniform flow distribution. The settling chamber, as well as the included screens and honeycomb, were designed according to Mehta and Bradshaw (1979). The contraction ratios between the settling chamber flow area and the test bundle flow area were in the range 7–14, i.e. in the range of good engineering practice according to Mehta and Bradshaw (1979).

The three screens used in the settling chamber had a wire diameter of 0.3mm and a mesh opening of 1mm, which resulted in a porosity of 58%. According to the suggestions of Mehta and Bradshaw (1979), the screens were placed at 20% of the settling chamber diameter (equivalent to 220mm) away from the contraction section entrance and from each other.

The honeycomb, serving as a turbulence damper, has the dimensions shown in Figure 3-3. As suggested by Mehta and Bradshaw (1979), the cell diameter was chosen as 6.4mm (1/4”), which was roughly 170 cells across the settling chamber diameter. Also in accordance to Mehta and Bradshaw (1979), the length of the honeycomb cells was 7.8 times the cell diameter. Figure 3-4 shows the dimensions of the settling chamber and the positions of the screens and honeycomb.

Contraction section

The contraction section consisted of two parts. As the test section was 500mm wide for all tested geometries, the first part decreased the width of the square flow channel from 1100 to 500mm. The second part decreased the height from 1100mm to the required height of the test section, depending on the transversal tube pitch. This second part of the contraction section is made specifically for each test section. Figure 3-5 shows the view of the contraction section from the top and the side.

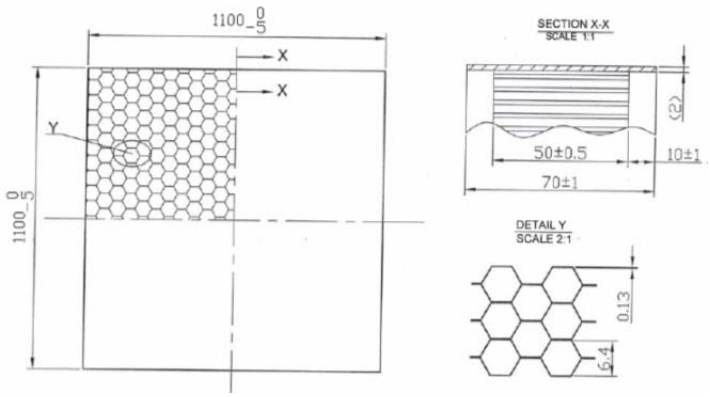

Figure 3-3: Dimensions of the honeycomb

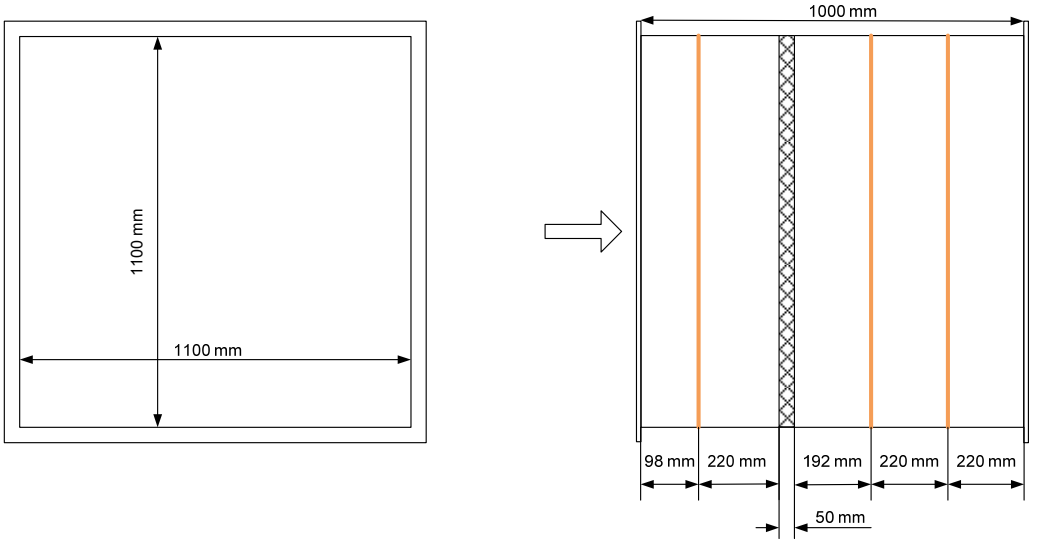

Figure 3-4: Dimensions of the settling chamber. Left: view in the flow direction, right: view from the side and the locations of the screens (orange) and the honeycomb. The arrow indicates the flow direction

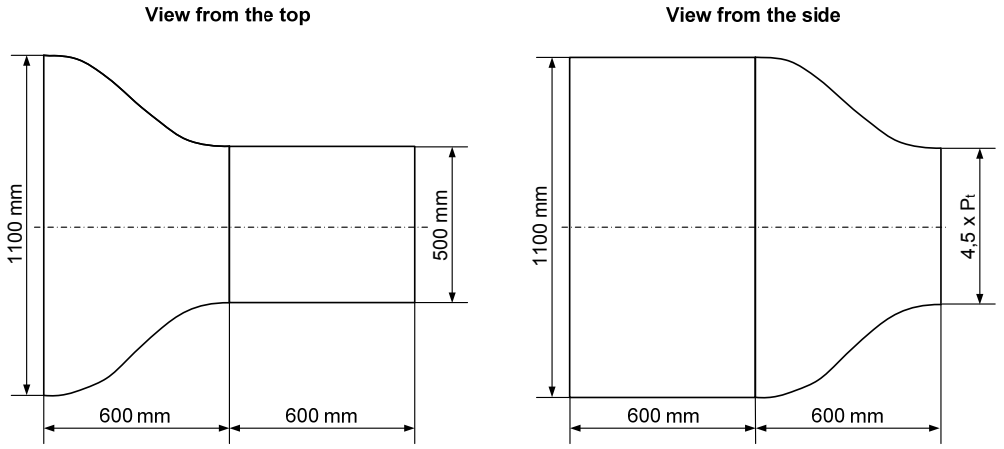

Figure 3-5: Views on the contraction section

The contraction section was designed according to Bell and Mehta (1988). To avoid boundary layer separation on the walls and to obtain reasonable mean flow uniformity at the contraction outlet, it was curved. Bell and Mehta (1988) found that the best-length-to-inlet-height ratio is 0.89. However, Mehta and Bradshaw (1979) argued that the length needs to be 25% longer for a 2D contraction. The length of each contraction section was calculated as 600mm.

Bell and Mehta (1988) investigated shapes as represented by different polynomial equations. The result of their investigation was that a contraction section shape represented by a fifth order polynomial equation best fulfils the requirements of the contraction section. The fifth order polynomial equation used by Bell and Mehta (1988), and adopted in the present work is

$$Y(X) = H_i - (H_i - H_o) \cdot \left[6 \cdot X^5 - 15 \cdot X^4 + 10 \cdot X^3 \right] \qquad \textit{Eq. 3-1}$$

where H_i is the contraction height at the inlet and H_o the contraction height at the outlet. Y represents the calculated height at a relative length X which represents the specific length x divided by the overall contraction section length of 600mm.

Cooling circuit

In order to prevent corrosion in the tubes, the cooling circuit was operated with a mixture of 70 (w)% water and 30 (w)% ethylene glycol.

Pump

The pump in the cooling circuit was from Grundfos (CRN 10-2, 50 Hz) and had a variable speed drive.

Plate heat exchanger

The plate heat exchanger in the cooling circuit transfers heat from the closed-loop water-glycol mixture to the city water. The heat exchanger was a brazed plate heat exchanger from Alfa Laval, model BHE type CB60-30L. The capacity was 150kW under the maximum test rig operating conditions.

Expansion tank

The purpose of the expansion tank was to maintain constant pressure in the water-glycol circuit. The expansion tank was from Grundfos (GT-HR-50 V) and had a volume of 50 litres.

City water supply regulation

The supply of cold water from the city water circuit was regulated by an automatic valve that adjusted the flow rate of cold water into the plate heat exchanger, keeping the water-glycol inlet temperature into the test section constant. The valve could be set to manual mode; its opening could then be controlled manually and kept constant during stable operating conditions.

Turning chambers

In order to measure the water-glycol temperature after each tube pass, turning chambers were constructed. Each turning chamber had four inlets and four outlets. A mesh was welded in the middle of each turning chamber to act as a turbulence generator and mix the water-glycol before it enters a new pass. The opening of the inlets and outlets could be adjusted to the tube diameter by screwing in an insert. The tubes were connected to the turning chambers using flexible hoses. Sensors for the temperature measurement were mounted in the middle of the outlet section of each turning chamber.

Figure 3-6: Turning chambers mounted in a frame. Left: connection between the finned tubes and the turning chambers with hoses; right: turning chambers and temperature sensors

3.3 Instrumentation

Logging system

The logging system was based on National Instruments, type *NI CompactDAQ*, which was built in a modular fashion and used LabView for monitoring and controlling the test rig. Table 3-1 gives an overview of the logging modules and their accuracy.

Table 3-1: Overview of the logging modules

Module	Type	Accuracy
NI c-DAQ 9172	Module chassis	N.A.
NI 9217	Temperature logging module	± 0.15 K
NI 9203	Pressure logging module	± 0.02% of the set range

Temperature Sensors

The temperature sensors were Pt100 sensors from Endress and Hauser. The sheath diameter was 3mm. Table 3-2 gives an overview of their location, the medium they are measuring and their length. All the sensors were calibrated in the laboratory. The given accuracy was 0.15 K ± 0.2% of the measured temperature in °C.

Table 3-2: Overview of the temperature sensors

Location	Medium	Length
Before the orifice	Air	250mm
Before the test section	Air	350mm
After the test section	Air	350mm
Before, between and after the tube rows	Water-Glycol	120mm

Pressure Sensors

The pressure sensors used were from the Deltabar S series from Endress and Hauser. Differential pressure cells as well as absolute pressure transmitters were used. Table 3-3 gives an overview of their location and their range. All sensors were delivered pre-calibrated and the given accuracy is ± 0.075% of the set range.

Table 3-3: Overview of the pressure sensors

Location	Measurement	Range	Sensor
At the orifice	differential pressure	0–8 000 Pa	PMD 75
At the orifice	absolute pressure	0.5–1.5 bar	PMC 71
At the test section	differential pressure	0–5 000 Pa	PMD 75
At the test section	absolute pressure	0.75–1.25 bar	PMC 71

Flow Meters

Air flow rate was measured using an orifice. Two orifice plates were used for low and high flow rates, having diameters of 140 and 221mm, respectively. The orifice was designed in accordance with ISO5167-1 (2003) and ISO5167-2 (2003). Figure 3-7 shows the measurement range of each orifice plate.

Upstream the orifice, a honeycomb was placed 3.9m upstream to dampen turbulence in the flow, as shown in the flow diagram of the test rig in Figure 3-1.

The water-glycol mixture flow rate was measured by a Promag 50 electromagnetic flow meter from Endress and Hauser. The measuring range

was from 0–2 l/s and the accuracy was 0.025% of the measuring range (equivalent to ± $5 \cdot 10^{-4}$ l/s).

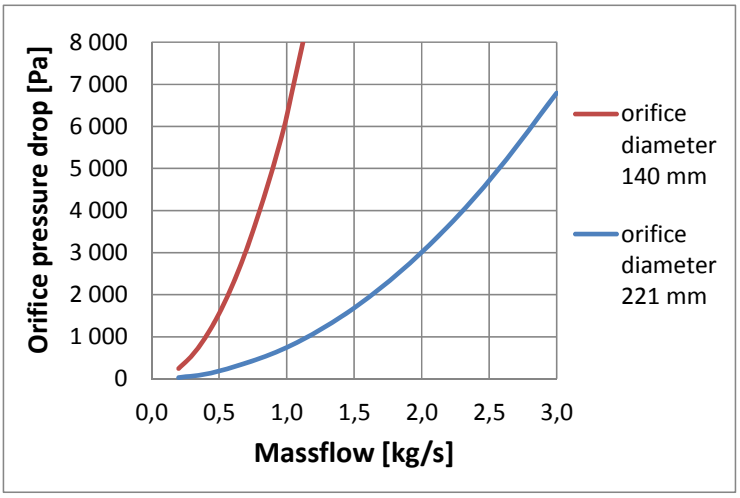

Figure 3-7: Measurement range of the orifice plates (at 125°C and atmospheric pressure)

3.4 Test bundles

Table 3-4 gives an overview of the eight tested tube bundles. The geometric parameters of the finned tubes and tube bundles are shown in Figure 2-13 and Figure 2-14. The geometries were selected to fill the gap in the existing literature and to vary one parameter at the time.

All finned tubes were arranged in tube bundles having a staggered 30 degree layout (shown in Figure 3-8) because this layout is the most compact. Each test section was 500mm in width, 4.5 times the transversal tube pitch P_t in height, and contained 32 active tubes with eight longitudinal tube rows each containing four tubes in the transversal direction. In addition, each transversal tube row had half a dummy tube, which was added to obtain a realistic flow distribution through the test section.

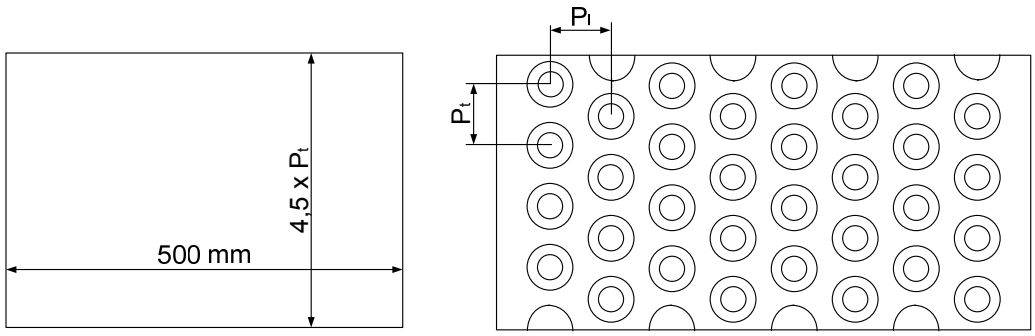

Figure 3-8: Test section dimensions and arrangement. Left: view in flow direction; right: view from the side–transversal tube pitch (P_t), longitudinal tube pitch (P_l)

The finned tubes used in tube bundles 1–7 were made from carbon steel and were manufactured by Spiro Gills Thermal Products Ltd, England. The tubes were made by winding a metal strip helically around the tube and welding it to the tube using high frequency resistance welding; thus producing an I-foot finned tube. The tubes had different fin types, tube diameters, fin heights and fin pitches. Tube bundles 4, 5 and 6 used the same finned tubes; however, they were arranged differently, having varying fin-tip clearance. Figure 3-9 shows pictures of the tubes. The tube diameter of these tubes was limited due to the production to a minimum of 19.05mm.

Table 3-4: Overview of the tube bundle parameters

Parameter	Unit	1	2	3	4	5	6	7	8
Fin type	-	serrated	solid	solid	serrated	serrated	serrated	serrated	solid
Tube material	-	Carbon Steel–St 38.5 (A179)							Aluminium AW 6060
Fin material	-	Carbon Steel–DC 01 (CS4)							
Tube outside diameter	mm	31.75	31.75	31.75	19.05	19.05	19.05	19.05	13.5
Tube wall thickness	mm	2.77	2.77	2.77	2.77	2.77	2.77	2.77	1.5
Fin height	mm	18	18	18	18	18	18	10	10
Segment height	mm	11.0	-	-	11.0	11.0	11.0	5.0	-
Segment width	mm	4.5	-	-	4.5	4.5	4.5	4.5	-
Number of fins	1/m	277	270	170	268	268	268	277	356
Fin thickness	mm	1.0	1.0	1.0	1.0	1.0	1.0	1.0	0.5
Fin-tip clearance	mm	2.0	2.0	2.0	5.0	10.0	0.0	5.0	5.2

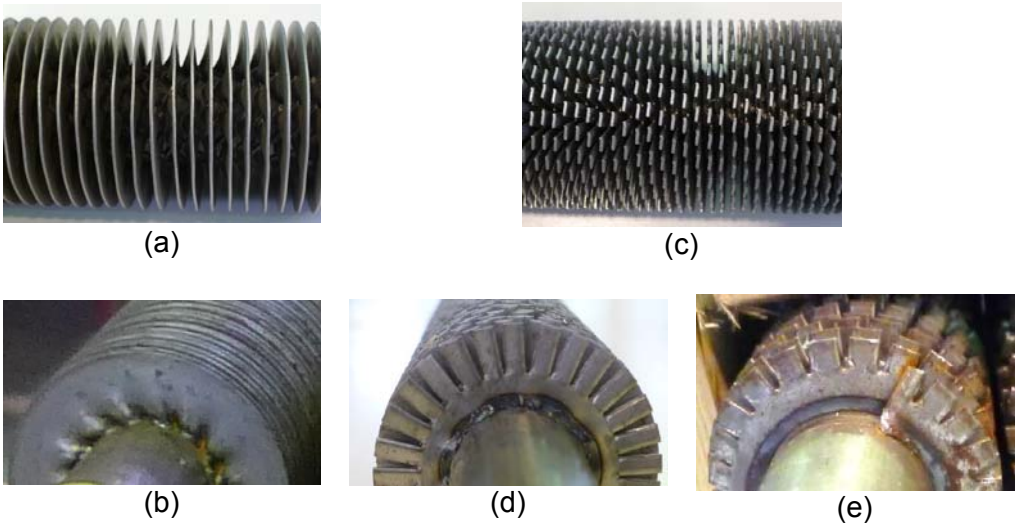

Figure 3-9: Pictures of the used carbon steel finned tubes. (a) solid finned tube, view from the side–geometry 3; (b) solid finned tube–Geometry 2; (c) serrated finned tube, view from the side–Geometry 1; (d) serrated finned tube with high fins–Geometry 1; (e) serrated finned tube with low fins–Geometry 7

In addition, a small diameter finned tube bundle, which used aluminium as the tube and fin material, (manufactured by Wieland-Werke AG, Germany) was tested (tube bundle 8). The fins on the tubes were made by roll forming them from the tube wall. Pictures of the tubes are shown in Figure 3-10.

Figure 3-10: Pictures of the aluminium finned tubes–Geometry 8. Left: view from the side; right: view of the fins

Figure 3-11 shows the tested tube bundles in comparison to tube bundles reported in the literature, arranged in a staggered 30 degree (±10%) layout having a minimum of 4 tube rows. The tube bundles were selected to have a

high surface area (represented by the high fin height), small tube diameter and varying one parameter at the time (see Table 3-5).

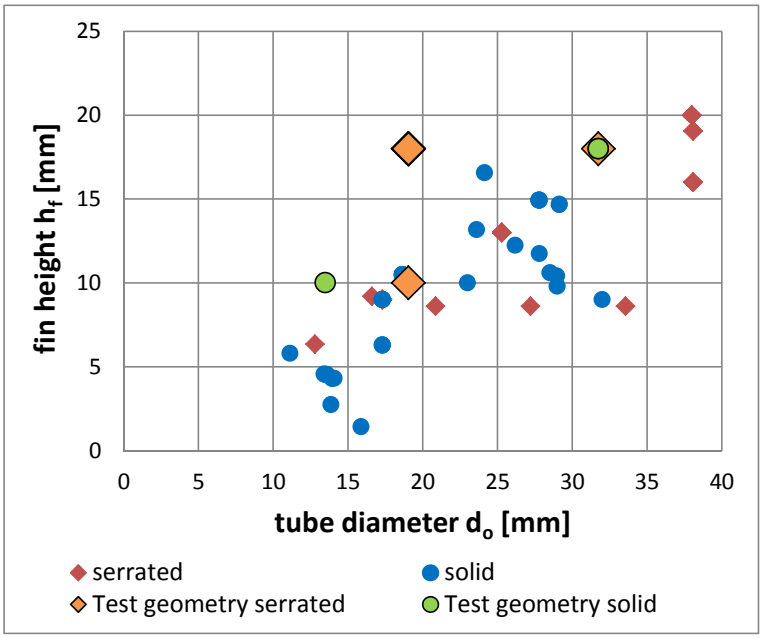

Figure 3-11: Comparison of the tested tube bundle geometries in comparison to tube bundles in the literature

Table 3-5: Variation of one parameter at the time and the tube bundles used of the variation

Varied parameter	**Tube bundles used for the comparison**
Fin type	1 and 2
Tube diameter d_o	1 and 4
Fin height h_f	4 and 7
Fin pitch s_f	2 and 3
Fin-tip clearance c_f	4, 5 and 6

4 DATA REDUCTION

This chapter describes the data reduction procedures for determining heat transfer and pressure loss coefficients. Further, fin efficiency, and the necessity to correct it for a non-uniform heat transfer distribution, are discussed. The calculation procedure for the row-to-row heat transfer coefficients is given, together with the results of the uncertainty analysis performed.

4.1 Average gas side heat transfer coefficient

From the calculated heat transfer rate in the test section, the air side heat transfer coefficient h_{air} could be evaluated. The heat transfer was calculated as the heat uptake in the water glycol circuit.

$$Q = \left(\dot{m} \cdot c_p\right)_{wg} \cdot \left(t_{wg,out} - t_{wg,in}\right) \qquad \textit{Eq. 4-1}$$

From the heat duty Q, the overall heat transfer coefficient U was calculated according to Eq. 4-2.

$$U = \frac{Q}{\left(A_f + A_t\right) \cdot LMTD} \qquad \textit{Eq. 4-2}$$

where LMTD is the logarithmic mean driving temperature difference for counter-current flow, given by

$$LMTD = \frac{\left(t_{wg,in} - t_{air,out}\right) - \left(t_{wg,out} - t_{air,in}\right)}{\ln \dfrac{\left(t_{wg,in} - t_{air,out}\right)}{\left(t_{wg,out} - t_{air,in}\right)}} \qquad \textit{Eq. 4-3}$$

The average air side heat transfer coefficient h_{air} was determined from

$$h_{air} = \left[\left(\eta_f \cdot A_f + A_t \right) \cdot \left(\frac{1}{U \cdot \left(A_f + A_t \right)} - \frac{1}{h_{wg} \cdot A_i} - \frac{\ln\left(\frac{d_o}{d_i} \right)}{k_t \cdot A_{bt}} \right) \right]^{-1} \qquad \textit{Eq. 4-4}$$

The tube side heat transfer coefficient h_{wg} was evaluated using the Gnielinski (1975) correlation (Eq. 4-5) and the fanning type friction coefficient from Kays et al. (2005) (Eq. 4-6).

$$Nu_{wg} = \frac{h_{wg} \cdot d_i}{k_{wg}} = \frac{\frac{c_f}{2} \cdot \left(Re_i - 1000 \right) \cdot Pr_{wg}}{1 + 12.7 \cdot \sqrt{\frac{c_f}{2}} \cdot \left(Pr_{wg}^{2/3} - 1 \right)} \cdot \left(1 + \left(\frac{d_i}{L} \right)^{2/3} \right) \qquad \textit{Eq. 4-5}$$

$$\frac{c_f}{2} = \left(2.236 \cdot \ln\left(Re_i \right) - 4.639 \right)^{-2} \qquad \textit{Eq. 4-6}$$

The Gnielinski (1975) correlation is a modification of the correlation of Petukhov (1970) in order to get better predictions of the heat transfer coefficient in the transition region with Reynolds number below $1 \cdot 10^4$. Petukhov estimated the uncertainty of his correlation with ±5%. A comparison of both correlations showed a ±3% variation in the range of interest. Therefore the uncertainty considered for Eq. 4-5 is to be assumed ±8%.

4.2 Fin efficiency

In Chapter 2.3, the fin efficiency calculation for solid-fin tubes (Eq. 2-6) and serrated-fin tubes (Eq. 2-7) is presented along with the corrections for the non-uniform heat transfer distribution of Weierman (1976) in Eq. 2-8, Hashizume et al. (2002) in Eq. 2-9 and Eq. 2-10, Žukauskas et al. (1966) in Eq. 2-14 and Yudin and Tokhtorova (1973) in Eq. 2-15.

In general, it can be stated that most authors assume uniform heat transfer coefficient distribution and use the theoretical fin efficiency in their data reduction. Næss (2010) and Ma et al. (2012) used the Weierman fin efficiency correction for a non-uniform heat transfer coefficient distribution in the data reduction of their experimental work on serrated finned tube bundles. Therefore, the proposed correction of Weierman for a non-uniform heat transfer coefficient distribution (Eq. 2-8) will be used in the data reduction for serrated-fin tube bundles.

Because of the large variation in the effect of the correction on the heat transfer coefficient, and given that most of the solid fin data in the literature are based on the theoretical fin efficiency (shown in Figure 2-12), it was decided to use the theoretical fin efficiency in the data reduction (Eq. 2-6) for solid-fin tubes.

4.3 Pressure drop

The pressure drop across a tube bundle consists of two main terms, the frictional pressure loss Δp_f and the pressure change because of flow acceleration Δp_a.

$$\Delta p_g = \Delta p_f + \Delta p_a \qquad \textit{Eq. 4-7}$$

The pressure drop measurements were carried out under adiabatic conditions; hence, the fluid properties remained nearly constant. Furthermore, the measured pressure drop was small (less than 4.5%) relative to the absolute pressure. Consequently, the pressure change due to acceleration was small too (1% relative to the measured pressure drop) and could be neglected.

The dimensionless pressure loss coefficient, Euler number Eu, was calculated according to Eq. 4-8, where Δp_{air} is the measured pressure difference, ρ_{air} is the arithmetic average of the air density at the bundle inlet and outlet, $\dot{m}_{air}$ is the air mass flow rate in the narrowest flow passage and N_L is the number of tube rows in the longitudinal direction.

$$Eu = \frac{2 \cdot \Delta p_{air} \cdot \rho_{air}}{\left(\dot{m}_{air} / A_{f,min} \right)^2 \cdot N_L} \qquad \textit{Eq. 4-8}$$

4.4 Thermophysical properties

Fluid properties

For all temperature dependent properties, the reference temperature used in the evaluation was the arithmetic mean temperature between the inlet and outlet.

$$T_{ref} = 0.5 \cdot \left(T_{in} + T_{out} \right) \qquad \textit{Eq. 4-9}$$

Air

The air density was calculated, assuming an ideal gas, using Eq. 4-10, where R_s = 287 J/kg·K is the specific gas constant for dry air.

$$\rho_{air} = \frac{p_{air}}{\left(T_{ref} + 273.15 \right) \cdot R_s} \qquad \textit{Eq. 4-10}$$

A dry air condition was assumed for all calculations as the humidity was not measured. However, an uncertainty of 0.35% was added to the specific gas constant, according to the assumptions and calculations of Næss (2007).

The correlations for the calculation of the temperature dependent fluid properties of the air were taken from VDI (2010). The thermal conductivity and viscosity were calculated according to Eq. 4-11 and the specific heat capacity according to Eq. 4-12, where T is the reference temperature in Kelvin and the factors A to G are given in Table 4-1.

$$k_{air} / \mu_{air} = A + B \cdot T + C \cdot T^2 + D \cdot T^3 + E \cdot T^4 \qquad \textit{Eq. 4-11}$$

$$c_{p,air} = B + (C - B) \cdot \left(\frac{T}{A + T} \right)^2 \cdot \left[1 - \frac{A}{A + T} \cdot \left(D + E \cdot \frac{T}{A + T} + F \cdot \left(\frac{T}{A + T} \right)^2 + G \cdot \left(\frac{T}{A + T} \right)^3 \right) \right] \qquad \textit{Eq. 4-12}$$

Table 4-1: Coefficients for Eq. 4-11 and Eq. 4-12

	Thermal conductivity	**Dynamic viscosity**	**Specific heat capacity**
	k_{air} [W/m·K]	**μ_{air} [Pa·s]**	**$c_{p,air}$ [J/kg·K]**
A	$-0.908 \cdot 10^{-3}$	$-0.01702 \cdot 10^{-5}$	2548.9320
B	$0.112 \cdot 10^{-3}$	$0.79965 \cdot 10^{-7}$	3.5248
C	$-0.084333 \cdot 10^{-6}$	$-0.72183 \cdot 10^{-10}$	-0.6366
D	$0.056964 \cdot 10^{-9}$	$0.04960 \cdot 10^{-12}$	-3.4281
E	$-0.015631 \cdot 10^{-12}$	$-0.01388 \cdot 10^{-15}$	49.8238
F	N.A.	N.A.	-120.3466
G	N.A.	N.A.	98.8658

Water-glycol mixture

The correlations for the 30 w% ethylene glycol mixture property calculations were taken from an NTNU internal database.

The density, thermal conductivity and dynamic viscosity and specific heat capacity can be calculated according to Eq. 4-13 where t is the reference temperature in degree Celsius and the factors A to F are given in Table 4-2.

$$\rho_{wg} / k_{wg} / \upsilon_{wg} / c_{p,wg} = A + B \cdot t + C \cdot t^2 + D \cdot t^3 + E \cdot t^4 + F \cdot t^5 \qquad \textit{Eq. 4-13}$$

Table 4-2: Coefficients for Eq. 4-13

	Density	**Thermal conductivity**	**Kinematic viscosity**	**Specific heat capacity**
	ρ_{wg} [kg/m^3]	**k_{wg} [W/m·K]**	**υ_{wg} [m^2/s]**	**$c_{p,wg}$ [J/kg·K]**
A	1045	0.44434	$3.9643 \cdot 10^{-6}$	3678
B	-0.3019	$1.2402 \cdot 10^{-3}$	$-1.3939 \cdot 10^{-7}$	2.1634
C	-0.0029	$-3.3807 \cdot 10^{-6}$	$2.8192 \cdot 10^{-9}$	$5.2946 \cdot 10^{-3}$
D	$3 \cdot 10^{-6}$	$-1.4638 \cdot 10^{-8}$	$-3.3462 \cdot 10^{-11}$	$-1.5312 \cdot 10^{-6}$
E			$2.1181 \cdot 10^{-13}$	
F			$-5.4615 \cdot 10^{-16}$	

Material properties

The thermal conductivity of the fin k_f, and tube k_t, material was calculated according to Eq. 4-14.

$$k = A + B \cdot t_{ref} + C \cdot t_{ref}^{\ 2} \qquad \textit{Eq. 4-14}$$

The coefficients A, B and C can be found in Table 4-3.

Table 4-3: Coefficients for the thermal conductivity calculation

Material	**A**	**B**	**C**	**Reference**
Aluminium AW 6060 (fin and tube)	190	0.074	-	Lundberg (1997)
Carbon steel ST 38.5 (A179) (for the tube)	58.4	$-2.21 \cdot 10^{-2}$	$-2.33 \cdot 10^{-5}$	Richter (1983)
Carbon steel DC 01 (CS4) (for the fin)	55.3	$-3.35 \cdot 10^{-2}$	$-0.50 \cdot 10^{-5}$	Hofmann (2009)

The tube reference temperature t_{ref_tube} was calculated according to Eq. 4-15 as the average temperature of the inside tube wall t_{wi} and outside tube wall (fin base temperature) t_{fb}.

$$t_{ref\_tube} = \frac{t_{wi} + t_{fb}}{2} \qquad \textit{Eq. 4-15}$$

The inner tube wall temperature t_{wi} (Eq. 4-16) and the outer tube wall temperature t_{fb} (Eq. 4-17) were calculated as:

$$t_{wi} = t_{wg} + U \cdot A_{0,i} \cdot \left(t_{air} - t_{wg}\right) \cdot R_i \qquad \textit{Eq. 4-16}$$

$$t_{fb} = t_{wg} + U \cdot A_{0,i} \cdot \left(t_{air} - t_{wg}\right) \cdot \left(R_i + R_w\right) \qquad \textit{Eq. 4-17}$$

with the inner heat transfer resistance R_i,

$$R_i = \frac{1}{h_{wg} \cdot A_{0,i}} \qquad \textit{Eq. 4-18}$$

and the wall heat transfer resistance R_w,

$$R_w = \frac{\ln\left(\frac{d_o}{d_i}\right)}{2 \cdot \pi \cdot k_t \cdot l_t \cdot N_t \cdot N_l} \qquad \textit{Eq. 4-19}$$

For the calculation of the wall resistance R_w, an iteration was performed as the tube wall resistance is a function of the temperature dependent tube thermal conductivity.

The fin reference temperature was calculated according to Eq. 4-20 as the average temperature of the fin base t_{fb} and fin tip t_{ft}.

$$t_{ref\_fin} = \frac{t_{fb} + t_{ft}}{2} \qquad \textit{Eq. 4-20}$$

From the differential equation of the temperature distribution in the solid fin,

$$0 = \frac{\partial^2 t}{\partial r^2} + \frac{1}{r} \cdot \frac{\partial t}{\partial r} + \frac{1}{r^2} \cdot \frac{\partial^2 t}{\partial r^2} + \frac{2 \cdot h_{air}}{k_f \cdot t_f} \cdot \left(t_{air} - t\right) \qquad \textit{Eq. 4-21}$$

with the boundary conditions

$$t = t_{fb} \text{ for } x = r_0$$

$$\frac{dt}{dx} = 0 \text{ for } x = r_2$$

the fin tip temperature can be calculated. Here, r_0 is the radius at the fin base and r_2 the radius at the fin tip plus half of the fin thickness (see also Figure 2-9).

Hofmann (2009) presented the following solution of Eq. 4-21 for solid fins:

$$t_{ft\_sol} = t_{air} - \frac{I_0\left(m \cdot r_2\right) \cdot K_1\left(m \cdot r_2\right) + I_1\left(m \cdot r_2\right) \cdot K_0\left(m \cdot r_2\right)}{I_0\left(m \cdot r_0\right) \cdot K_1\left(m \cdot r_2\right) + I_1\left(m \cdot r_2\right) \cdot K_0\left(m \cdot r_0\right)} \cdot \left(t_{air} - t_{fb}\right) \qquad \textit{Eq. 4-22}$$

where I and K are modified Bessel functions of the first, respective second kind.

For serrated fins, Hofmann (2009) considered the solid part as well as the serrations. The solution of Eq. 4-21 for serrated fins is

$$t_{ft\_ser} = t_{air} - \left(\Phi \cdot e^{m \cdot r_2} + \Psi \cdot e^{-m \cdot r_2}\right) \qquad \textit{Eq. 4-23}$$

where

$$\Phi = \frac{\left(t_{air} - t_{fb}\right)}{\Omega} \cdot \left[-e^{-m \cdot r_2} \cdot \left(I_0(m \cdot r_1) \cdot K_1(m \cdot r_1) + I_1(m \cdot r_1) \cdot K_0(m \cdot r_1)\right)\right] \qquad \textit{Eq. 4-24}$$

$$\Psi = \frac{\left(t_{air} - t_{fb}\right)}{\Omega} \cdot \left[-e^{m \cdot r_2} \cdot \left(I_0(m \cdot r_1) \cdot K_1(m \cdot r_1) + I_1(m \cdot r_1) \cdot K_0(m \cdot r_1)\right)\right] \qquad \textit{Eq. 4-25}$$

$$\begin{aligned}\Omega = &-I_0(m\cdot r_0)\cdot K_0(m\cdot r_1)\cdot e^{m\cdot r_1}\cdot e^{-m\cdot r_2} + I_0(m\cdot r_0)\cdot K_0(m\cdot r_1)\cdot e^{-m\cdot r_1}\cdot e^{m\cdot r_2} - \\ &-I_0(m\cdot r_0)\cdot K_1(m\cdot r_1)\cdot e^{m\cdot r_1}\cdot e^{-m\cdot r_2} - I_0(m\cdot r_0)\cdot K_1(m\cdot r_1)\cdot e^{-m\cdot r_1}\cdot e^{m\cdot r_2} + \\ &+I_0(m\cdot r_1)\cdot K_0(m\cdot r_0)\cdot e^{m\cdot r_1}\cdot e^{-m\cdot r_2} - I_0(m\cdot r_1)\cdot K_0(m\cdot r_0)\cdot e^{-m\cdot r_1}\cdot e^{m\cdot r_2} - \\ &-I_1(m\cdot r_1)\cdot K_0(m\cdot r_0)\cdot e^{m\cdot r_1}\cdot e^{-m\cdot r_2} - I_1(m\cdot r_1)\cdot K_0(m\cdot r_0)\cdot e^{-m\cdot r_1}\cdot e^{m\cdot r_2}\end{aligned} \qquad \textit{Eq. 4-26}$$

4.5 Evaluation of the row to row heat transfer coefficient

There were a total of eight longitudinal tube rows in the test section, where, relative to the air flow, the water-glycol mixture makes each pass in a cross flow arrangement. As shown in Figure 3-6, the water-glycol mixture temperature was measured between passes.

The heat duty for each pass was evaluated using the measured temperatures of the water-glycol mixture according to Eq. 4-27.

$$Q_n = \dot{m}_{wg}\cdot c_{p,wg,n}\cdot\left(t_{wg,out,n} - t_{wg,in,n}\right) \qquad \textit{Eq. 4-27}$$

where $c_{p,wg,n}$ is the water-glycol mixture specific heat capacity at the arithmetic mean temperature of the water-glycol mixture inlet temperature $t_{wg,in,n}$ and outlet temperature $t_{wg,out,n}$.

Starting with the first tube row in the air flow direction, the air outlet temperature for this row was calculated according to Eq. 4-28. The calculated air outlet temperature was then used as the air inlet temperature for the following tube row.

$$t_{air,out,n} = t_{air,in,n+1} = t_{air,in,n} - \frac{Q_n}{\dot{m}_{air}\cdot c_{p,air,n}} \qquad \textit{Eq. 4-28}$$

In order to evaluate the overall heat transfer coefficient U for each tube row, the results of two methods were compared: the P-NTU method as described in VDI (2010) and the LMTD method as described in chapter 4.1.

For the P-NTU method, different dimensionless numbers are calculated, as shown in Eq. 4-29 to Eq. 4-32:

- Dimensionless temperature changes of the air stream

$$P_{air,n} = \frac{t_{air,in,n} - t_{air,out,n}}{t_{air,in,n} - t_{wg,in,n}} \qquad \textit{Eq. 4-29}$$

- Heat capacity of the air and water-glycol mixture

$$W_{air} = \frac{Q_n}{t_{air,in,n} - t_{air,out,n}} = \dot{m}_{air} \cdot c_{p,air,n} \qquad \textit{Eq. 4-30}$$

$$W_{wg} = \frac{Q_n}{t_{wg,out,n} - t_{wg,in,n}} = \dot{m}_{wg} \cdot c_{p,wg,n} \qquad \textit{Eq. 4-31}$$

- Heat capacity ratio of the two heat capacity rates

$$H_{air,n} = \frac{W_{air,n}}{W_{wg,n}} = \frac{\dot{m}_{air} \cdot c_{p,air,n}}{\dot{m}_{wg} \cdot c_{p,wg,n}} \qquad \textit{Eq. 4-32}$$

From the dimensionless temperature change and the heat capacity ratio of the two streams, the number of transfer units NTU can be calculated. The configuration of one tube row with several transversal tubes and perpendicular air flow is treated, according to Baehr and Stephan (2006), as cross flow with one tube row, laterally mixed on one side. It is calculated according to Eq. 4-33.

$$NTU_n = -\frac{1}{H_{air,n}} \cdot \ln\left(1 + H_{air,n} \ln\left(1 - P_{air,n}\right)\right) \qquad \textit{Eq. 4-33}$$

The overall heat transfer coefficient U_{NTU} is calculated from Eq. 4-34

$$U_{NTU,n} = NTU_n \cdot \frac{W_{air,n}}{A_{o,t,n} + A_{0,f,n}} \qquad \textit{Eq. 4-34}$$

Comparing the obtained values for U_{NTU} and U (based on LMTD), showed that their difference is less than 0.2%. Therefore, it was decided to use the same calculation method for the row specific heat transfer coefficient $h_{air,n}$ as for the whole bundle heat transfer coefficient h_{air}.

Turbulence Measurements

In order to test the influence of air inlet free stream turbulence on the heat transfer coefficient development in the first tube rows, a turbulence generating grid was installed and free stream turbulence was measured using hot wire anemometry.

The calibration of the hot wire anemometer was performed using a Venturi tube. The hot wire anemometer was placed at point 2, the minimum cross section (Figure 4-1).The pressure drop over the Venturi tube was monitored by a manometer. From the pressure drop of the air, the velocity at point 2 was calculated using the Bernoulli equation according to Eq. 4-35.

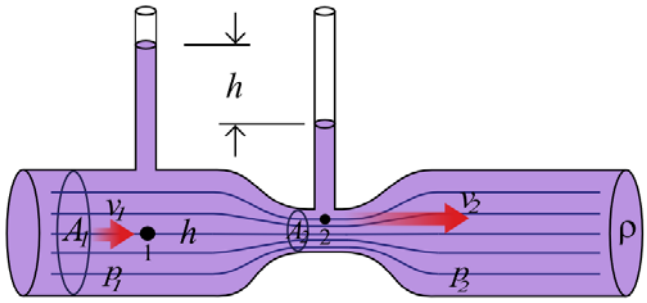

Figure 4-1: Schematic view of a venturi tube [Picture taken from: www.commons.wikimedia.org]

$$u_2 = \frac{\dot{V}}{A_2} = \sqrt{\frac{2}{\rho_{air,1}} \cdot \frac{p_1 - p_2}{1 - \left(\frac{A_2}{A_1}\right)^2}} \qquad \textit{Eq. 4-35}$$

The uncertainty of the velocity measurements was estimated to ±1.6% (Valsø Klynderud (2014)).

For evaluation of the turbulence intensity, the root mean square (rms) velocity fluctuation was calculated according to Eq. 4-36.

$$u_{rms} = \left[\frac{1}{n} \cdot \sum_{i=1}^{n} \left(u_i - u_m \right)^2 \right]^{1/2} \qquad \textit{Eq. 4-36}$$

The turbulence intensity τ was evaluated as the velocity fluctuation, represented by u_{rms} over the mean velocity u_m:

$$\tau = \frac{u_{rms}}{u_m} \qquad \textit{Eq. 4-37}$$

The grid used for turbulence generation was placed 600mm upstream of the tube bundle and the turbulence measurements were carried out 450mm downstream of the grid. The grid dimensions are shown in Figure 4-2. The width of the grid was 500mm and the height 293mm. The porosity of the grid was 55%.

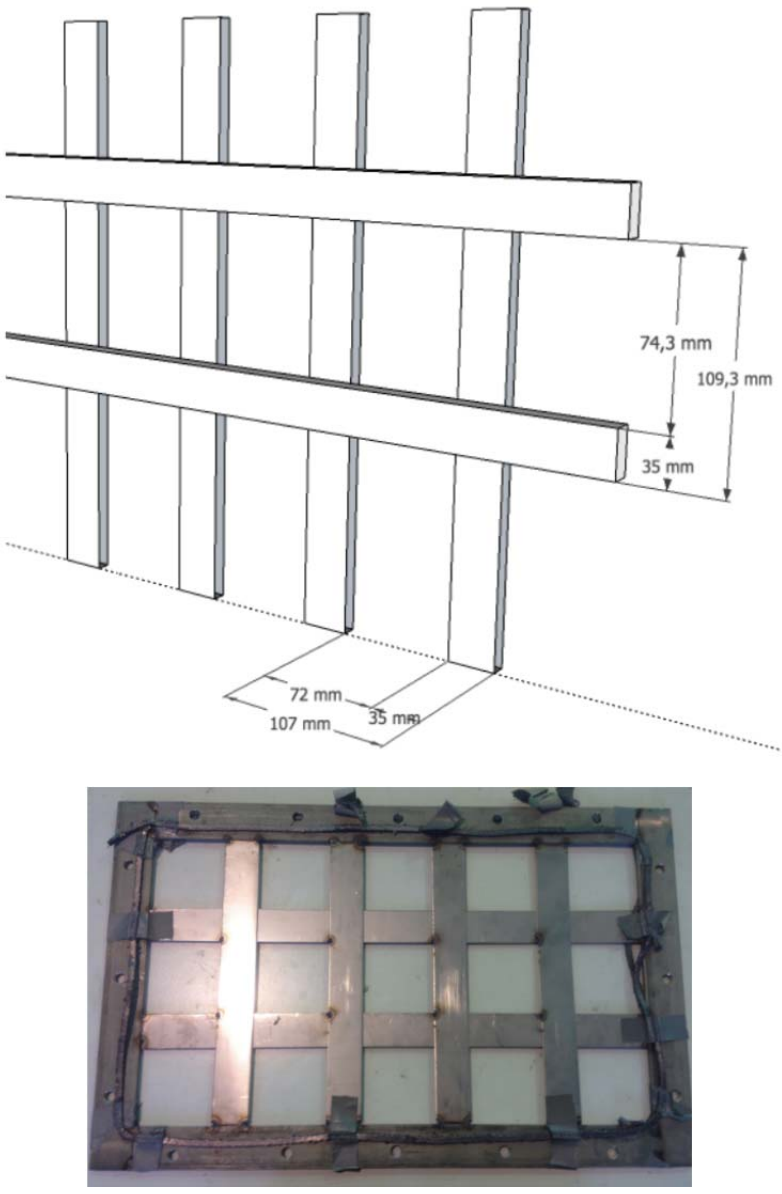

Figure 4-2: Dimensions (top) and picture (bottom) of the grid used for turbulence generation (Valsø Klynderud (2014))

4.6 Uncertainty analysis

An uncertainty analysis was performed in order to estimate the accuracy of the measurements and results. For the presented parameters an uncertainty range is given, as well as an average uncertainty value, which is the arithmetic mean uncertainty value of all experimental measurements.

Measured values

For each measured value there are three contributions to the uncertainty:

- The random error of the measurement
- The sensor accuracy
- The data logger accuracy

The random error of the measurements was calculated, as described by Moffat (1988), using the Student's t distribution and the standard deviation σ, as shown in Eq. 4-38.

$$\delta X_{i\_random} = t \cdot \sigma \qquad \textit{Eq. 4-38}$$

As the number of measurement points was larger than 120 and the confidence interval was chosen to be 95%, the Student's t multiplier is 1.96. The sensor and data logger accuracies are given in Chapter 3.3. The uncertainty ranges of the measured values are shown in Table 4-4.

Table 4-4: Uncertainty of the measured values

Parameter	Symbol	Unit	Uncertainty range (Average)
Air temperatures	T	K	± (0.3% – 1.3%) (± 0.4%)
Water-glycol temperatures	T	K	± (0.6% – 1.3%) (± 1.0%)
Differential pressures	Δp	Pa	± (0.6% – 19.9%) (± 3.5%)
Absolute pressures	p	Pa	± (0.2% – 13.3%) (± 2.1%)
Water-glycol volume flow	$\dot{V}_{wg}$	l/s	± (1.4% – 3.9%) (± 2.4%)

Calculated values

Moffat (1988) reported that the uncertainty of calculated values is estimated by using the partial derivative of each variable in the formula. These are combined using the root-sum-square method (Eq. 4-39). The partial derivatives are weighting factors used to consider the contribution of each factor to the result.

$$\delta R = \sqrt{\sum_{i=1}^{N}\left(\frac{\partial R}{\partial X_i}\delta X_i\right)^2} \qquad \textit{Eq. 4-39}$$

Geometry

For each tested finned tube geometry, the finned length l_t was measured and the number of fins N_f per tube was counted. Their variation, as well as the given production tolerances of the tubes, were considered in the uncertainty analysis.

Table 4-5: Considered uncertainty for the tube geometry parameters, given by the production tolerances and own measurements

Parameter	**Symbol**	**Uncertainty**
Tube outside diameter	d_o	± 0.25mm
Tube thickness	b_t	± 0.05mm
Fin height	h_f	± 0.25mm
Fin thickness	b_f	± 0.05mm
Segment height	h_s	± 0.25mm
Segment width	w_s	± 0.05mm
Finned length	l_t	$\pm \frac{t \cdot \sigma}{\sqrt{N}} = \pm \frac{2.042 \cdot \sigma}{\sqrt{32}}$
Number of fins per tube	N_f	$\pm \frac{t \cdot \sigma}{\sqrt{N}} = \pm \frac{2.042 \cdot \sigma}{\sqrt{32}}$

In the specifications of the tested welded I-foot fins, it is stated that a welding interruption shall not exceed five wraps and shall not occur more than once within a 150mm tube length.

For the tubes of the tested geometry the welded length is estimated by

$$l_w = \pi \cdot d_o \cdot N_f \cdot l_t \qquad \textit{Eq. 4-40}$$

And the uncertainty of the welded length

$$\frac{\delta l_w}{l_w} = 1 - \frac{\pi \cdot d_o \cdot (N_f - \frac{l_t}{l_{wi}} \cdot 5) \cdot l_t}{\pi \cdot d_o \cdot N_f \cdot l_t} = 1 - \frac{N_f - \frac{l_t}{l_{wi}} \cdot 5}{N_f} = \frac{\frac{l_t}{l_{wi}} \cdot 5}{N_f} \qquad \textit{Eq. 4-41}$$

With l_{wi} being the length within one welding interruption can occur; l_{wi} = 150mm.

As the non-welded fins are inactive in the heat transfer, this uncertainty is taken into account in the calculated fin heat transfer surface $A_{o,f}$ together with the uncertainties due to the variation of the fin height, fin pitch and fin thickness. The uncertainty due to the fin variation can both increase and decrease the fin heat transfer surface. The improperly welded fins can only decrease the active fin heat transfer surface. In the analysis all fins are assumed active and attached to the tube. This results in an approximately 3 to 6% lower heat transfer coefficient than assuming a Gaussian distribution of the non-attached fins.

Table 4-6 shows the results for the different heat transfer surfaces and flow areas.

Table 4-6: Uncertainty of the calculated heat transfer surfaces and flow areas

Parameter	**Symbol**	**Unit**	**Uncertainty range (Average)**
Fin heat transfer surface	$A_{0,f}$	m^2	± (3.7% – 9.0%) (± 6.3%)
Tube outside heat transfer surface	$A_{0,t}$	m^2	± (1.3% – 2.9%) (± 2.1%)
Tube inside heat transfer surface	$A_{0,i}$	m^2	± (0.8% – 2.6%) (± 1.6%)
Minimum free-flow area	$A_{f,min}$	m^2	± (1.3% – 2.1%) (± 1.8%)
Flow area inside the tubes	$A_{f,i}$	m^2	± (1.7% – 5.2%) (± 3.1%)

Mass flow rate

For the estimation of the uncertainty of the air mass flow rate from the orifice, the calculation given in the standard ISO5167-1 (2003) was used (Eq. 4-42), where C is the discharge coefficient, ε is the expansion factor, β is the diameter ratio d/D, D is the pipe diameter, d is the orifice diameter, Δp is the pressure drop and ρ_1 is the density upstream of the orifice.

$$\frac{\delta \dot{m}_{air}}{\dot{m}_{air}} = \sqrt{\left(\frac{\delta C}{C}\right)^2 + \left(\frac{\delta \varepsilon}{\varepsilon}\right)^2 + \left(\frac{2\beta^4}{1-\beta^4}\right)^2 + \left(\frac{\delta D}{D}\right)^2 + \left(\frac{2}{1-\beta^4}\right)^2 + \left(\frac{\delta d}{d}\right)^2 + \frac{1}{4}\left(\frac{\delta \Delta p}{\Delta p}\right)^2 + \left(\frac{\delta \rho_1}{\rho_1}\right)^2} \qquad \textit{Eq. 4-42}$$

The water-glycol mixture mass flow rate was calculated from the measured volume flow.

$$\frac{\delta \dot{m}_{wg}}{\dot{m}_{wg}} = \sqrt{\left(\frac{\delta \dot{V}_{wg}}{\dot{V}_{wg}}\right)^2 + \left(\frac{\delta \rho_{wg,in}}{\rho_{wg,in}}\right)^2} \qquad \textit{Eq. 4-43}$$

The uncertainty of the air and water-glycol mass flow rate is given in Table 4-7.

Table 4-7: Uncertainty of the mass flow rates

Parameter	**Symbol**	**Unit**	**Uncertainty range (Average)**
Air mass flow rate	$\dot{m}_{air}$	kg/s	± (0.7% – 9.7%) (± 5.4%)
Water-glycol mass flow rate	$\dot{m}_{wg}$	kg/s	± (1.4% – 3.9%) (± 2.4%)

Heat transfer

The uncertainties for the calculated heat duty, heat transfer coefficients and fin efficiencies were estimated by calculating the partial derivatives according to Eq. 4-39. Table 4-8 shows the uncertainties obtained.

Table 4-8: Uncertainties of calculated values related to heat transfer

Parameter	Symbol	Unit	Corresponding Equation	Uncertainty range (Average)
Heat duty	Q_{gl}	W	Eq. 4-1	± (3.2% – 9.1%) (± 4.7%)
Overall heat transfer coefficient	U	$W/m^2 K$	Eq. 4-2	± (6.2% – 13.2%) (± 8.4%)
LMTD	LMTD	°C	Eq. 4-3	± (1.4% – 3.7%) (± 2.0%)
Inside heat transfer coefficient	h_{wg}	$W/m^2 K$	Eq. 4-5	± (8.2% – 9.3%) (± 8.5%)
Solid-fin tubes Theoretical fin efficiency	$\eta_{f,th,sol}$	-	Eq. 2-6	± (0.5% – 3.4%) (± 2.3%)
Serrated-fin tubes Corrected fin efficiency	$\eta_{f,W,ser}$	-	Eq. 2-7 & Eq. 2-8	± (0.4% – 1.8%) (± 1.0%)
Air side heat transfer coefficient	h_{air}	$W/m^2 K$	Eq. 4-4	± (9.0% – 16.7%) (± 11.9%)
Nusselt number	Nu	-	$Nu = \frac{h \cdot d_o}{k}$	± (9.0% – 16.7%) (± 11.9%)
Prandtl number	Pr_{air}	-	$Pr = \frac{c_p \cdot \mu}{k}$	± (0.4% – 0.6%) (± 0.4%)

Pressure drop

The uncertainties of the Reynolds number and Euler number are shown in Table 4-9.

Table 4-9: Uncertainties related to gas side pressure drop

Parameter	Symbol	Unit	Corresponding Equation	Uncertainty range (Average)
Reynolds number	Re	-	$Re = \frac{\dot{m} \cdot d_o}{A_{f,min} \cdot \mu}$	± (2.5% – 9.4%) (± 5.4%)
Euler number	Eu	-	$Eu = \frac{2 \cdot \Delta p}{\rho \cdot u_{max}^2 \cdot N_l}$	± (4.3% – 25.2%) (± 11.3%)

5 EXPERIMENTAL RESULTS

In this chapter the experimental results are presented, discussed and compared to correlations as well as to data published in the literature.

5.1 Comparison of the experimental data to published correlations

The experimental results from the serrated-fin tubes are compared to the heat transfer and pressure drop correlations of Ma et al. (2012), Nir (1991), Næss (2010), PFR (1976) and Weierman (1976), whereas the experimental results for the solid-fin tube geometry are compared to the correlations published by Nir (1991), PFR (1976), Stasiulevičius et al. (1988) and Weierman (1976). The correlations are presented in chapter 2.4 as well as in Appendix I.

The solid lines in Figure 5-1 and Figure 5-2 indicate that the correlation predictions are within their stated validity range of the correlation, whereas the dashed lines indicate an extrapolation of the correlations that fall outside their stated validity range. The literature correlations were selected on the basis of being frequently used or of a new origin.

Table 5-1 and Table 5-2 present the prediction accuracy of the different correlations for the measured heat transfer and pressure drop data. For each correlation the difference between the prediction value and the experimental value was put in relation to the experimental value. The spread between the correlations was calculated as the difference of the highest and lowest prediction value of the different correlations in relation to the lowest prediction.

Heat transfer

Figure 5-1 shows the experimentally obtained heat transfer data as well as the predictions of the published correlations. Larger diagrams are included in Appendix II. Table 5-1 shows the prediction accuracy of each correlation and the total spread between all correlations.

The first three diagrams in Figure 5-1 (Geometries 1 - 3) show the data for the tested large diameter tube bundles (d_o = 31.75mm). It can be seen that all correlations underpredict the results. The Weierman correlation fits the data best, even though it underpredicts the measured data by up to 23%. For the smaller tube diameters (Geometries 4 - 8) Weierman (1976) overpredicts the heat transfer. The reason for this might be that large diameter tubes were used in his tests (in the range of d_o = 50.8mm).

The second row of diagrams in Figure 5-1 (Geometries 4 - 6) shows the heat transfer data of the same tubes, tested in different arrangements. Only the fin-tip clearance varied from 5mm (Geometry 4) and 10mm (Geometry 5) to 0mm (Geometry 6). The correlation of PFR (1976) predicts the results best.

For a lower finned tube (Geometry 7), the correlation of Nir (1991) predicts the measurement results within +4% and -10%. All other correlations overpredict the data.

Experimental data of the smallest diameter tubes having solid fins (Geometry 8) are covered by Stasiulevičius et al. (1988) within +1/-9%.

As shown in all the diagrams in Figure 5-1, the spread between correlations is quite large, up to 77%.

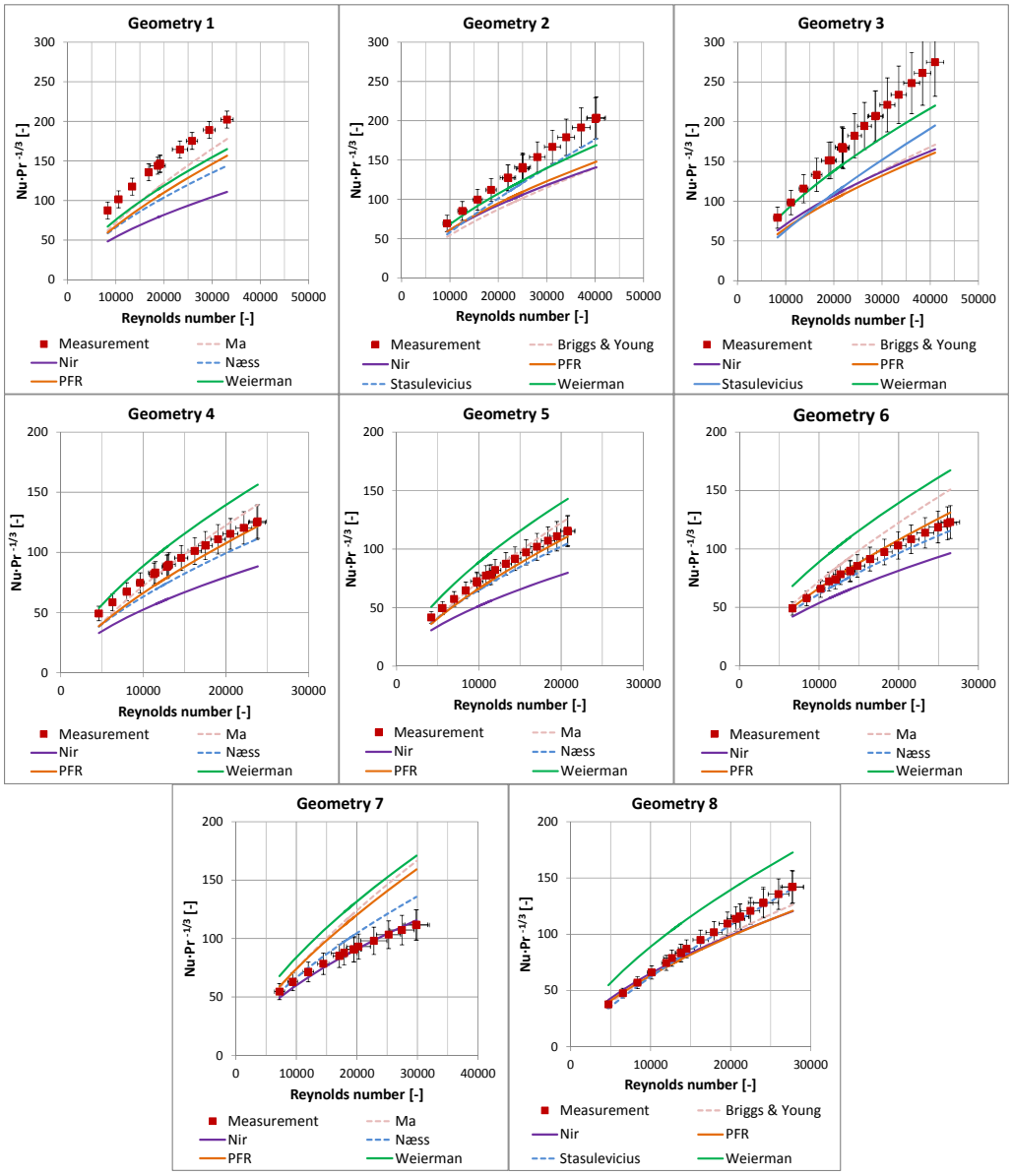

Figure 5-1: Comparison of the experimental heat transfer results to published correlations (diagrams repeated larger in the appendix)

Table 5-1: Prediction accuracy of the different correlations for the measured heat transfer data

Geo.	Briggs and Young (1963)	Ma et al. (2012)	Nir (1991)	Næss (2010)	PFR (1976)	Stasiulevičius et al. (1988)	Weierman (1976)	Spread between the correlations
	[%]	[%]	[%]	[%]	[%]	[%]	[%]	[%]
1		-12 / -29	-45 / -46	-33 / -29	-32 / -23		-23 / -18	+39 / +60
2	-25 / -31		-15 / -31		-15 / -27	-20 / -13	-5 / -17	+14 / +26
3	-23 / -34		-16 / -36		-22 / -38	-28 / -24	+4 / -15	+34 / +43
4		-21 / +11	-33 / -29	-22 / -11	-22/ -3		+9 / +25	+63 / +77
5		-13 / +10	-26 / -31	-11 / -9	-13 / -4		+20 / +24	+65 / +77
6		+7 /+23	-14 / -22	-4/ -8	+0 / +7		+39 / +33	+62 / +72
7		+6 / +49	-10 / +4	-1 / +22	+8 / +43		+25 / +53	+38 / +48
8	+1 / -11		+11 / -15		+5 / -15	-9 / +1	+46 / +21	+41 / +60

Best prediction of the measured data

Pressure drop

Figure 5-2 shows the experimentally obtained Euler numbers as well as the predictions of published correlations. Larger diagrams are included in Appendix II. Table 5-2 shows the prediction accuracy of each correlation as well as the spread between all correlations for each geometry.

Aside from Geometry 8, all correlations underpredict the measured data. The diagrams in the first row of Figure 5-2 show the experimental results for large tubes (d_o = 31.75mm). For the solid-fin tube bundles (Geometries 2 and 3) the correlation of Stasiulevičius et al. (1988) fits the data best, even though it underpredicts within a range from 8 to 18%. For the serrated-fin tubes (Geometry 1), the correlation of Nir (1991) agrees best with the measurements.

The diagrams in the second row of Figure 5-2 show a set of 19.05mm diameter tubes in different arrangements having various fin-tip clearance c_f. The correlations of Nir (1991), Næss (2010) and Weierman (1976) estimate the results as being within the same range. However, the Næss (2010) estimation is slightly better for Geometry 5 and also Geometry 7, which has a lower fin height.

For small diameter solid-fin tubes (Geometry 8), the correlation of Nir (1991) predicts the data within +15 to +4%.

Overall, for serrated-fin tubes the pressure drop correlation of Næss (2010) best predicts the data although it underpredicts the Euler number by up to 38%. The correlations of Ma et al. (2012) and PFR (1976) significantly underpredict the results by up to 80%, and 72% respectively. The spread between the correlations is also considerable - up to 410%.The reason for the mismatch can be found in the relatively low fin-tip clearance in this study. The large tube diameter tubes were measured with c_f = 2mm and the smaller diameter tubes with c_f = 5mm (see Table 3-4). Most previous studies were conducted with a less compact arrangement. For their measurements, Næss (2010) used a minimum fin-tip clearance c_f of 8mm, Weierman (1976a) used 11mm, Stasiulevičius et al. (1988) tested with a minimum fin-tip clearance of 13mm and Ma et al. (2012) used 18mm as a minimum.

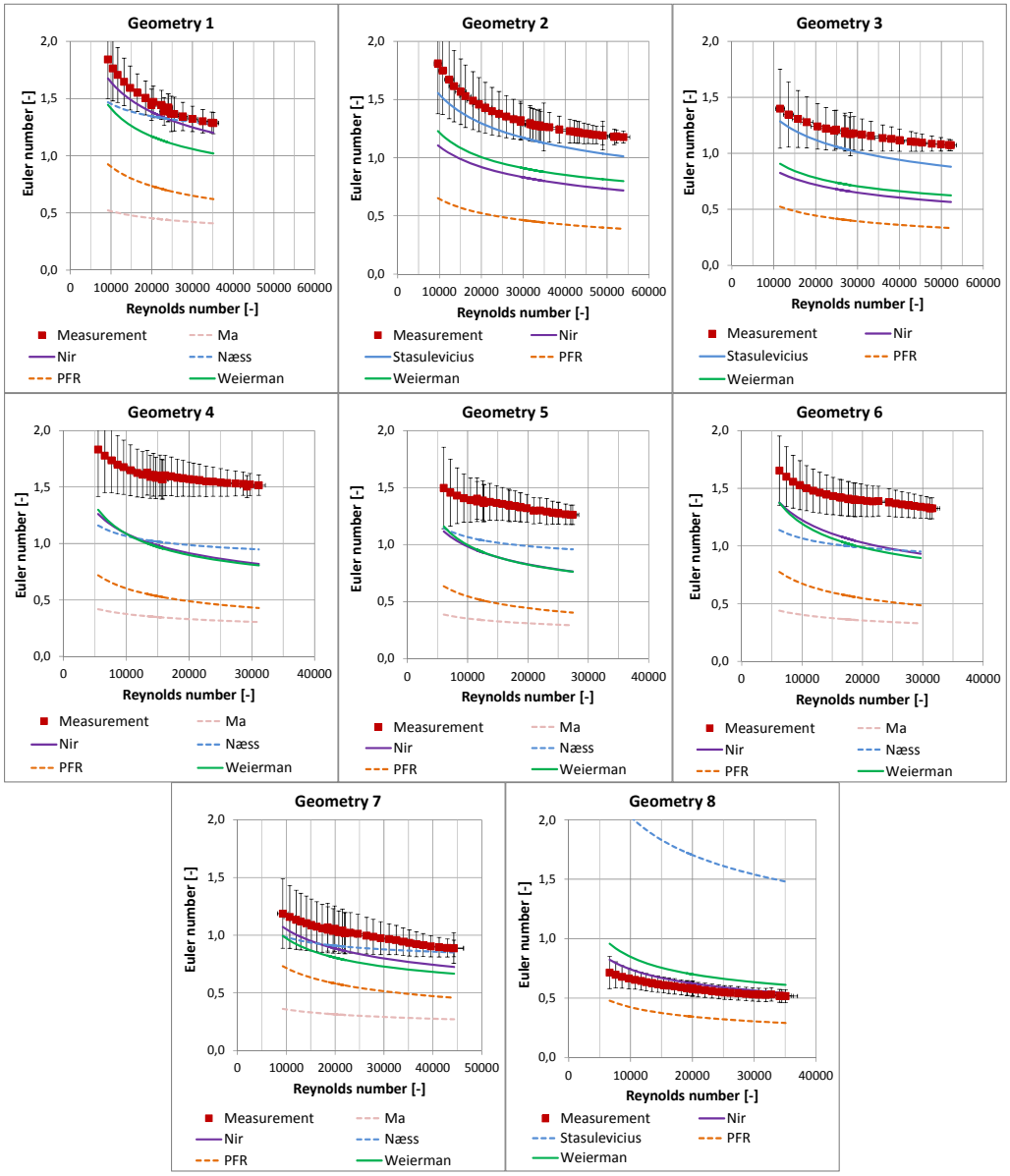

Figure 5-2: Comparison of the experimental pressure drop results to published correlations (diagrams repeated larger in the appendix)

Table 5-2: Prediction accuracy of the different correlations for the measured pressure drop data

Geo.	Ma et al. (2012)	Nir (1991)	Næss (2010)	PFR (1976)	Stasiulevičius et al. (1988)	Weierman (1976)	Spread between the correlations
	[%]	[%]	[%]	[%]	[%]	[%]	[%]
1	-72 / -68	-4 / -9	-20/ -0	-49 / -52		-19 / -22	+202 / +221
2		-36 / -39		-64 / -67	-14 / -10	-32 / -30	+139 / +160
3		-41 / -47		-63 / -69	-8 / -18	-35 / -42	+145 / +165
4	-77 / -80	-31 / -46	-36 / -38	-61 / -72		-29 / -47	+187 / +211
5	-74 / -77	-25 / -39	-23 / -25	-58 / -68		-23 / -40	+198 / +228
6	-73 /-75	-17 / -31	-28/ -31	-53 / -64		-17 / -33	+185 / +213
7	-69 / -70	-10 / -18	-16 / -4	-38 / -48		-16 / -25	+186 / +214
8		+15 / +4		-33 / -44	+215 / +184	+34 / 17	+370 / +410

Best prediction of the measured data

5.2 Reynolds number dependency

In order to determine the influence of flow on the heat transfer coefficient, a simplified heat transfer equation was used, as shown in Eq. 5-1. The Reynolds number exponent m for each geometry was evaluated using least-squares regression.

$$\frac{Nu}{Pr^{1/3}} = c \cdot Re^{m} \qquad \textit{Eq. 5-1}$$

Table 5-3 shows the obtained coefficient c, the Reynold exponent m and the obtained coefficient of determination R^2 for each regression, using Eq. 5-1.

The obtained Reynolds number exponent m for each geometry is shown in Figure 5-3. The average exponent of the serrated-fin geometries is 0.60 and for the solid-fin geometries 0.76. The reason for this difference could be that serrated-fin tubes introduce additional turbulence to the flow due to the serration of the fins, which than interrupts the flow. However, this is not the case for solid-fin tubes. Therefore, the dependency of the heat transfer on the Reynolds number Re, respectively the flow velocity, could be higher for solid-fin tubes than for serrated-fin tubes.

Figure 5-4 shows the fit of the data points for the obtained regression. It can be seen that the regression coefficients for the serrated-fin geometries are spread between 0.15 and 0.64 while the coefficients for the solid-fin geometries remain nearly constant at 0.07 and 0.06 respectively.

Table 5-3: Coefficient c and Reynolds number exponent m for each geometry based on Eq. 5-1, coefficient of determination for each regression as a degree of goodness

	Fin type	Coefficient c	Exponent m	Coefficient of determination R^2
Geo 1	Serrated	0.36	0.609	0.999
Geo 4	Serrated	0.40	0.571	0.999
Geo 5	Serrated	0.20	0.642	0.999
Geo 6	Serrated	0.15	0.660	0.998
Geo 7	Serrated	0.64	0.501	0.999
Geo 2	Solid	0.07	0.747	0.999
Geo 3	Solid	0.07	0.777	0.999
Geo 8	Solid	0.06	0.757	0.999

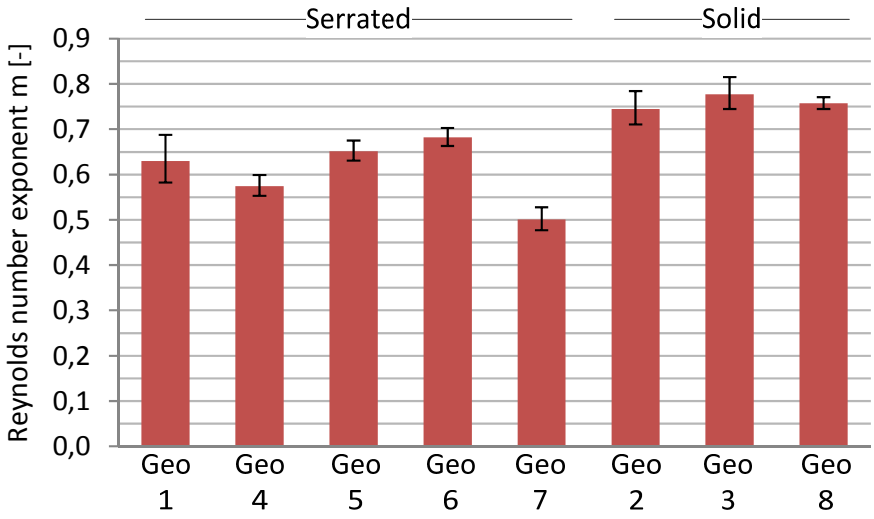

Figure 5-3: Measured Reynolds number exponent for heat transfer

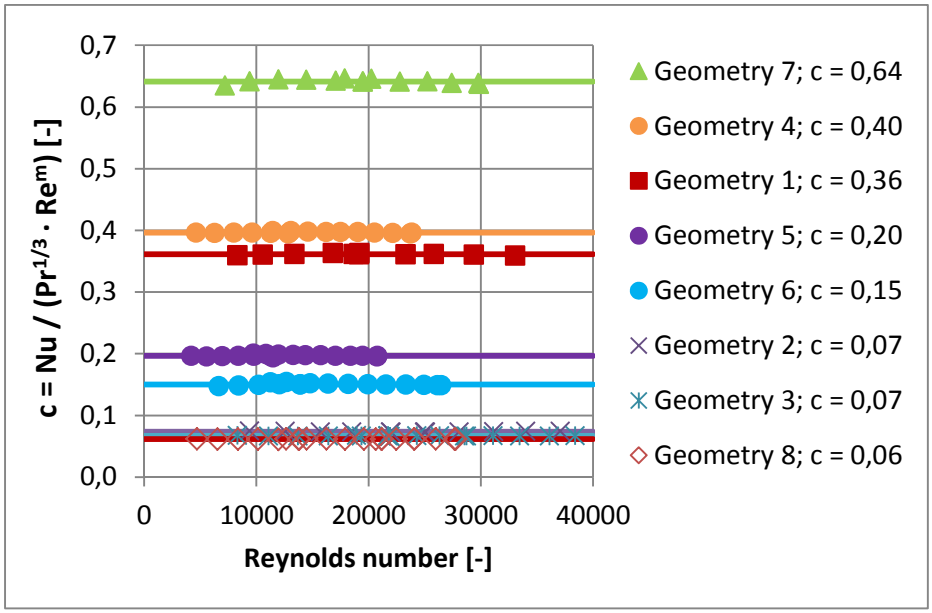

Figure 5-4: Coefficient c from Eq. 5-1 for the different geometries

The same linear regression was used for the pressure drop coefficient, Eu.

$$Eu = c \cdot Re^{m} \qquad \textit{Eq. 5-2}$$

Table 5-4 shows the obtained coefficient c, Reynold exponent m and the obtained coefficient of determination R^2 for each regression based on Eq. 5-2.

Figure 5-5 shows the Reynolds number exponent m obtained for each geometry. The average Reynolds number exponent for serrated-fin tubes is -0.16 and for solid-fin tubes -0.20. Again the Reynolds number dependency and therefore the flow velocity dependency of the Euler number is higher for solid-fin tubes than for serrated-fin tubes. It can be seen in Figure 5-5 that the spread of the exponent is large, especially for serrated-fin geometries.

Figure 5-6 presents the fit of the data points to the obtained regression. It can be noticed, that Geometries 1 and 2 have particularly high coefficients, 16.4 and 21.2, respectively, and fit the regressions less well than the other geometries. One reason for the spread and the high coefficients could be that after measuring Geometries 1 and 2, an additional honeycomb was installed in the test rig to further decrease turbulence in the air flow. Thereafter the measurements values from Geometries 3 and onwards are smoother and better fit the regressions.

Table 5-4: Coefficient c and Reynolds number exponent m for each geometry based on Eq. 5-2, coefficient of determination for each regression as a degree of goodness

	Fin type	**Coefficient c**	**Exponent m**	**Coefficient of determination R^2**
Geo 1	Serrated	21.2	-0.269	0.988
Geo 4	Serrated	4.1	-0.098	0.976
Geo 5	Serrated	3.7	-0.106	0.979
Geo 6	Serrated	4.7	-0.123	0.998
Geo 7	Serrated	6.6	-0.187	0.991
Geo 2	Solid	16.4	-0.244	0.986
Geo 3	Solid	6.6	-0.168	0.993
Geo 8	Solid	4.1	-0.197	0.998

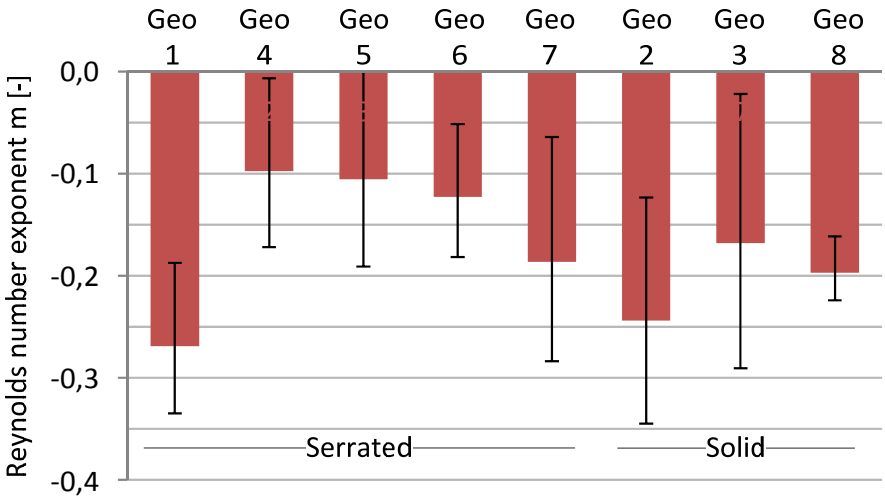

Figure 5-5: Measured Reynolds number exponent m for pressure drop

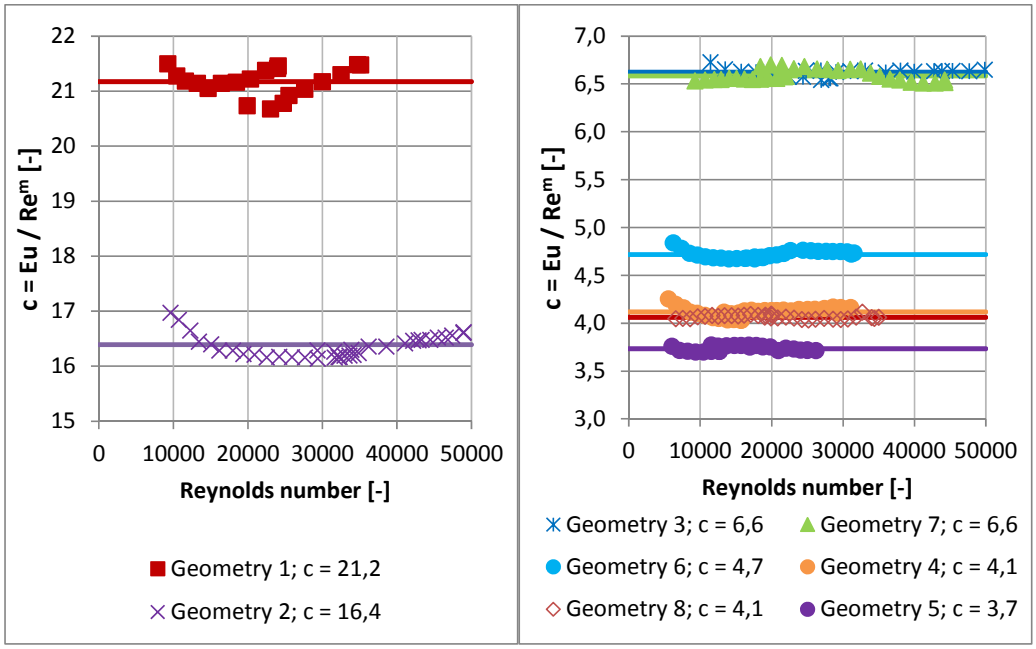

Figure 5-6: Coefficient c from Eq. 5-2 for the different geometries

Figure 5-7 shows a comparison of the measured Reynolds number exponent to published exponents from heat transfer and pressure drop correlations. It can be seen that for the measured heat transfer data the average serrated-fin Reynolds number exponent of 0.60 is in the range of the published exponents, between 0.59 and 0.88. This is also the case for the average solid-fin Reynolds number exponent of 0.76, which is in the range of the published exponents, between 0.60 and 0.80. For the pressure drop, the measured average Reynolds number exponents are slightly lower than those published, -0.16 vs. a range from -0.18 to -0.32 for serrated-fin tubes and -0.20 vs a range from -0.23 to -0.30 for solid-fin tubes.

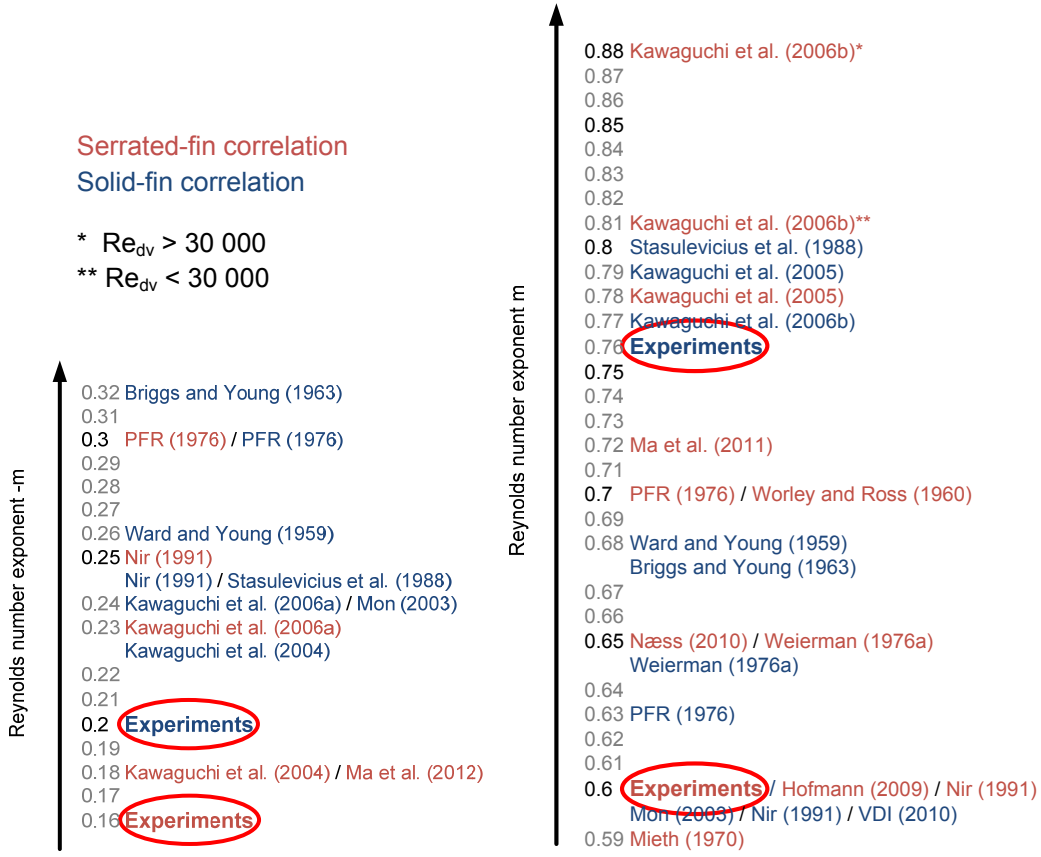

Figure 5-7: Comparison of the Reynolds number exponent –m for pressure drop correlations (left) and m for heat transfer correlations (right)

5.3 Influence of different parameters on the heat transfer and pressure drop performance

Two different methods are used to present the experimental results with respect to the influence of different parameters on heat transfer and pressure drop. First is a comparison of the results of two measured geometries, while varying only one parameter. A second comparison is then provided of this study's experimental data with experimental data from the literature. An elasticity factor E is introduced in order to visualise the manner in which a parameter influences the heat transfer coefficient, the Nusselt number and the Euler number.

The elasticity E is evaluated using Eq. 5-3. The resulting relative change in the heat transfer coefficient or Euler number is divided by the relative change in the varying parameter:

$$E = \frac{\Delta Y / Y}{\Delta x / x} \qquad \textit{Eq. 5-3}$$

where

- Y is either the heat transfer coefficient h_{air}, the dimensionless heat transfer coefficient $Nu \cdot Pr^{-1/3}$ or the Euler number Eu.
- x is the varied parameter (tube diameter d_o, fin height h_f, fin pitch s_f or fin-tip clearance c_f)

E can take values above, below and equal to 0.

- E > 0: an increase in the varied parameter increases the heat transfer coefficient or Euler number
- E = 0: an increase in the varied parameter has no effect on the heat transfer coefficient or Euler number
- E < 0: an increase in the varied parameter decreases the heat transfer coefficient or Euler number

5.3.1 Influence of fin type

A comparison between Geometries 1 and 2, while varying only the fin type was carried out by comparing the apparent heat transfer coefficients h_{app} (Eq. 5-4). As discussed in chapter 4.2, the correction of the fin efficiency for a solid-fin tube is quite high (12 to 33%) compared to the correction for serrated-fin tubes (3 to 7%). Therefore, only the theoretical fin efficiency was used in the data reduction for solid-fin tubes. To compare both fin types on an equal basis, the apparent heat transfer coefficient is chosen, where the fin efficiency is of no importance.

$$h_{app} = h_{air} \cdot \frac{A_{0,t} + \eta_f \cdot A_{0,f}}{A_{0,t} + A_{0,f}} \qquad \textit{Eq. 5-4}$$

The comparison shows that the apparent heat transfer coefficient h_{app} is higher for serrated-fin tubes than for solid-fin tubes (Figure 5-8 left). This is attributed to the frequent boundary layer break-up due to the serration of the fins and the introduced turbulence. The advantage of serrated-fin tubes is observed to be higher for low flow rates than for high flow rates, in that the apparent heat transfer coefficients are higher by 30% at low flow rates and by only 18% at high flow rates. This is also the case for the product of ($h_{app} \cdot A_{ht}$). The overall heat transfer surface area of the tested tubes vary only by 3% ($A_{ht,sol}$ = 25.68 m^2 compared to $A_{ht,ser}$ = 26.49 m^2). The cut out surface of the serrated-fin is compensated by all four side of the segment distributing to the heat transfer surface.

The measured Euler numbers (Figure 5-8 right) for serrated-fin tubes is essentially the same as for solid-fin tubes, within ± 2%.

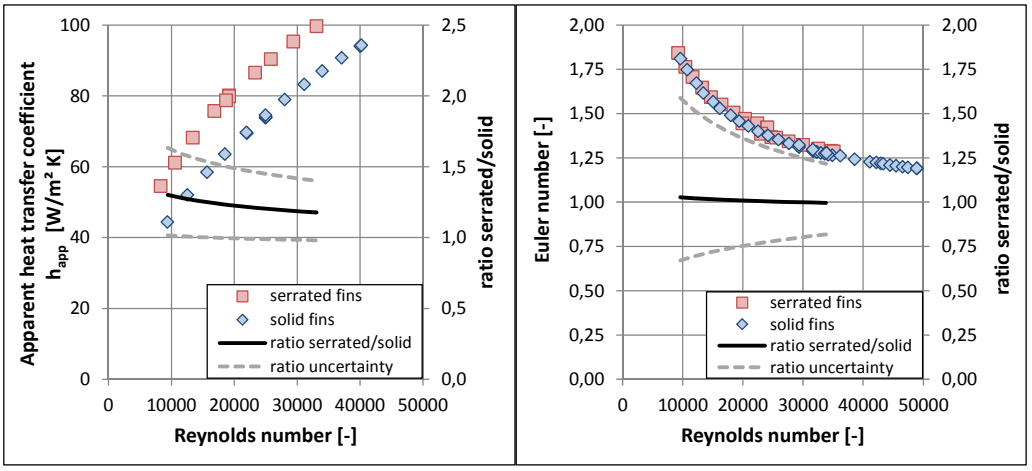

Figure 5-8: Experimental results for heat transfer (left) and pressure drop (right) for serrated (Geometry 1) and solid-fin tubes (Geometry 2)

Among the other influences of serrated fins, the associated turbulence due to the boundary layer break up improve the heat transfer. Due to the additional turbulence a high mixing of the flow is introduced and the heat transfer is reliably improved in serrated-fin tube bundles compared to solid-fin tubes. Higher Nusselt numbers for serrated-fin tubes than for solid-fin tubes were also reported by Hofmann (2009) and Kawaguchi et al. (2005). Figure 5-9 (left) shows the ratio of the apparent heat transfer coefficient of serrated over solid-fin tubes. Table 5-5 shows the parameters of the geometries used. It can be seen that Kawaguchi et al. (2005) measured a lower flow rate dependent advantage of serrated-fin tubes than is found for this work. However, their measurements showed an influence of the number of fins. For a high number of fins (SR/SP300) there is less advantage than for a smaller number of fins (SR/SP200). In addition, Kawaguchi et al. (2006b) measured two serrated-fin tubes with different degrees of serration h_s/h_f, 0.27 and 0.49. (The degree of serration is the ratio of the segment height h_s to the fin height h_f and can vary from 0 for solid fins, to 1 for serrated L-foot fins.) The dashed line in Figure 5-9 on the left shows that an increasing degree of serration, ranging from a mainly solid-fin to a more serrated-fin, increases the heat transfer coefficient as well.

For the pressure drop Hofmann (2009) reported higher pressure drops for serrated-fin tubes as compared to solid-fin tubes. However, the results of Kawaguchi et al. (2004) were again dependent on the number of fins (Figure 5-9, right). For a smaller number of fins (SR/SP200) their results are in accordance with those of Hofmann and Weierman. For a higher number of fins (SR/SP300), the opposite was the case. The experimental results of Geometries 1 and 2 fall between the measurements of Kawaguchi et al. This is also the case for the number of fins, which are 276 fins per meter tube for Geometries 1 and 2 as compared with 200 fins per meter tube for SR/SP200 and 300 fins per meter tube for SR/SP300. Kawaguchi et al. (2006a) also reported pressure drop measurements for serrated-fin tubes with different degrees of serration. Those tubes had 200 fins per meter tube. The authors reported that for an increasing degree of serration, the pressure drop decreases. He argues that according to his velocity measurements the friction on the surface of the less segmented fins is higher due to a larger heat transfer surface.

Table 5-5: Overview of the geometries to compare the influence of fin type on the heat transfer coefficient and Euler number

Author	Geo.	Fin type (degree of serration) h_s/h_f [%]	Tube diameter d_o [mm]	Fin height h_f [mm]	Fin pitch s_f [mm]	Fin-tip clearance c_f [mm]
Measurement	1	Serrated (61%)	31.75	18.00	3.70	2.00
	2	Solid (0%)	31.75	18.00	3.70	2.00
Kawaguchi et al. (2004, 2005)	SP 200	Solid (0%)	17.3	9.0	5.0	4.7
	SP 300	Solid (0%)	17.3	9.0	3.3	4.7
	SR 200	Serrated*	17.3	9.0	5.0	4.7
	SR 300	Serrated*	17.3	9.0	3.3	4.7
Kawaguchi et al. (2006a, 2006b)	SR 211 HK	Serrated (49%)	25.3	9.0	5.0	15.2
	SR 211 LK	Serrated (27%)	25.3	9.0	5.0	15.2

* Kawaguchi did not state the segment height h_s

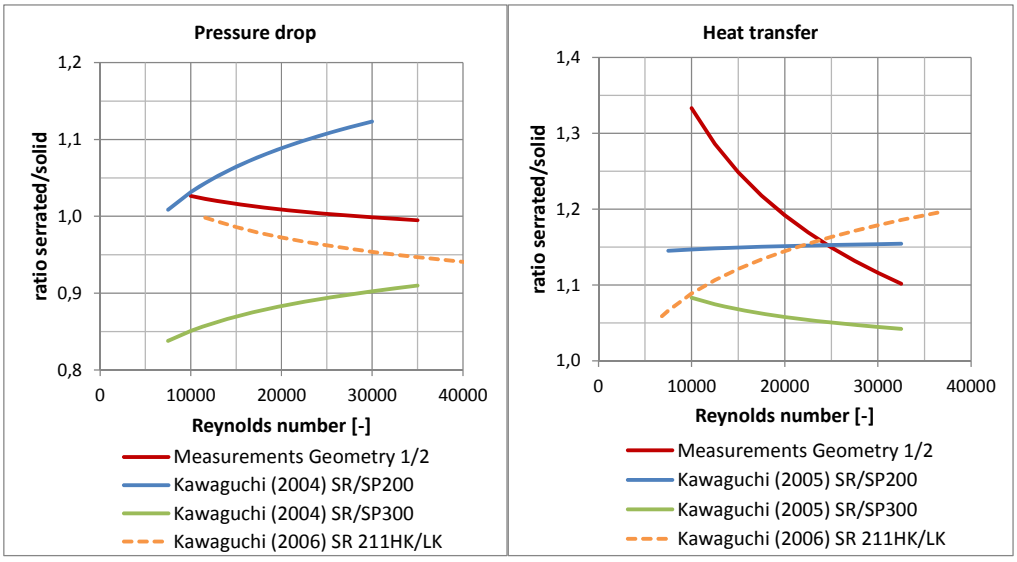

Figure 5-9: Performance of serrated and solid-fin tubes in comparison, left: heat transfer coefficient; right: Euler number

5.3.2 Influence of tube diameter

Typically, dimensionless numbers are used in comparisons of different geometries. In the case of finned tubes these numbers usually contain the tube diameter as the specific length scale. Instead of the Nusselt number (Eq. 5-5) and the Reynolds number (Eq. 5-7), in the comparison of Geometries 1 and 4 in which the tube diameter varies, the heat transfer coefficient (Eq. 5-6) and the velocity in the minimum flow area (Eq. 5-8) are used. This is done in order to establish the same basis for a comparison of the two geometries.

$$\frac{Nu}{Pr^{1/3}} = \frac{h_{air} \cdot d_o}{k_{air} \cdot Pr_{air}^{1/3}} \qquad \textit{Eq. 5-5}$$

$$h_{air} = \frac{Nu}{Pr^{1/3}} \cdot \frac{k_{air} \cdot Pr_{air}^{1/3}}{d_o} \qquad \textit{Eq. 5-6}$$

$$Re = \frac{\rho_{air} \cdot u_{max} \cdot d_o}{\mu_{air}} \qquad \textit{Eq. 5-7}$$

$$u_{max} = \frac{Re \cdot \mu_{air}}{\rho_{air} \cdot d_o} \qquad \textit{Eq. 5-8}$$

On the other hand, the fin-tip clearances of both geometries differed due to the experimental set up. The fin-tip clearance was 2mm for the large diameter tubes (d_o = 31.75mm) and 5mm for the small diameter tubes (d_o = 19.05mm) This resulted in a larger minimum free-flow area (Eq. 5-9) for the small diameter tubes (0.72 m^2 vs 0.63 m^2) and therefore a lower flow velocity and lower percentage of flow passing between the fins. The measured results were compared with respect to the velocity in the minimum free-flow area $A_{f,min}$:

$$A_{f,min} = l_t \cdot N_t \cdot \left(P_t - d_o - 2 \cdot N_f \cdot h_f \cdot t_f\right) = l_t \cdot N_t \cdot \left(c_f + 2 \cdot N_f \cdot h_f \cdot \left(s_f - t_f\right)\right) \qquad \textit{Eq. 5-9}$$

Figure 5-10 shows a comparison of the heat transfer and pressure drop performance of the two serrated-fin tube bundles (Geometries 1 and 4). The left plot of Figure 5-10 shows that the heat transfer coefficient was slightly higher for the tubes with the larger diameter (Geometry 1) as compared those with the smaller diameter (Geometry 4). The heat transfer coefficient of the larger tubes was 4 to 7% higher with respect to the velocity in the minimum free-flow area. This finding, however, was within the uncertainty range of the compared results, which is shown by the dotted grey lines.

The measured Euler number (Figure 5-10 right) was lower for the larger diameter tubes by 4 to 16%.

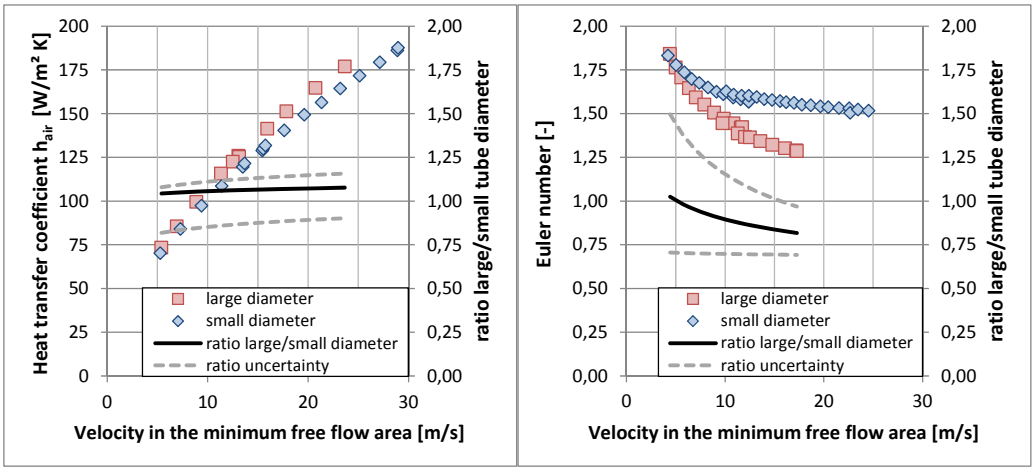

Figure 5-10: Experimental results for different tube diameters, 31.75mm (Geometry 1) and 19.05mm (Geometry 4); left: heat transfer coefficient; right: pressure drop

To compare the measurement results of this study with those in the literature, the heat transfer coefficient and the velocity in the minimum free-flow area $A_{f,min}$ were calculated using air as the fluid at 100°C. According to Kays et al. (2005) the thermal conductivity is $k_{air} = 3.126 \cdot 10^{-2}$W/m·K, the dynamic viscosity $\mu_{air} = 2.177 \cdot 10^{-5}$kg/m·s, the density is $\rho_{air} = 0.9463$kg/m^3 and the Prandtl number $Pr_{air} = 0.703$.

Figure 5-11 shows the change in the heat transfer coefficient per unit change in the tube diameter. Table 5-6 shows the geometry parameters used in the comparison. The elasticity E was calculated using Eq. 5-10. Næss (2010) reported opposite results to those of Geometries 1 and 4. From his measurements, it can be concluded that a 1% increase in tube diameter results in an approximately 0.15% decrease in the heat transfer coefficient. For solid-fin tubes, Briggs and Young (1963) measured a slight decrease in the heat transfer coefficient with increasing tube diameter.

$$E = \frac{\Delta h_{air} / h_{air,d_{o,small}}}{\Delta d_o / d_{o,small}} \quad \text{respectively} \quad E = \frac{\Delta Eu / Eu_{d_{o,small}}}{\Delta d_o / d_{o,small}} \qquad \textit{Eq. 5-10}$$

Table 5-6: Overview of the geometries used to compare the influence of tube diameter on the heat transfer coefficient and Euler number

Author	Geo.	Fin type (degree of serration) h_s/h_f [%]	Tube diameter d_o [mm]	Fin height h_f [mm]	Fin pitch s_f [mm]	Fin-tip clearance c_f [mm]
Measurement	1	Serrated (61%)	31.75	18.00	3.61	2.00
	4	Serrated (61%)	19.05	18.00	3.73	5.00
Briggs and Young (1963)	13	Solid (0%)	29.1	14.68	3.18	3.84
	16	Solid (0%)	40.9	14.48	3.22	1.68
Næss (2010)	1	Serrated (100%)	20.89	8.61	5.08	7.99
	5	Serrated (100%)	27.24	8.61	5.08	8.04
	8	Serrated (100%)	33.59	8.61	5.08	7.99
Worley and Ross (1960)	4	Studs (100%)	50.8	19.05	6.35	15.88
	11	Studs (100%)	38.1	19.05	6.35	3.18

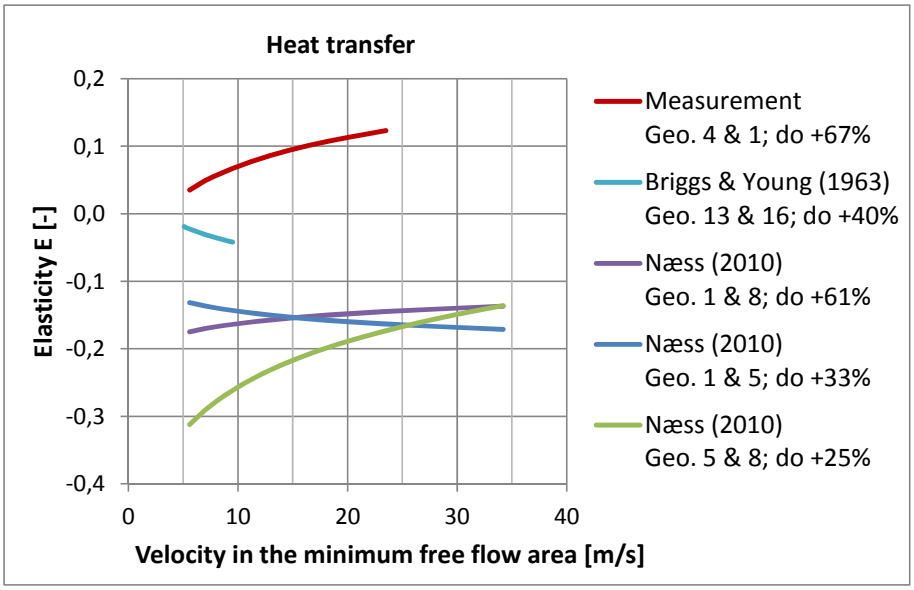

Figure 5-11: Elasticity of heat transfer coefficient vs. tube diameter (Eq. 5-10)

Overall it can be concluded that a change in tube diameter has only a small effect on the heat transfer coefficient.

Figure 5-12 shows the change in the Euler number per unit change in tube diameter for the measurements of Geometries 1 and 4 and the measurements of Næss (2010) and Worley and Ross (1960). It can be seen that the measurement results of Geometries 1 and 4 fall between those of the other two studies. Næss (2010) showed that for an increasing tube diameter the Euler number increased. Worley and Ross reported the opposite, as is also the case in this study. However, the influence measured in this study was four times less sensitive than that reported by Worley and Ross (1960).

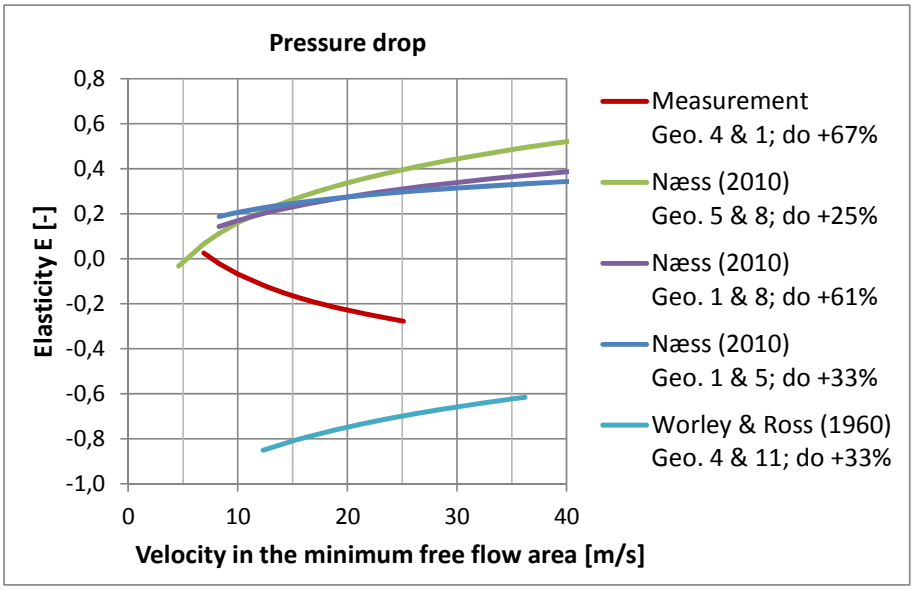

Figure 5-12: Elasticity of Euler number vs. tube diameter (Eq. 5-10)

5.3.3 Influence of fin height

A comparison of Geometries 4 and 7, while varying only the fin height, showed that both the heat transfer coefficient and the pressure drop coefficient were higher for higher fins, as shown in Figure 5-13. For higher finned tubes, the heat transfer coefficient increased by 15 to 25% and the Euler number increased by 41 to 57%, as compared with lower finned tubes. The increase in the pressure drop can be explained by the increase in the friction surface. The heat transfer surface is 1.9 times as large in a high-fin tube as in a low-fin tube.

As the fin-tip clearance was the same in both tube bundles, the ratio of the flow-area-between-the-fins-to-the-minimum-free-flow-area $A_{f,fin}/A_{f,min}$ varied from 0.84 for high-fin tubes to 0.73 for low-fin tubes. More air flowed between the fins of the high-fin tubes to take part in the heat transfer (increased heat transfer coefficient), and the air was exposed to a larger surface area, thus causing higher skin friction (increased pressure drop).

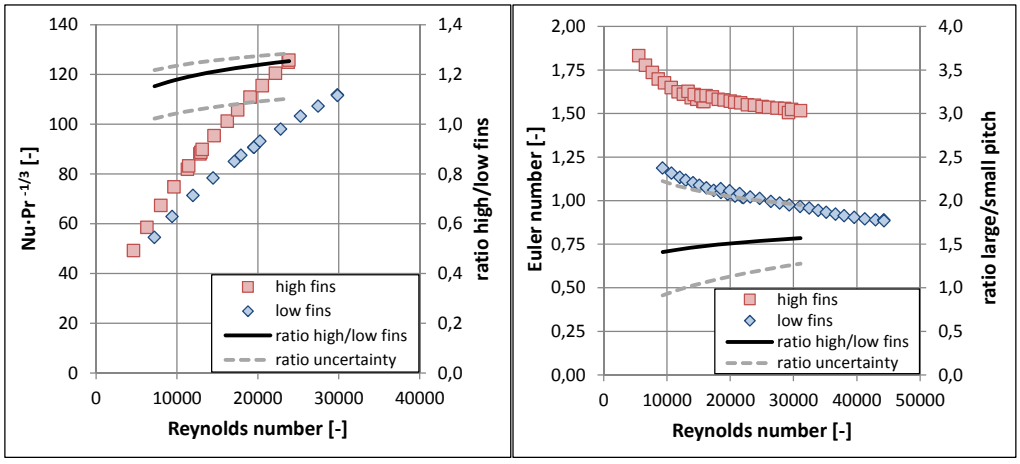

Figure 5-13: Experimental results for different fin heights, 18mm (Geometry 4) and 10mm (Geometry 7); left: heat transfer coefficient; right: Euler number

The comparison of the study measurement results with those reported in the literature was made using elasticity E, calculated with Eq. 5-11. Table 5-7 shows the geometric parameters used in the comparison.

$$E = \frac{\Delta Nu / Nu_{h_{f,low}}}{\Delta h_f / h_{f,low}} \quad \text{respectively} \quad E = \frac{\Delta Eu / Eu_{h_{f,low}}}{\Delta h_f / h_{f,low}} \qquad \textit{Eq. 5-11}$$

The comparison shows that Kawaguchi et al. (2006b) and Næss (2010) reported similar findings for serrated-fin tubes, as shown in Figure 5-14. However, Kawaguchi et al. (2006b) found the opposite behaviour for solid-fin tubes. The authors argue that for solid-fin tubes, higher fins act like a channel to straighten the flow. For serrated-fin tubes, Kawaguchi et al. measured a higher velocity between the segments of the high-fin tubes, which were claimed to cause the increased heat transfer.

Figure 5-15 shows the results of the measured Euler numbers compared to the data reported in the literature. The measurement results are in good agreement with the findings of Kawaguchi et al. (2006a) for serrated-fin tubes.

The reported results of Næss (2010) and for solid-fin tubes from Kawaguchi et al. (2006a) show the same trends but are less distinct.

Table 5-7: Overview of the geometries used to compare the influence of fin height on the Nusselt number and Euler number

Author	Geo.	Fin type (degree of serration) h_s/h_f [%]	Tube diameter d_o [mm]	Fin height h_f [mm]	Fin pitch s_f [mm]	Fin-tip clearance c_f [mm]
Measurement	4	Serrated (61%)	19.05	18.00	3.73	5.00
	7	Serrated (50%)	19.05	11.00	3.61	5.00
Kawaguchi et.al (2006a, 2006b)	SP 200	Solid (0%)	17.3	9.0	5.0	4.7
	SP 201	Solid (0%)	17.3	6.3	5.0	10.1
	SR 210	Serrated (48%)	25.3	13.0	5.0	7.2
	SR 211	Serrated (49%)	25.3	9.0	5.0	15.2
Næss (2010)	9	Serrated (100%)	27.24	11.38	3.36	29.8
	10	Serrated (100%)	27.24	8.61	3.36	35.3

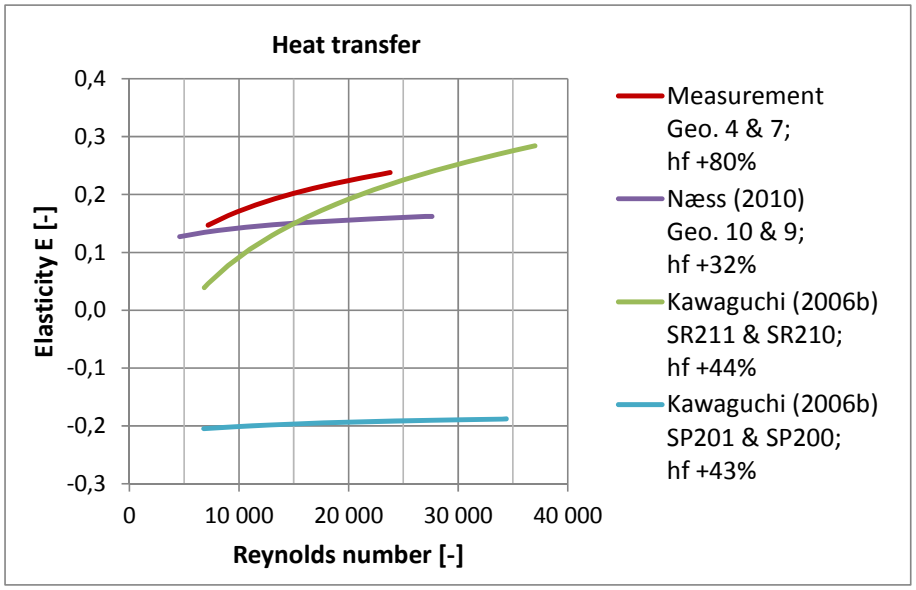

Figure 5-14: Elasticity of Nusselt number vs. fin height (Eq. 5-11)

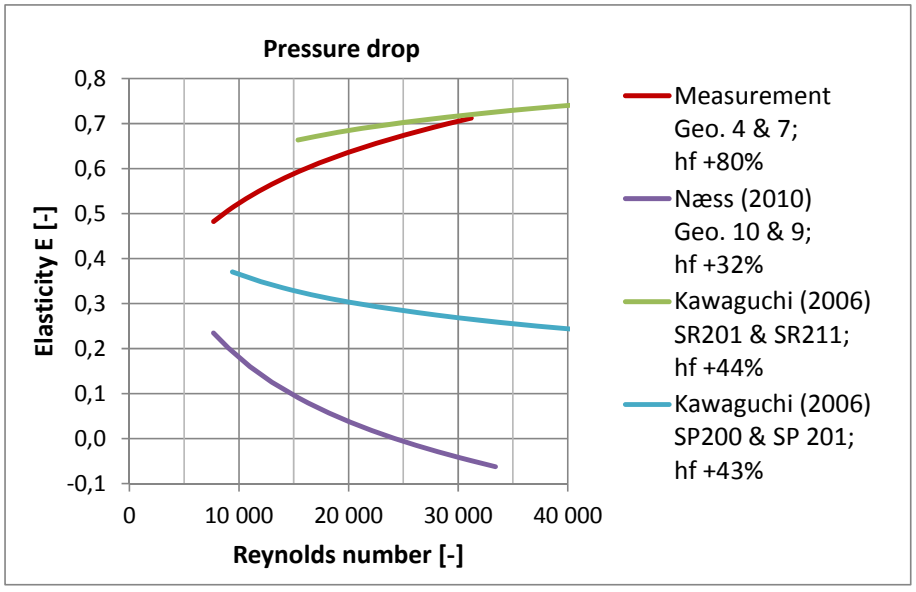

Figure 5-15: Elasticity of Euler number vs. fin height (Eq. 5-11)

5.3.4 Influence of fin pitch

Geometries 2 and 3 were used to compare the influence of the fin pitch on the heat transfer and pressure drop of finned tubes. Figure 5-16 shows the experimental results for heat transfer and pressure drop with respect to the velocity in the minimum free-flow area. It can be seen in the left plot that the heat transfer coefficient is the same as that for the large fin pitch (Geometry 3) and the Nusselt number is only 1 to 4% higher than for the small fin pitch (Geometry 2). Due to the different fin pitches, the minimum free-flow area is smaller for the small fin pitch (Geometry 2) than for the large fin pitch (Geometry 3). Therefore, the velocity in the minimum free-flow area is bigger for the same mass flow rate. This means that, in addition to the larger fin surface, for the same mass flow rate, a small-fin pitch geometry transfers more heat due to the higher velocity in the minimum free-flow area, resulting in higher heat transfer coefficients. In the case of the tested Geometries 2 and 3, the heat transfer surface is 54% larger in the small-fin pitch of Geometry 2 and the minimum free-flow area is 11% smaller than in the large-fin pitch of Geometry 3.

The Euler number decreases with increasing fin pitch. The measurement results show a decrease of 8 to 18% as compared to small fin pitch tubes. This Euler number decrease is related to the decreased surface area with an increased fin pitch, resulting in a lower pressure drop due to less skin friction.

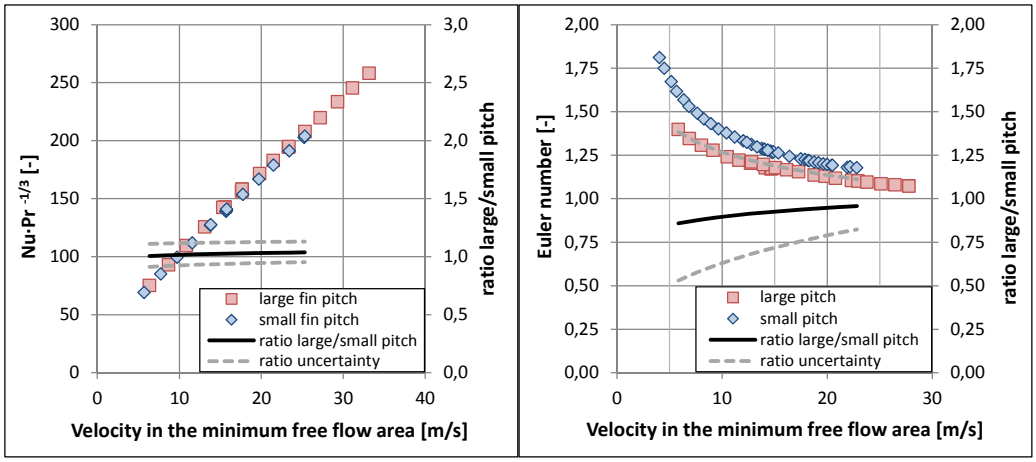

Figure 5-16: Experimental results for fin pitches, 5.6mm (Geometry 3) and 3.7mm (Geometry 2); left: heat transfer coefficient; right: pressure drop

Table 5-8 lists the geometries used to compare the influence of the fin pitch. A comparison with the literature data results was made using Eq. 5-12 and shows that regarding the heat transfer (Figure 5-17) both Ma et al. (2012) and Næss (2010) reported an increasing heat transfer coefficient for an increasing fin pitch. Kawaguchi et al. (2006b) reported the opposite for both serrated and solid-fin tubes. Note that the measurements of Ma et al. (2012) showed an extremely large impact of the velocity on the performance of the tubes.

Regarding the pressure drop, as shown in Figure 5-18, all authors agree that increasing the fin pitch decreases the Euler number. Kawaguchi et al. (2006a) again reported a higher influence of the fin pitch on solid-fin tubes than on serrated-fin tubes.

$$E = \frac{\Delta Nu / Nu_{s_{f,small}}}{\Delta s_f / s_{f,small}} \quad \text{respectively} \quad E = \frac{\Delta Eu / Eu_{s_{f,small}}}{\Delta s_f / s_{f,small}} \qquad \textit{Eq. 5-12}$$

Table 5-8: Overview of the geometries used to compare the influence of fin pitch on the Nusselt number and Euler number

Author	Geo.	Fin type (degree of serration) h_s/h_f [%]	Tube diameter d_o [mm]	Fin height h_f [mm]	Fin pitch s_f [mm]	Fin-tip clearance c_f [mm]
Measurement	2	Solid (0%)	31.75	18.00	3.70	2.00
	3	Solid (0%)	31.75	18.00	5.89	2.00
Kawaguchi et al. (2004, 2005)	SP 200	Solid (0%)	17.3	9.0	5.0	4.7
	SP 300	Solid (0%)	17.3	9.0	3.3	4.7
	SR 200	Serrated*	17.3	9.0	5.0	4.7
	SR 300	Serrated*	17.3	9.0	3.3	4.7
Ma et al. (2012)	1	Serrated (63%)	38.1	16	3.89	17.9
	4	Serrated (63%)	38.1	16	4.15	17.9
Næss (2010)	9	Serrated (100%)	27.24	11.38	3.36	29.8
	10	Serrated (100%)	27.24	8.61	3.36	35.3

* Kawaguchi does not state the segment height h_s

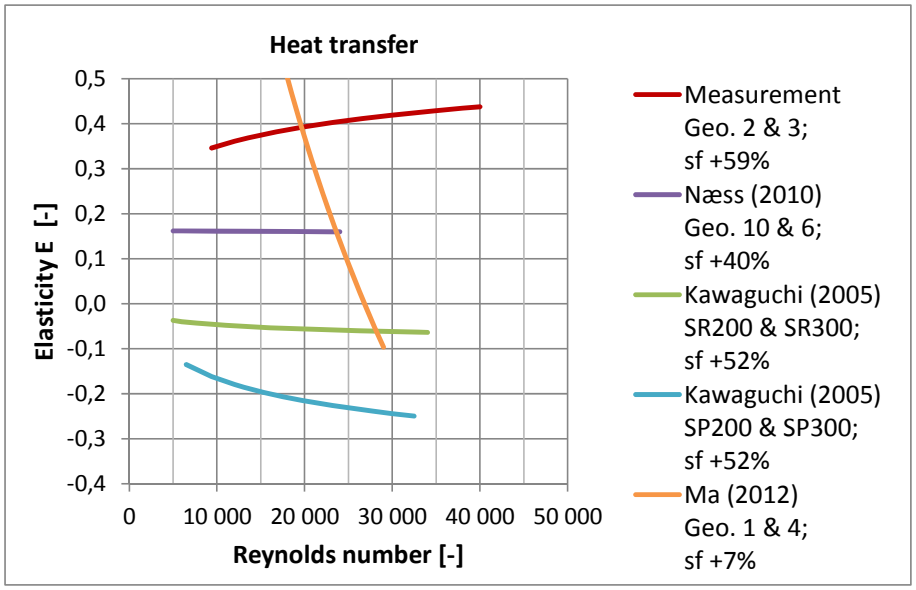

Figure 5-17: Elasticity of Nusselt number vs. fin pitch (Eq. 5-12)

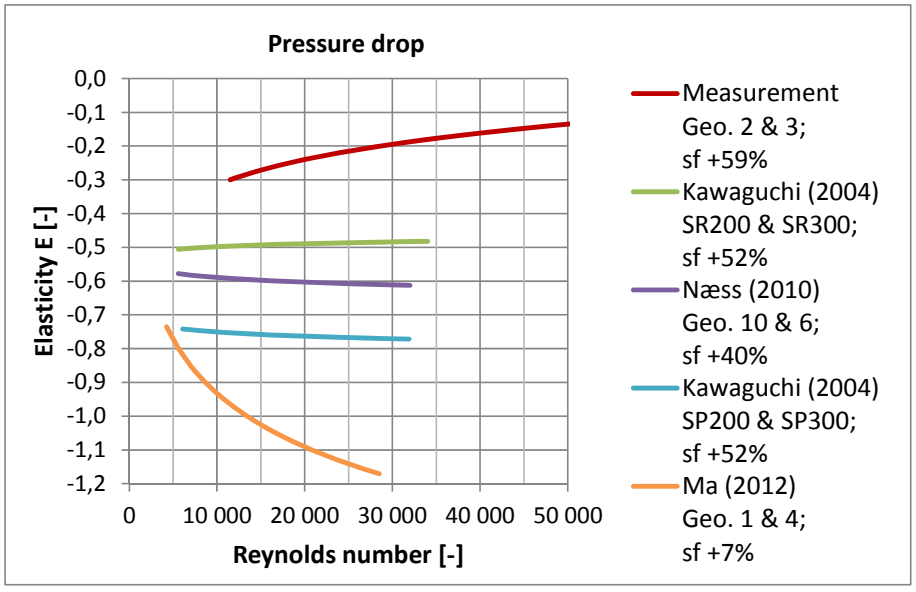

Figure 5-18: Elasticity of Euler number vs. fin pitch (Eq. 5-12)

5.3.5 Influence of fin-tip clearance

The influence of the fin tip clearance c_f on the heat transfer and pressure drop was evaluated with Geometries 4 to 6. Geometries 4 and 5 had a fin-tip clearance of 5mm and 10mm, respectively. Geometry 6 had a fin-tip clearance of 0mm, which resulted in the fin tips touching.

Figure 5-19 shows the experimental heat transfer results. Increasing the fin-tip clearance from 5mm to 10mm had only a small negative effect on the Nusselt number (decrease of 0 to 10%). As the ratio of the flow-area-between-the-fins-to-the-minimum-free-flow-area ($A_{f,fin}/A_{f,min}$) was decreased for a larger fin-tip clearance, more air bypassed the fins and the velocity between the fins decreased. In the case of the zero fin-tip gap, the Nusselt number was reduced by 8 to 18% compared to the 5mm fin gap (Figure 5-19, bottom left). For a 0mm fin-tip clearance, the fins act like a channel and the flow between the fins is likely to be laminar. The bypass flow in the fin gap, which is responsible for the mixing, stops for a zero fin gap. Even though the velocities are higher between the fins due to the reduced flow area, the reduced mixing results in a reduced heat transfer.

The right-hand diagrams in Figure 5-19 show the Euler numbers for the three geometries. The highest Euler number was measured for the 5mm fin gap, followed by the geometries with touching fins (-12 to 8%), and the lowest Euler number was measured for Geometry 5 with the largest fin gap (-15 to 16%). As described above, a decrease in the fin-tip clearance leads to a smaller bypass flow area and higher velocities between the fins. When the fins are touching, the mixing of the bypass flow disappears and therefore due to there being less turbulence, the pressure drop is reduced.

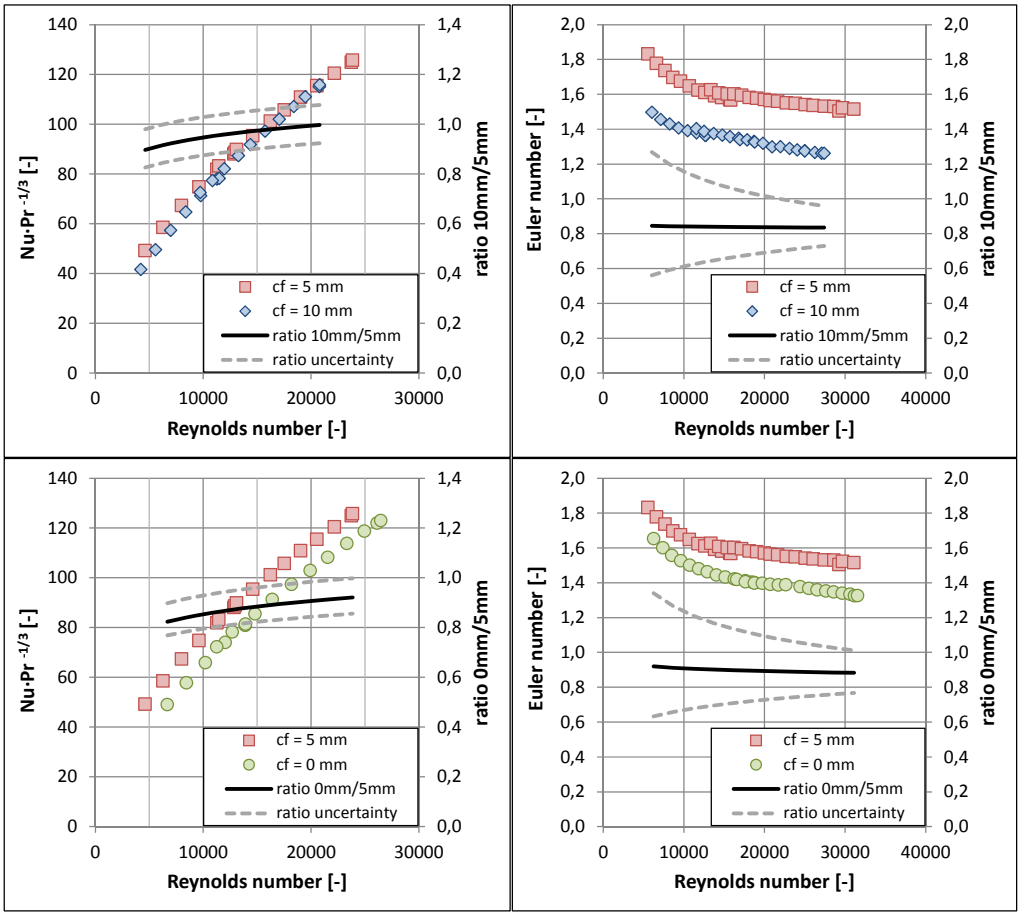

Figure 5-19: Experimental heat transfer and pressure drop results for different fin-tip clearances, 10mm (Geometry 5), 5mm (Geometry 4) and 0mm (Geometry 6); left: heat transfer, right: pressure drop

The actual pressure drop per tube row can be seen in the diagrams in Figure 5-20. The smaller the fin-tip clearance, the larger the measured pressure drop per tube row for the same mass flow rate, mainly due to the different velocities between the tubes. A comparison of the pressure drops for the same velocity in the minimum free-flow area (Figure 5-20, on the right) shows that the 5mm fin-tip clearance geometry yields the highest pressure drop per tube row. The pressure drop for the 10mm fin-tip clearance configuration is reduced due to a wider fin tip gap causing reduced skin friction. The pressure drop for the geometry with touching fins is reduced due to the channel flow established, resulting in less turbulence.

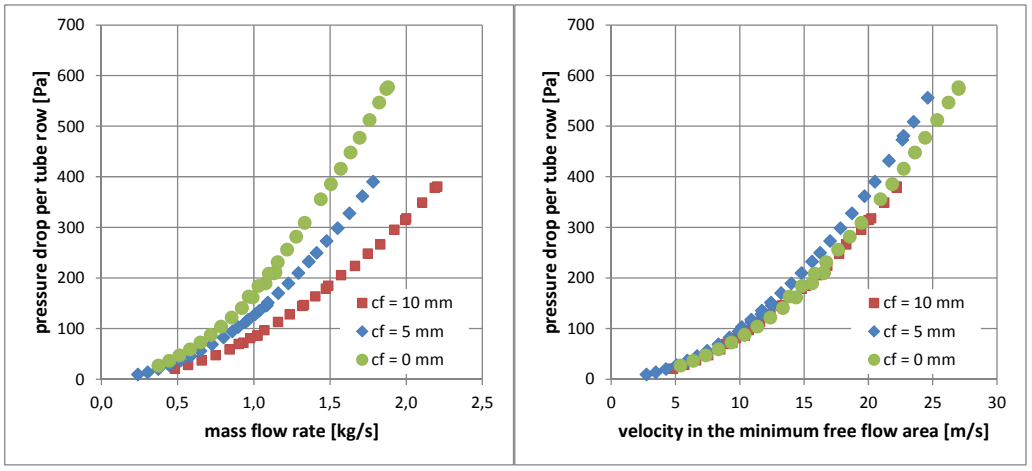

Figure 5-20: Experimental pressure drop per tube row for different fin-tip clearances, 10mm (Geometry 5), 5 mm (Geometry 4) and 0mm (Geometry 6); left: per mass flow rate; right: per velocity in the minimum free-flow area

Figure 5-21 shows the influence of the fin-tip clearance on the Nusselt number as calculated using Eq. 5-13, and Table 5-9 provides an overview of the compared geometries. The measurements reported by Ackerman and Brunsvold (1970) and Ward and Young (1959) show a negligible influence of the fin-tip clearance on the heat transfer. Both have a rather high increase in the fin-tip clearance of 800% (from 3.2mm to 28.6mm) and 1772% (from 4.7mm to 88.4mm). Ma et al. (2012) reported a positive influence on the heat transfer from an increased fin-tip clearance.

$$E = \frac{\Delta Nu / Nu_{c_f=5mm}}{\Delta c_f / c_f = 5mm} \quad \text{respectively} \quad E = \frac{\Delta Eu / Eu_{c_f=5mm}}{\Delta c_f / c_f = 5mm} \qquad \textit{Eq. 5-13}$$

Figure 5-22 shows various measurement results with respect to the influence of the fin-tip clearance on the Euler number. All measurement results show that an increase in the fin-tip clearance reduces the Euler number. Ackerman and Brunsvold (1970) show a rather negligible effect. The arrangement angles of the measurements were 26.6° for Briggs and Young (1963) and Robinson and Briggs (1966) and 30° for Ackerman and Brunsvold (1970), Ma et al. (2012) and this study, all having the minimum flow area in the transversal plane. The

influence of a 100% increase in the fin-tip clearance (as in this study) was determined to be the same for the same increase by Briggs and Young (1963), Geometries 34 and 35, and by Robinson and Briggs (1966), Geometries 24 and 25.

Table 5-9: Overview of the geometries used to compare the influence of fin pitch on the Nusselt number and Euler number

Author	Geo.	Fin type (degree of serration) h_s/h_f [%]	Tube diameter d_o [mm]	Fin height h_f [mm]	Fin pitch s_f [mm]	Fin-tip clearance c_f [mm]
Measurement	4	Serrated (61%)	19.05	18.00	3.73	5.00
	5	Serrated (61%)	19.05	18.00	3.73	10.00
Ackerman and Brunsvold (1970)	3	Pins (100%)	47.6	25.4	6.35	28.6
	6	Pins (100%)	47.6	25.4	6.35	3.2
Briggs and Young (1963)	22	Solid (0%)	18.6	10.5	2.32	9.4
	23	Solid (0%)	18.6	10.5	2.32	3.2
	24	Solid (0%)	18.6	10.5	2.32	22.6
	25	Solid (0%)	18.6	10.5	2.32	45.7
Ma et al. (2012)	7	Serrated (63%)	38.1	16	4.15	33.9
	11	Serrated (63%)	38.1	16	4.15	49.9
Robinson and Briggs (1966)	33	Solid (0%)	26.6	12.3	2.75	1.55
	34	Solid (0%)	26.6	12.3	2.75	34.57
	35	Solid (0%)	26.6	12.3	2.75	17.42
	36	Solid (0%)	26.6	12.3	2.75	5.46
Ward and Young (1959)	4	Solid (0%)	14.07	4.3	2.27	4.72
	9	Solid (0%)	13.49	4.5	2.35	88.44

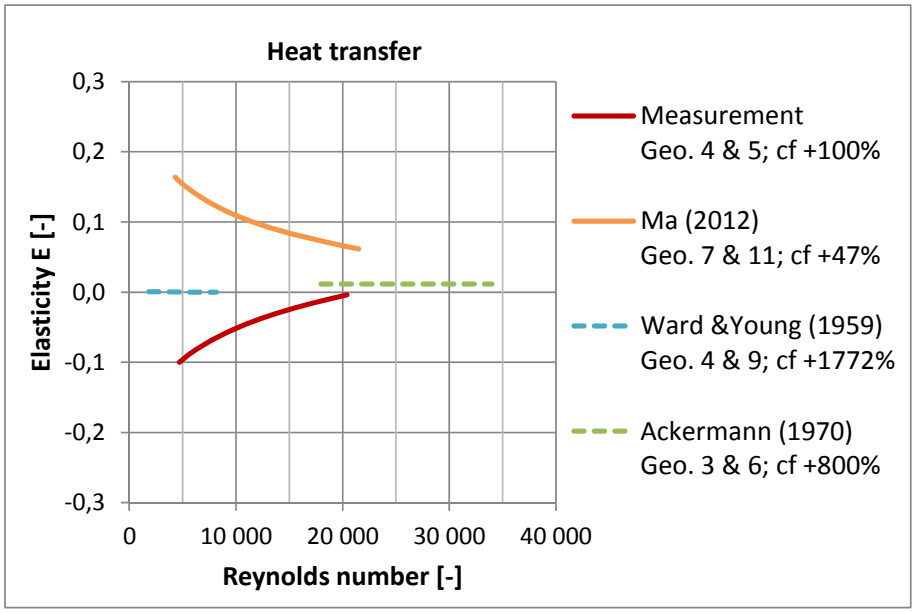

Figure 5-21: Elasticity of Nusselt number vs. vs. fin-tip clearance (Eq. 5-13)

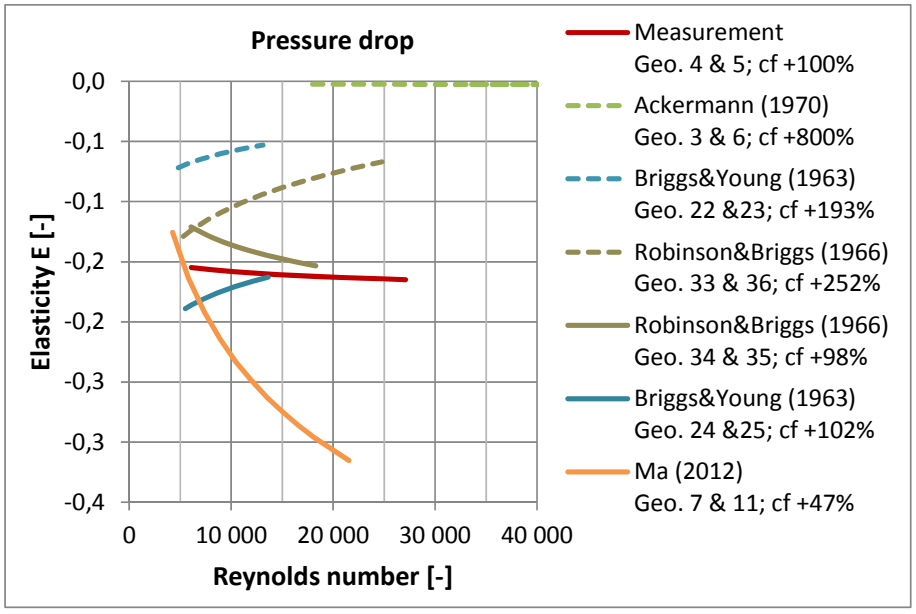

Figure 5-22: Elasticity of Euler number vs. fin-tip clearance (Eq. 5-13)

5.3.6 Summary

Sections 5.3.1 to 5.3.5 showed the influence of different parameters on the heat transfer and pressure drop behaviour of finned tube bundles. Table 5-10 shows an overview of the findings of the heat transfer measurements of this study and those in the literature, and Table 5-11 shows the same for pressure drop. The observation results of this study are indicated by the green highlighted cells.

From the tables, it can be seen that the present study showed that:

1. A compact arrangement, corresponding to decreased tube pitches P_t and P_l, has no influence on the heat transfer coefficient but increases the pressure drop.
2. An increased surface area, by increasing the tube diameter d_o and the fin height h_f and decreasing the fin pitch s_f, increases the transferred heat not only through the increased heat transfer surface area but also through an increased heat transfer coefficient. However, the pressure drop is increased as well.
3. Further enhancing the heat transfer by means of serrated fins increases the heat transfer coefficient, but has no influence on the pressure drop.

Table 5-10: Overview of the findings on the influence of different geometric parameters on the heat transfer coefficient, the green cells highlight the findings of this study

Parameter	**Heat transfer coefficient increased**	**Heat transfer coefficient decreased**	**No effect**
P_t decreased		Worley and Ross (1960); Ackerman and Brunsvold (1970)	Kawaguchi et al. (2005) ; Ma et al. (2012)
P_l decreased		Ma et al. (2012)	Worley and Ross (1960); Ackerman and Brunsvold (1970); Kawaguchi et al. (2005)
Serrated fins vs. solid fins	Weierman (1977); Kawaguchi et al. (2005); Hofmann (2009)		
d_o increased			Worley and Ross (1960)
h_f increased	Stasiulevičius et al. (1988); Kawaguchi et al. (2006b) *for serrated fins;* Næss (2010)	Kawaguchi et al. (2006b) *for solid fins*	Worley and Ross (1960)
s_f decreased	Kawaguchi et al. (2005; Næss (2010)	Žukauskas et al. (1966); Ma et al. (2012)	Worley and Ross (1960)

Table 5-11: Overview of the findings on the influence of different geometric parameters on the pressure drop, the green cells highlight the findings of this study

Parameter	**Pressure drop larger**	**Pressure drop smaller**	**No effect**
P_t decreased	Ma et al. (2012)		Kawaguchi et al. (2004); Næss (2010)
P_l decreased	Robinson and Briggs (1966); Ma et al. (2012)		Kawaguchi et al. (2004); Næss (2010)
Serrated fins vs. solid fins	Weierman (1977); Kawaguchi et al. (2005) *for a high fin pitch;* Hofmann (2009)	Kawaguchi et al. (2005) *for a low fin pitch*	
d_o increased			Worley and Ross (1960)
h_f increased	Kawaguchi et al. (2006a) Næss (2010)	Stasiulevičius et al. (1988)	Worley and Ross (1960)
s_f decreased	Worley and Ross (1960); Kawaguchi et al. (2004); Næss (2010); Ma et al. (2012)		

5.4 Row-to-row heat transfer coefficient variation

As described in chapter 3, the test rig was equipped with turning chambers following each tube row, wherein the water-glycol mixture temperature was measured after each pass. Knowing the temperature increase of the water-glycol for each pass, the heat transfer coefficient was evaluated as presented in chapter 4.5.

Figure 5-23 compares the measured heat transfer coefficient per tube row of different geometries for the same Reynolds number and for the same air mass flow rate, respectively. In both cases, the behaviour is the same. The heat transfer coefficient in the first tube row is reduced by 20 to 35% as compared with the other tube rows. The results of rows two to eight vary in a range of ± 10%, which is within the limits of uncertainty. According to Neal and Hitchcock (1967), the reason for the increasing heat transfer coefficient is the increasing level of turbulence in the tube bank.

In their studies, Jameson (1945) and Brauer (1961) found that from the 4th row and on the heat transfer coefficient remained constant. Therefore, the heat transfer coefficient per tube row is set in relation to the average heat transfer coefficient from rows four to eight. The high variation of the heat transfer coefficient from rows two to row eight might be due to insufficient mixing of the water-glycol and the placement of the turning chambers, as well as the uncertainty limits. For this reason, the results of Geometries 3 and 7 have been omitted, as they seemed unreliable with variations of up to 20%.

Figure 5-24 shows a comparison of the heat transfer coefficient per tube row, h_n, for Geometry 5 for different Reynolds numbers. The behaviour of the heat transfer coefficient per tube row is the same, independent of the flow rate. The first tube row shows an 18 to 21% lower heat transfer coefficient than subsequent tube rows.

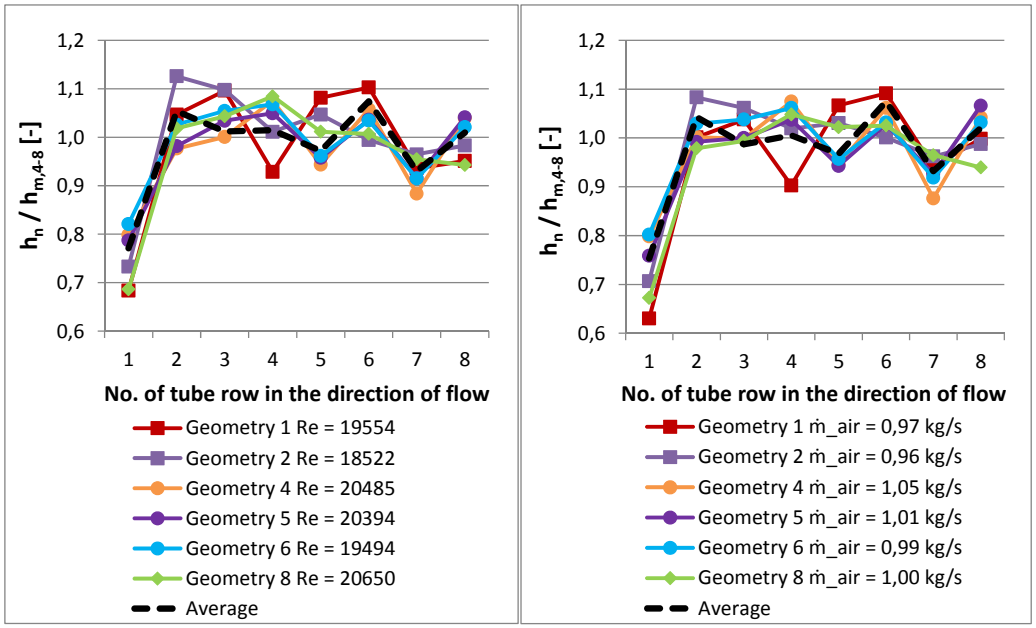

Figure 5-23: Comparison of the heat transfer coefficient per tube row h_n relative to average heat transfer coefficient of row 4 to 8 $h_{m,4-8}$; left: for the same Reynolds number of approximately 20000; right: for the same air mass flow rate of approximately 1 kg/s

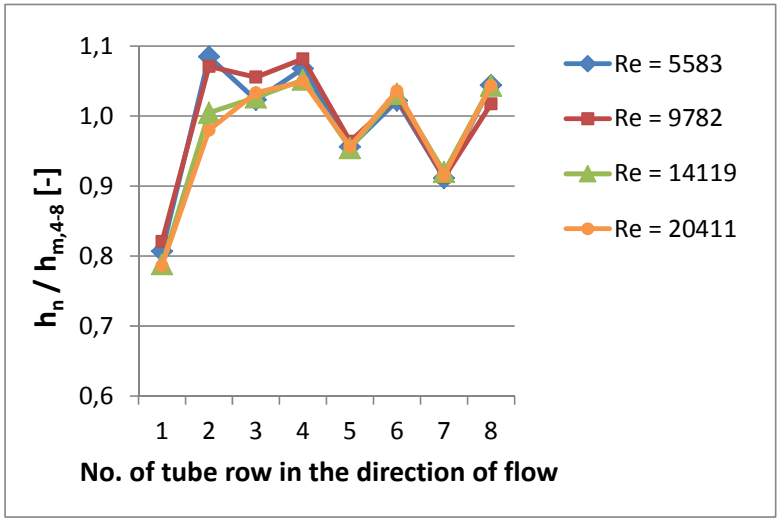

Figure 5-24: Comparison of the heat transfer coefficient per tube row, h_n, relative to the average heat transfer coefficient for rows 4 to 8 $h_{m,4-8}$ of Geometry 5 for different Reynolds numbers

In order to test the influence of the free-stream turbulence upstream of the tube bundles, a grid was placed 600mm upstream of the tube bundles and the turbulence level was evaluated using a hot-wire anemometer (as described in chapter 4.5). The measured turbulence level was 2% without a grid and 37% with the grid in position.

The coloured solid lines in Figure 5-25 show the results from measurements without a grid (T_u=2%) and with the grid (T_u=37%) providing higher turbulence upstream of the test section. The heat transfer coefficient per tube row does not change significantly. The results of Zozulya et al. (1973), as indicated by the grey dashed lines, show a strong influence of the free stream turbulence on the heat transfer coefficient for the first tube row. However, this is not the case for the results measured in the present study, where the difference for the first tube row is an increase of about 5% when T_u is increased from 2% to 37% and otherwise the curves show the same behaviour from the second tube row on.

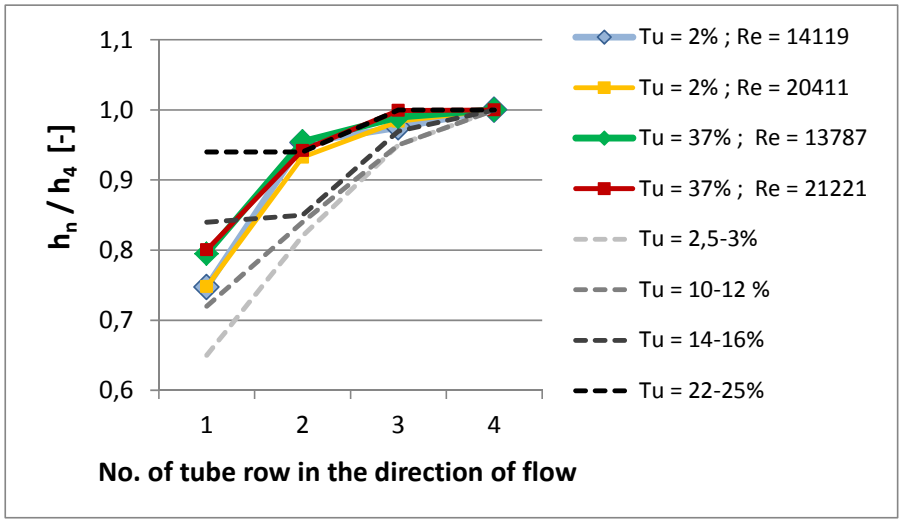

Figure 5-25: Heat transfer coefficient per tube row of Geometry 5 at different upstream turbulence levels compared to the findings of Zozulya et al. (1973) (grey dashed lines) at the indicated turbulence levels

6 CORRELATION DEVELOPMENT

In order to further use the obtained experimental data, correlations for predicting the heat transfer and pressure drop of serrated and solid-fin tube bundles were developed. This chapter presents the database used for the correlations and the approach used to develop the correlation. In addition, the results are presented and compared to published correlations.

6.1 Introduction to the data base

A database containing published experimental data on heat transfer and pressure drop was established for serrated and solid-fin tube bundles having a staggered layout. Table 6-1 gives an overview of the data from the literature included in the database. The data is also shown in Figure 6-1 (serrated-fin heat transfer), Figure 6-2 (solid-fin heat transfer), Figure 6-3 (serrated-fin pressure drop) and Figure 6-4 (solid-fin pressure drop).

The data used for the correlation development was restricted to Reynolds numbers below 50 000, a minimum of four longitudinal tube rows and a tube bundle arrangement angle below 45° (with the ratio of the tube pitches (P_t/P_l) < 2). The Reynolds number limitation was based on the findings of Stasiulevičius et al. (1988) who showed that for a higher Reynolds number, flow transition may occur, which changes the Reynolds number dependency for both heat transfer and pressure drop. Also, for most heat recovery operations, the Reynolds number will normally be below 50 000. The limitation to at least four longitudinal tube rows is based on the argument that the flow structure and hence the heat transfer coefficient develops through the first tube rows (PFR (1976), Zozulya et al. (1973)) as discussed in chapter 5.4. Therefore, shallow tube bundles may experience a different behaviour and are excluded. Næss (2005) showed that for transversal-to-longitudinal-tube-pitch ratios (P_t/P_l) above ca. 2, heat transfer and pressure drop experienced a decrease with increasing pitch ratio. However, data covering this area is at present very limited, and has therefore been excluded from this investigation. Also, from a thermal-hydraulic design perspective, the most attractive tube-pitch ratios are close to 1.15 (30° layout angle), which provides the most heat transfer surface area per unit volume, combined with the highest heat transfer coefficient (Næss (2007)).

In the interpretation of the fin-side heat transfer coefficient from the experimental data, all sources with the exception of Ma et al. (2012) and Næss (2010) assumed uniform heat transfer coefficient distribution on the heat transfer surface. However, the correction made by Ma et al. (2012) and Næss (2010) for uneven heat transfer coefficient distribution was moderate, in the range of 3 to 7%, and the data were therefore accepted without modifications. The results from Ma et al. (2012) and Næss (2010) were therefore about 3%-7% higher than they would have appeared assuming uniform heat transfer coefficient distribution.

From Table 6-2 it can be seen that the experimental data expand the database data. The fin-height-to-tube-diameter ratio increased from 0.63 to 0.91 for the serrated-fin and from 0.71 to 0.74 for the solid-fin tube bundles. Note that the tested tube bundles were arranged in a more compact manner. The extended-surface ratio Ar and the heat-transfer-surface-to-minimum-flow-area ratio $A_{ht}/A_{f,min}$ for the tested tube bundles is in the upper range of all tube bundles of the database.

Figure 6-5 to Figure 6-8 compare the experimental data of this study with data from the database. The heat transfer data of the serrated-fin tubes (Figure 6-5) extends the database data both on the upper and lower limits. The solid-fin heat transfer experimental data (Figure 6-6) is in the same range as the literature data. However, this is not the case for the pressure drop. The Euler number of the new experiments is generally higher for both the serrated-fin data (Figure 6-7) and solid-fin data (Figure 6-8). Only Geometry 8, which has the smallest tube diameter of 13.5mm, is in the range of the literature data.

Table 6-1: Experimental data from the literature included in the databases and used for correlation development with the experimental data of this study

Reference	Serrated fins		Solid fins	
	Heat transfer	**Pressure drop**	**Heat transfer**	**Pressure drop**
Ackerman and Brunsvold (1970)	X	X		
Brauer (1964)				X
Briggs and Young (1963)			X	X
Cox (1973)		X		
Hashizume (1981)	X	X	X	X
Hofmann (2009)	X	X		
Kawaguchi et al. (2004)		X		X
Kawaguchi et al. (2005)	X		X	
Kawaguchi et al. (2006a)		X		X
Kawaguchi et al. (2006b)	X		X	
Kays and London (1984)			X	X
Ma et al. (2012)	X	X		
Næss (2007)	X	X		
Robinson and Briggs (1966)				X
Stasiulevičius et al. (1988)			X	X
Vampola (1966)	X	X		
Ward and Young (1959)			X	X
Weierman (1977)		X		X
Weierman et al. (1978)	X	X		
Worley and Ross (1960)	X	X		

Table 6-2: Range of parameters from the database and test bundles. Data in parentheses are from the present investigation.

Parameter	Range*	
	Serrated fins	**Solid fins**
Tube diameter d_o	17.20 / 12.83 – 63.50 *(19.05 – 31.75)*	9.65 – 40.89 / 50.80 *(13.50 – 31.75)*
Fin height h_f	8.61 / 6.35 – 31.75 *(10.0 – 18.0)*	2.74 / 4.32 – 16.57 / 19.0 *(10.0 – 18.0)*
Fins per meter - N_f	78.7 – 446.5 *(268.4 - 277.3)*	125.0 / 118.0 – 451.2 *(169.9- 354.0)*
Fin height to tube diameter - h_f/d_o	0.26 – 0.63 *(0.52 – 0.94)*	0.19 – 0.71 *(0.57 – 0.74)*
Degree of serration - h_s/h_f	0.53 – 0.99** *(0.50 – 0.61)*	-
Fin pitch to tube diameter - s_f/d_o	0.08 – 0.33 *(0.11 – 0.20)*	0.08 – 0.36 *(0.12 – 0.21)*
Transversal tube pitch to tube diameter - P_t/d_o	1.75 – 3.50 *(2.20 – 3.41)*	1.72 – 3.13 / 3.43 *(2.20 – 2.87)*
Transversal tube pitch to longitudinal tube pitch - P_t/P_l	0.75 – 2.00 *(1.15)*	0.88 / 0.67 – 1.83 *(1.15)*
Extended surface area - Ar	4.75 – 18.89 *(9.82 – 18.85)*	3.47 – 22.53 / 17.43 *(10.77 – 16.56)*
Heat transfer surface to minimum flow area ratio - $A_{ht}/A_{f,min}$	8.2 – 60.6 / 61.7 *(30.2 – 59.1)*	7.45 – 64.42 / 55.08 *(26.8 – 58.5)*
Minimum flow area ratio to flow area between the fins - $A_{f,min}/A_{f,fin}$	1.00 – 3.24 *(1.00 – 1.38)*	1.07 / 1.05 – 3.39 / 4.52 *(1.00 – 1.38)*

* Database: Minimum (heat transfer / pressure drop) - Maximum (heat transfer / pressure drop)
Test bundles: Minimum – Maximum

** For L-foot fins, the degree of serration was set to 0.99 instead of 1

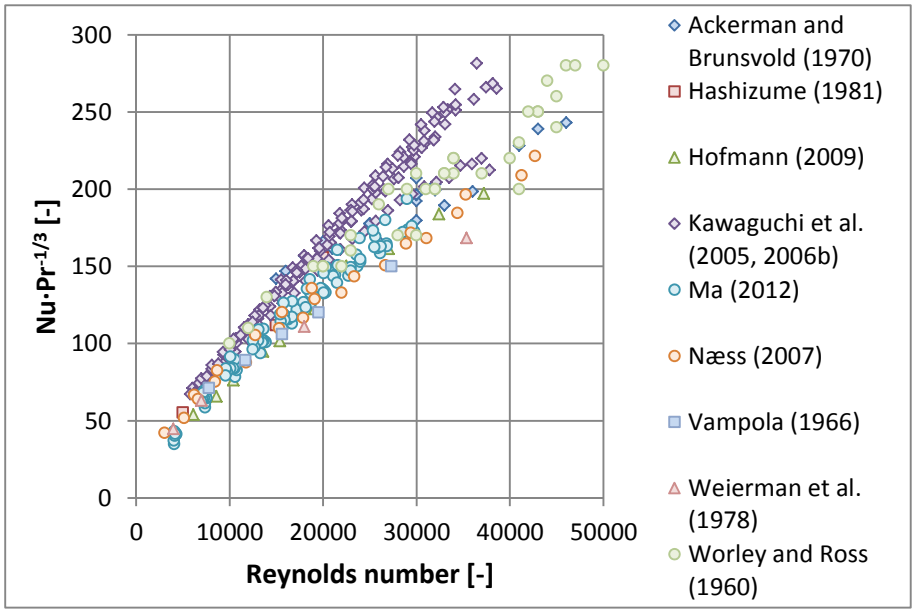

Figure 6-1: Serrated-fin heat transfer data from the literature used for correlation development

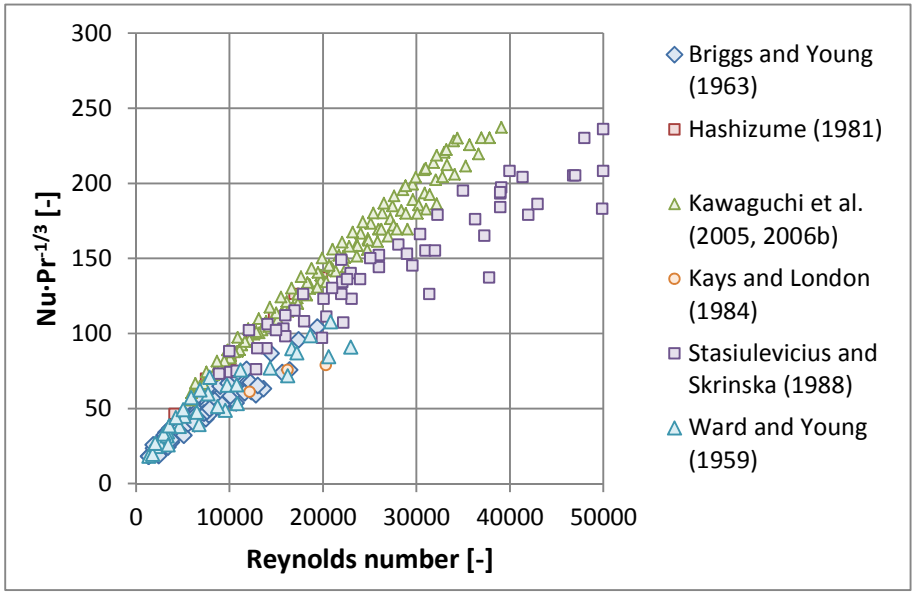

Figure 6-2: Solid-fin heat transfer data from the literature used for correlation development

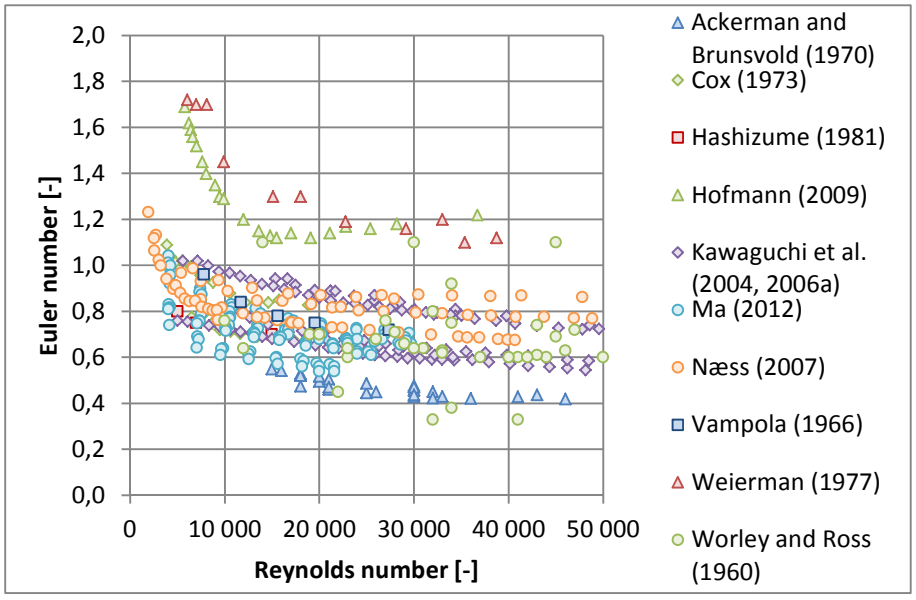

Figure 6-3: Serrated-fin pressure drop data from the literature used for correlation development

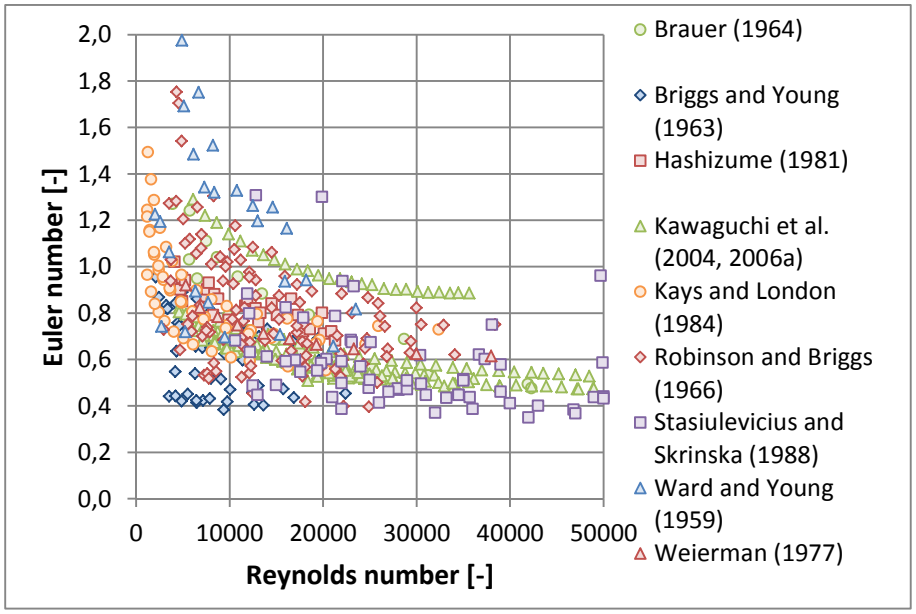

Figure 6-4: Solid fin pressure drop data from the literature used for correlation development

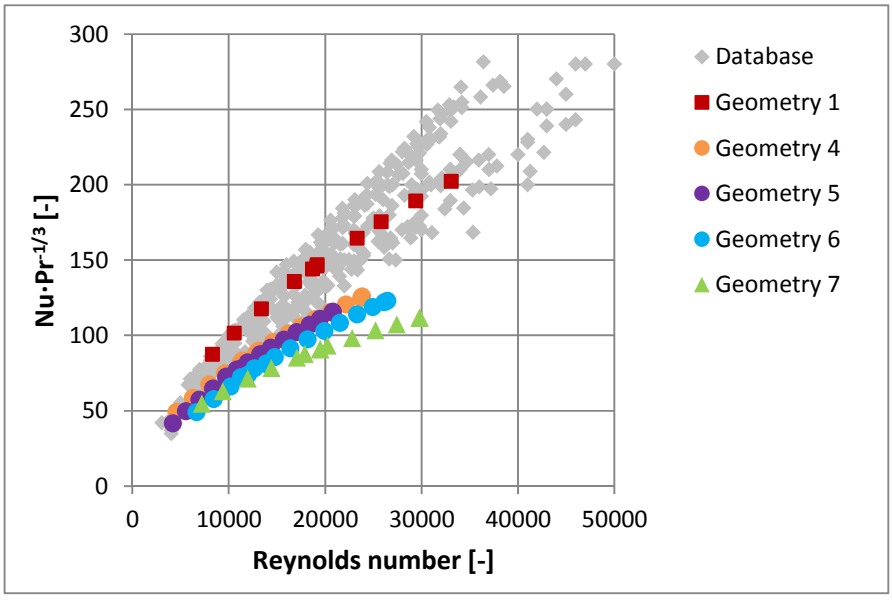

Figure 6-5: Comparison of the experimental serrated-fin heat transfer data to the database data

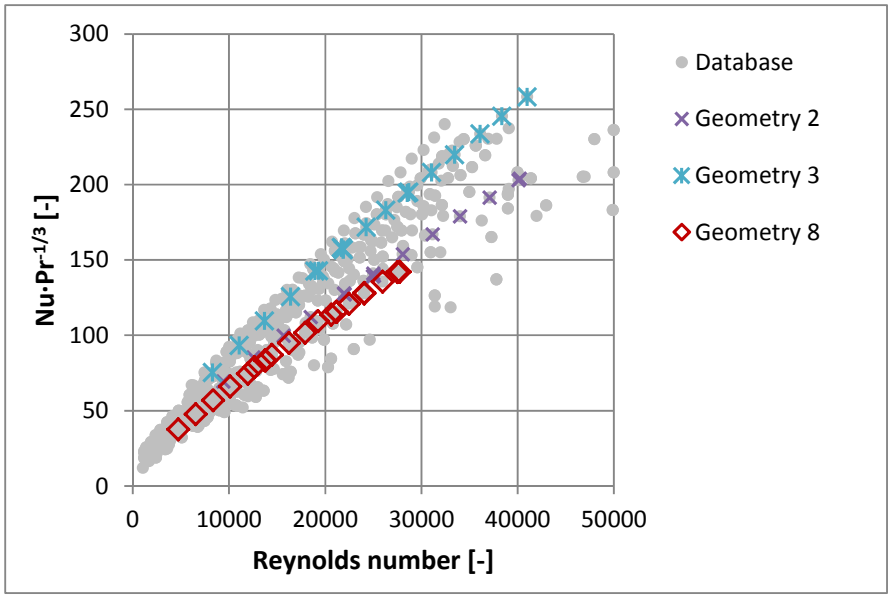

Figure 6-6: Comparison of the experimental solid-fin heat transfer data to the database data

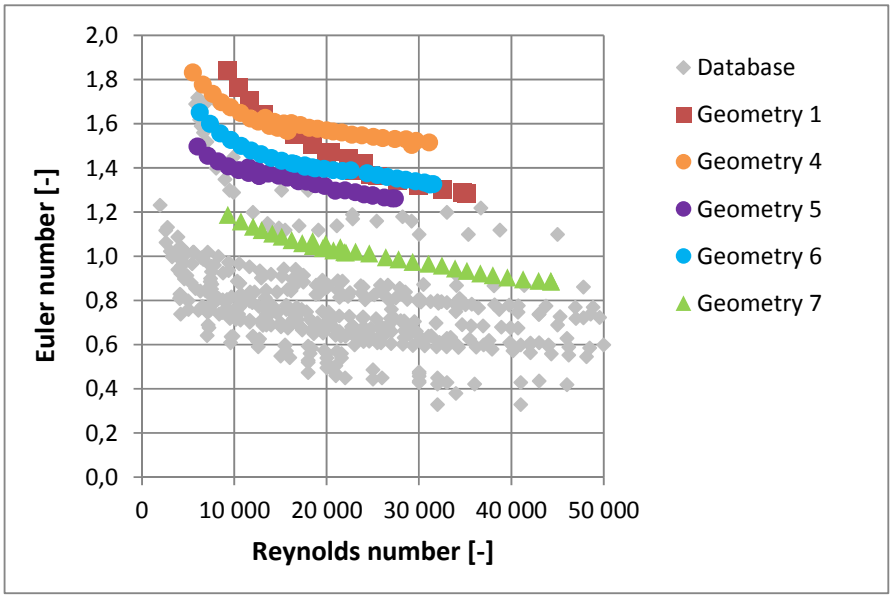

Figure 6-7: Comparison of the experimental serrated-fin pressure drop data to the database data

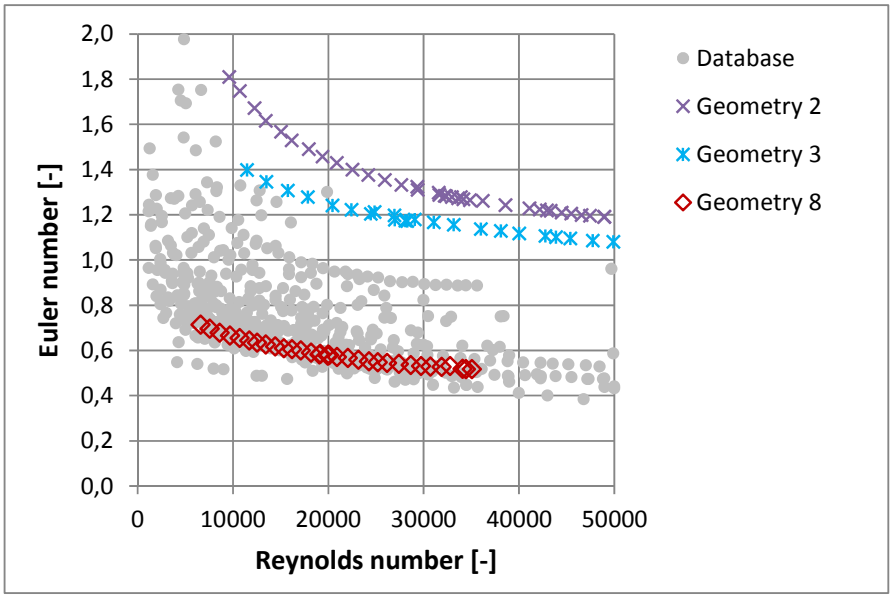

Figure 6-8: Comparison of the experimental solid -fin pressure drop data to the database data

6.2 Approach to the correlation development

The collected data were used to generate correlations for the heat transfer and pressure drop in solid and serrated-fin tube bundles. Different types of correlations were derived. The first type was based on dimensionless groups, such as those of Næss (2010) and Weierman (1976). Sets of dimensionless groups were formed to represent the tube and bundle layout according to those presented in chapter 2.4. The tube and fin geometry, for example, were represented by the ratio (h_f/d_o) (alternatively (d_f/d_o)), (h_f/s_f) and (t_f/s_f). In addition, for serrated-fin tubes the degree of serration ($1-h_s/h_f$) was used. The tube bundle layout was reflected by using the tube-pitch ratios (P_t/d_o), (P_l/d_o), (P_d/d_o), or alternatively (P_t/P_l).

In a second approach, arguing that it is the extension of the total surface contact area (i.e. fin surface area) that dominates the heat transfer and pressure drop (i.e. governing the boundary layer build-up and friction surface), area ratios were used. PFR (1976) based their correlations on the ratio of the overall surface-to-base tube area, Ar, which is calculated according to Eq. 2-19 and Eq. 2-20 for serrated and Eq. 2-18 for solid-fin tubes, respectively. Nir (1991) used dimensionless area ratios to define the flow distribution, such as the heat transfer surface area to the minimum free-flow area ($A_{ht}/A_{f,min}$), minimum free-flow area to the free-flow area between the fins ($A_{f,min}/A_{f,fin}$) and the diagonal to transversal free-flow area ($A_{f,d}/A_{f,t}$).

A third approach involved using both dimensionless groups and extension ratios.

The regression analysis was performed in multiple steps using *Minitab 17 Statistical Software* (2015). In the first step a best subset regression was carried out to identify the most relevant predictors (dimensionless groups and area ratios). This best subset regression presents different combinations of four predictors:

1. the coefficient of determination (R^2),
2. the adjacent R^2 ($\bar{R}^2$),
3. the Mallows C_p and
4. the root mean square of error (RMSE).

These values are evaluated to select the combination of predictors that will yield the best model. Their calculation and the explanation of the model are taken from Reddy (2011) and the Minitab (2015) user guide.

The ***coefficient of determination R^2*** is a number that indicates how well data fit a statistical model. It can take a value between 0 and 1, with an R^2 value close to 1 indicating a good fit of the data to the model. R^2 is calculated, using Eq. 6-1, as the ratio of the regression sum of squares (SSR) to the total sum of squares (SST):

$$R^2 = \frac{SSR}{SST} = \frac{\sum_{1=1}^{n}\left(\hat{y}_i - \bar{y}\right)^2}{\sum_{1=1}^{n}\left(y_i - \bar{y}\right)^2} \qquad \textit{Eq. 6-1}$$

where

- y_i … is the original value of an observation
- $\bar{y}$ … is the mean value of all observations
- $\hat{y}_i$ … is the value of y estimated from the model.

However, R^2 is not sufficient to compare models or correlations with different numbers of predictors, as R^2 would always increase with an increasing number of predictors. The ***adjacent*** $\bar{R}^2$ (Eq. 6-2) takes into account the number of predictors and only increases if an added predictor improves the model.

$$\bar{R}^2 = 1 - \left(1 - R^2\right) \cdot \frac{n-1}{n-p} \qquad \textit{Eq. 6-2}$$

where

- n … is the total number of observations
- p … is the number of predictors

The ***Mallow C_p*** is another criterion for comparing models with different numbers of predictors. A good fit of the model to the data is indicated by the Mallows C_p value being approximately equal to the number of predictors p used. Mallow C_p is calculated using Eq. 6-3:

$$C_p = \frac{SSE_p}{SSE_{all}} + (2p - n) \qquad \textit{Eq. 6-3}$$

where

- SSE … is the error sum of the squares $SSE = \sum_{i=1}^{n} (y_i - \hat{y}_i)^2$
- SSE_p…is the error sum of the squares of the model with p predictors
- SSE_{all}…is the error sum of the squares of the model with all predictors

The ***root mean square of error (RMSE)*** (Eq. 6-4) estimates the absolute error of the model and should be as small as possible.

$$RMSE = \frac{SSE}{n-p} = \frac{1}{n-p} \cdot \sum_{1=1}^{n} (y_i - \hat{y}_i)^2 \qquad \textit{Eq. 6-4}$$

In the second step, a multiple regression analysis was carried out using the best predictors found in the best subset regression. For the obtained correlation, the variance inflation factor (VIF) was checked. This factor measures the multicollinearity of the regression. Correlations with predictors that are moderately correlated were accepted. This is the case for VIF < 10, according to Reddy (2011), and for VIF < 5, according to Minitab (2015).

The correlations showing the best agreement with the data are presented below.

6.3 Heat transfer correlations

In the first approach, the heat transfer data were correlated using only the Reynolds number, which already gave high prediction rates. 95% of the heat transfer data were correlated within ±32% for serrated-fin tubes (Eq. 6-5) and within ±39% for solid-fin tubes (Eq. 6-7).

In the second stage dimensionless numbers were added to the prediction to find the best fitting correlation. For the heat transfer correlation, it was found that the useful predictors were the overall extended surface area Ar, the transversal-tube-pitch-to-tube-diameter ratio P_t/d_o, the fin-height-to-tube-diameter ratio h_f/d_o and, for serrated fins, the fin-pitch-to-tube-diameter ratio s_f/d_o. The predictions of the correlations improved by adding the predictors to the Reynolds number Re (see

Table 6-4 for serrated-fin tubes and

Table 6-6 for solid-fin tubes). The fit of the obtained correlations to the data is shown in Figure 6-9 for serrated-fin tubes (Eq. 6-6) and in Figure 6-10 for solid-fin tubes (Eq. 6-8). Both correlations were the best result of the regression analysis, even though the coefficients point towards different directions. Both a small Area extension (Ar), and a larger heat transfer surface due to a larger fin height h_f (Eq. 6-6 and Eq. 6-8) and a smaller fin pitch s_f (Eq. 6-6), point towards higher heat transfer coefficients.

The influence of the tube bundle layout on the heat transfer depends only on the transversal tube pitch P_t. This is in accordance with Worley and Ross (1960) and Ackerman and Brunsvold (1970), who showed that increasing the transversal tube pitch P_t lead to higher heat transfer coefficients, whereas varying the longitudinal tube pitch P_l had no effect.

Serrated-fin tubes

For serrated-fin tubes, increasing the fin height h_f or decreasing the fin pitch s_f and therefore also increasing the overall extended surface area Ar, increases the heat transfer coefficient. This is according to the experimental results and the findings of Næss (2010) and Kawaguchi et al. (2005, 2006b).

The influence of the overall extended surface area Ar on the heat transfer behaviour of finned tubes is different in the new correlations compared to the

published correlations of PFR (1976) and VDI (2010). Ar in Eq. 6-6 for serrated-fins has an exponent of -0.655 and in Eq. 6-8 for solid-fins has an exponent of -0.350. The PFR (1976) and VDI (2010) Ar exponents were -0.17 and -0.15, respectively. However, their correlations include only the Reynolds number Re and the overall extended surface area Ar as predictors.

Table 6-4 shows the accuracy of the developed heat transfer correlations for serrated-fin tubes for the new correlation (Eq. 6-6) and the correlations of Nir (1991), PFR (1976) and Weierman (1976). Figure 6-9 shows the fit of the serrated-fin heat transfer data to Eq. 6-6. Similar diagrams are shown for the correlations of Nir (1991), PFR (1976) and Weierman (1976) in Appendix III. For Eq. 6-6, 81% of the data were correlated within ±10% and 95% of the data were correlated within ±21%. The correlation of Nir (1991), in particular, underestimates the experimental data. From

Table 6-4, note that Eq. 6-6 estimates the data best, followed by PFR (1976). However, not all the correlations can predict all the data points from the database due to restrictions in their validity ranges and due to the lacking geometry details of Kawaguchi et al. (2005, 2006b) which does not allow the calculation of the overall extended surface area, Ar.

In Figure 6-9 the fit of the data to the correlation is shown. For the measured data in this study it can be said, that the small tubes with high fins (Geometry 4 to 6) fit the correlation best, within ±10%. The results for Geometry 1 (large tube, high fins) are underpredicted and the results for Geometry 7 (small tube, low fins) are overpredicted. The measured Reynolds number exponent for Geometry 7 was much lower (0.50) compared to the Reynolds number exponent in the correlation (0.69)

Solid-fin tubes

For solid-fin tubes, the new correlation (Eq. 6-8) predicts that an increasing fin height h_f will increase the heat transfer coefficient. However, the overall performance of the correlation shows a decreasing heat transfer coefficient for an increasing fin height. Similar behaviour was also observed experimentally by Kawaguchi et al. (2006b) and numerically by Mon (2003). Mon argued that with an increased fin height h_f the boundary layer on the fins becomes thicker and reduces the heat transfer.

Table 6-6 shows the accuracy of the developed heat transfer correlations for solid-fin tubes and the correlations of Nir (1991), PFR (1976) and Weierman (1976). Figure 6-10 shows a comparison of Eq. 6-8 to the experimental data. The comparisons for Nir, PFR and Weierman can be found in Appendix III. Nir (1991) and PFR (1976) underpredict the heat transfer data whereas Weierman (1976) overpredicts the data. From

Table 6-6 it appears that the new correlation Eq. 6-8 estimates the data best followed by Nir (1991) and PFR (1976). For the new solid-fin tubes correlation (Eq. 6-8), 64% of the data were correlated within 10% and 95% of the data were correlated within 26%.

The comparison of the measured data to the correlation shows (see Figure 6-10) that Geometry 8 is predicted best by it. The two large diameter solid-fin tubes, Geometry 2 and 3, are underpredicted by -10% and -15%.

Table 6-3: Correlations for predicting the heat transfer of serrated-fin tubes

Data used	Correlation	Equation
Serrated DB and exp. Data	$Nu \cdot Pr^{-1/3} = 0.081 \cdot Re^{0.751}$	Eq. 6-5
Serrated DB and exp. data	$Nu \cdot Pr^{-1/3} = 0.184 \cdot Re^{0.696} \cdot Ar^{-0.655} \cdot \left(\frac{P_t}{d_o}\right)^{0.262} \cdot \left(\frac{h_f}{d_o}\right)^{0.602} \cdot \left(\frac{s_f}{d_o}\right)^{-0.729}$	Eq. 6-6

Table 6-4: Accuracy of correlations predicting the heat transfer of serrated-fin tubes

Equation / Author	Points covered	Percentage of the data within ± 10%	95% of the data are within	R^2
Eq. 6-5	364	53%	± 32%	0.890
Eq. 6-6	284	81%	± 21%	0.958
Nir (1991)	263	11%	± 45%	-
PFR (1976)	243	63%	± 27%	-
Weierman (1976)	364	59%	± 62%	-

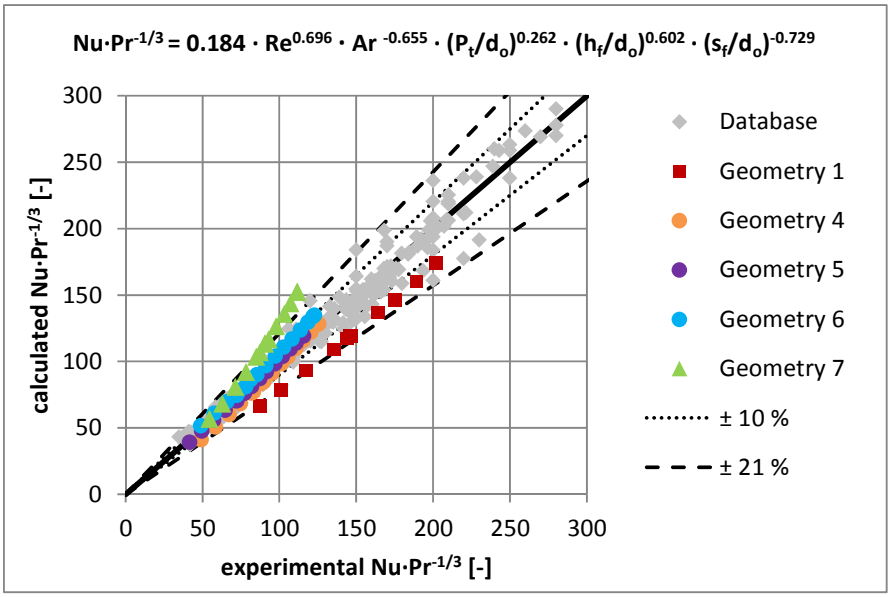

Figure 6-9: Fit of the serrated-fin heat transfer data to Eq. 6-6

Table 6-5: Correlations for predicting the heat transfer of solid-fin tubes

Data used	Correlation	Equation
Solid DB and exp. data	$Nu \cdot Pr^{-1/3} = 0.084 \cdot Re^{0.735}$	**Eq. 6-7**
Solid DB and exp. data	$Nu \cdot Pr^{-1/3} = 0.346 \cdot Re^{0.751} \cdot Ar^{-0.350} \cdot \left(\frac{P_t}{d_o}\right)^{-0.575} \cdot \left(\frac{h_f}{d_o}\right)^{0.464}$	Eq. 6-8

Table 6-6: Accuracy of correlations predicting the heat transfer of solid-fin tubes

Equation / Author	Points covered	Percentage of the data within ± 10%	95% of the data are within	R^2
Eq. 6-7	325	28%	± 39%	0.934
Eq. 6-8	325	64%	± 26%	0.962
Nir (1991)	325	35%	± 39%	-
PFR (1976)	306	32%	± 31%	-
Weierman (1976)	325	23%	± 64%	-

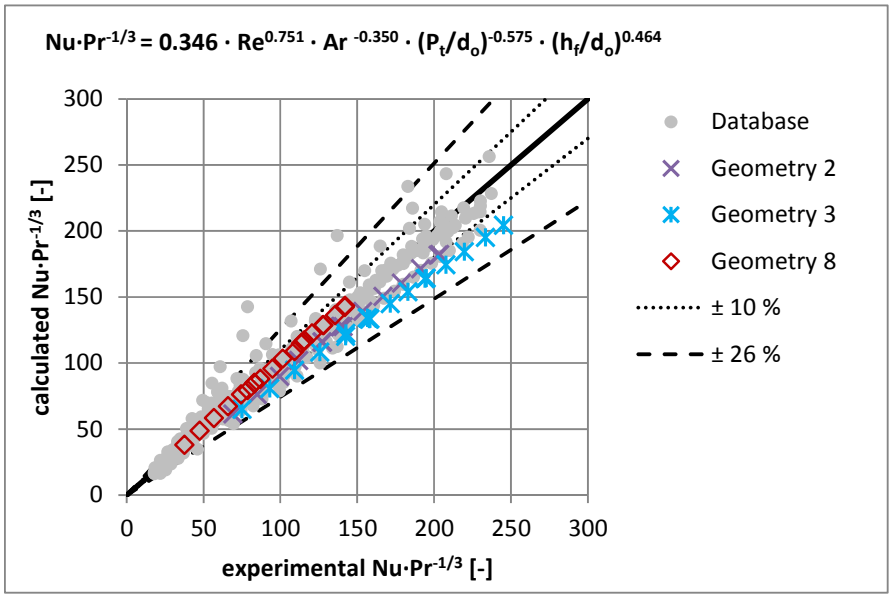

Figure 6-10: Fit of the solid-fin heat transfer data to Eq. 6-8

6.4 Pressure drop correlations

Serrated-fin tubes

The new correlations for the pressure loss coefficients (Euler number Eu) of serrated-fin (Eq. 6-10) and solid-fin tubes (Eq. 6-12) predict 95% of the data within ±34%. The predictors show that the bundle arrangement is more important for pressure drop than for heat transfer. The transversal-tube-pitch-to-longitudinal-tube-pitch ratio P_t/P_l as well as the minimum free-flow area $A_{f,min}$ are included in the correlations. For serrated-fin tubes the minimum-free-flow-area-to-the-flow-area-between-the-tubes ratio $A_{f,min}/A_{f,fin}$ is important as well as the degree of serrations h_s/h_f. For solid-fin tubes, the heat-transfer-surface-to-minimum-free-flow-area ratio $A_{ht}/A_{f,min}$, the fin-height-to-tube-diameter ratio h_f/d_o and the fin-pitch-to-tube-diameter ratio s_f/d_o are also important.

Keeping the fin tip clearance c_f constant and increasing the transversal tube pitch P_t, the fin height h_f or the fin pitch s_f leads to a decreased Euler number. All three measures increase the distance between the tube and/or the minimum free-flow area. This leads to a reduced flow through the fins and less skin friction, and accords with the findings of Ma et al. (2012), Næss (2010) and Stasiulevičius et al. (1988).

The comparison of the experimental serrated-fin heat transfer data to the correlations (Figure 6-11 and Table 6-8) shows that the new correlation (Eq. 6-10) predicts the data best, followed by Weierman (1976) and Nir (1991). The correlation of PFR (1976) can only be used for 11 data points of the database. This is due to the given validity range restriction of the correlation as well as the lacking geometry data on the segment width w_s for the serrated-fin tubes tested by Kawaguchi et al. (2004, 2006a). Eq. 6-10 predicts 44% of the data within ±10% and 95% of the data within ±34%.

The data overestimated by Eq. 6-10 are from Hashizume (1981), Ackerman and Brunsvold (1970) (Geometry 6) and Worley and Ross (1960) (Geometries 8 and 9). Ackerman and Brunsvold and Worley and Ross tested stud fins that were quite thick (t_f = 3.2mm). Worley and Ross tested tubes with a low number of fins, only 79 fins per meter tube length.

Figure 6-11 shows the comparison of the data to the new correlation. Geometry 1 is well predicted by the correlation. Geometry 4 to 6 have a good fit for lower Reynolds numbers. For higher Reynolds numbers the correlation

underpredicts the results. For Geometry 7 the Euler number is overpredicted by 10%.

Solid-fin tubes

Figure 6-12 and Table 6-10 show the prediction accuracy of Eq. 6-12 and the correlations of Nir (1991), PFR (1976) and Weierman (1976) to the experimental data. The correlation predicting the data best is Eq. 6-12 followed by Weierman (1976).

In Figure 6-12 it is shown that Geometry 8 is well predicted by the correlation, as it was the case for the Nusselt number. Geometry 3 is underpredicted by approximately 30%. Also for Geometry 2 lower Euler numbers are calculated, especially for low Reynolds numbers.

Table 6-7: Correlations predicting the pressure drop of serrated-fin tubes

Data used	Correlation	Equation
Serrated DB and exp. data	$Eu = 5.066 \cdot Re^{-0.180}$	Eq. 6-9
Serrated DB and exp. data	$Eu = 9.661 \cdot Re^{-0.197} \cdot \left(\frac{P_t}{P_l}\right)^{0.931} \cdot \left(\frac{A_{f,min}}{A_{f,fin}}\right)^{-0.776} \cdot \left(1-\frac{h_s}{h_f}\right)^{0.112}$	Eq. 6-10

Table 6-8: Accuracy of correlations predicting the pressure drop of serrated-fin tubes

Equation / Author	Points covered	Percentage of the data within ± 10%	95% of the data are within	R^2
Eq. 6-9	504	14%	± 65%	0.103
Eq. 6-10	442	44%	± 34%	0.739
Nir (1991)	382	11%	± 71%	-
PFR (1976)	17	6%	± 40%	-
Weierman (1976)	689	27%	± 51%	-

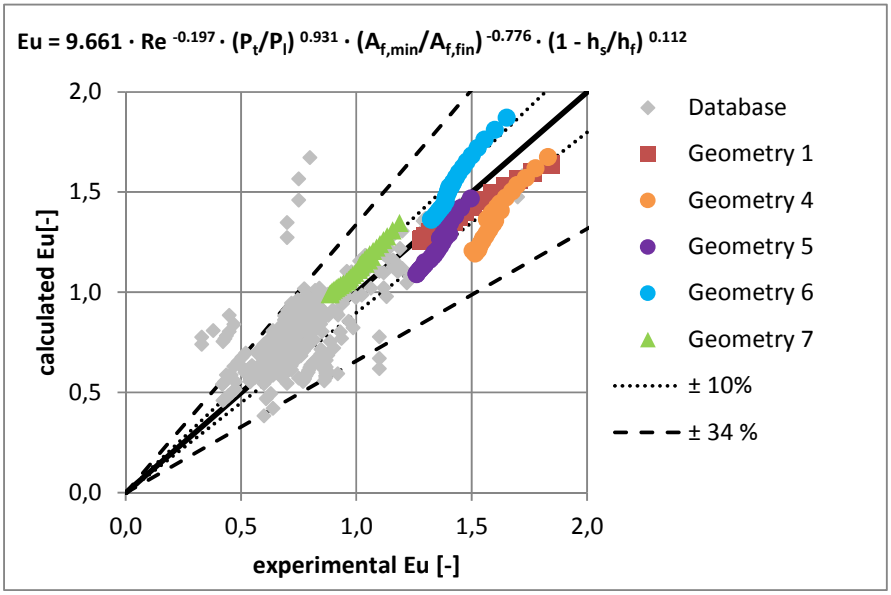

Figure 6-11: Fit of the serrated-fin pressure drop data to Eq. 6-10

Table 6-9: Correlations predicting the pressure drop of solid-fin tubes

Data used	Correlation	Equation
Solid DB and exp. data	$Eu = 3.270 \cdot Re^{-0.153}$	Eq. 6-11
Solid DB and exp. data	$Eu = 0.340 \cdot Re^{-0.132} \cdot \left(\frac{P_t}{P_l}\right)^{0.502} \cdot \left(\frac{A_{ht}}{A_{f,min}}\right)^{0.738} \cdot \left(\frac{h_f}{d_o}\right)^{-0.293} \cdot \left(\frac{s_f}{d_o}\right)^{0.333}$	Eq. 6-12

Table 6-10: Accuracy of correlations predicting the pressure drop of solid-fin tubes

Equation / Author	Points covered	Percentage of the data within ± 10%	95% of the data are within	R^2
Eq. 6-11	615	23%	± 49%	0.129
Eq. 6-12	615	50%	± 34%	0.729
Nir (1991)	90	46%	± 32%	-
PFR (1976)	86	9%	± 121%	-
Weierman (1976)	615	37%	± 42%	-

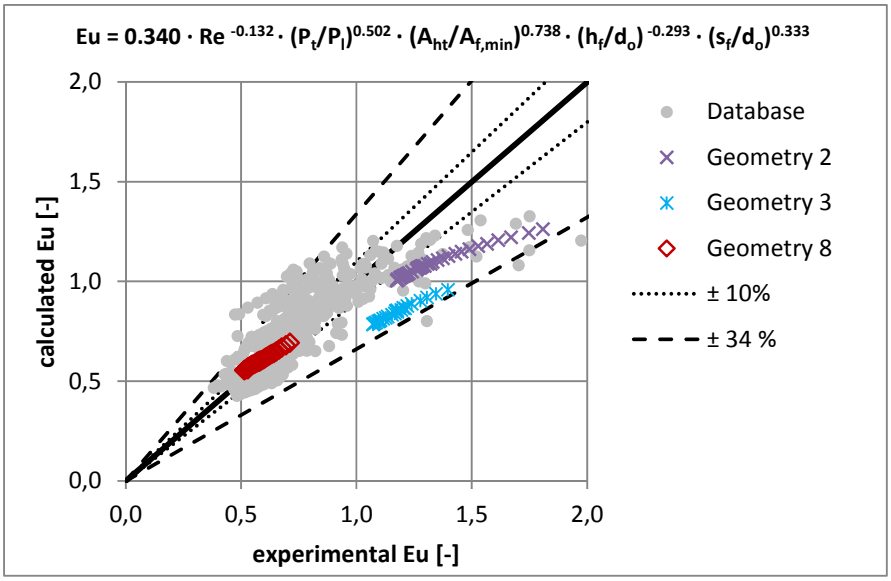

Figure 6-12: Fit of the solid fin pressure drop data to Eq. 6-12

7 IMPLEMENTATION OF THE DESIGN OF COMPACT WHRUS

In this chapter, the experimental results and developed correlations are used to define criteria for the design of compact waste heat recovery units (WHRUs). This is performed in two steps. First, the experimental results of the tested tubes are compared with regard to performance, volume and weight. Next, the correlations developed in chapter 6 are used to define the parameters necessary for an energy efficient and compact WHRU for a given design case where the maximum pressure loss and mass flow rate are given.

For both comparisons the material of the finned tubes was the same as for the tested tubes.

7.1 Comparison of the heat transfer performance of the tested geometries with respect to pressure drop, volume and weight

In order to compare the heat transfer performance of the tested tube bundles (tested tube geometries and tube and fin material according to Table 3-4) with respect to pressure drop, volume and weight, a control volume was defined. This control volume, shown in Figure 7-1, includes the space occupied by a tube row in a tube bundle. This can be calculated using to Eq. 7-1.

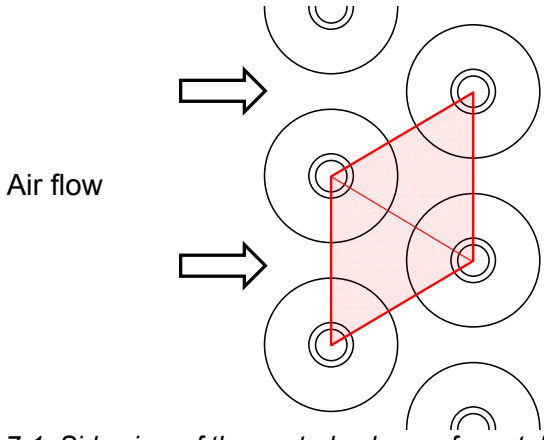

Figure 7-1: Side view of the control volume of one tube row

$$V_c = 2 \cdot \left(\frac{P_t}{2} \cdot P_l \right) \cdot l_t \qquad \textit{Eq. 7-1}$$

For each comparison of the fin type, fin height h_f, fin pitch s_f, fin-tip clearance c_f and tube diameter d_o, the heat transferred per unit pressure drop, unit volume and unit weight were calculated.

7.1.1 Comparison of fin type

Geometries 1 and 2 were used in the comparison of different fin types, and the finned tube bundles varied only with respect to fin type (see Table 7-1). Table 7-2 shows further comparisons of the two geometries, and it can be seen that they occupy the same volume and have practically the same heat transfer surface area and almost the same weight. The heat transfer surface loss due to fin serration is nearly fully compensated by a slightly smaller fin pitch and the contribution of the four cut sides of the segment to the heat transfer surface.

This parameter comparison shows that the cuts in the fins on the serrated-fin tubes have little impact on the heat transfer surface of a tube bundle; however, the weight is reduced by 9%.

Table 7-1: Geometric parameters of the tubes used in the fin type comparison

Geo.	Fin type	Tube diameter	Fin height	Fin pitch	Fin-tip clearance
	-	d_o [mm]	h_f [mm]	s_f [mm]	c_f [mm]
1	Serrated	31.75	18.00	3.60	2.00
2	Solid	31.75	18.00	3.70	2.00

Table 7-2: Geometric parameters of the one-tube tube bundle used in the fin-type comparison

Geo.	Fin type	Heat transfer surface	Volume	Weight
	-	A_{ht} [m^2/m tube]	V [m^3/m tube]	m [kg/m tube]
1	Serrated	1.655	0.0084	7.283
2	Solid	1.652	0.0084	7.922
Serrated vs Solid	-	0 %	0 %	- 9 %

Figure 7-2 and Figure 7-3 show the heat transferred per unit pressure drop, pumping power and volume and weight. Serrated fins perform better than solid fins in all three comparisons. The heat transfer is 18% to 34% higher for serrated-fin tubes compared to than solid-fin tubes per unit pressure drop, 25% to 35% higher heat transfer per unit tube bundle volume and 37% to 48% higher heat transfer per unit mass.

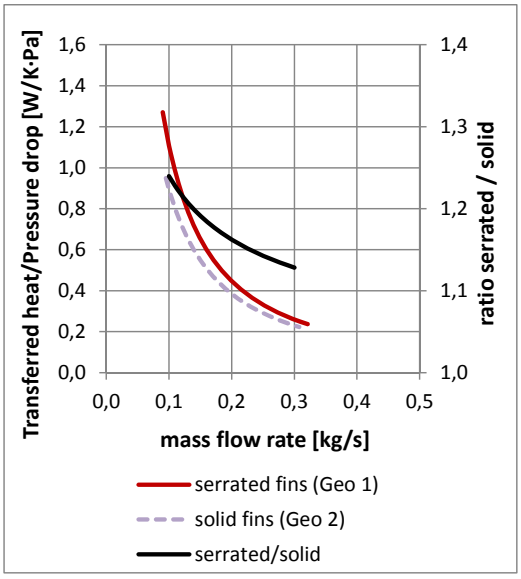

Figure 7-2: Transferred heat per unit pressure drop for different fin types

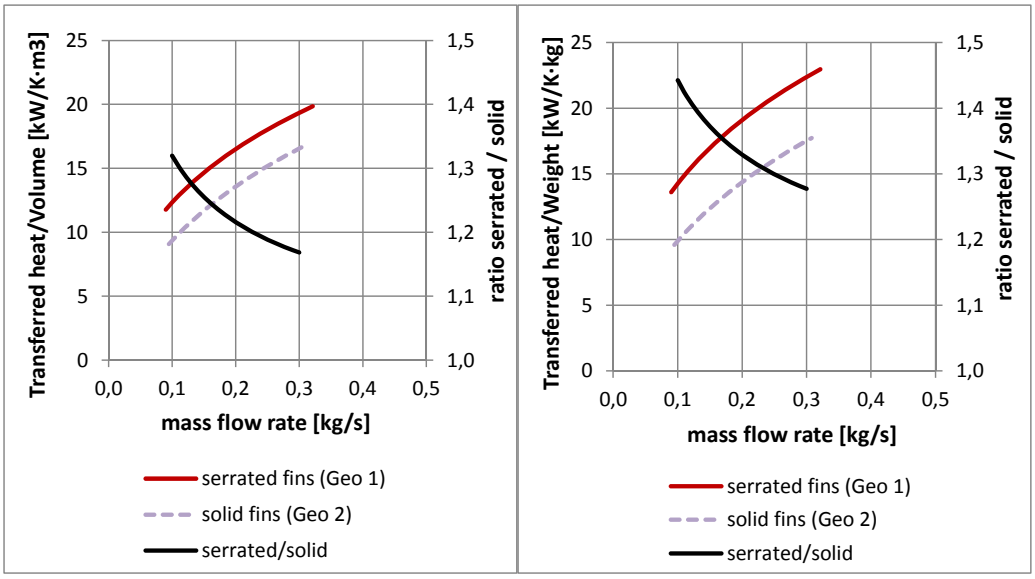

Figure 7-3: Transferred heat per unit volume (left) and per unit weight (right) for different fin types

7.1.2 Comparison of fin height

Geometries 4 and 7, i.e. serrated-fin tubes, were used in the comparison of the influence of fin height on heat transferred per unit pressure drop, volume and weight. Their geometric parameters are given in Table 7-4. The fin height was increased by 80% from 10mm to 18mm and therefore the heat transfer surface, tube bundle volume and weight increased as well by 92%, 82% and 61%, respectively.

Table 7-3: Geometric parameters of the tubes used in the fin-height comparison

Geo.	Fin type	Tube diameter	Fin height	Fin pitch	Fin-tip clearance
	-	d_o [mm]	h_f [mm]	s_f [mm]	c_f [mm]
4	Serrated	19.05	18.00	3.73	5.00
7	Serrated	19.05	10.00	3.61	5.00

Table 7-4: Geometric parameters of the tube bundle used in the fin-height comparison

Geo.	Fin height h_f [mm]	Heat transfer surface A_{ht} [m^2/m tube]	Volume V [m^3/m tube]	Weight m [kg/m tube]
4	18.00	1.128	0.0062	4.731
7	10.00	0.587	0.0034	2.931
4 vs 7	+ 80 %	+ 92 %	+ 82 %	+ 61 %

Figure 7-4 shows the heat transferred per unit pressure drop. In the left-hand figure, the comparison shows that for the same mass flow rate and the same pressure drop, high-fin tubes transfer more than twice the heat than low-fin tubes. For the same velocity in the minimum free-flow area, high-fin tubes still transfer more heat than low-fin tubes; however, the result is less significant. The advantage of the increased heat transfer surface of the high fin tubes is almost completely compensated by the decreased fin efficiency for higher fins.

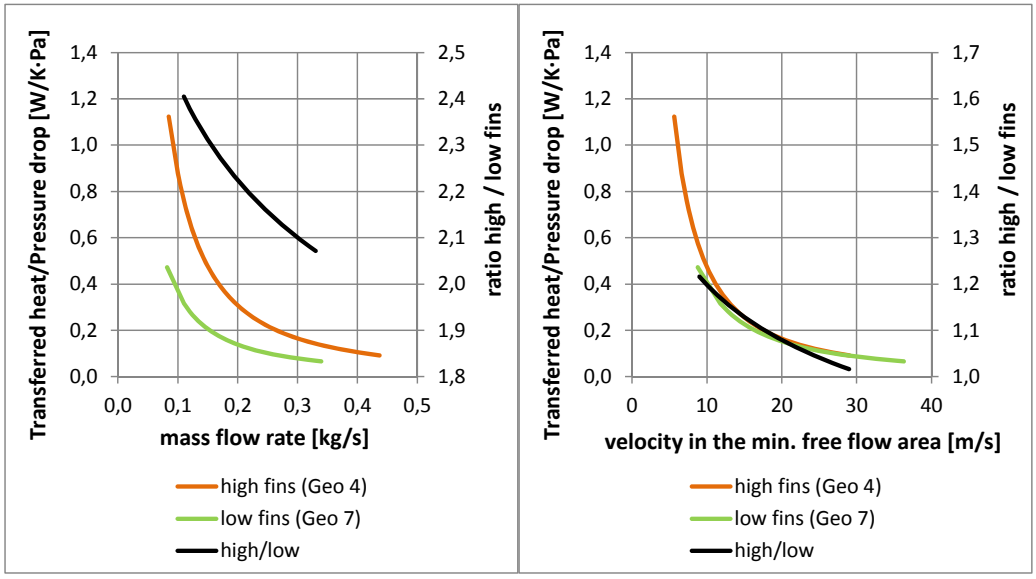

Figure 7-4: Transferred heat per unit pressure drop for different fin heights

Figure 7-5 shows a comparison of the heat transferred per unit tube bundle volume (left) and weight (right). From this comparison it is clear that, for the same amount of heat transferred, the lower fins lead to a more compact tube bundle. An 80% increase in the fin height leads to an 82% increase in tube bundle volume; however, the heat duty has not increased by the same magnitude (compare to chapter 5.3.3). One reason for this is that the fin efficiency decreases with increasing fin height. The increase in the heat duty is less than the increase in the heat transfer surface. Therefore, tubes with lower fins transfer more heat per volume and weight for the same mass flow rate, and they also transfer more heat per unit volume for the same velocity in the minimum free-flow area. Comparing the transferred heat per unit weight with respect to the velocity in the minimum free-flow area, the tube bundles both geometries have comparable performance.

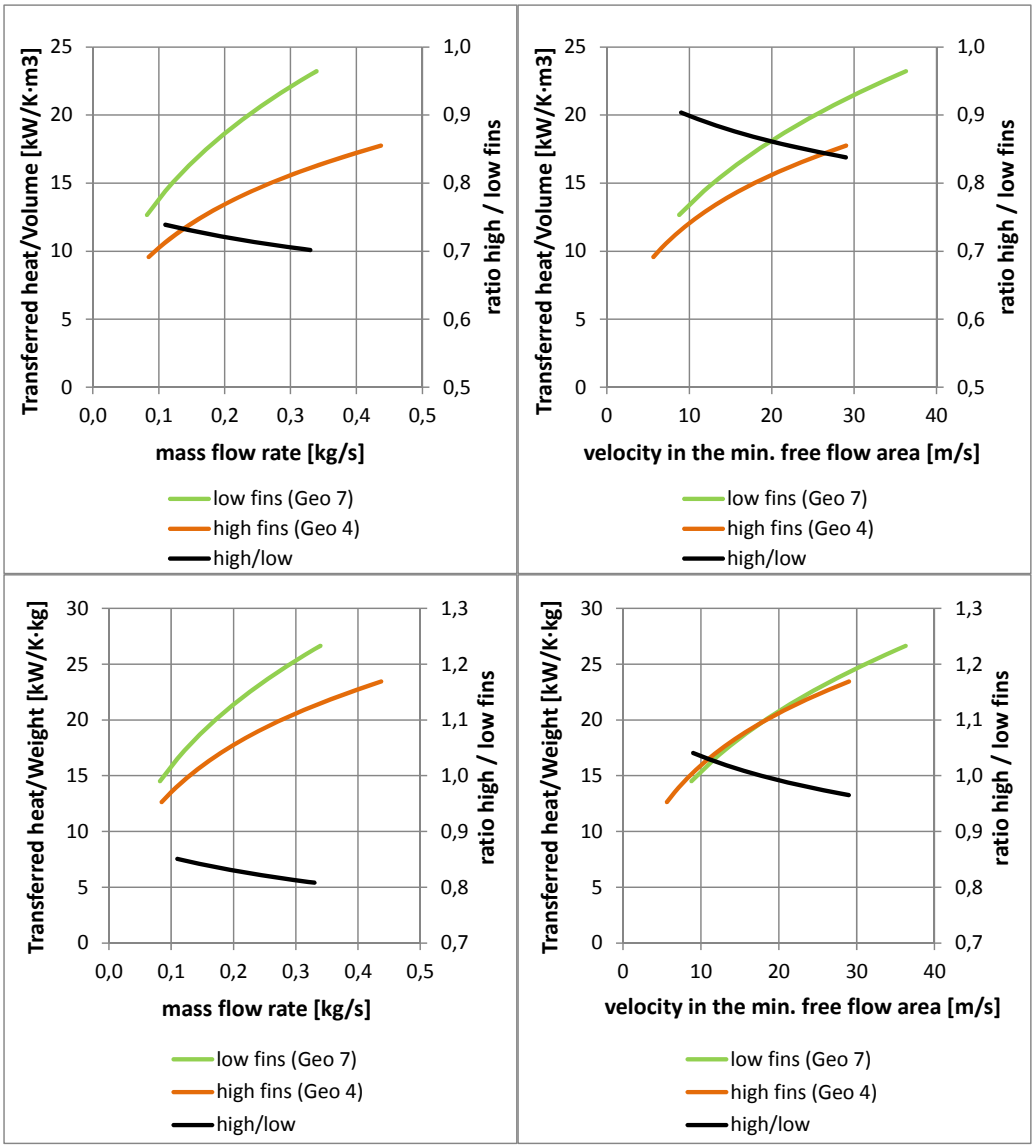

Figure 7-5: Transferred heat per unit volume (left) and per unit weight (right) for different fin heights

7.1.3 Comparison of fin pitch

Solid fin Geometries 2 and 3 were used for this comparison (Table 7-5) in which only the fin pitch varies, i.e. the number of fins per unit tube length. By decreasing the fin pitch by 37%, the heat transfer surface was increased by 54% and the weight of the tube by 39%. The volume was the same due to the geometries having the same fin height (Table 7-6).

Table 7-5: Geometric parameters of the tubes used in the fin pitch comparison

Geo.	Fin type	Tube diameter	Fin height	Fin pitch	Fin-tip clearance
	-	d_o [mm]	h_f [mm]	s_f [mm]	c_f [mm]
2	Solid	31.75	18.00	3.70	2.00
3	Solid	31.75	18.00	5.89	2.00

Table 7-6: Geometric parameters of the tube bundles used in the fin pitch comparison

Geo.	Fin pitch	Heat transfer surface	Volume	Weight
	s_f [mm]	A_{ht} [m^2/m tube]	V [m^3/m tube]	m [kg/m tube]
2	3.70	1.706	0.0084	7.962
3	5.89	1.109	0.0084	5.738
2 vs 3	- 37 %	54 %	0 %	39 %

Figure 7-6 and Figure 7-7 show the heat transferred per unit pressure drop, volume and weight. A comparison of both geometries for the same mass flow rate shows that the heat transferred per unit pressure drop and weight is the same for both geometries. This means that the heat transferred per unit pressure drop and weight is independent of the fin pitch. This is not the case for the heat transferred per unit volume for which denser fins and a smaller fin pitch are advantageous (Figure 7-7 on the upper left).

A comparison of both geometries for the same velocity in the minimum free-flow area shows that the tubes having a smaller fin pitch transfer approximately 8 to 16% more heat per pressure drop and 31% more heat per unit volume. Only in tubes with a larger fin pitch does the heat transferred per unit weight show a small advantage, having a 6% higher performance.

In general, these results indicate that tubes with a higher number of fins should be used in compact finned tube heat exchangers.

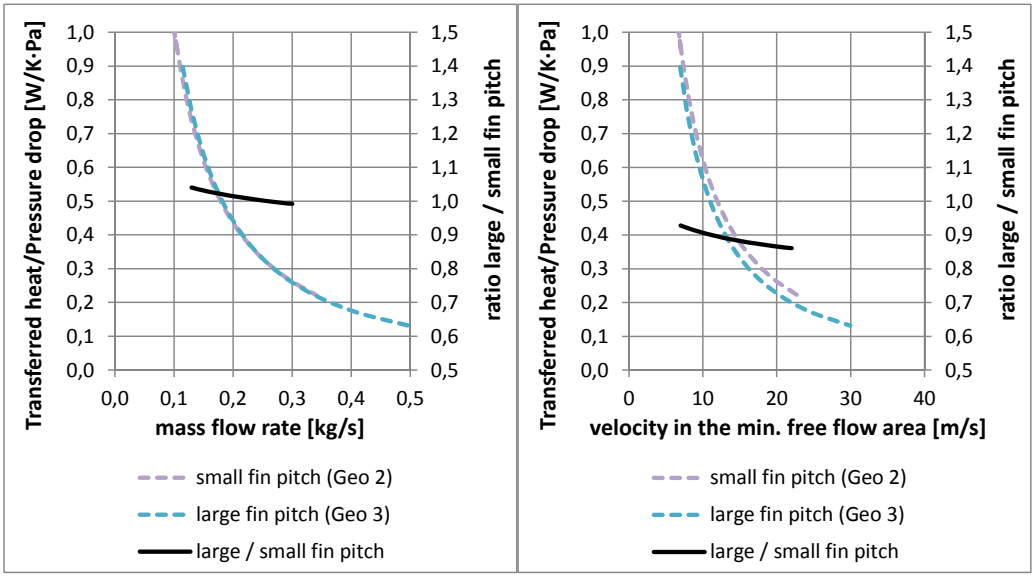

Figure 7-6: Transferred heat per unit pressure drop for different fin pitches

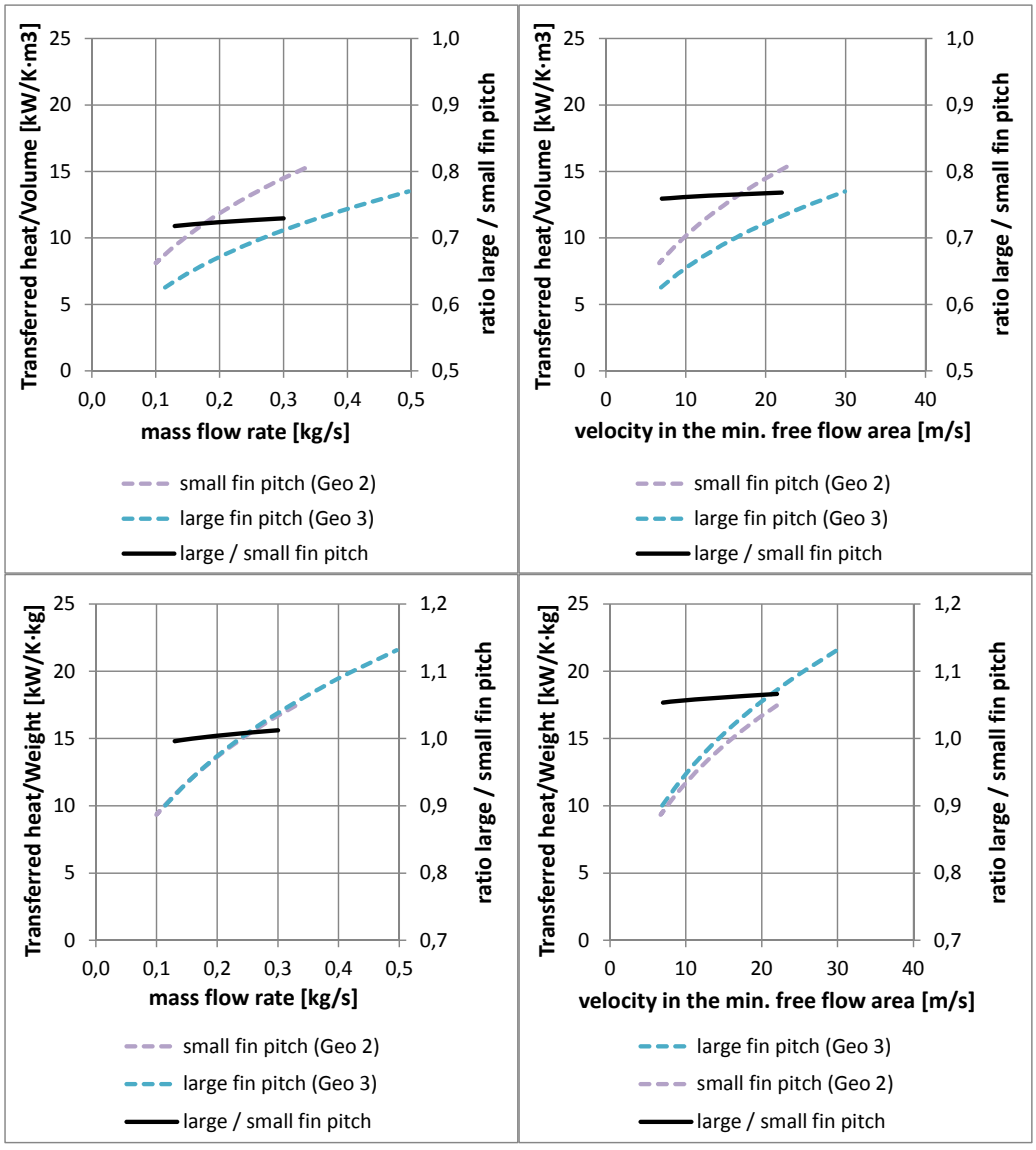

Figure 7-7: Transferred heat per unit volume (left) and per unit weight (right) for different fin pitches

7.1.4 Comparison of fin-tip clearance

The fin-tip clearance determines the gap between fins of two neighbouring tubes (see Figure 2-13). In the experiments on the influence of fin-tip clearance, the same tubes were used but they were arranged in three different ways. One setup had touching fins, and the second and third a gap between the fins of 5mm and 10mm, respectively (Table 7-7). The tube layout angle β was maintained at 30°, which resulted in there being only a change in the tube bundle volume, while the heat transfer surface and the tube bundle weight remained the same (Table 7-8).

Table 7-7: Geometric parameters of the tubes used in the fin-tip clearance comparison

	Fin type	Tube diameter	Fin height	Fin pitch	Fin-tip clearance
Geo.	-	d_o [mm]	h_f [mm]	s_f [mm]	c_f [mm]
4	Serrated	19.05	18.00	3.73	5.00
5	Serrated	19.05	18.00	3.73	10.0
6	Serrated	19.05	18.00	3.73	0.00

Table 7-8: Geometric parameters of the tube bundle used in the fin-tip clearance comparison

	Fin-tip clearance	Heat transfer surface	Volume	Weight
Geo.	c_f [mm]	A_{ht} [m^2/m tube]	V [m^3/m tube]	m [kg/m tube]
4	5.00	1.128	0.0062	4.731
5	10.00	1.128	0.0073	4.731
6	0.00	1.128	0.0052	4.731
5 and 6 vs 4	± 100 %	0 %	± 17 %	0 %

As described above, the fin-tip clearance primarily influences the distance between the tubes, thus, increasing the fin-tip clearance increases the volume. For a compact heat exchanger it is therefore preferable to decrease the fin-tip clearance. The heat transferred per unit volume and weight (Figure 7-9) is higher for a small fin-tip clearance. The drawback of this more compact heat

exchanger is an increase in the pressure drop. Higher fin-tip clearances lead to an increased bypass flow between the tubes. The smaller the gap between neighbouring fins, the higher the resulting velocity, leading to increased friction. As such, the heat transferred per unit pressure drop is reduced with a decreased fin-tip clearance (see Figure 7-8).

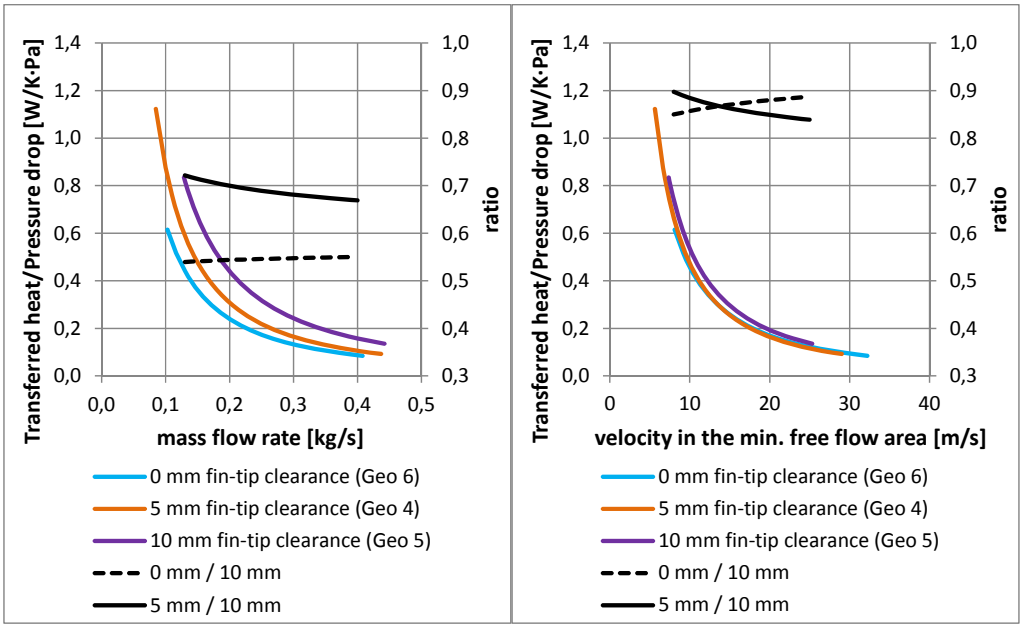

Figure 7-8: Transferred heat per unit pressure drop for different fin-tip clearances

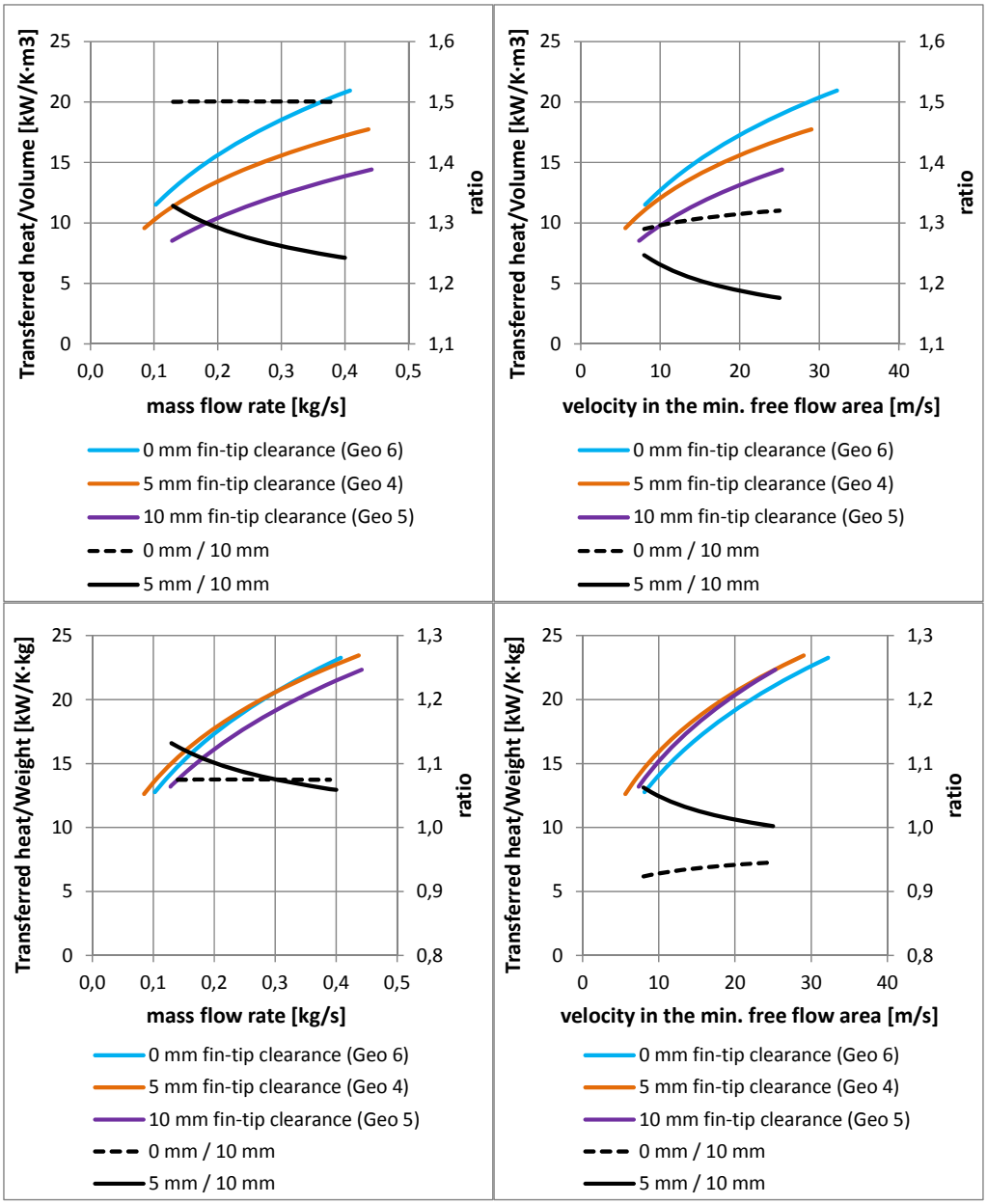

Figure 7-9: Transferred heat per unit volume (left) and per unit weight (right) for different fin-tip clearances

7.1.5 Comparison of tube diameter

For the comparison of the influence of tube diameter, Geometries 1 and 4 were used, both of which varied geometrically in their tube diameters. While their fin heights and fin pitches were the same, their tested fin-tip clearances varied. Geometry 1 was tested with a 2mm fin-tip clearance and Geometry 4 with 5mm (see Table 7-9). As shown earlier in chapter 7.1.4, the fin-tip clearance does not significantly influence the heat transferred per tube. Therefore, the fin-tip clearance of Geometry 1 was adjusted to 5mm in order to compare both geometries with respect to the heat transferred per volume and weight, while omitting any comparison of the heat transferred per unit pressure drop. A change in the fin-tip clearance would affect the pressure drop significantly; a correction for the change in pressure drop due to the increased fin-tip clearance was not calculated.

Table 7-10 shows the resulting differences between the geometries. An increase in the tube diameter by 67% resulted in a 47% increase in the tube and fin surface. The fin surface also increased as the strip length increased, which is wrapped around the tube to form the fins. The volume is 48% larger in the larger diameter tube and the weight increased by 54%.

Table 7-9: Geometric parameters of the tubes used in the tube diameter comparison

Geo.	Fin type	Tube diameter	Fin height	Fin pitch	Fin-tip clearance
	-	d_o [mm]	h_f [mm]	s_f [mm]	c_f [mm]
1	Serrated	31.75	18.00	3.60	*5.00**
4	Serrated	19.05	18.00	3.73	5.00

**tested with 2mm fin-tip clearance, adjusted to 5mm fin-tip clearance for comparison*

Table 7-10: Geometric parameters of the tube bundle used in the tube diameter comparison

Geo.	Tube diameter d_o [mm]	Heat transfer surface A_{ht} [m^2/m tube]	Volume V [m^3/m tube]	Weight m [kg/m tube]
1	31.75	1.655	*0.0092**	7.283
4	19.05	1.128	0.0062	4.731
1 vs 4	+ 67 %	+ 47 %	+ 48 %	+54 %

Even though the heat transfer coefficient for both tubes is almost the same (see Figure 5-8), the increased heat transfer surface of the larger diameter tubes is advantageous with respect to the heat transferred. Figure 7-10 shows that larger tube diameters lead to slightly higher rates of heat transferred per unit volume (0%–5%) and weight (4%–10%). As the relationship between the mass flow rate and the velocity in the minimum free flow area is the same for Geometry 1 and 4, the results are the same for both comparisons and the diagrams look similar.

This shows that for compact heat exchangers, a larger tube diameter may be preferable, but the advantage is very small and is inside the measurement uncertainty range.

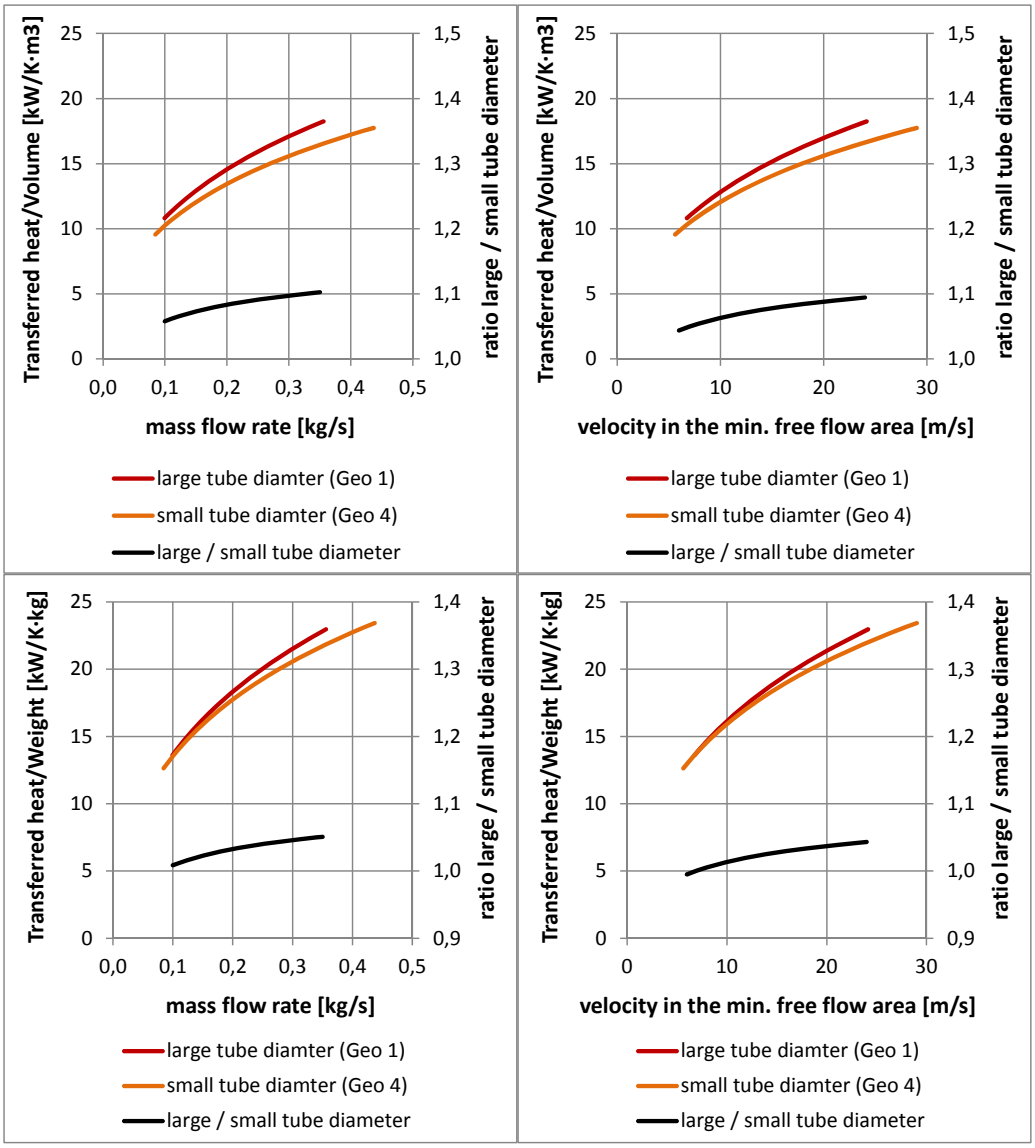

Figure 7-10: Transferred heat per volume (left) and weight (right) for different tube diameters

7.1.6 Summary

Table 7-11 summarizes the findings from the comparisons made in this section with finned tubes made of carbon steel. If the heat transferred per unit pressure drop can be increased, then the use of high serrated fins with a large fin-tip clearance is preferable. In a compact heat exchanger having a small volume and low weight, low serrated fins should be used that have a small fin pitch and that are arranged as closely together as possible.

Table 7-11: Summary of the optimization of different parameters

	Optimization for maximum transferred heat per		
	Pressure drop	**Volume**	**Weight**
Fin type (Geometries 1 & 2)	Serrated fins	Serrated fins	Serrated fins
Fin height (Geometries 4 & 7)	High fins	Low fins	Low fins
Fin pitch (Geometries 2 & 3)	No difference	Small fin pitch	No difference
Tube diameter (Geometries 1 & 4)	-	Large tubes	Large tubes
Fin-tip clearance (Geometries 4, 5 & 6)	Large clearance	Small clearance	Small clearance

Figure 7-11 illustrates the above findings. The diagrams show the heat transferred per unit volume and weight for the different tested geometries, respectively. (The fin-tip clearance was adjusted to 5mm for the large diameter tubes of Geometries 1, 2 and 3). The results indicate the following performance per unit volume and weight:

- Serrated-fin tubes (Geometries 7, 1 and 4) perform better than solid-fin tubes (Geometries 2 and 3).
- Low-fin tubes (Geometry 7) have a higher performance than high-fin tubes (Geometry 4).
- Large diameter tubes (Geometry 1) transfer more heat than small diameter tubes (Geometry 4).
- Denser fins (Geometry 2 compared to Geometry 3) are better for achieving a smaller heat exchanger volume.
- An arrangement with a small fin-tip clearance yields a higher performance (Figure 7-9).

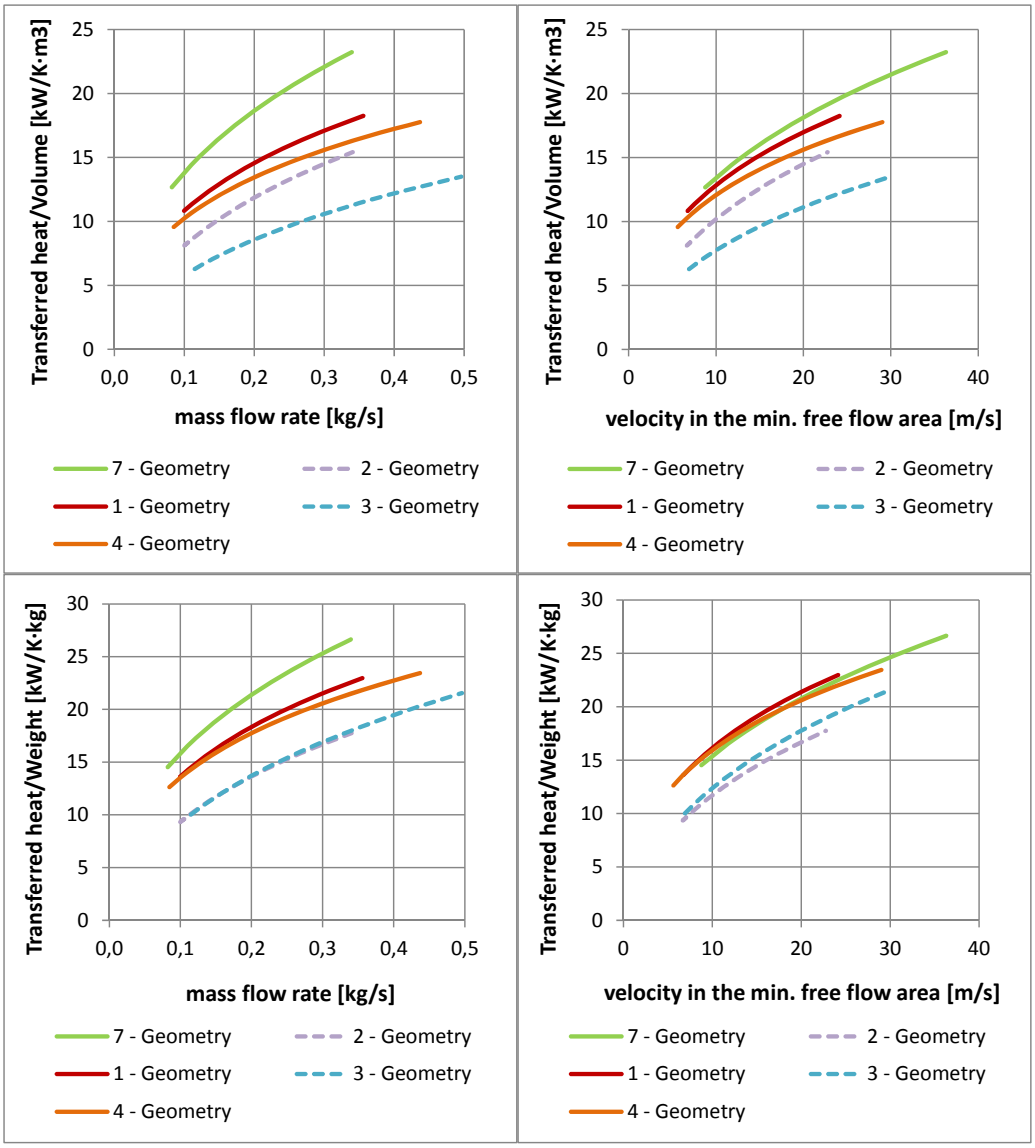

Figure 7-11: Transferred heat per unit volume (left) and per unit weight (right) for the different geometries tested with an adjusted fin-tip clearance of 5mm

In order to see an general effect of the geometry parameters on the performance on the finned tube bundles an ideal heat transfer was assumed, represented by a fin efficiency of unity (η_f = 1). For the comparison the experimental Nusselt and Euler numbers were used and the transferred heat

per unit Volume and per unit pressure drop was calculated. The results are shown in the Table 7-12 and Figure 7-12. It can be seen, that the ratio of the transferred heat per unit volume and pressure drop has in general increased. The findings summarized in the table, are the same to those for carbon steel tubes. There are only two differences on the influence of the fin height and the tube diameter.

Lower fin tubes have a higher transferred heat per unit volume for the same mass flow rate. If they are compared for the same velocity in the minimum free flow area, high finned tubes perform better. As the minimum flow area for a low finned tube bundle is small the velocity is higher, which yields a higher heat transfer coefficient.

The effect of the bigger attached fin respectively heat transfer surface of larger tube diameter seems to be more visible for an assumed ideal heat transfer.

Table 7-12: Summary of the optimization of different parameters with an ideal heat transfer

	Maximum transferred heat per	
	Pressure drop	**Volume**
Fin type (Geometries 1 & 2)	Serrated fins	Serrated fins
Fin height (Geometries 4 & 7)	High fins	High fins[1] Low fins[2]
Fin pitch (Geometries 2 & 3)	No difference	Small fin pitch
Tube diameter (Geometries 1 & 4)	Large tubes	Large tubes
Fin-tip clearance (Geometries 4, 5 & 6)	Large clearance	Small clearance

1: for the same velocity in the minimum flow area

2: for the same mass flow rate

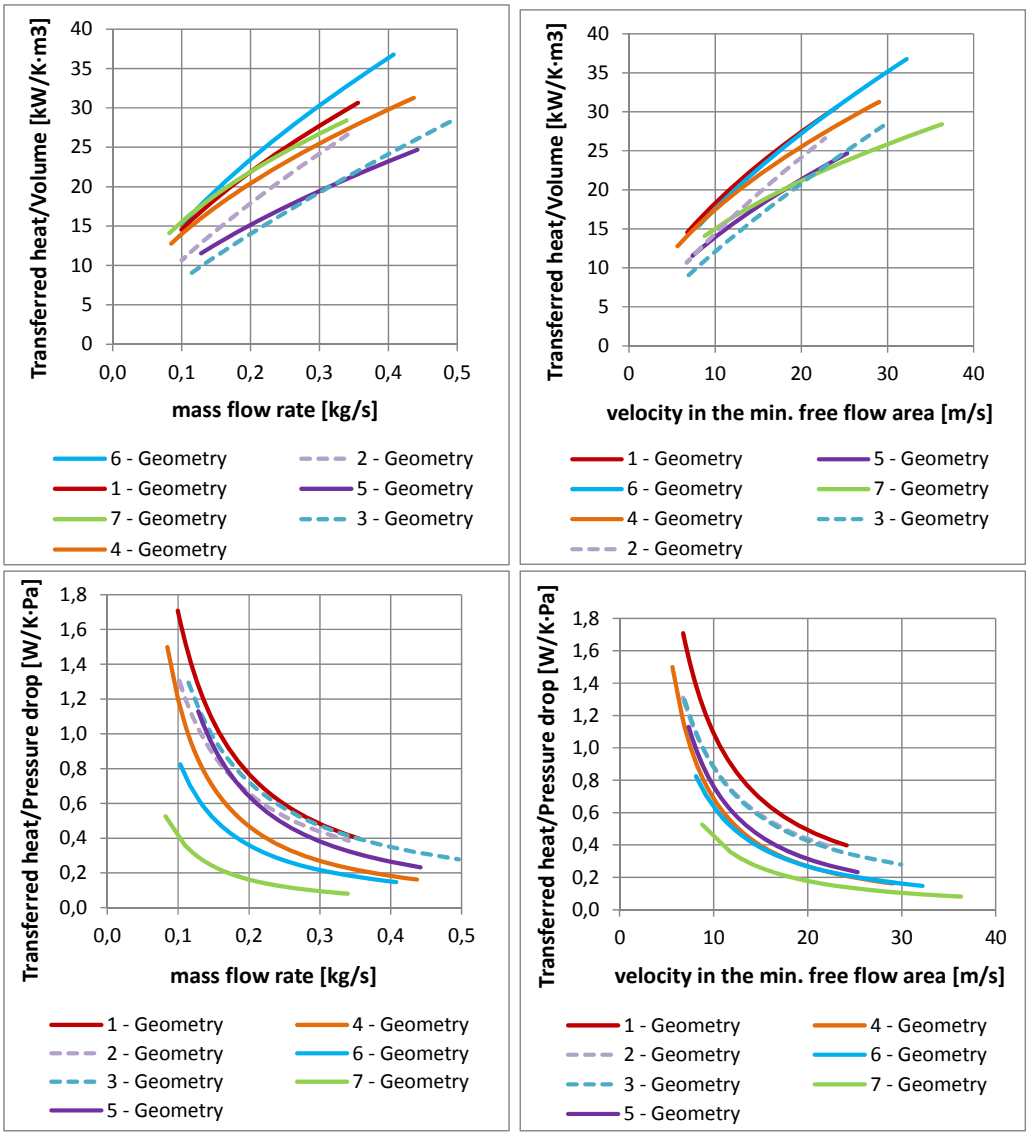

Figure 7-12: Transferred heat per unit volume (top) and per unit pressure drop (bottom) for the different geometries tested with an assumed ideal heat transfer

7.2 Optimization of tube bundle for a given design case

To optimize the design of a compact WHRU, the correlations developed in chapter 6 were used. For a real application scenario it was assumed that heat is recovered form a gas turbine exhaust gas. The tubes used in the finned tube heat exchanger are made of carbon steel.

In addition, the boundary conditions were defined as follows:

1. The mass flow rate ṁ on the gas side is set to 90kg/s.
2. The maximum allowed pressure drop over the tube bundles Δp_{max} is 3000Pa.
3. The tube bundle inlet flow cross-sectional area measures 3.0m x 6.0m.
4. The average gas temperature is assumed to be 300°C, and all gas properties were calculated at this temperature.
5. The coolant side was excluded by assuming constant conditions and using only the air side heat transfer coefficient h_{air} for the calculation of the transferred heat (see Eq. 7-3).

Condition 1 corresponds to the gas flow from a gas turbine, as reported in Walnum et al. (2013). Conditions 2 and 3 accord with the assumptions and findings of Skaugen et al. (2014).

The air inlet section is 3.0m x 6.0m. For a given tube and tube bundle geometry the minimum free-flow area $A_{f,min}$, the maximum velocity in the tube bundle u_{max} (Eq. 7-2) and the Reynolds number Re can be calculated.

$$u_{max} = \frac{\dot{m}_{gas}}{\rho_{gas} \cdot A_{f,min}} \qquad \textit{Eq. 7-2}$$

With the Reynolds number Re and Eq. 6-10 and Eq. 6-12, respectively (depending on the fin type), the Euler number Eu and the pressure drop per tube row can be calculated. The 3000 Pa maximum allowed pressure drop defines the maximum number of longitudinal tube rows N_l. With the Reynolds number Re and Eq. 6-6 and Eq. 6-8, respectively (again depending on the fin type) the Nusselt number Nu and the heat transfer coefficient h_{air} can be determined. The heat recovered from the hot turbine exhaust gas is calculated using Eq. 7-3.

$$Q = h_{air} \cdot \left(\eta_f \cdot A_{0,f} + A_{0,t} \right) \cdot \Delta T \qquad \textit{Eq. 7-3}$$

Table 7-13 shows the reference geometry and the variation range of each parameter. The tube bundle layout was kept constant at an angle of β = 30°.

Table 7-13: Geometry parameters

	Fin type	**Tube diameter**	**Fin height**	**Number of fins**	**Fin-tip clearance**
	-	**d_o [mm]**	**h_f [mm]**	**N_f [1/m]**	**c_f [mm]**
Reference (0)		20	10	250	5
Variations (n)	Serrated / Solid	10 - 34	5 - 20	150 - 350	0 - 10

For each geometry the heat transferred per unit pressure drop (Eq. 7-4) and the heat transferred per unit tube bundle volume (Eq. 7-5) was calculated with Q' = Q/ΔT being the heat transferred per unit temperature difference.

$$\frac{Q'}{dp} = \frac{h_{air} \cdot \left(\eta_f \cdot A_{0,f} + A_{0,t} \right)}{dp_{tb}} \qquad \textit{Eq. 7-4}$$

$$\frac{Q'}{V} = \frac{h_{air} \cdot \left(\eta_f \cdot A_{0,f} + A_{0,t} \right)}{V_{tb}} \qquad \textit{Eq. 7-5}$$

Figure 7-13 and Figure 7-14 show the change in the variation with respect to the reference geometry for serrated-fin and solid-fin tubes by varying one parameter at the time. The optimum would maximise the heat transferred per unit volume and per unit pressure drop. This would be signified in the upper right quadrant in the figure. The arrows indicate the increase of each geometric parameter (tube diameter d_o, fin height h_f, number of fins N_f, fin-tip clearance c_f).

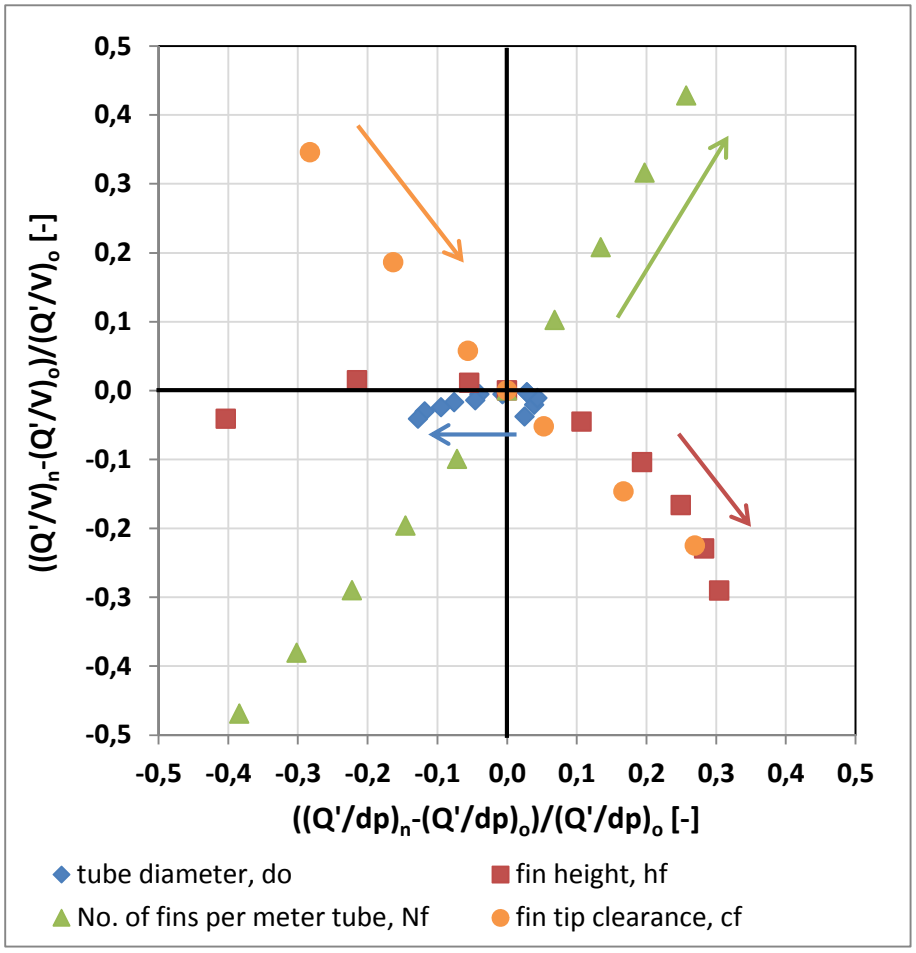

Figure 7-13: Serrated-fin variations (arrows indicate an increase in the respective parameter)

For serrated-fin tubes (Figure 7-13), the following is observed:

- Tube diameter d_o has little influence on the performance of the tube bundle. The heat transferred per unit volume varies within 5%. Only the heat transferred per unit pressure drop is reduced in larger tube diameters, pointing slightly toward the use of smaller diameter tubes.
- Lower fins lead to a reduced heat transfer per unit pressure drop. Increasing the fin height h_f leads to higher heat transfer per pressure drop; however, the heat transferred per unit volume is reduced as the

design moves away from that of a compact tube bundle. (The degree of serration was kept at 0.5 for this comparison.)

- Increasing the number of fins N_f has a positive effect on the heat transferred per unit volume and per unit pressure drop. A high fin density should be applied in compact tube trundles.
- Fin-tip clearance c_f should be low in compact tube bundles, as increasing the fin-tip clearance reduces the heat transferred per unit volume, while increasing the heat transferred per unit pressure drop.

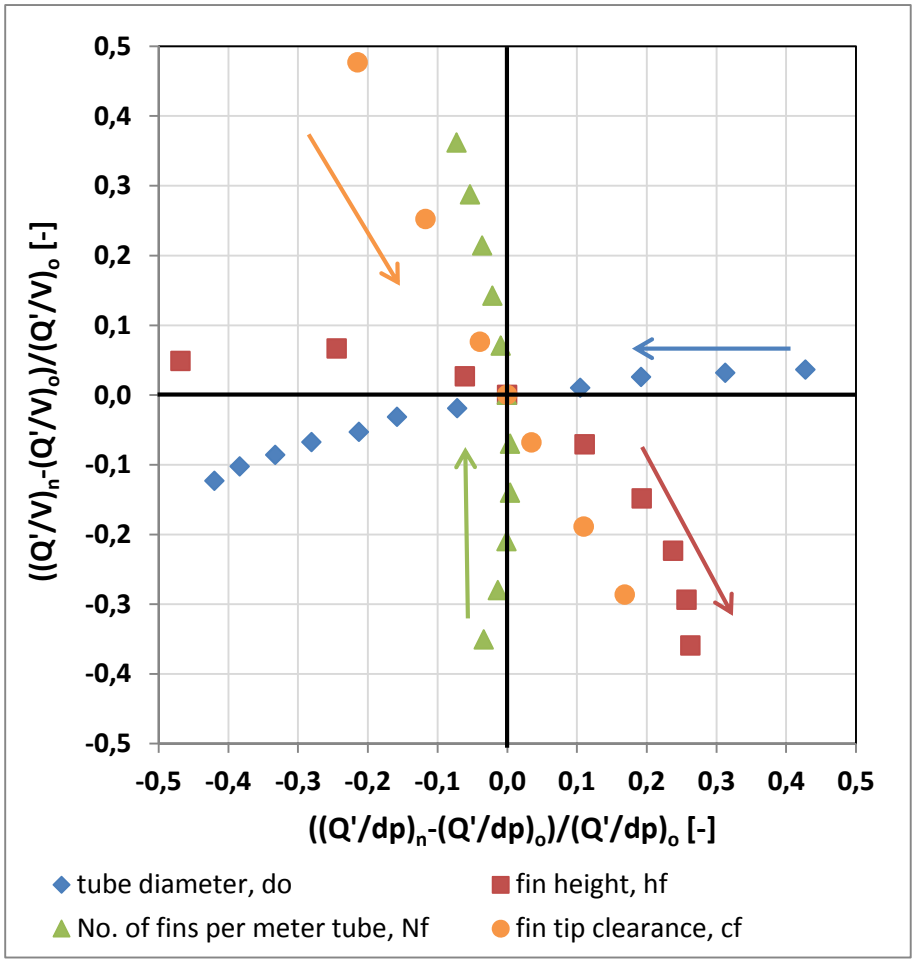

Figure 7-14: Solid-fin variations (arrows indicate an increase in the respective parameter)

For solid-fin tubes (Figure 7-14), the following is observed:

- Tube diameter d_o has little influence on the heat transferred per unit volume However, the heat transferred per unit pressure drop is influenced significantly, showing clearly that smaller, rather than larger, tube diameters yield better results.
- Lower fin height h_f leads to an increase in the heat transferred heat per unit volume and a reduction in the heat transferred per unit pressure drop. For serrated-fin tubes, increasing the fin height leads to a higher amount of heat transferred per unit pressure drop; however, the heat transfer per unit volume ratio is reduced.
- The number of fins N_f is positively correlated with the heat transferred per unit volume, but seems to have only a minor effect on the heat transferred per unit pressure drop.
- Fin-tip clearance c_f should be kept low for compact tube bundles. Increasing the fin-tip clearance reduces the heat transferred per unit volume and increases the heat transferred heat per unit pressure drop.

From this comparison, the optimal tube parameters for a compact WHRU tube bundle can be summarised as follows:

- a small tube diameter (for solid-fin tubes),
- low fin height,
- high fin density and
- a tube arrangement that is as closely packed as possible.

7.3 Summary

Table 7-14 and Table 7-15 summarize the findings from the comparison of the heat transfer performances of the tested geometries with respect to pressure drop, volume and weight and of the proposed optimization for the given design case. Based on the results of this study, depending on the optimization goal, different finned tubes are recommended.

To achieve a maximized heat transfer per unit pressure drop, the experimental results and the newly obtained correlations agree on the use of high fins and a large fin-tip clearance. However, there is disagreement in the findings with respect to fin type. From the experimental results, the use of serrated-fin tubes is suggested, but the correlations suggest the use of solid-fin tubes.

To optimise the heat transferred per unit volume and weight, the experimental results and the correlations agree that finned tubes should have a low fin height so that a large number of fins can be used as well as a fin-tip clearance that is as small as possible. With respect to solid-fin tubes, the correlations indicate that a small tube diameter is beneficial for compact and light-weight tube bundles. For serrated-fin tubes, the correlations show no clear trend with respect to the influence of the tube diameter on the heat transferred per unit volume. Regarding the heat transferred per unit weight, larger tube diameters seem to be beneficial. The experiments performed with serrated-finned tubes also showed that larger tube diameters transfer more heat per unit volume and weight.

Table 7-14: Experimental results on the influence of parameter on the heat transferred per unit pressure drop, volume and weight

Parameter	**Heat transferred per unit pressure drop is higher for**	**Heat transferred per unit volume is higher for**	**Heat transferred per unit weight is higher for**
Fin type	Serrated	Serrated	Serrated
Tube diameter d_o	*Not measured*	Large	Large
Fin height h_f	High	Low	Low
Number of fins N_f	No difference	Large	No difference
Fin-tip clearance c_f	Large	Small	No difference

Table 7-15: Correlation results on the influence of parameter on the heat transferred per unit pressure drop, volume and weight

Parameter	**Heat transferred per unit pressure drop is higher for**	**Heat transferred per unit volume is higher for**	**Heat transferred per unit weight is higher for**
Fin type	Solid	No clear trend	Serrated
Tube diameter d_o	No clear trend/Small*	No clear trend/Small*	Large/Small*
Fin height h_f	High	Low	Low
Number of fins N_f	Small	Large	Large
Fin-tip clearance c_f	Large	Small	Small

*Results for serrated / solid-fin tubes

8 SUMMARY, CONCLUSION AND RECOMMENDATIONS

8.1 Summary and conclusions

Finned tubes have the advantage of an extended heat transfer surface, which is beneficial for heat exchangers used, for example, to recover heat from hot gases, such as waste heat recovery units where the effective heat transfer coefficient on the exhaust side is orders of magnitude lower than that on the working fluid side. In this study, literature was reviewed, experimental data collected and correlations developed with respect to thermal-hydraulic performance. Gaps in published experimental data were identified, as well as discrepancies in the findings. On this basis, an experimental test setup was built to measure heat transfer and pressure drop in finned tube bundles and an experimental programme was undertaken. The research goal was to define design criteria for compact and light-weight waste heat recovery units and to make the associated data available.

Eight different tube bundles were tested. The finned tubes in each tube bundle were arranged in four transverse and eight longitudinal active tube rows in a staggered arrangement and with an equilateral 30° layout. The tested geometrical range of the tubes is shown in the Table 8-1.

Table 8-1: Range of the tested parameters

Parameter	**Tested range**
Fin type	Serrated and Solid
Tube diameter d_o	13.5 – 31.75 mm
Fin height h_f	10 – 18 mm
Number of fins N_f	170 – 356 1/m
Fin-tip clearance c_f	0 – 10mm

The experiments showed that the tube and tube bundle parameters had an impact on both the heat transfer coefficient as well as on the pressure drop (see Table 8-2). The heat transfer coefficient was higher for tubes with serrated fins, large diameters, high fins and those with a small number of fins per tube.

The pressure drop decreased for tubes with a small diameter, and in those with lower fins, larger fin pitch and a large fin-tip clearance.

Table 8-2: Influence of parameter on the heat transfer and pressure drop

Parameter	**Heat transfer coefficient / Nusselt number is increased**	**Pressure drop / Euler number is decreased**
Fin type	Serrated	No difference
Tube diameter d_o	Large	Small
Fin height h_f	High	Low
Number of fins N_f	Small	Small
Fin-tip clearance c_f	No difference	Large

Most of the published correlations were determined on the basis of only the experiments performed by the authors and therefore have limited validity. For generating more general correlations; experimental data from various authors was collected. Together with the experimental data from this study, the collected data were used to develop new correlations for predicting heat transfer and pressure drop for serrated- and solid-fin tubes. These new correlations have a wider validity range and can predict 95% of the data to within 21% and 26%, respectively, for heat transfer and within 34% for pressure drop.

The design implications depend on the target optimization desired for the waste heat recovery unit in question. If the aim is to optimize heat transfer and pressure drop, then the tubes should have high fins, with a large fin pitch and large tube pitch. However, if the aim is to have a small and light-weight unit, the fins should be serrated and be low in height, the number of fins should be large and a dense tube arrangement should be used to minimize the space used.

8.2 Recommendations for further work

The scope of this study was restricted to focusing on a limited set of parameters. Based on the literature reviewed and the experiments conducted, new research questions arise:

1. How uneven is the heat transfer distribution and how should fin efficiency be addressed? This issue is especially relevant for new materials when fin materials with different thermal conductivities are considered.
2. What is the influence of the degree of serration on heat transfer and pressure drop?
3. What alternative fin and tube materials could be used to further decrease the weight of the tube bundle in waste heat recovery units?
4. How does the tube layout, especially in a tube with larger tube bundle layout angles, influence the volume and weight of the tube bundle?
5. Can numerical analysis help in the understanding of the flow structure inside tube bundles and be used to forecast the heat transfer and pressure drop behaviour outside the validity range of correlations?

A review was conducted as part of the present study of the different corrections for fin efficiency accounting for uneven heat transfer distribution. Some corrections have only a small impact, but others correct the fin efficiency quite strongly, especially for solid-fin tubes. There is no clear trend visible in the corrections in terms of their magnitude, or whether only the tube geometry or the fluid flow influences the uneven heat transfer distribution.

The degree of serration determines the percentage of serration present on a fin, from 0% for a solid-fin to 100% for a serrated L-foot fin tube. It is unknown what influence the degree of serration has on heat transfer and pressure drop. Also, for low-fin tubes in particular, where the serration is small, less than 50%, this might be an important question.

Most authors used a 30° tube bundle layout for their investigations as it appears to be the most compact. However, there is data lacking on the influence of the tube angle, especially in the range between 45° to 90°.

Today, waste heat recovery unit tube bundles are manufactured from steel. Finding and using a high-conductivity light-weight material suitable for high-temperature applications could further improve the weight of the tube bundle. Titanium alloys may be a possibility.

REFERENCES

ACKERMAN, J. W. & BRUNSVOLD, A. R. 1970. Heat Transfer and Draft Loss Performance of Extended Surface Tube Banks. *Journal of Heat Transfer, Transactions ASME,* 92 Ser C**,** 215-220

BAEHR, H. D. & STEPHAN, K. 2006. *Heat and Mass Transfer,* Berlin, Heidelberg, Springer-Verlag Berlin Heidelberg

BELL, J. H. & MEHTA, R. D. 1988. Contraction design for small low-speed wind tunnels. *JIAA TR - 84.* Joint Institute for Aeronautics and Acoustics

BRAUER, H. 1961. Wärme- und strömungstechnische Untersuchungen an quer angeströmten Rippenrohrbündeln. Teil 2: Einfluß der Rippen- und der Rohranordnung. *Chemie Ingenieur Technik,* 33**,** 431-438

BRAUER, H. 1964. Compact heat exchangers. *Chem. Prog. Eng.,* 45**,** 315-321

BRIGGS, D. E. & YOUNG, E. H. 1963 Convection heat transfer and pressure drop of air flowing across triangular pitch banks of finned tubes. Chemical Engineering Process Symposium Series, 1963. 1-10

CHU, C. M. & RALSTON, T. 1998. HTFS2: Improved models for heat transfer and pressure drop applied to staggered arrangements of tubes with plain helical fins. HTFS RS 1036

CLÉIRIGH, C. T. Ó. & SMITH, W. J. 2014. Can CFD accurately predict the heat-transfer and pressure-drop performance of finned tube bundles? *Applied Thermal Engineering,* 73**,** 681-690

COX, B. 1973. Heat transfer and pumping power performance in tube banks: finned and bare. *ASME Paper 73-HT-27.*

EDENHOFER, O., PICHS-MADRUGA, R., SOKONA, Y., FARAHANI, E., KADNER, S., SEYBOTH, K., ADLER, A., BAUM, I., BRUNNER, S. & EICKEMEIER, P. 2014. Climate change 2014: Mitigation of climate change. *Contribution of Working Group III to the Fifth Assessment Report of the Intergovernmental Panel on Climate Change***,** 511-597

FIEBIG, M., VALENCIA, A. & MITRA, N. K. 1993. Wing-type vortex generators for fin-and-tube heat exchangers. *Experimental Thermal and Fluid Science,* 7**,** 287-295

GARDNER, K. A. 1945. Efficiency of extended surfaces. *Trans. ASME,* 67

GNIELINSKI, V. 1975. Neue Gleichungen für den Wärme- und den Stoffübergang in turbulent durchströmten Rohren und Kanälen. *Forschung im Ingenieurwesen,* 41**,** 8-16

HASHIZUME, K. 1981. Heat Transfer and Pressure Drop Characteristics of Finned Tubes in Cross Flow. *Heat Transfer Engineering,* 3**,** 15-20

HASHIZUME, K., MORIKAWA, R., KOYAMA, T. & MATSUE, T. 2002. Fin Efficiency of Serrated Fins. *Heat Transfer Engineering,* 23**,** 6-14

HENRY, J. A. R. 1994. Effect of fin frequency and tube pitch on bundle pressure loss. HTFS RS 953

HOFMANN, R. 2009. *Experimental and Numerical Gas-Side Performance Evaluation of Finned tube Heat Exchangers.* Dr-Ing thesis, Technische Universität Wien

HU, X. & JACOBI, A. M. 1993. Local heat transfer behavior and its impact on a single-row, annularly finned tube heat exchanger. *Journal of heat transfer,* 115**,** 66-74

ISO5167-1 2003. Measurement of fluid flow by means of pressure differential devices inserted in circular cross-section conduits running full - Part 1: General principles and requirements.

ISO5167-2 2003. Measurement of fluid flow by means of pressure differential devices inserted in circular cross-section conduits running full - Part 2: Orifice plates.

JAMESON, S. L. 1945. Tube spacing in finned tube banks. *Trans. ASME,* 67**,** 633-642

KAWAGUCHI, K., OKUI, K., ASAI, T. & HASEGAWA, Y. 2006a. The heat transfer and pressure drop characteristics of finned tube banks in forced

convection (effects of fin height on pressure drop characteristics). *Heat Transfer—Asian Research,* 35**,** 179-193

KAWAGUCHI, K., OKUI, K., ASAI, T. & HASEGAWA, Y. 2006b. The heat transfer and pressure drop characteristics of the finned tube banks in forced convection (effects of fin height on heat transfer characteristics). *Heat Transfer—Asian Research,* 35**,** 194-208

KAWAGUCHI, K., OKUI, K. & KASHI, T. 2004. The heat transfer and pressure drop characteristics of finned tube banks in forced convection (comparison of the pressure drop characteristics of spiral fins and serrated fins). *Heat Transfer—Asian Research,* 33**,** 431-444

KAWAGUCHI, K., OKUI, K. & KASHI, T. 2005. Heat transfer and pressure drop characteristics of finned tube banks in forced convection (comparison of the heat transfer characteristics between spiral fin and serrated fin). *Heat Transfer—Asian Research,* 34**,** 120-133

KAYS, W. M., CRAWFORD, M. E. & WEIGAND, B. 2005. *Convective heat and mass transfer,* Boston, McGraw-Hill

KAYS, W. M. & LONDON, A. L. 1984. *Compact heat exchangers 3rd edition,* New York, McGraw-Hill

KRÜCKELS, W. & KOTTKE, V. 1970. Untersuchung über die Verteilung des Wärmeübergangs an Rippen und Rippenrohr-Modellen. *Chemie Ingenieur Technik,* 42**,** 355-362

LEMOUEDDA, A., SCHMID, A., FRANZ, E., BREUER, M. & DELGADO, A. 2011. Numerical investigations for the optimization of serrated finned tube heat exchangers. *Applied Thermal Engineering,* 31**,** 1393-1401

LUNDBERG, S. 1997. TALAT Lecture 2502 - Material Aspects of Fire Design. *Training in Aluminium Application Technologies.* Training in Aluminium Application Technologies

LYMER, A. & RIDAL, B. 1961 Finned Tubes in a Cross-Flow of Gas. J. Brit. Nuclear Energy Conf., 1961. Flexibox Ltd., Manchester, Eng., 301-313

MA, Y., YUAN, Y., LIU, Y., HU, X. & HUANG, Y. 2012. Experimental investigation of heat transfer and pressure drop in serrated finned tube banks with staggered layouts. *Applied Thermal Engineering,* 37**,** 314-323

MCILWAIN, S. R. 2003. *Improved Prediction Methods of Finned Tube Bundle Heat Exchangers in Crossflow.* PhD Thesis PhD Thesis, University of Strathclyde

MCKETTA, J. J. 1992. *Heat transfer design methods,* New York, Marcel Dekker

MEHTA, R. D. & BRADSHAW, P. 1979. Design rules for small low speed wind tunnels. *Aeronautical Journal,* 83**,** 443-449

MIETH, H. C. 1970. Method for Heat Transfer Calculation of Helical-Wound Fin Tubes. *ASME-70, Pet 4,*

MINITAB. 2015. *Minitab Statistical Software,* http://www.minitab.com/en-us/products/minitab/. [Accessed 2015-03-22

MIRKOVIC, Z. 1974. Heat transfer and flow resistance correlation for helically finned and staggered tube banks in crossflow. *In:* AFGAN, N. H. & SCHLÜNDER, E. U. (eds.) *Heat Exchanger: Design and Theory Source Book.* New York: McGraw-Hill

MOFFAT, R. J. 1988. Describing the uncertainties in experimental results. *Experimental Thermal and Fluid Science,* 1**,** 3-17

MON, M. S. 2003. *Numerical Investigation of Air-Side Heat Transfer and Pressure Drop in Circular Finned tube Heat Exchangers.* Dr.-Ing thesis, TU Bergakademie Freiberg

NEAL, S. B. H. C. & HITCHCOCK, J. A. 1967 A study of the heat transfer processes in banks of finned tubes in cross flow, using a large scale model technique. pp 290-8 of Proceedings of the Third International Heat Transfer Conference, Chicago, Illinois, August 7--12, 1966. Volume III. New York, American Institute of Chemical Engineers, 1966., 1967. Central Electricity Research Labs., Leatherhead, Eng.,

NIR, A. 1991. Heat transfer and friction factor correlations for crossflow over staggered finned tube banks. *Heat Transfer Engineering,* 12**,** 43-58

NÆSS, E. 2005. Heat Transfer and Pressure Drop in Serrated-Fin Tube Bundles for Waste Heat Recovery Applications. *Proceedings of 6th World Conference on Heat Transfer Fluid Mechanics and Thermodynamics.* Matsushima:

NÆSS, E. 2007. *An experimental study of heat transfer and pressure drop in serrated-fin tube bundles and investigation of particulate fouling in waste heat recovery heat exchangers.* Dr.-Ing. thesis NTNU 2007:70 PhD thesis NTNU 2007:70, Norwegian University of Science and Technology

NÆSS, E. 2010. Experimental investigation of heat transfer and pressure drop in serrated-fin tube bundles with staggered tube layouts. *Applied Thermal Engineering,* 30**,** 1531-1537

O'BRIEN, J., SOHAL, M. & WALLSTEDT, P. 2003 Heat Transfer Testing of Enhanced Finned tube Bundles Using the Single-Blow Technique. 2003. ASME,

PETUKHOV, B. 1970. Heat transfer and friction in turbulent pipe flow with variable physical properties. *Advances in heat transfer,* 6**,** i565

PFR 1976. Heat Transfer and Pressure Drop Data Characteristics of Dry Tower Extended Surfaces. PFR Report BNWL-PFR-7-100: PFR Engineering Systems Inc.

RALSTON, T., BYSKOV, R. K., FARRANT, P. E. & CHU, C. M. 1997. HTFS models for heat transfer and pressure drop applied to staggered arrangements of tubes with plain helical fins. HTFS RS 1016:

REDDY, T. A. 2011. *Applied Data Analysis and Modeling for Energy Engineers and Scientists,* Boston, MA, Springer US

RICHTER, F. 1983. *Physikalische Eigenschaften von Stählen und ihre Temperaturabhängigkeit: Polynome und graphische Darstellungen: Mitteilung aus dem Forschungsinstitut der Mannesmann AG,* Düsseldorf, Verlag Stahleisen M.B.H.

ROBINSON, K. K. & BRIGGS, D. E. 1966 Pressure drop of air flowing across triangular pitch banks of finned tubes. Chemical Engineering Process Symposium Series, 1966. 177-184

RYGVOLD, E. M. 2010. *Varmeovergang og trykktap i varmevekslere.* MSc thesis, NTNU

SKAUGEN, G., WALNUM, H. T., HAGEN, B. A., CLOS, D. P., MAZZETTI, M. J. & NEKSÅ, P. 2014 Design and Optimization of Waste Heat Recovery Unit Using Carbon Dioxide as Cooling Fluid. ASME 2014 Power Conference, 2014. American Society of Mechanical Engineers, V001T03A006-V001T03A006

SPIRO-GILLS. 2012. *http://www.spiro-gills.com/images/heatexchangerbrochure.pdf*. [Accessed 30.11.2012]

STASIULEVIČIUS, J., SKRINSKA, A. & ŽUKAUSKAS, A. 1988. *Heat transfer of finned tube bundles in crossflow*, Hemisphere, Washington

VALSØ KLYNDERUD, T. 2014. *The influence of free-stream turbulence on heat transfer in finned tube bundles.* Master thesis, Norwegian University of Science and Technology

VAMPOLA, J. 1966. Přestup tepla a tlakové ztráty při proudění plynu svazkem žebrovaných trubek. *Strojirenstri,* 16**,** 501-507

VDI 2010. *VDI Heat Atlas,* Berlin, Heidelberg, Springer

WALNUM, H. T., NEKSÅ, P., NORD, L. O. & ANDRESEN, T. 2013. Modelling and simulation of CO2 (carbon dioxide) bottoming cycles for offshore oil and gas installations at design and off-design conditions. *Energy,* 59**,** 513-520

WARD, D. & YOUNG, E. 1959. Heat transfer and pressure drop of air in forced convection across triangular pitch banks of finned tubes. *Chemical Engineering Progress Symposium Series.*

WEBB, R. L. & KIM, N.-H. 2005. *Principles of enhanced heat transfer,* Boca Raton, Taylor & Francis

WEIERMAN, C. 1976. Correlations ease the selection of finned tubes. *Oil and Gas Journal,* 74**,** 94-100

WEIERMAN, C. 1977. Pressure drop data for heavy-duty finned tubes. *Chemical Engineering Progress,* 73**,** 69-72

WEIERMAN, C., TABOREK, J. & MARNER, W. J. 1978. Comparison of the performance of in-line and staggered banks of tubes with segmented fins. *AIChE Symposium Series,* 74**,** 39-46

WORLEY, N. G. & ROSS, W. 1960. Heat transfer and pressure loss characteristics of cross-flow tubular arrangements with studded surfaces. *Inst. Mech. Engrs.***,** 15 - 26

YUDIN, V. & TOKHTOROVA, L. 1973. Investigation of the correction factor Ψ for the theoretical effectiveness of a round fin. *Teploenergetika,* 20**,** 48-50

ZOZULYA, N. V., VOROBYEV, Y. P. & KHAVIN, A. A. 1973. Effect of Flow Turbulization on Heat Transfer in a Finned Tube Bundle. *Heat Transfer Soviet Research,* 5**,** 154-156

ŽUKAUSKAS, A., STASIULEVIČIUS, J. & SKRINSKA, A. 1966 Experimental Investigation of Efficiency of Heat Transfer of a Tube with Spiral Fins in Cross-Flow. 3rd International Heat Transfer Conference, 1966 Chicago. 299-305

APPENDIX

I. Published literature correlations

Heat Transfer – Serrated-fin tubes

Reference	Correlation	Validity / Test geometries
Worley and Ross (1960)	$Nu = 0.125 \cdot Re^{0.7} \cdot Pr^{1/3}$	Based on own experimental data 20 000 ≤ Re 38.1mm ≤ d_o ≤ 63.5mm 15.88mm ≤ h_f ≤ 31.75mm 5.07mm ≤ s_f ≤ 12.7mm 2.38mm ≤ t_f ≤ 3.18mm 79.38mm ≤ P_t ≤ 177.8mm 63.5mm ≤ P_l ≤ 88.9mm
Mieth (1970) [see Næss (2007)]	$Nu = 0.412 \cdot Re^{0.59} \cdot Pr^{1/3} \cdot \left(\frac{s_f}{h_f}\right)^{0.3} \cdot \left(\frac{s_f}{t_f}\right)^{0.1}$	Not specified
Weierman (1976), [See McKetta (1992)]	$Nu = 0.25 \cdot Re^{0.65} \cdot Pr^{1/3} \cdot \left[0.55 + 0.45 \cdot e^{\left(-0.35 \cdot h_f / s_f\right)}\right] \cdot \left[0.7 + \left(0.7 - 0.8 \cdot e^{-0.15 \cdot N_l^2}\right) \cdot \left(e^{-P_l / P_t}\right)\right] \cdot \left(\frac{d_f}{d_o}\right)^{0.5} \cdot \left(\frac{T_b}{T_w}\right)^{0.25}$	Based on own experimental data 0.7 kg/s m^2≤ j_{max} ≤ 40.7 kg/s m^2
PFR (1976)	$Nu = 0.195 \cdot Re^{0.7} \cdot Pr^{1/3} \cdot Ar^{-0.17}$	Based on data of various authors 1 000 ≤ Re ≤ 40 000 4 ≤ Ar ≤ 34 9.53mm ≤ d_o ≤ 50.8mm 1.524m/s ≤ u ≤ 7.62m/s $1.75 \cdot 10^{-5}$ Pa s ≤ η ≤ $2.1 \cdot 10^{-5}$ Pa s

Heat Transfer – Serrated-fin tubes

Reference	Correlation	Validity / Test geometries
Nir (1991)	$Nu = 1.0 \cdot Re^{0.6} \cdot Pr^{1/3} \cdot \left(\frac{A_{ht}}{A_{f,min}}\right)^{-0.266} \cdot \left(\frac{A_{f,min}}{A_{f,fin}}\right)^{-0.4} \cdot \left(\frac{d_f}{d_o}\right)^{-0.4}$	Based on data of various authors $300 \le Re_h \le 10\,000$ $10 \le (A_{ht}/A_{f,min}) \le 60$ $1.0 \le (A_{f,min}/A_{f,fin}) \le 3.0$ $N_l \ge 4$
Kawaguchi et al. (2005)	$Nu = 0.0635 \cdot Re_{dv}^{0.784} \cdot Pr^{1/3} \cdot \left(\frac{g_f}{d_v}\right)^{-0.062}$ $d_v = d_o + 2 \cdot h_f \cdot t_f \cdot N_f$	Based on own experimental data $7\,000 \le Re_v \le 50\,000$ $0.112 \le (h_f/d_v) \le 0.198$ $N_l = 6$
Kawaguchi et al. (2006b)	$5\,000 \le Re_v \le 30\,000$: $Nu = 0.068 \cdot Re_{dv}^{0.81} \cdot Pr^{1/3} \cdot \left(\frac{h_f}{d_v}\right)^{0.24} \cdot \left(\frac{g_f}{s_f}\right)^{-0.07}$ $30\,000 \le Re_v \le 50\,000$: $Nu = 0.041 \cdot Re_{dv}^{0.88} \cdot Pr^{1/3} \cdot \left(\frac{h_f}{d_v}\right)^{0.44} \cdot \left(\frac{g_f}{s_f}\right)^{-0.38}$ $d_v = d_o + 2 \cdot h_f \cdot t_f \cdot N_f$	Based on own experimental data $0.31 \le (h_f/d_v) \le 0.45$ $0.76 \le (g_f/s_f) \le 0.82$ $N_l = 6$
Hofmann (2009)	$Nu = 0.36475 \cdot Re^{0.6013} \cdot Pr^{1/3} \cdot \left[1 - 0.392 \cdot \log\left(\frac{N_{l,\infty}}{N_l}\right)\right]$	Based on own experimental data $4\,500 \le Re \le 35\,000$ $15.5\text{mm} \le h_f \le 20\text{mm}$ $0.8\text{mm} \le t_f \le 1.0\text{mm}$ $3.39\text{mm} \le s_f \le 3.62\text{mm}$ $1 \le N_l \le 8$

Heat Transfer – Serrated-fin tubes

Reference	**Correlation**	**Validity / Test geometries**
Næss (2010)	$Nu = 0.107 \cdot Re^{0.65} \cdot Pr^{1/3} \cdot \left(\frac{P_t}{d_o}\right)^{0.35} \cdot \left(\frac{h_f}{d_o}\right)^{-0.13} \cdot \left(\frac{h_f}{s_f}\right)^{-0.14} \cdot \left(\frac{s_f}{d_o}\right)^{-0.2}$	Based on own experimental data $2\,000 \le Re \le 60\,000$ $1.75 \le (P_t/d_o) \le 3.82$ $0.26 \le (h_f/d_o) \le 0.42$ $1{,}69 \le (h_f/s_f) \le 3.13$ $0.13 \le (s_f/d_o) \le 0.24$ $N_l = 8$
Ma et al. (2012)	$Nu = 0.117 \cdot Re^{0.717} \cdot Pr^{1/3} \cdot \left(0.6 + 0.4 \cdot e^{-\frac{250}{Re} \cdot \frac{h_f}{s_f}}\right) \cdot \left(\frac{P_t}{P_l}\right)^{0.06}$	Based on own experimental data $4\,000 \le Re \le 30\,000$ $5.0 \le (h_f / g_f) \le 5.5$ $0.75 \le (P_t / P_l) \le 1.30$ $N_l = 8$

Heat Transfer – Solid-fin tubes

Reference	**Correlation**	**Validity / Test geometries**
Ward and Young (1959)	$Nu = 0.364 \cdot Re^{0.68} \cdot Pr^{1/3} \cdot \left(\frac{d_f}{d_o}\right)^{0.45} \cdot \left(\frac{t_f}{d_f}\right)^{0.3}$	Based on own experimental data $1\,000 \le Re \le 28\,000$ $1.18 \le (d_f/d_o) \le 2.04$ $0.007 \le (t_f/d_f) \le 0.025$
Briggs and Young (1963)	$Nu = 0.134 \cdot Re^{0.681} \cdot Pr^{1/3} \cdot \left(\frac{g_f}{h_f}\right)^{0.2} \cdot \left(\frac{g_f}{t_f}\right)^{0.1134}$	Based on own experimental data $1\,100 \le Re \le 18\,000$ $0.13 \le (g_f/h_f) \le 0.66$ $1.0 \le (g_f/t_f) \le 6.6$
Weierman (1976), [See McKetta (1992)]	$Nu = 0.25 \cdot Re^{0.65} \cdot Pr^{1/3} \cdot \left[0.35 + 0.65 \cdot e^{\left(-0.25 \cdot h_f / s_f\right)}\right] \cdot \left[0.7 + \left(0.7 - 0.8 \cdot e^{-0.15 \cdot N_l^2}\right)\left(e^{-P_l / P_t}\right)\right] \cdot \left(\frac{d_f}{d_o}\right)^{0.5} \cdot \left(\frac{T_b}{T_w}\right)^{0.25}$	Based on own experimental data 0.7 kg/s m$^2 \le j_{max} \le 40.7$ kg/s m^2
PFR (1976)	$Nu = 0.29 \cdot Re^{0.633} \cdot Pr^{1/3} \cdot Ar^{-0.17}$	Based on data of various authors $1\,000 \le Re \le 40\,000$ $4 \le Ar \le 34$ $9.53\text{mm} \le d_o \le 50.8\text{mm}$ $1.524\text{m/s} \le u \le 7.62\text{m/s}$ $1.75 \cdot 10^{-5}$ Pa s $\le \eta \le$ $2.1 \cdot 10^{-5}$ Pa s
Stasiulevičius et al. (1988)	$Nu = 0.044 \cdot Re^{0.8} \cdot \left(\frac{P_t}{P_l}\right)^{0.2} \cdot \left(\frac{s_f}{d_o}\right)^{0.18} \cdot \left(\frac{h_f}{d_o}\right)^{-0.14}$	Based on own experimental data $20\,000 < Re < 200\,000$ $1.30 \le (P_t/P_l) \le 2.83$ $0.13 \le (h_f/d_o) \le 0.59$ $0.13 \le (s_f/d_o) \le 0.28$

Heat Transfer – Solid-fin tubes

Reference	**Correlation**	**Validity / Test geometries**
Nir (1991)	$Nu = 1.0 \cdot Re^{0.6} \cdot Pr^{1/3} \cdot \left(\frac{A_{ht}}{A_{f,min}}\right)^{-0.266} \cdot \left(\frac{A_{f,min}}{A_{f,fin}}\right)^{-0.4} \cdot \left(\frac{d_f}{d_o}\right)^{-0.4}$	Based on data of various authors $300 \le Re_h \le 10\,000$ $10 \le (A_{ht}/A_{f,min}) \le 60$ $1.0 \le (A_{f,min}/A_{f,fin}) \le 3.0$ $N_l \ge 4$
Mon (2003)	$Nu = 0.284 \cdot Re^{0.6} \cdot Pr^{1/3} \cdot Ar^{-0.15} \cdot F^{-0.75} \cdot \left(\frac{P_t}{P_d}\right)^{1.06}$ $F = \frac{1}{\frac{A_{ht}}{A_{f,min}} + 1}$	Based on own modelled data $5\,000 \le Re \le 70\,000$ $3.7 \le Ar \le 25.0$ $0.01 \le F \le 0.08$ $11.5 \le (A_{ht}/A_{f,min}) \le 92.0$ $P_t/P_d = 1$ $N_l = 4$
Kawaguchi et al. (2005)	$Nu = 0.0382 \cdot Re_{dv}^{0.787} \cdot Pr^{1/3} \cdot \left(\frac{g_f}{d_v}\right)^{-0.264}$ $d_v = d_o + 2 \cdot h_f \cdot t_f \cdot N_f$	Based on own experimental data $7\,000 \le Re_v \le 50\,000$ $0.107 \le (g_f/d_v) \le 0.185$ $N_l = 6$
Kawaguchi et al. (2006b)	$Nu = 0.045 \cdot Re_{dv}^{0.77} \cdot Pr^{1/3} \cdot \left(\frac{h_f}{d_v}\right)^{0.24} \cdot \left(\frac{g_f}{s_f}\right)^{-1.38}$ $d_v = d_o + 2 \cdot h_f \cdot t_f \cdot N_f$	Based on own experimental data $5\,000 \le Re_v \le 30\,000$ $0.32 \le (h_f/d_v) \le 0.42$ $0.76 \le (g_f/s_f) \le 0.82$ $N_l = 6$
VDI (2010)	$Nu = 0.38 \cdot Re^{0.6} \cdot Pr^{1/3} \cdot Ar^{-0.15}$	Based on experimental data of various sources $1\,000 \le Re \le 100\,000$ $5 \le Ar \le 30$ $N_l \ge 4$

Pressure Drop – Serrated-fin tubes

Reference	Correlation	Validity / Test geometries
Weierman (1976), [See McKetta (1992)]	$Eu = \left(0.28 + \frac{32}{Re^{0.45}}\right) \cdot \left(\frac{d_f}{d_o}\right)^{0.5} \cdot \left[0.11 \cdot \left(0.05 \cdot \frac{P_t}{d_o}\right)^{\left(-0.7 \cdot \left(h_f / s_f\right)^{0.23}\right)}\right] \cdot \left[1.1 + \left(1.8 - 2.1 \cdot e^{-0.15 \cdot N_l^2}\right) \cdot \left(e^{-2 \cdot P_l / P_t}\right) - \left(0.7 - 0.8 \cdot e^{-0.15 \cdot N_l^2}\right) \cdot \left(e^{-0.6 \cdot P_l / P_t}\right)\right]$	Based on own experimental data 0.7 kg/s $m^2 \leq j_{max} \leq$ 40.7 kg/s m^2
PFR (1976)	for $(P_l/d_o) \leq 4{,}0$: $Eu = 1.4 \cdot \left(\frac{13.6}{Re_h^{0.3}}\right) \cdot \left(\frac{P_l}{d_o}\right)^{-0.42}$ for $(P_l/d_o) > 4{,}0$: $Eu = 1.4 \cdot \left(\frac{150}{Re_h} + \frac{1.8}{Re_h^{0.2}}\right) \cdot \left(\frac{P_l}{d_o}\right)^{0.35}$ $d_h = 4 \cdot \left[\left(N_l - 1\right) \cdot P_l + d_f\right] \cdot \left(\frac{A_{f,min}}{A_{ht}}\right)$	Based on data of various authors $400 \leq Re_h \leq 10\,000$
Nir (1991)	$Eu = \frac{1.24}{Re^{0.25}} \cdot \left(\frac{A_{ht}}{A_{f,min}}\right)^{0.68} \cdot \left(\frac{d_f}{d_o}\right)^{-0.25}$	Based on data of various authors $300 \leq Re_h \leq 10\,000$ $8.5 \leq (A_{ht}/A_{f,min}) \leq 60$ $N_l \geq 4$
Kawaguchi et al. (2004)	$Eu = \frac{6.46}{Re_h^{0.179}} \cdot \left(\frac{g_f}{t_f}\right)^{-0.354}$ with $d_h = 4 \cdot \frac{A_{f,min}}{2 \cdot N_f \cdot \left(s_f + 2 \cdot h_f\right)}$	Based on own experimental data $3\,000 \leq Re \leq 30\,000$ $3.07 \leq (s_f/t_f) \leq 5.07$

Pressure Drop – Serrated-fin tubes

<table>
<tr><th>Reference</th><th>Correlation</th><th>Validity /
Test geometries</th></tr>
<tr><td>Kawaguchi et al. (2006a)</td><td>$Eu = \frac{4.99}{Re_h^{0.23}} \cdot \left(\frac{h_f}{d_h}\right)^{0.13} \cdot \left(\frac{g_f}{s_f}\right)^{-1.19}$ with

$d_h = 4 \cdot \frac{A_{f,min}}{2 \cdot N_f \cdot (s_f + 2 \cdot h_f)}$</td><td>Based on own experimental data

3 000 ≤ Re ≤ 30 000
0.42 ≤ (h_f/d_h) ≤ 1.08
0.76 ≤ (s_f/g_f) ≤ 0.82</td></tr>
<tr><td>Hofmann (2009)</td><td>$Eu = \left(a_{hy} + \frac{b_{hy}}{Re} + \frac{c_{hy}}{Re^2}\right) = \left(a_{po} + b_{po} Re^{c_{po}}\right)$

Coefficients of Regression:
<table><tr><td></td><td>hy - Hyperbolia</td><td>po – Power</td></tr><tr><td>a</td><td>1.3550</td><td>1.1321</td></tr><tr><td>b</td><td>-7189.7055</td><td>148575379605.4982</td></tr><tr><td>c</td><td>55970438.4750</td><td>-3.0312</td></tr></table></td><td>Based on own experimental data

4 500 ≤ Re ≤ 50 000
1 ≤N_l ≤ 8</td></tr>
<tr><td>Næss (2010)</td><td>$Eu = \left(0.24 + \frac{8.2}{Re^{0.5}}\right) \cdot \cdot \min\left(1.0\,; 0.52 + 964.5 \cdot e^{-3.24 \cdot P_t/P_l}\right) \cdot \cdot \left(\frac{h_f}{d_o}\right)^{0.18} \cdot \left(\frac{s_f}{d_o}\right)^{-0.74}$</td><td>Based on own experimental data

2 000 ≤ Re ≤ 60 000
1.75 ≤ (P_t/d_o) ≤ 3.82
0.26 ≤ (h_f/d_o) ≤ 0.42
0.13 ≤ (s_f/d_o) ≤ 0.24
N_l = 8</td></tr>
<tr><td>Ma et al. (2012)</td><td>$Eu = \frac{1.773}{Re^{0.184}} \cdot \left(\frac{h_f}{g_f}\right)^{0.556} \cdot \left(\frac{P_t}{d_o}\right)^{-0.673} \cdot \left(\frac{P_l}{d_o}\right)^{-0.133}$</td><td>Based on own modelled data

4 000 ≤ Re ≤ 30 000
5.0 ≤ (h_f/g_f) ≤ 5.5
2.3 ≤ (P_t/d_o) ≤ 3.2
2.4 ≤ (P_l/d_o) ≤ 3.1
N_l = 8</td></tr>
</table>

Pressure Drop – Solid-fin tubes

Reference	Correlation	Validity / Test geometries
Ward and Young (1959)	$Eu = \frac{0.256}{Re^{0.264}} \cdot \left(\frac{t_t}{d_f}\right)^{-0.377} \cdot \left(\frac{g_f}{d_o}\right)^{-0.396}$	Based on own experimental data $1\,000 \le Re \le 28\,000$ $0.015 \le (t_f/d_f) \le 0.05$ $0.06 \le (g_f/d_o) \le 0.27$ $N_l \ge 3$
Robinson and Briggs (1966)	$Eu = \frac{18.93}{Re^{0.316}} \cdot \left(\frac{P_t}{d_o}\right)^{-0.927} \cdot \left(\frac{P_t}{P_d}\right)^{0.515}$	Based on own experimental data $2\,000 \le Re \le 50\,000$ $1.8 \le (P_t/d_o) \le 4.6$
Weierman (1976), [See McKetta (1992)]	$Eu = \left(0.28 + \frac{32}{Re^{0.45}}\right) \cdot \left(\frac{d_f}{d_o}\right)^{0.5} \cdot \left[0.11 \cdot \left(0.05 \cdot \frac{P_t}{d_o}\right)^{\left(-0.7 \cdot \left(h_f/s_f\right)^{0.20}\right)}\right] \cdot \left[1.1 + \left(1.8 - 2.1 \cdot e^{-0.15 \cdot N_l^2}\right) \cdot \left(e^{-2 \cdot P_l/P_t}\right) - \left(0.7 - 0.8 \cdot e^{-0.15 \cdot N_l^2}\right) \cdot \left(e^{-0.6 \cdot P_l/P_t}\right)\right]$	Based on own experimental data $0.7\ kg/s\ m^2 \le j_{max} \le 40.7\ kg/s\ m^2$
PFR (1976)	for $(P_l/d_o) \le 4{,}0$: $Eu = \left(\frac{13.6}{Re_h^{0.3}}\right) \cdot \left(\frac{P_l}{d_o}\right)^{-0.42}$ for $(P_l/d_o) > 4{,}0$: $Eu = \left(\frac{150}{Re_h} + \frac{1.8}{Re_h^{0.2}}\right) \cdot \left(\frac{P_l}{d_o}\right)^{0.35}$ $d_h = 4 \cdot \left[\left(N_l - 1\right) \cdot P_l + d_f\right] \cdot \left(\frac{A_{f,min}}{A_{ht}}\right)$	Based on data of various authors $400 \le Re_h \le 10\,000$

Pressure Drop – Solid-fin tubes

Reference	Correlation	Validity / Test geometries
Stasiulevičius et al. (1988)	$Eu = \frac{13.1}{Re^{0.25}} \cdot \left(\frac{P_t}{d_o}\right)^{-0.55} \cdot \left(\frac{P_l}{d_o}\right)^{-0.5} \cdot \left(1-\frac{h_f}{d_o}\right)^{-1.4} \cdot \left(1-\frac{s_f}{d_o}\right)^{1.8}$	Based on own experimental data $10\,000 \le Re \le 100\,000$ $2.17 \le (P_t/d_o) \le 4.13$ $0.17 \le (P_l/d_o) \le 2.14$ $0.13 \le (h_f/d_o) \le 0.59$ $0.13 \le (s_f/d_o) \le 0.28$
Nir (1991)	$Eu = \frac{2.12}{Re^{0.25}} \cdot \left(\frac{A_{ht}}{A_{f,min}}\right)^{0.45} \cdot \left(\frac{d_f}{d_o}\right)^{-0.25}$	Based on data of various authors $300 \le Re_h \le 10\,000$ $8.5 \le (A_{ht}/A_{f,min}) \le 60$ $N_l \ge 4$
Mon (2003)	$Eu = \frac{0.75}{Re^{0.24}} \cdot F^{-0.75} \cdot \left(\frac{P_t}{P_d}\right)^{0.64}$ $F = \frac{1}{\frac{A_{ht}}{A_{f,min}} + 1}$	Based on own modelled data $5\,000 \le Re \le 70\,000$ $3.7 \le Ar \le 25.0$ $0.01 \le F \le 0.08$ $11.5 \le (A_{ht}/A_{f,min}) \le 92.0$ $P_t/P_d = 1$ $N_l = 4$
Kawaguchi et al. (2004)	$Eu = \frac{6.46}{Re_h^{0.228}} \cdot \left(\frac{g_f}{t_f}\right)^{-0.872}$ with $d_h = 4 \cdot \frac{A_{f,min}}{2 \cdot N_f \cdot (s_f + 2 \cdot h_f)}$	Based on own experimental data $2\,000 \le Re \le 27\,000$ $2.95 \le (s_f/t_f) \le 4.39$
Kawaguchi et al. (2006a)	$Eu = \frac{2.60}{Re_h^{0.24}} \cdot \left(\frac{h_f}{d_h}\right)^{0.004} \cdot \left(\frac{g_f}{s_f}\right)^{-4.13}$ with $d_h = 4 \cdot \frac{A_{f,min}}{2 \cdot N_f \cdot (s_f + 2 \cdot h_f)}$	Based on own experimental data $2\,000 \le Re \le 27\,000$ $0.38 \le (h_f/d_h) \le 1.24$ $0.76 \le (s_f/g_f) \le 0.82$

II. Experimental results

Tube bundle 1

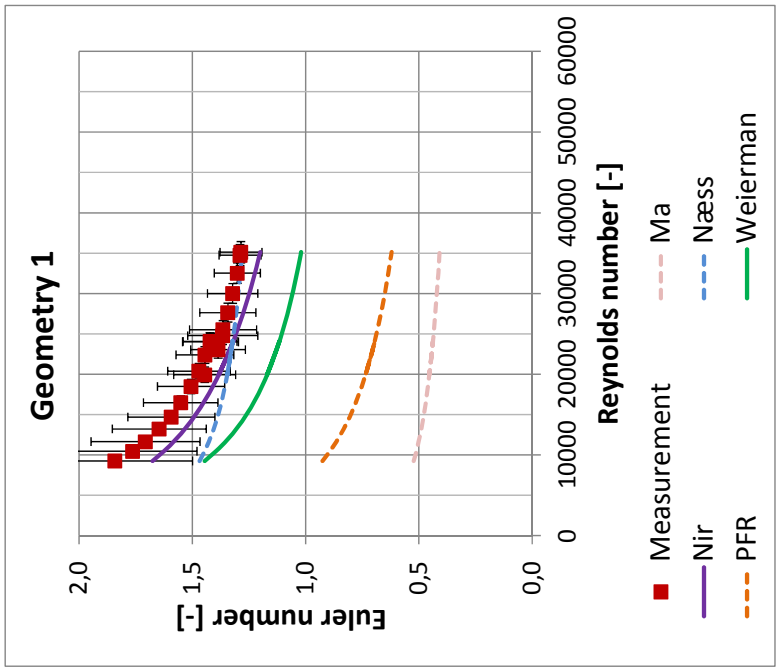

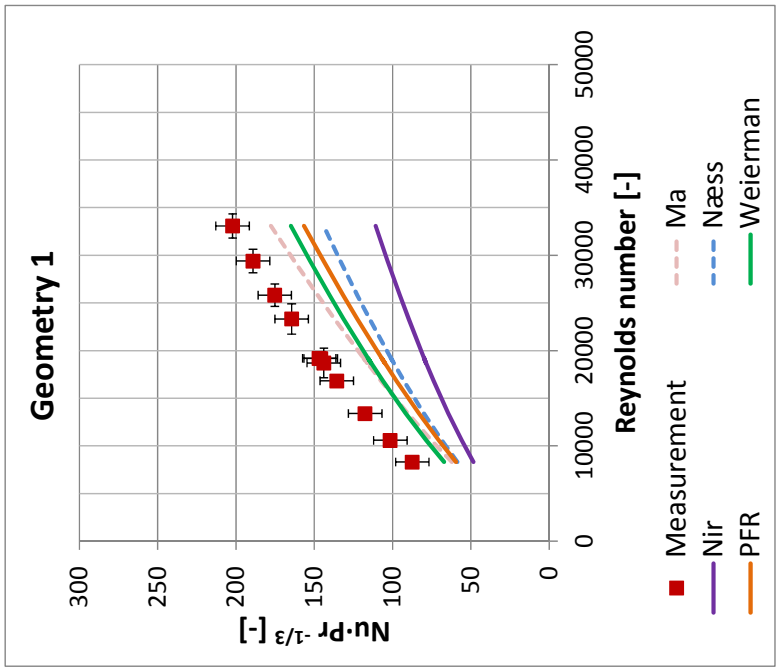

Heat transfer

air			water-glycol									
mass flow	inlet temper-ature	outlet temper-ature	mass flow	inlet temper-ature	outlet temper-ature	heat duty	overall htc	tube side htc	corrected fin efficiency	air side htc	Reynolds number	Nusselt·Prandtl number
$\dot{m}_{air}$	$T_{air\text{-}in}$	$T_{air\text{-}out}$	$\dot{m}_{wg}$	$T_{wg\text{-}in}$	$T_{wg\text{-}out}$	Q_{wg}	U_{wg}	h_i	$\eta_{f,W}$	h_{air}	Re	$Nu \cdot Pr^{-1/3}$
kg/s	°C	°C	kg/s	°C	°C	W	W/m^2K	W/m^2K	-	W/m^2K	-	-
0.34	117.9	32.0	1.67	24.4	29.4	31534	36	2372	0.73	73	8312	87
0.44	118.3	35.4	1.67	24.4	30.5	38301	39	2389	0.70	85	10586	101
0.56	118.5	39.7	1.67	24.3	31.7	45808	42	2411	0.67	100	13398	118
0.71	119.7	44.9	1.66	24.3	33.1	54508	45	2434	0.64	116	16830	136
0.81	120.3	48.2	1.66	24.3	34.0	59795	46	2450	0.62	126	19196	147
0.81	121.6	48.6	1.66	24.4	34.1	60533	46	2454	0.62	125	19171	146
0.79	116.4	46.2	1.66	24.4	33.3	55709	46	2442	0.63	122	18698	144
0.99	118.9	52.3	1.66	24.4	34.9	65702	49	2475	0.59	141	23315	164
1.10	119.9	55.4	1.66	24.4	35.7	70573	50	2489	0.58	151	25812	175
1.26	122.7	60.1	1.66	24.4	36.9	78286	52	2512	0.56	165	29403	189
1.43	123.6	63.9	1.66	24.4	37.9	83937	53	2531	0.54	177	33078	202

Pressure drop

differential pressure	mass flow	orifice diameter	absolute pressure	mean temper-ature	Reynolds number	Euler number
dp	$\dot{m}_{air}$	d_{or}	$p_{ts\text{-}in}$	$T_{m\text{-}air}$	Re	Eu
Pa	kg/s	mm	Pa	°C	-	-
173	0.33	140	100092	18.6	9257	1.84
211	0.38	140	100030	18.5	10461	1.76
253	0.42	140	100059	18.5	11644	1.71
315	0.48	140	100051	18.6	13224	1.65
377	0.53	140	100087	18.8	14695	1.59
463	0.60	140	100098	19.1	16484	1.55
567	0.67	140	100070	19.5	18483	1.51
678	0.74	140	100077	20.3	20380	1.47
806	0.81	140	100021	20.6	22390	1.44
909	0.87	140	100080	20.3	24018	1.42
925	0.88	140	99984	21.5	24076	1.42
647	0.73	221	99889	21.8	19935	1.44
833	0.84	221	99909	22.3	23048	1.39
936	0.90	140	100057	20.8	24783	1.37
1008	0.93	221	99966	22.6	25529	1.36
1166	1.01	221	100015	23.0	27633	1.34
1360	1.10	221	99951	23.5	30007	1.32
1576	1.19	221	100023	23.8	32531	1.30
1790	1.28	221	99988	24.2	34752	1.29
1806	1.29	221	100114	23.2	35127	1.29

Tube bundle 2

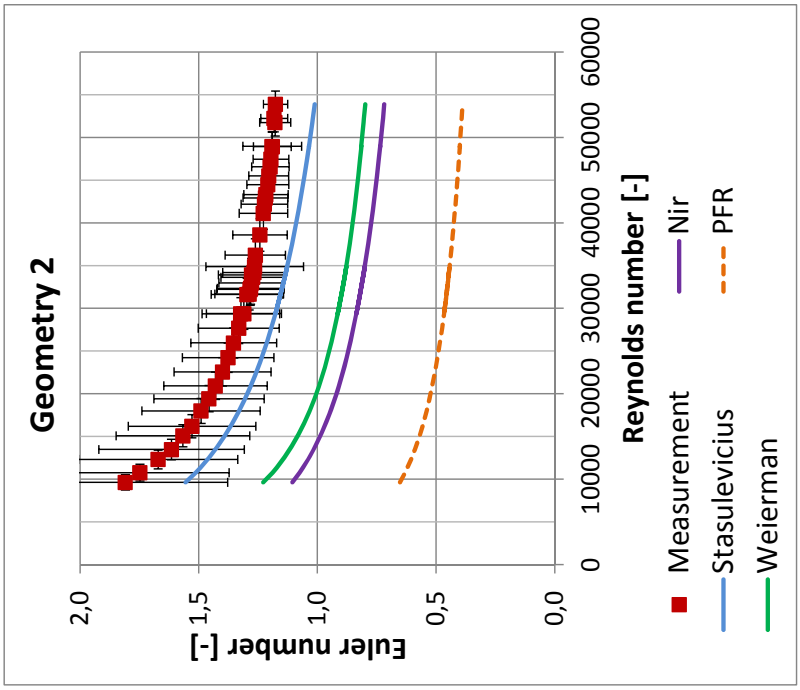

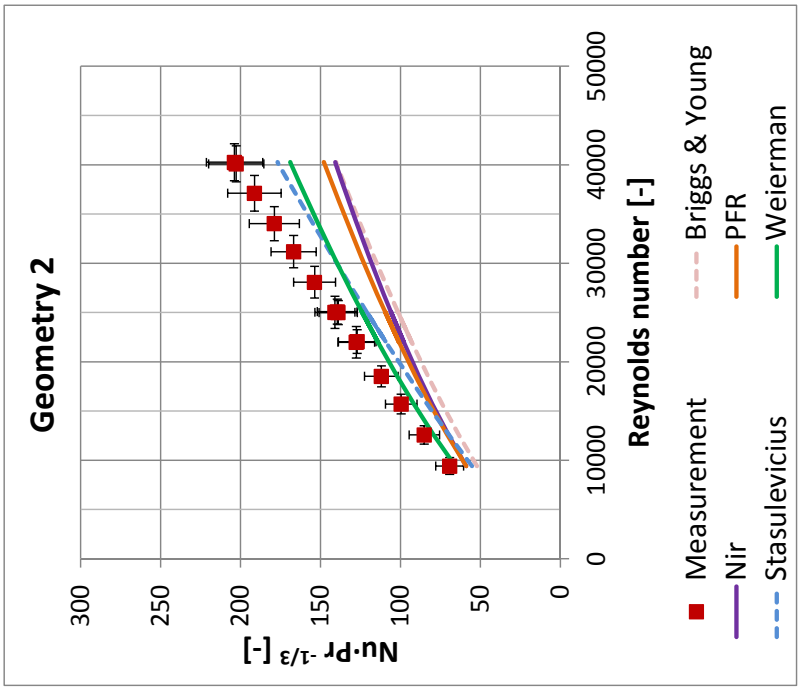

Heat transfer

air			water-glycol									
mass flow	inlet temper-ature	outlet temper-ature	mass flow	inlet temper-ature	outlet temper-ature	heat duty	overall htc	tube side htc	theoretic al fin efficiency	air side htc	Reynolds number	Nusselt· Prandtl number
$\dot{m}_{air}$	T_{air-in}	$T_{air-out}$	$\dot{m}_{wg}$	T_{wg-in}	T_{wg-out}	Q_{wg}	U_{wg}	h_i	$\eta_{f,th}$	h_{air}	Re	$Nu \cdot Pr^{-1/3}$
kg/s	°C	°C	kg/s	°C	°C	W	W/m^2K	W/m^2K	-	W/m^2K	-	-
0.40	25.3	29.9	2.12	126.2	39.0	36463	34	2971	0.74	59	9413	69
0.54	24.8	30.6	2.12	126.3	43.8	45851	38	2979	0.70	73	12572	85
0.68	25.0	31.8	2.12	126.3	48.6	53895	41	3011	0.66	86	15706	100
0.81	25.0	32.6	2.12	126.5	52.4	60517	44	3029	0.64	97	18522	112
0.96	25.2	33.7	2.12	126.0	56.6	67409	46	3060	0.61	111	22038	127
1.09	24.8	34.0	2.12	125.8	59.5	72882	48	3059	0.59	121	24988	139
1.10	25.0	34.2	2.12	126.2	59.9	73327	48	3070	0.59	122	25074	140
0.96	25.0	33.5	2.12	126.2	56.8	67941	46	3050	0.61	111	21968	128
1.10	25.1	34.4	2.12	126.2	60.2	73818	49	3077	0.59	123	25016	141
1.23	25.2	35.1	2.12	126.3	63.2	79102	51	3097	0.57	135	28076	154
1.37	24.9	35.5	2.12	126.2	65.8	84185	52	3101	0.55	147	31173	167
1.50	25.0	36.1	2.12	126.1	68.1	88418	54	3119	0.53	158	34024	179
1.64	25.2	36.9	2.12	126.4	70.5	92732	56	3145	0.51	169	37110	191
1.78	25.0	37.1	2.12	125.9	72.3	96152	57	3146	0.50	179	40094	203
1.79	25.1	37.2	2.12	125.8	72.4	96165	57	3149	0.50	180	40252	204

Pressure drop

differential pressure	mass flow	orifice diameter	absolute pressure	mean temper-ature	Reynolds number	Euler number
dp	$\dot{m}_{air}$	d_{or}	$p_{ts\text{-}in}$	$T_{m\text{-}air}$	Re	Eu
Pa	kg/s	mm	Pa	°C	-	-
178	0.35	140	100365	15.9	9622	1.81
215	0.39	140	100168	15.9	10752	1.75
270	0.45	140	99997	15.9	12299	1.67
313	0.49	140	99981	16.0	13466	1.62
382	0.55	140	99933	16.4	15069	1.57
431	0.59	140	100045	16.9	16185	1.53
522	0.66	140	100007	17.5	17981	1.49
598	0.71	140	100159	18.3	19411	1.46
686	0.77	140	100325	19.2	20921	1.43
784	0.83	140	100530	20.0	22549	1.40
895	0.90	140	100746	21.0	24213	1.38
1016	0.96	140	100971	21.9	25939	1.35
1145	1.03	140	101194	23.0	27668	1.33
1279	1.10	140	101414	24.1	29371	1.31
1461	1.18	140	101706	24.4	31665	1.29
1504	1.20	140	101784	24.3	32207	1.28
1515	1.21	140	101789	24.3	32337	1.28
1570	1.23	140	101889	24.4	32980	1.28
1626	1.26	140	101978	24.6	33628	1.27
1673	1.29	140	101975	20.2	34876	1.26
1680	1.28	140	102059	25.0	34185	1.27
1227	1.08	221	101351	18.3	29354	1.32
1401	1.16	221	101645	19.1	31617	1.30
1595	1.25	221	101961	19.9	33915	1.28
1808	1.34	221	102279	20.9	36221	1.26
2033	1.43	221	102623	22.0	38602	1.24
2281	1.53	221	102981	22.4	41122	1.23
2385	1.57	221	103132	22.2	42203	1.22
2462	1.60	221	103238	22.4	42933	1.22
2488	1.61	221	103313	21.8	43326	1.22
2603	1.65	221	103482	21.9	44476	1.21
2718	1.69	221	103638	22.1	45504	1.21

differential pressure	mass flow	orifice diameter	absolute pressure	mean temper-ature	Reynolds number	Euler number
dp	$\dot{m}_{air}$	d_{or}	$p_{ts\text{-}in}$	$T_{m\text{-}air}$	Re	Eu
Pa	kg/s	mm	Pa	°C	-	-
2831	1.73	221	103788	22.3	46566	1.20
2935	1.76	221	103916	22.6	47454	1.20
3071	1.81	221	104024	21.2	48962	1.19
3081	1.82	221	104116	21.9	48922	1.19
3471	1.93	221	104562	24.3	51753	1.18
3545	1.94	221	103404	22.9	52236	1.18
3746	2.01	221	103718	23.0	53892	1.18

Tube bundle 3

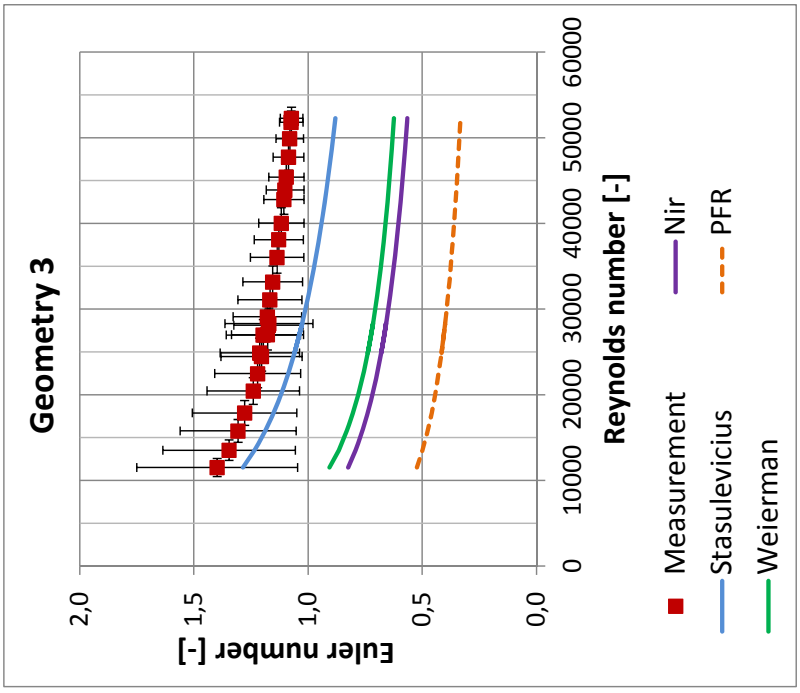

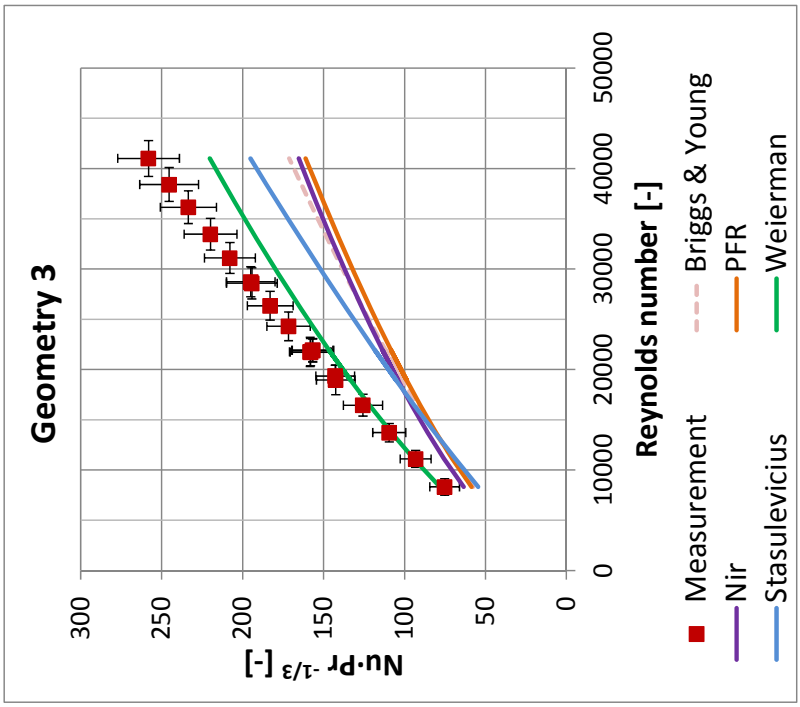

Heat transfer

air			water-glycol									
mass flow	inlet temper-ature	outlet temper-ature	mass flow	inlet temper-ature	outlet temper-ature	heat duty	overall htc	tube side htc	theoretic al fin efficiency	air side htc	Reynolds number	Nusselt· Prandtl number
$\dot{m}_{air}$	T_{air-in}	$T_{air-out}$	$\dot{m}_{wg}$	T_{wg-in}	T_{wg-out}	Q_{wg}	U_{wg}	h_i	$\eta_{f,th}$	h_{air}	Re	$Nu \cdot Pr^{-1/3}$
kg/s	°C	°C	kg/s	°C	°C	W	W/m^2K	W/m^2K	-	W/m^2K	-	-
0.40	24.8	29.0	2.11	125.8	46.8	32867	39	2963	0.72	65	8318	75
0.54	25.1	30.3	2.11	126.0	52.7	40696	45	3001	0.68	81	11103	93
0.67	25.0	31.0	2.11	126.0	56.9	47237	49	3013	0.64	95	13724	109
0.81	25.4	32.1	2.11	125.6	61.0	52890	53	3054	0.61	110	16444	126
0.95	25.1	32.5	2.11	126.2	64.7	59256	57	3054	0.58	125	19358	143
1.08	24.9	33.0	2.11	126.0	67.4	63798	59	3062	0.56	138	21917	157
1.08	25.3	33.3	2.11	125.9	67.5	63519	60	3081	0.56	138	21913	157
0.93	24.9	32.4	2.11	126.3	64.4	59201	57	3045	0.58	125	18956	142
1.08	24.9	33.1	2.11	126.3	67.7	64313	60	3061	0.56	140	21751	158
1.07	25.1	33.2	2.11	126.3	67.8	64190	60	3071	0.56	139	21729	158
1.20	25.0	33.7	2.11	126.3	70.4	68401	62	3080	0.54	152	24300	172
1.31	25.0	34.1	2.11	126.3	72.3	71792	64	3092	0.52	162	26348	183
1.42	25.2	34.6	2.11	125.8	74.1	74420	66	3111	0.51	172	28578	194
1.43	25.2	34.6	2.11	125.8	74.2	74640	66	3115	0.51	173	28730	195
1.55	25.1	35.0	2.11	125.8	76.1	78056	68	3115	0.49	185	31102	208
1.67	25.1	35.3	2.11	125.7	77.7	80968	70	3127	0.48	196	33467	220
1.81	25.1	35.8	2.11	125.6	79.5	84072	72	3136	0.47	208	36145	234
1.92	25.2	36.2	2.11	126.0	81.1	87024	73	3150	0.46	219	38407	245
2.06	25.1	36.5	2.11	126.1	82.7	90090	75	3154	0.44	231	41009	258

Pressure drop

differential pressure	mass flow	orifice diameter	absolute pressure	mean temper-ature	Reynolds number	Euler number
dp	$\dot{m}_{air}$	d_{or}	$p_{ts\text{-}in}$	$T_{m\text{-}air}$	Re	Eu
Pa	kg/s	mm	Pa	°C	-	-
133	0.38	140	100249	10.6	9481	1.46
188	0.46	140	100228	10.6	11501	1.40
251	0.54	140	100199	10.9	13519	1.35
332	0.64	140	100377	11.3	15770	1.31
419	0.72	140	100377	11.9	17871	1.28
535	0.83	140	100607	12.8	20442	1.24
642	0.91	140	100619	13.7	22463	1.22
758	1.00	140	100628	15.0	24463	1.20
910	1.10	140	100903	16.1	26999	1.18
979	1.15	140	100676	14.1	28303	1.17
988	1.15	140	100828	16.6	28103	1.17
777	1.01	221	100581	13.2	24871	1.21
906	1.10	221	100676	13.8	26973	1.20
1044	1.18	221	100764	14.4	29097	1.18
1184	1.27	221	100890	15.0	31085	1.17
1342	1.35	221	100946	15.7	33166	1.15
1559	1.48	221	101649	16.6	36029	1.14
1730	1.56	221	101723	16.6	38093	1.13
1888	1.64	221	101846	16.6	40023	1.12
2149	1.76	221	102001	17.5	42788	1.11
2259	1.80	221	102135	17.9	43899	1.10
2417	1.87	221	102271	18.7	45403	1.09
2667	1.97	221	102522	19.8	47732	1.09
2927	2.07	221	102355	20.7	49900	1.08
3190	2.16	221	102717	23.0	51809	1.07
3206	2.17	221	102756	21.7	52276	1.07

Tube bundle 4

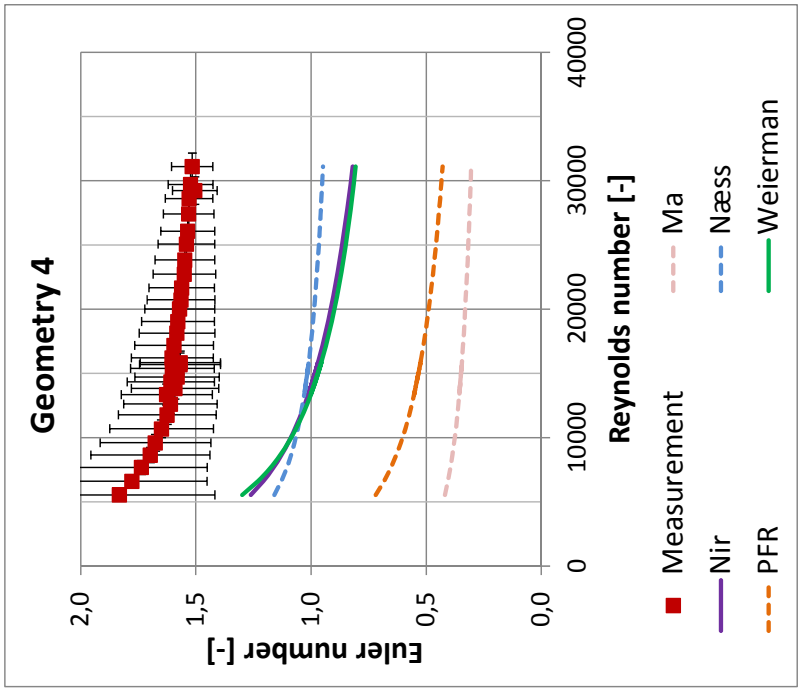

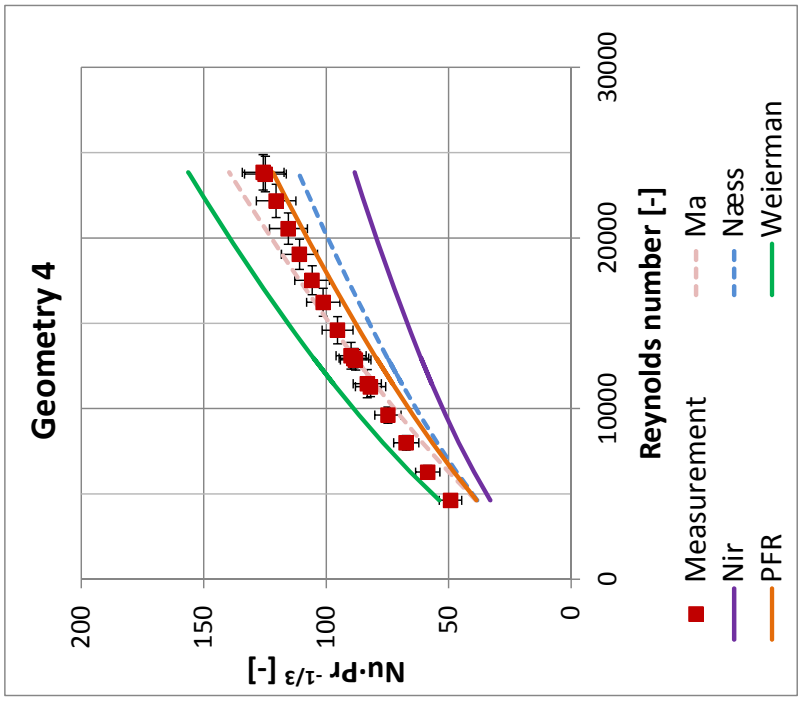

Heat transfer

air			water-glycol									
mass flow	inlet temper-ature	outlet temper-ature	mass flow	inlet temper-ature	outlet temper-ature	heat duty	overall htc	tube side htc	corrected fin efficiency	air side htc	Reynolds number	Nusselt·Prandtl number
$\dot{m}_{air}$	$T_{air\text{-}in}$	$T_{air\text{-}out}$	$\dot{m}_{wg}$	$T_{wg\text{-}in}$	$T_{wg\text{-}out}$	Q_{wg}	U_{wg}	h_i	$\eta_{f,W}$	h_{air}	Re	$Nu \cdot Pr^{-1/3}$
kg/s	°C	°C	kg/s	°C	°C	W	W/m^2K	W/m^2K	-	W/m^2K	-	-
0.37	24.3	30.7	1.38	125.8	39.8	32930	41	6831	0.72	70	4624	49
0.50	25.9	33.7	1.38	125.7	47.4	40559	46	7103	0.69	84	6280	59
0.65	25.1	34.4	1.38	126.0	52.8	48336	50	7096	0.65	97	7996	67
0.78	24.7	35.3	1.38	126.3	57.4	54681	52	7127	0.63	109	9621	75
0.92	24.5	36.1	1.38	126.2	61.6	60131	55	7162	0.61	119	11285	82
1.05	24.8	37.2	1.39	125.8	65.2	64199	57	7257	0.59	129	12853	88
1.06	24.4	36.8	1.39	125.8	65.2	64749	57	7205	0.59	130	12955	89
0.93	25.2	36.8	1.39	126.0	62.6	60585	56	7244	0.61	122	11461	83
1.07	25.1	37.7	1.39	126.3	66.3	65549	58	7293	0.59	132	13099	90
1.20	25.1	38.4	1.39	126.3	69.4	69354	60	7339	0.57	140	14600	95
1.33	24.8	38.8	1.39	125.6	71.8	72766	61	7349	0.56	149	16229	101
1.45	24.8	39.4	1.39	126.2	74.2	76072	63	7384	0.55	156	17519	106
1.57	24.8	39.9	1.39	125.7	76.3	78715	64	7425	0.54	164	19045	111
1.70	25.0	40.6	1.39	126.1	78.6	81609	65	7470	0.53	172	20550	115
1.84	25.0	41.2	1.39	126.1	80.6	84302	67	7512	0.52	179	22175	120
1.97	24.9	41.5	1.39	125.8	82.2	86456	68	7525	0.51	186	23748	125
1.98	25.1	41.7	1.39	126.1	82.4	86886	68	7549	0.51	188	23849	126

Pressure drop

differential pressure	mass flow	orifice diameter	absolute pressure	mean temper-ature	Reynolds number	Euler number
dp	$\dot{m}_{air}$	d_{or}	$p_{ts\text{-}in}$	$T_{m\text{-}air}$	Re	Eu
Pa	kg/s	mm	Pa	°C	-	-
74	0.24	140	100266	12.3	3572	2.03
110	0.30	140	100324	12.1	4503	1.90
161	0.37	140	100311	12.2	5539	1.83
222	0.44	140	100301	12.3	6597	1.78
293	0.52	140	100339	12.5	7674	1.74
365	0.58	140	100420	12.9	8643	1.70
446	0.65	140	100359	13.5	9596	1.68
548	0.72	140	100393	14.2	10689	1.65
658	0.80	140	100460	14.8	11772	1.62
754	0.85	140	100483	15.5	12610	1.61
902	0.94	140	100674	16.5	13833	1.59
1024	1.00	140	100577	17.3	14719	1.58
1162	1.07	140	100749	18.3	15686	1.57
1169	1.08	140	101259	17.6	15834	1.57
825	0.90	221	101319	12.6	13353	1.63
939	0.96	221	101533	12.8	14335	1.61
1083	1.04	221	101769	13.4	15395	1.60
1210	1.09	221	101009	13.5	16208	1.60
1361	1.16	221	101026	14.1	17183	1.59
1513	1.22	221	101123	15.0	18126	1.58
1678	1.29	221	101240	16.0	19041	1.58
1858	1.36	221	101282	16.8	20018	1.57
1996	1.41	221	101355	17.5	20724	1.56
2185	1.48	221	101364	18.0	21659	1.56
2384	1.55	221	101506	17.9	22730	1.55
2622	1.62	221	101429	18.0	23837	1.55
2891	1.71	221	101615	18.4	25066	1.54
3122	1.78	221	101740	18.7	26074	1.54
3453	1.87	221	101906	19.3	27417	1.53

differential pressure	mass flow	orifice diameter	absolute pressure	mean temper-ature	Reynolds number	Euler number
dp	$\dot{m}_{air}$	d_{or}	$p_{ts\text{-}in}$	$T_{m\text{-}air}$	Re	Eu
Pa	kg/s	mm	Pa	°C	-	-
3784	1.96	221	102066	20.2	28622	1.53
3846	2.02	221	105769	23.2	29234	1.50
4069	2.04	221	102505	21.0	29703	1.52
4448	2.14	221	103090	21.8	31106	1.52

Tube bundle 5

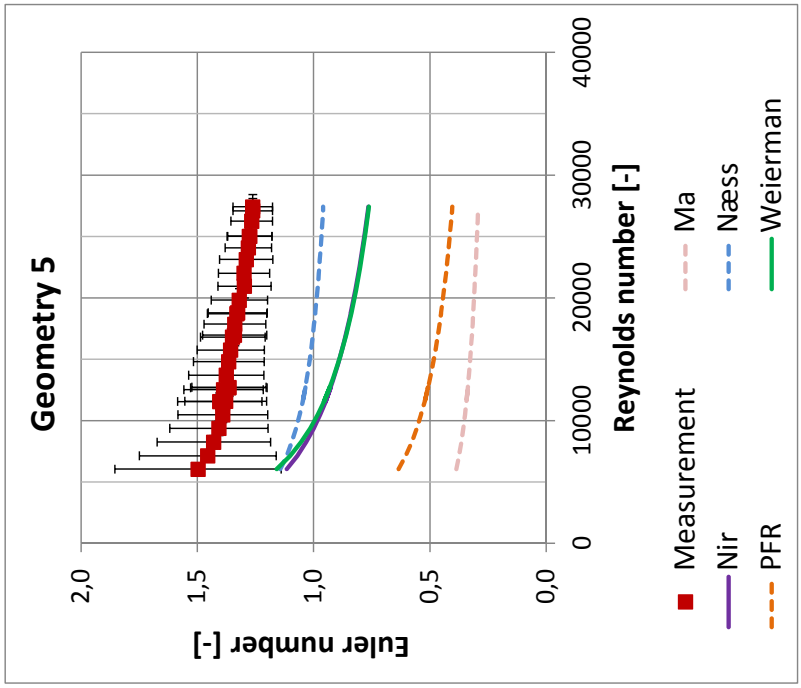

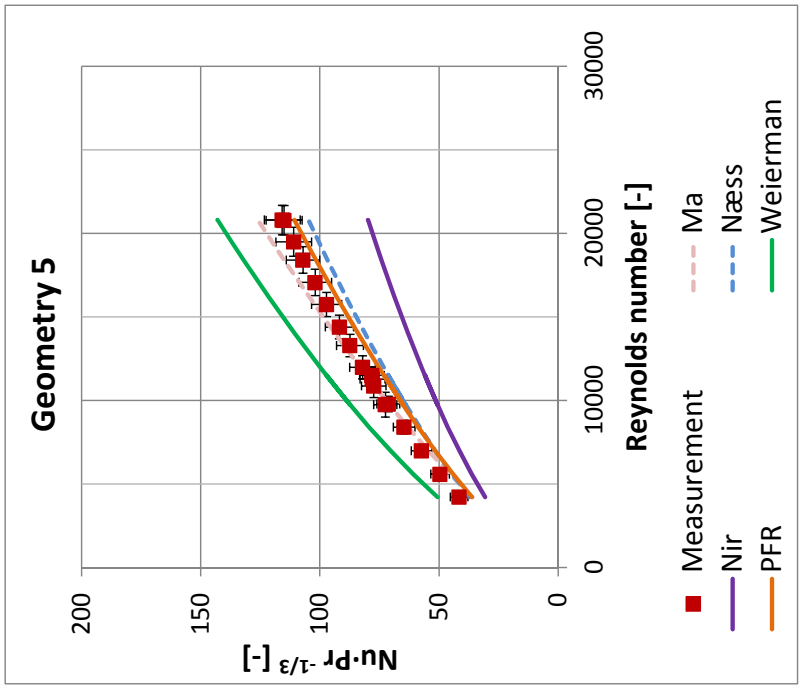

Heat transfer

air			water-glycol									
mass flow	inlet temper-ature	outlet temper-ature	mass flow	inlet temper-ature	outlet temper-ature	heat duty	overall htc	tube side htc	corrected fin efficiency	air side htc	Reynolds number	Nusselt·Prandtl number
$\dot{m}_{air}$	T_{air-in}	$T_{air-out}$	$\dot{m}_{wg}$	T_{wg-in}	T_{wg-out}	Q_{wg}	U_{wg}	h_i	$\eta_{f,W}$	h_{air}	Re	$Nu \cdot Pr^{-1/3}$
kg/s	°C	°C	kg/s	°C	°C	W	W/m^2K	W/m^2K	-	W/m^2K	-	-
0.39	25.2	31.5	1.37	126.0	45.1	32504	37	6916	0.75	60	4215	42
0.52	25.4	33.1	1.38	125.8	51.2	39793	42	7015	0.72	71	5583	50
0.66	25.0	34.0	1.38	126.1	56.2	46711	45	7054	0.69	83	6980	57
0.79	25.1	35.2	1.38	125.8	60.6	52429	49	7130	0.66	94	8397	65
0.93	25.2	36.3	1.38	126.1	64.6	57589	52	7205	0.64	104	9782	71
1.07	24.9	36.9	1.38	126.2	68.1	62696	54	7228	0.62	115	11276	78
1.09	25.1	37.1	1.38	126.1	68.2	62633	54	7253	0.62	115	11498	78
0.92	25.0	36.3	1.38	126.0	65.3	58593	52	7178	0.64	106	9741	73
1.03	25.3	37.3	1.38	126.1	68.2	62096	54	7254	0.62	114	10862	77
1.14	25.5	38.1	1.38	125.8	70.7	65199	56	7304	0.61	121	11976	82
1.27	25.1	38.4	1.38	125.8	73.1	68925	57	7307	0.59	129	13282	87
1.38	25.2	39.1	1.38	125.8	75.2	71700	59	7361	0.58	136	14388	92
1.51	25.1	39.6	1.38	126.4	77.8	75546	60	7391	0.57	144	15741	97
1.64	25.2	40.3	1.38	126.1	80.0	78273	62	7438	0.55	152	17059	102
1.77	25.0	40.6	1.38	125.8	81.6	80964	63	7453	0.54	160	18402	107
1.88	25.0	41.0	1.38	125.7	83.0	82980	64	7470	0.53	166	19487	111
2.01	25.1	41.6	1.38	126.6	85.1	85954	66	7518	0.53	172	20784	115
2.01	25.1	41.6	1.39	126.2	84.9	85832	66	7526	0.52	173	20801	116

Pressure drop

differential pressure	mass flow	orifice diameter	absolute pressure	mean temper-ature	Reynolds number	Euler number
dp	$\dot{m}_{air}$	d_{or}	$p_{ts\text{-}in}$	$T_{m\text{-}air}$	Re	Eu
Pa	kg/s	mm	Pa	°C	-	-
165	0.48	140	101012	19.1	6043	1.50
224	0.57	140	100993	19.5	7130	1.45
296	0.66	140	100998	20.0	8247	1.43
380	0.75	140	100984	21.0	9368	1.41
472	0.84	140	101026	21.8	10478	1.39
576	0.93	140	101033	22.8	11577	1.38
689	1.02	140	100895	22.6	12718	1.36
690	1.02	140	101022	23.8	12675	1.36
558	0.91	221	101017	17.4	11557	1.40
650	0.99	221	101005	17.9	12519	1.39
777	1.08	221	101024	18.7	13695	1.38
905	1.17	221	101040	19.3	14803	1.36
1024	1.25	221	101013	19.9	15751	1.36
1160	1.33	221	101056	20.2	16796	1.35
1171	1.35	221	100996	19.7	16963	1.34
1307	1.42	221	100998	20.6	17859	1.34
1433	1.49	221	100999	21.2	18712	1.33
1476	1.51	221	100972	23.9	18784	1.33
1643	1.59	221	100965	24.6	19815	1.32
1791	1.68	221	101831	24.6	20949	1.30
1987	1.77	221	101524	24.7	22002	1.30
2129	1.85	221	102354	23.0	23124	1.29
2361	1.95	221	102307	26.4	24075	1.28
2515	2.02	221	103099	26.1	25016	1.28
2544	2.03	221	102674	27.2	25018	1.27
2793	2.13	221	103166	28.2	26249	1.27
3025	2.21	221	103446	30.8	27100	1.26
3047	2.23	221	103633	29.1	27416	1.26

Tube bundle 6

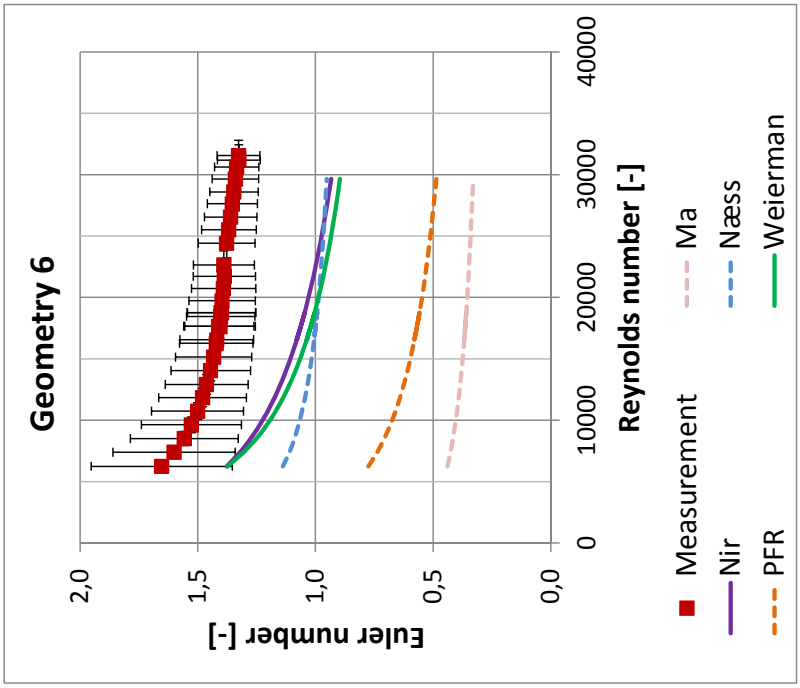

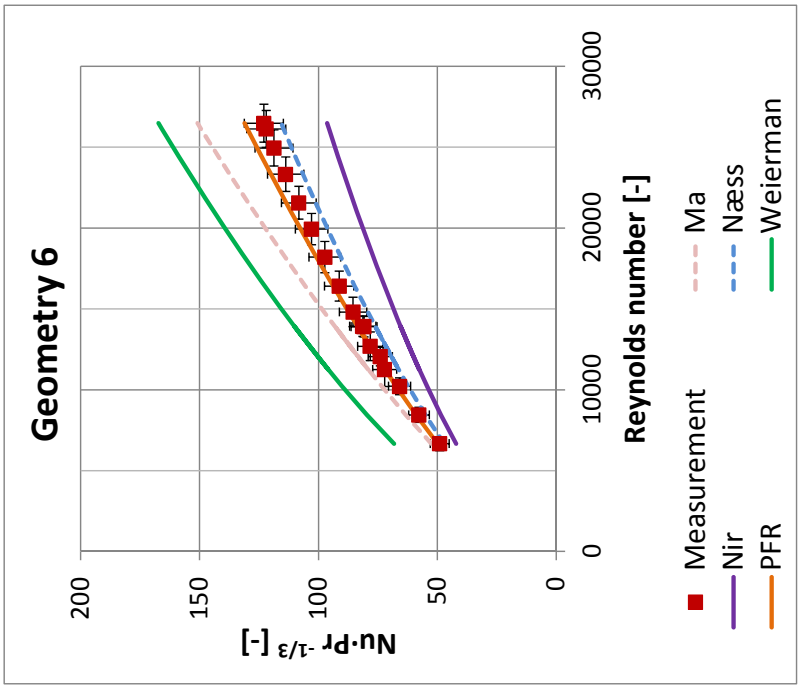

Heat transfer

air			water-glycol									
mass flow	inlet temper-ature	outlet temper-ature	mass flow	inlet temper-ature	outlet temper-ature	heat duty	overall htc	tube side htc	corrected fin efficiency	air side htc	Reynolds number	Nusselt·Prandtl number
$\dot{m}_{air}$	$T_{air\text{-}in}$	$T_{air\text{-}out}$	$\dot{m}_{wg}$	$T_{wg\text{-}in}$	$T_{wg\text{-}out}$	Q_{wg}	U_{wg}	h_i	$\eta_{f,W}$	h_{air}	Re	$Nu \cdot Pr^{-1/3}$
kg/s	°C	°C	kg/s	°C	°C	W	W/m^2K	W/m^2K	-	W/m^2K	-	-
0.45	23.9	31.2	1.36	125.2	46.0	37191	41	6745	0.72	70	6672	49
0.57	24.2	32.8	1.36	125.6	51.1	44074	45	6859	0.69	83	8448	58
0.69	23.8	33.7	1.37	126.4	55.5	50680	49	6896	0.66	96	10213	66
0.82	23.3	34.4	1.36	126.3	59.1	56515	52	6900	0.63	108	12054	74
0.95	23.3	35.2	1.37	126.0	62.7	61255	54	6953	0.61	118	13904	81
0.95	23.2	35.3	1.37	126.4	62.9	61772	55	6958	0.61	119	13928	81
0.77	23.6	34.4	1.35	126.2	57.6	54421	51	6870	0.64	105	11259	72
0.87	22.9	34.6	1.35	126.5	60.4	59153	53	6839	0.62	114	12689	78
1.02	22.8	35.5	1.35	126.4	64.0	64083	56	6894	0.60	125	14809	85
1.13	22.9	36.2	1.36	126.3	66.8	67842	58	6946	0.58	134	16407	91
1.26	22.9	36.9	1.36	125.9	69.4	71300	60	6992	0.57	143	18202	97
1.38	22.6	37.3	1.36	126.0	71.6	74749	61	7000	0.56	152	19935	103
1.49	21.9	37.3	1.36	126.4	73.5	78379	62	6969	0.54	160	21560	108
1.62	21.7	37.7	1.36	126.4	75.5	81529	64	6989	0.53	169	23328	114
1.74	21.8	38.4	1.36	127.3	77.7	84731	65	7049	0.52	176	24944	119
1.82	21.8	38.6	1.36	126.4	78.3	85565	66	7047	0.51	181	26132	122
1.84	21.7	38.6	1.36	126.3	78.5	86066	66	7050	0.51	183	26477	123

Pressure drop

differential pressure	mass flow	orifice diameter	absolute pressure	mean temper-ature	Reynolds number	Euler number
dp	$\dot{m}_{air}$	d_{or}	$p_{ts\text{-}in}$	$T_{m\text{-}air}$	Re	Eu
Pa	kg/s	mm	Pa	°C	-	-
213	0.37	140	100085	28.2	6255	1.65
290	0.44	140	100183	28.5	7400	1.60
374	0.50	140	100305	29.0	8510	1.56
472	0.57	140	100409	29.8	9631	1.53
582	0.64	140	100516	30.8	10744	1.50
702	0.70	140	100624	31.7	11845	1.48
831	0.77	140	100716	32.7	12915	1.46
975	0.84	140	100860	33.3	14048	1.44
1124	0.90	140	100947	33.5	15147	1.43
1291	0.97	140	100973	33.9	16266	1.42
1513	1.06	140	101012	34.2	17659	1.41
1675	1.11	140	101089	36.5	18459	1.40
1689	1.12	140	101062	33.7	18764	1.40
1304	0.98	221	100968	31.0	16559	1.42
1472	1.05	221	101000	31.5	17646	1.41
1667	1.12	221	101041	32.2	18771	1.40
1851	1.18	221	101040	33.0	19729	1.40
2049	1.24	221	101020	33.8	20734	1.39
2253	1.30	221	101008	34.4	21717	1.39
2470	1.36	221	100677	34.8	22645	1.39
2844	1.46	221	100987	35.0	24415	1.38
3085	1.53	221	101385	35.5	25516	1.37
3326	1.59	221	101771	36.2	26547	1.36
3582	1.66	221	102155	36.5	27629	1.35
3816	1.72	221	102527	36.9	28595	1.35
4097	1.79	221	102962	37.8	29648	1.34
4371	1.85	221	103372	38.9	30621	1.33
4588	1.90	221	103853	41.7	31187	1.33
4616	1.91	221	103738	39.4	31550	1.33

Tube bundle 7

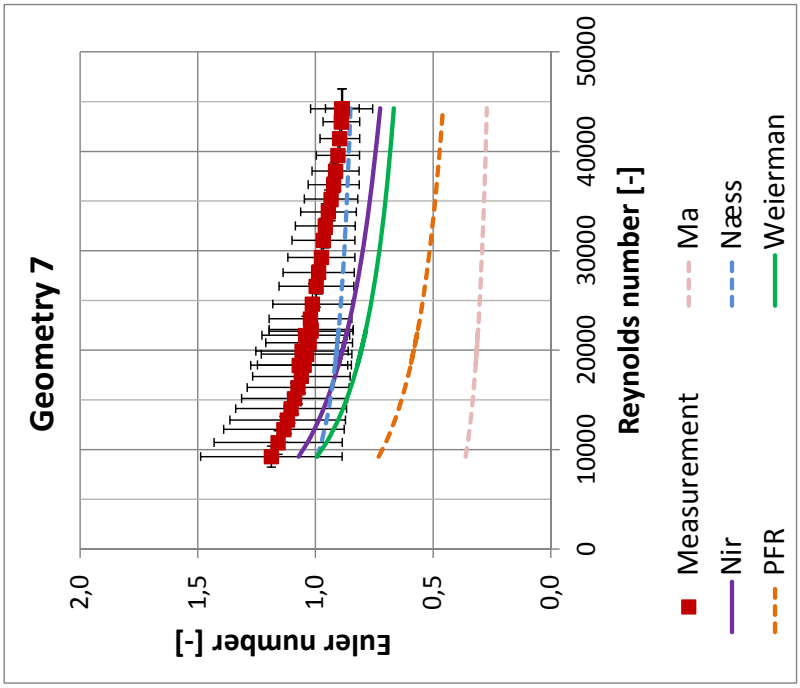

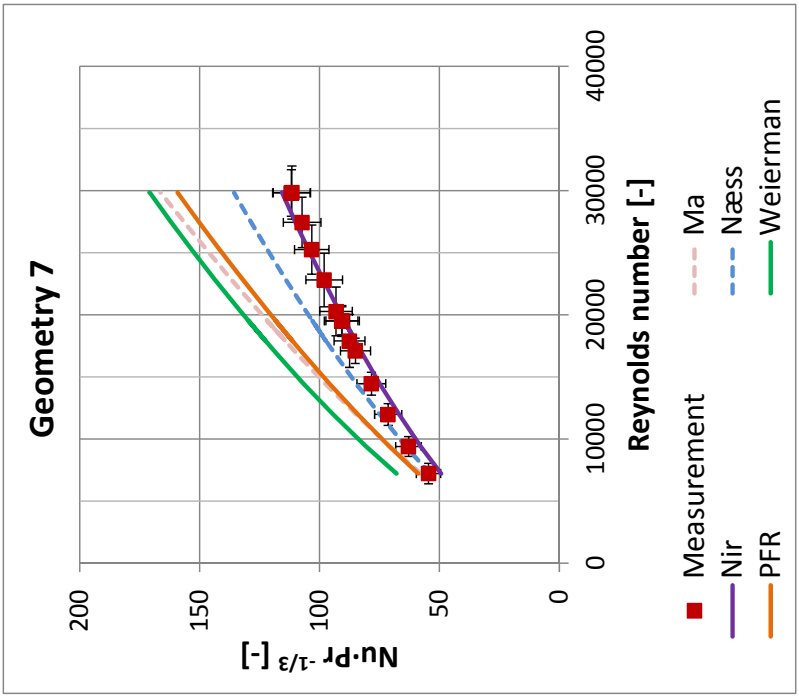

Heat transfer

air			water-glycol									
mass flow	inlet temper-ature	outlet temper-ature	mass flow	inlet temper-ature	outlet temper-ature	heat duty	overall htc	tube side htc	corrected fin efficiency	air side htc	Reynolds number	Nusselt·Prandtl number
$\dot{m}_{air}$	$T_{air\text{-}in}$	$T_{air\text{-}out}$	$\dot{m}_{wg}$	$T_{wg\text{-}in}$	$T_{wg\text{-}out}$	Q_{wg}	U_{wg}	h_i	$\eta_{f,W}$	h_{air}	Re	$Nu \cdot Pr^{-1/3}$
0.36	25.5	31.1	1.37	126.2	48.7	28756	59	6915	0.88	78	7216	55
0.47	25.1	31.8	1.37	125.7	53.9	34742	66	6927	0.87	91	9394	63
0.60	25.6	33.5	1.38	125.7	59.7	40660	73	7054	0.85	104	11968	71
0.73	25.7	34.6	1.38	126.0	64.4	45774	79	7136	0.84	115	14453	78
0.87	25.9	35.6	1.38	125.6	68.4	50161	83	7198	0.83	125	17093	85
1.00	25.1	35.7	1.38	126.4	71.7	54863	87	7175	0.82	134	19494	91
1.00	25.1	35.7	1.38	126.0	71.5	54614	87	7167	0.82	134	19513	91
0.91	25.2	35.4	1.38	126.1	69.7	52429	85	7140	0.82	129	17896	88
1.04	25.1	36.0	1.38	125.6	72.6	55997	89	7182	0.81	137	20264	93
1.17	25.8	37.3	1.38	126.3	76.2	59515	92	7299	0.81	145	22802	98
1.30	25.6	37.7	1.38	126.1	78.5	62776	96	7319	0.80	153	25250	103
1.41	25.5	38.0	1.38	125.7	80.2	65082	98	7324	0.79	160	27436	107
1.54	25.0	38.3	1.38	126.5	82.3	68505	101	7318	0.78	167	29806	112
1.54	25.4	38.5	1.38	126.3	82.4	68147	101	7352	0.78	166	29838	112

Pressure drop

differential pressure	mass flow	orifice diameter	absolute pressure	mean temper-ature	Reynolds number	Euler number
dp	$\dot{m}_{air}$	d_{or}	$p_{ts\text{-}in}$	$T_{m\text{-}air}$	Re	Eu
Pa	kg/s	mm	Pa	°C	-	-
145	0.27	140	100779	6.0	6512	1.27
207	0.32	140	100710	5.7	7934	1.22
276	0.38	140	100703	5.6	9305	1.19
357	0.44	140	100722	5.6	10715	1.16
441	0.49	140	100757	5.7	12035	1.13
507	0.53	140	100733	5.8	12984	1.12
592	0.58	140	100727	5.9	14125	1.10
672	0.62	140	100785	6.1	15143	1.09
764	0.66	140	100857	6.4	16241	1.07
864	0.71	140	100879	6.7	17370	1.06
974	0.76	140	100919	7.0	18520	1.05
1084	0.80	140	100835	7.4	19592	1.04
1210	0.85	140	100699	7.8	20749	1.03
1346	0.90	140	100617	8.3	21917	1.02
1353	0.91	140	100721	7.3	22086	1.02
977	0.75	221	100860	5.6	18481	1.07
1122	0.81	221	100936	5.7	19913	1.06
1289	0.88	221	100955	5.8	21495	1.04
1469	0.95	221	100910	5.9	23154	1.02
1655	1.01	221	100822	6.1	24642	1.01
1879	1.08	221	100861	6.5	26434	1.00
2061	1.14	221	101149	6.9	27810	0.99
2277	1.20	221	101078	7.3	29336	0.97
2540	1.28	221	101061	7.8	31053	0.97
2768	1.34	221	101223	8.3	32506	0.96
2976	1.40	221	101543	8.8	33906	0.94
3181	1.45	221	101885	9.6	35198	0.93
3429	1.52	221	102283	10.8	36642	0.92
3647	1.58	221	102805	11.0	38011	0.91

differential pressure	mass flow	orifice diameter	absolute pressure	mean temper-ature	Reynolds number	Euler number
dp	$\dot{m}_{air}$	d_{or}	$p_{ts\text{-}in}$	$T_{m\text{-}air}$	Re	Eu
Pa	kg/s	mm	Pa	°C	-	-
3909	1.64	221	103000	11.0	39603	0.90
4195	1.71	221	103441	11.1	41286	0.90
4516	1.79	221	103899	11.7	42972	0.89
4773	1.84	221	104166	11.6	44273	0.89
4784	1.84	221	104298	12.3	44313	0.88

Tube bundle 8

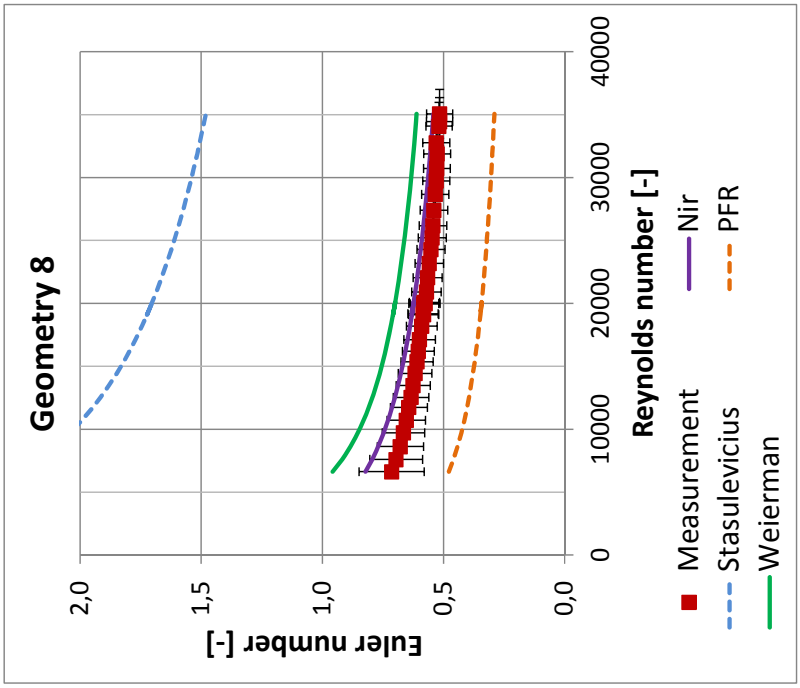

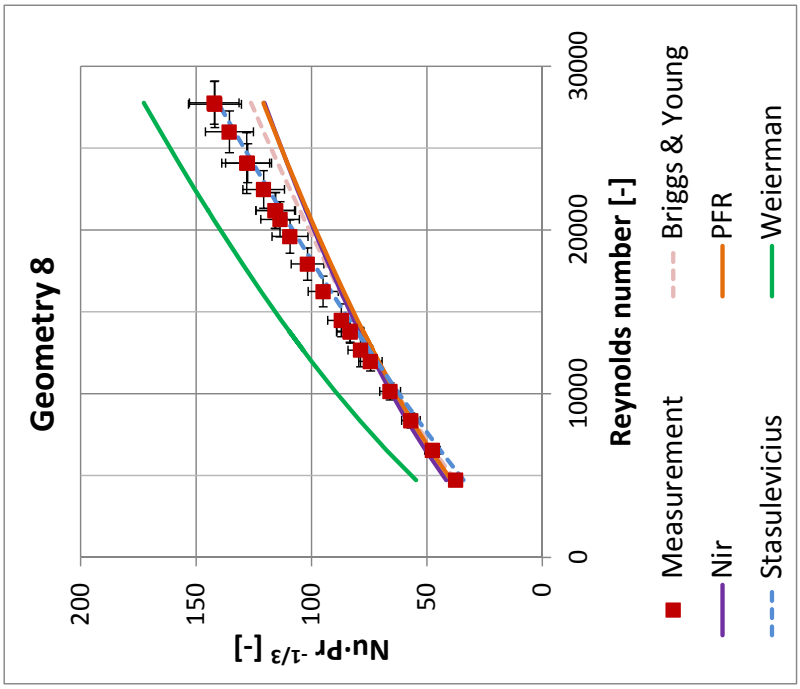

Heat transfer

air			water-glycol									
mass flow	inlet temper-ature	outlet temper-ature	mass flow	inlet temper-ature	outlet temper-ature	heat duty	overall htc	tube side htc	theoretic al fin efficiency	air side htc	Reynolds number	Nusselt· Prandtl number
$\dot{m}_{air}$	T_{air-in}	$T_{air-out}$	$\dot{m}_{wg}$	T_{wg-in}	T_{wg-out}	Q_{wg}	U_{wg}	h_i	$\eta_{f,th}$	h_{air}	Re	$Nu \cdot Pr^{-1/3}$
kg/s	°C	°C	kg/s	°C	°C	W	W/m^2K	W/m^2K	-	W/m^2K	-	-
0.37	25.2	33.5	0.89	126.0	50.4	27926	61	7570	0.92	76	4734	38
0.51	25.8	36.5	0.89	125.5	56.0	35622	73	7769	0.90	97	6545	48
0.65	25.5	38.4	0.89	125.3	60.4	42814	84	7857	0.88	117	8367	57
0.79	25.1	39.9	0.89	125.7	63.8	49583	94	7938	0.87	136	10138	66
0.94	24.8	41.4	0.89	125.8	67.2	55742	102	8006	0.85	154	11974	74
1.09	25.2	43.5	0.89	126.1	70.3	61341	111	8160	0.84	173	13823	83
1.09	24.7	43.1	0.89	126.2	70.2	61727	111	8126	0.84	173	13774	83
1.00	25.7	43.1	0.89	125.7	69.5	58268	107	8161	0.84	163	12666	79
1.14	25.6	44.5	0.89	125.8	71.7	63381	115	8239	0.83	181	14482	87
1.28	25.2	45.7	0.89	126.0	74.3	68688	121	8286	0.82	198	16244	95
1.42	25.4	46.8	0.89	125.7	75.8	72038	127	8373	0.81	213	17922	102
1.56	25.8	48.5	0.89	126.4	77.9	76295	133	8499	0.80	229	19603	109
1.64	24.9	48.5	0.89	126.2	78.7	78962	136	8444	0.79	238	20654	114
1.68	24.9	48.7	0.89	125.8	78.9	79749	138	8464	0.79	243	21196	116
1.69	25.0	49.0	0.89	126.7	79.5	80376	138	8488	0.79	243	21183	115
1.79	25.2	49.8	0.89	126.4	80.8	82808	142	8544	0.78	254	22478	121
1.92	25.0	50.6	0.89	126.1	81.8	85830	146	8585	0.77	269	24082	128
1.92	25.0	50.5	0.89	125.8	81.5	85625	147	8577	0.77	269	24083	128
2.08	25.1	51.7	0.89	126.1	83.5	89512	152	8671	0.76	286	25996	136
2.21	25.3	52.8	0.89	126.2	84.8	92124	156	8728	0.75	299	27679	142
2.22	25.4	52.8	0.89	126.1	84.9	92231	156	8748	0.75	300	27764	142

Pressure drop

differential pressure	mass flow	orifice diameter	absolute pressure	mean temper-ature	Reynolds number	Euler number
dp	$\dot{m}_{air}$	d_{or}	$p_{ts\text{-}in}$	$T_{m\text{-}air}$	Re	Eu
Pa	kg/s	mm	Pa	°C	-	-
134	0.36	140	100001	13.4	5617	0.73
181	0.43	140	100045	13.6	6622	0.71
233	0.49	140	100088	13.9	7594	0.70
293	0.56	140	100146	14.3	8621	0.68
366	0.63	140	100223	14.6	9714	0.67
440	0.69	140	100270	15.2	10714	0.65
521	0.76	140	100332	15.7	11730	0.64
589	0.82	140	100347	16.4	12534	0.63
675	0.88	140	100449	17.0	13473	0.63
769	0.94	140	100508	17.7	14436	0.62
866	1.01	140	100597	18.6	15371	0.61
959	1.06	140	100599	19.2	16193	0.60
1070	1.12	140	100572	20.1	17122	0.60
1187	1.20	140	100892	20.1	18190	0.59
1304	1.26	140	100884	20.0	19167	0.58
1415	1.31	140	100915	20.4	19984	0.58
1416	1.32	140	100847	19.7	20090	0.58
1277	1.25	221	100509	18.5	19096	0.58
1387	1.31	221	100515	19.0	19972	0.58
1514	1.37	221	100549	19.5	20906	0.57
1675	1.45	221	100582	20.0	22044	0.57
1835	1.52	221	100618	20.5	23174	0.56
1998	1.60	221	100636	21.0	24284	0.55
2141	1.66	221	100507	21.2	25210	0.55
2291	1.73	221	100761	21.2	26179	0.54
2483	1.80	221	100924	20.9	27405	0.54
2686	1.89	221	101032	21.1	28664	0.53
2877	1.96	221	101341	21.7	29735	0.53
3062	2.03	221	101635	22.3	30720	0.53

differential pressure	mass flow	orifice diameter	absolute pressure	mean temper-ature	Reynolds number	Euler number
dp	$\dot{m}_{air}$	d_{or}	$p_{ts\text{-}in}$	$T_{m\text{-}air}$	Re	Eu
Pa	kg/s	mm	Pa	°C	-	-
3301	2.11	221	101994	23.1	31886	0.53
3501	2.18	221	103803	24.8	32767	0.53
3732	2.26	221	102607	24.2	34080	0.52
3903	2.31	221	103116	28.0	34442	0.52
3939	2.33	221	102902	24.8	35061	0.52

III. Correlation development

Heat transfer

Serrated fins

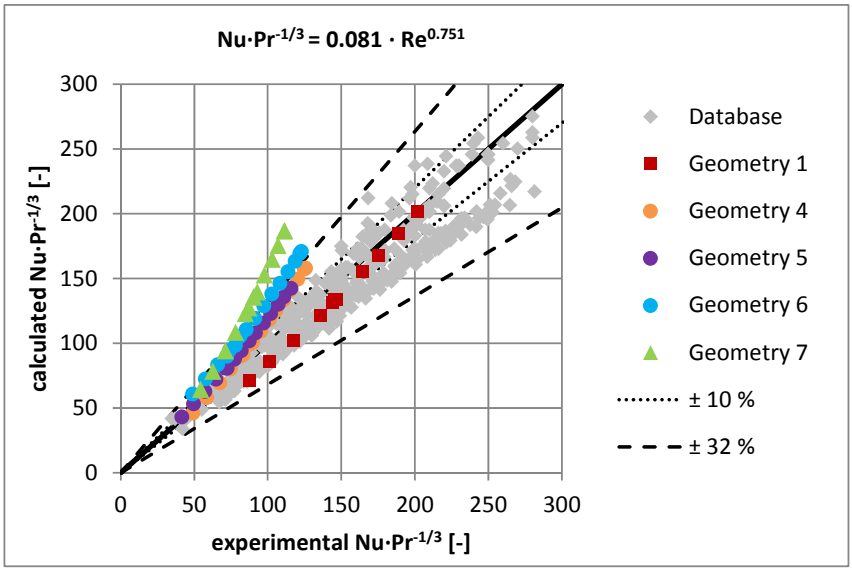

Figure 0-1: Fit of the serrated fin heat transfer data to Eq 6-5

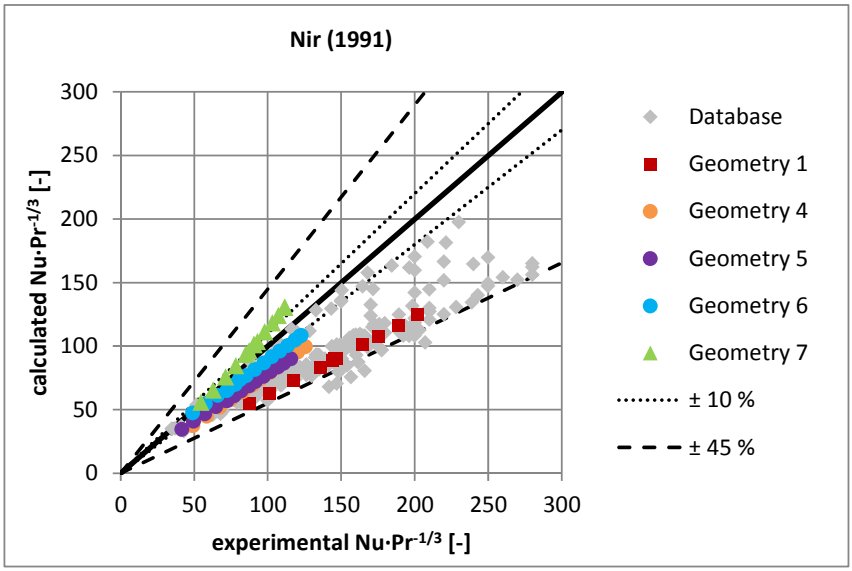

Figure 0-2 : Fit of the serrated fin heat transfer data to Nir (1991)

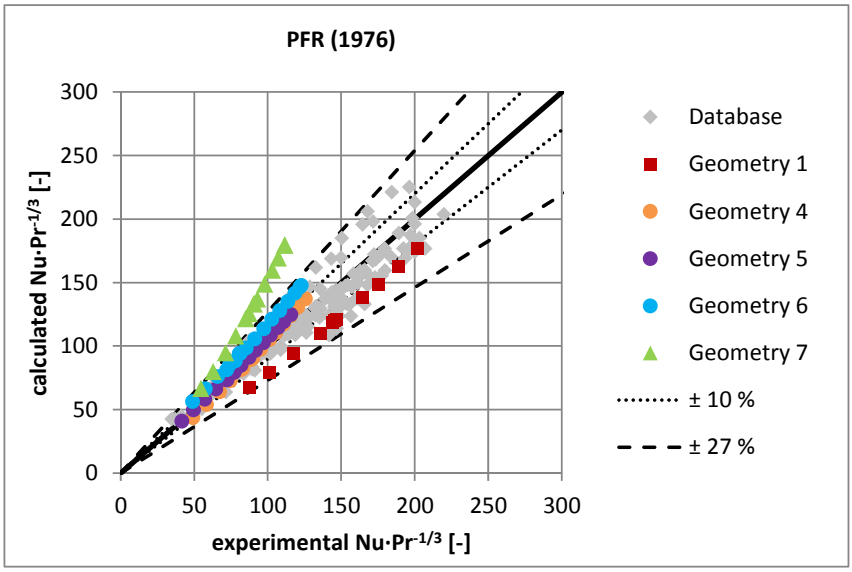

Figure 0-3: Fit of the serrated fin heat transfer data to PFR (1976)

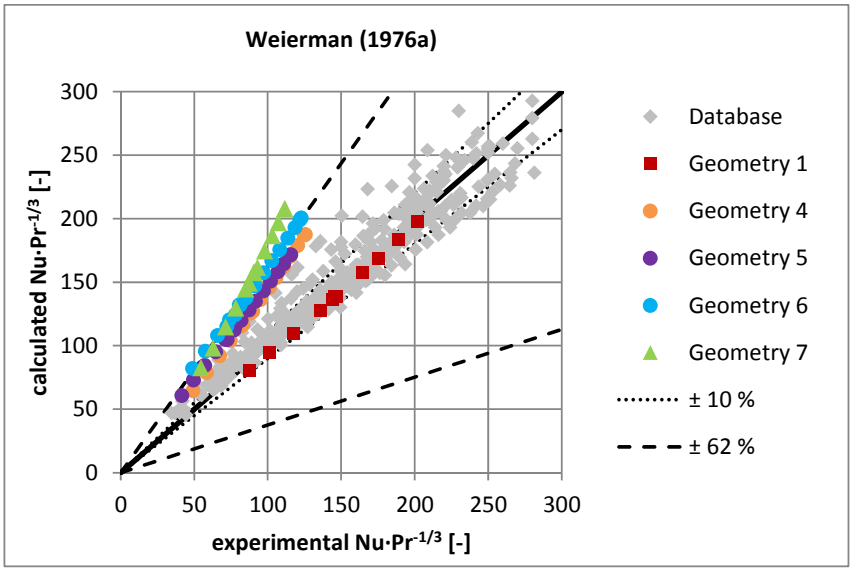

Figure 0-4: Fit of the serrated fin heat transfer data to Weierman (1976)

Solid fins

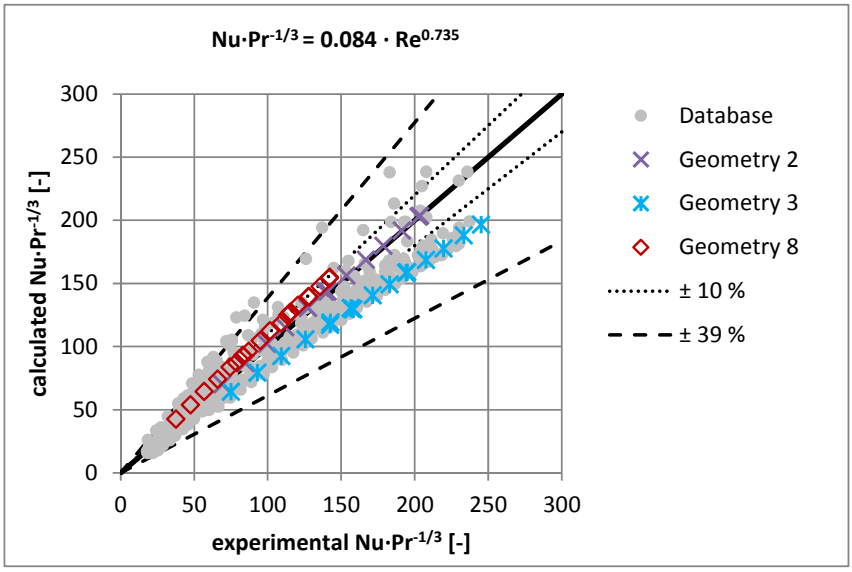

Figure 0-5: Fit of the solid fin heat transfer data to Eq 6-7

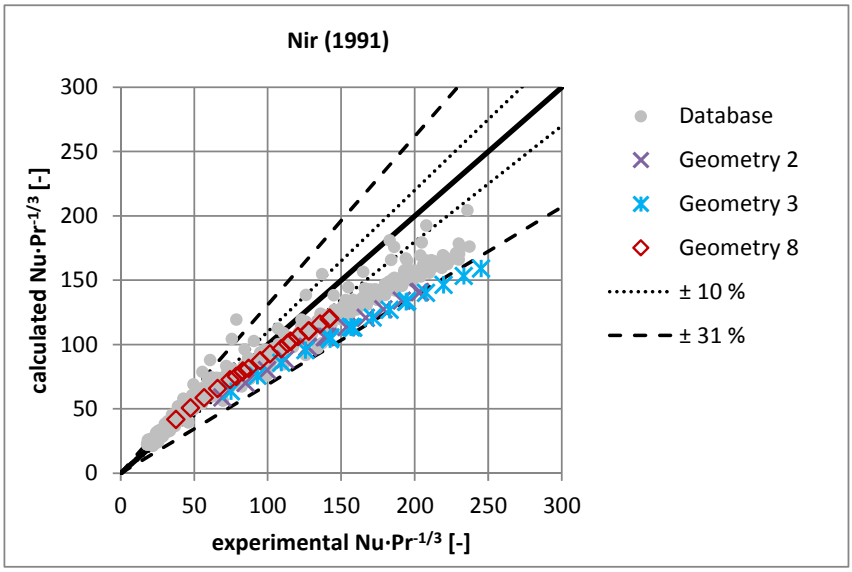

Figure 0-6: Fit of the solid-fin heat transfer data to Nir (1991)

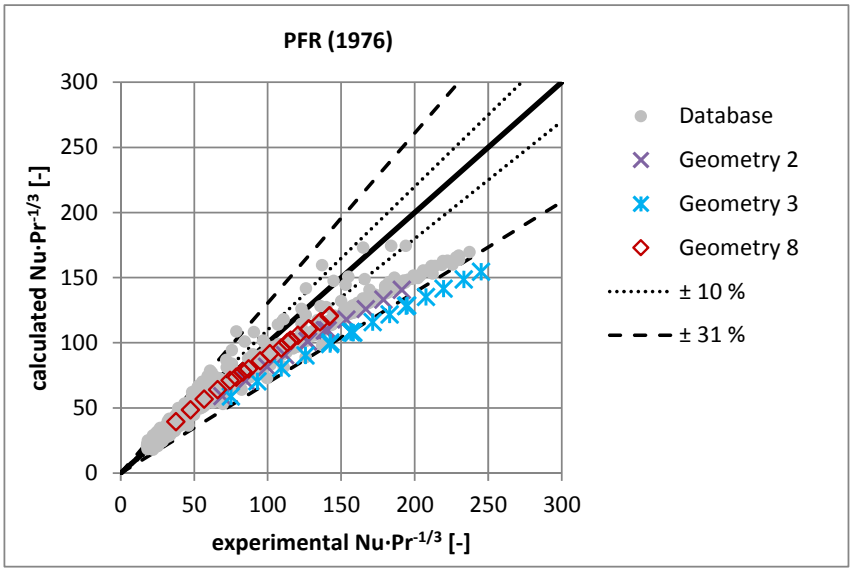

Figure 0-7: Fit of the solid fin heat transfer data to PFR (1976)

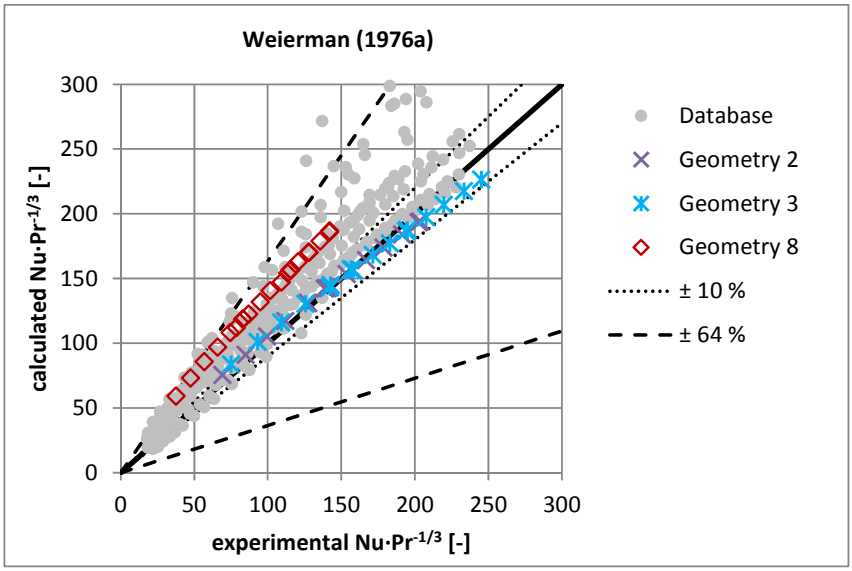

Figure 0-8: Fit of the solid fin heat transfer data to Weierman (1976)

Serrated and Solid fins

Table 0-1: Correlations for the heat transfer prediction of finned tubes

Equation	Data used	Correlation
Eq. 0-1	All DB and exp. data	$Nu \cdot Pr^{-1/3} = 0.069 \cdot Re^{0.762}$
Eq. 0-2	All DB and exp. data	$Nu \cdot Pr^{-1/3} = 0.101 \cdot Re^{0.724} \cdot Ar^{-0.103} \cdot \left(\frac{P_t}{d_o}\right)^{0.175} \cdot \left(1-\frac{h_s}{h_f}\right)^{-0.035}$

Table 0-2: Prediction accuracy of correlations for the heat transfer prediction of finned tubes

Equation	Points covered	Percentage of the data within ± 10%	95% of the data are within	R^2
Eq. 0-1	689	45%	41%	0.919
Eq. 0-2	609	53%	31%	0.944

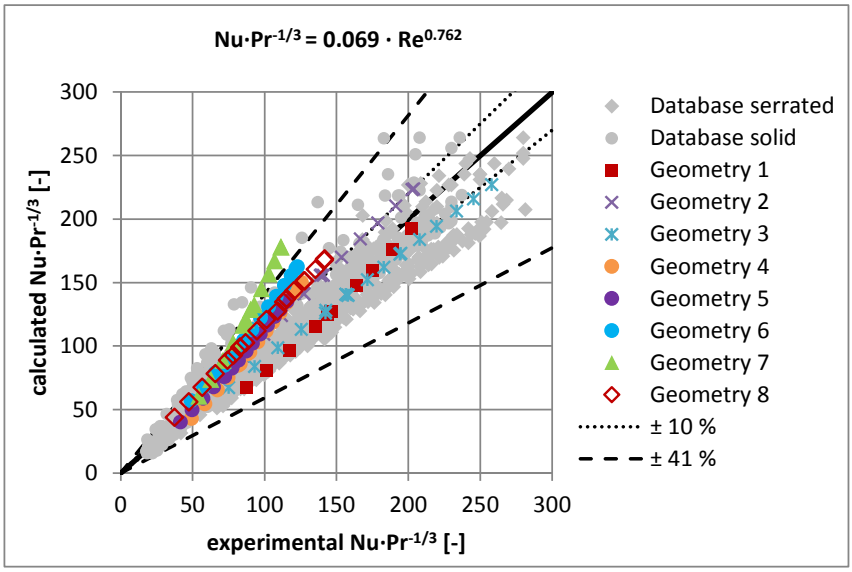

Figure 0-9: Fit of the heat transfer data to Eq. 0-1

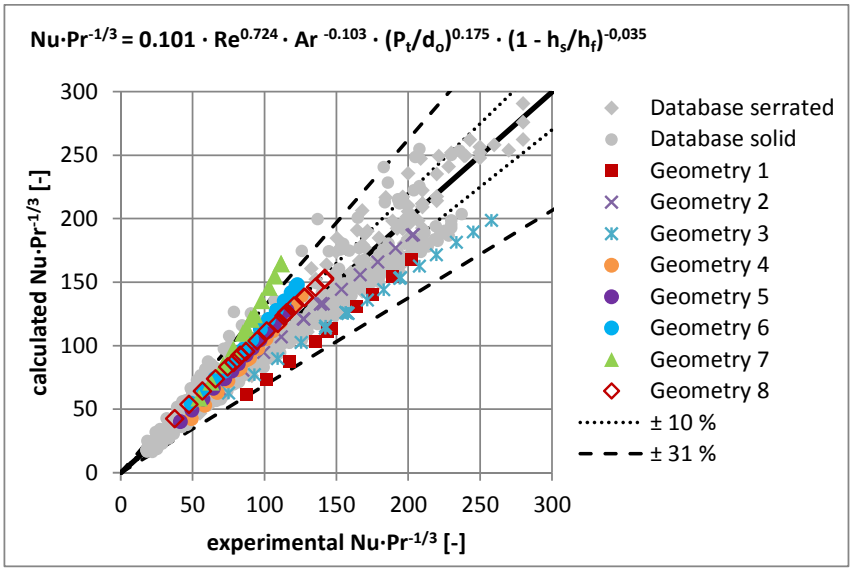

Figure 0-10: Fit of the heat transfer data to Eq. 0-2

Pressure drop

Serrated fins

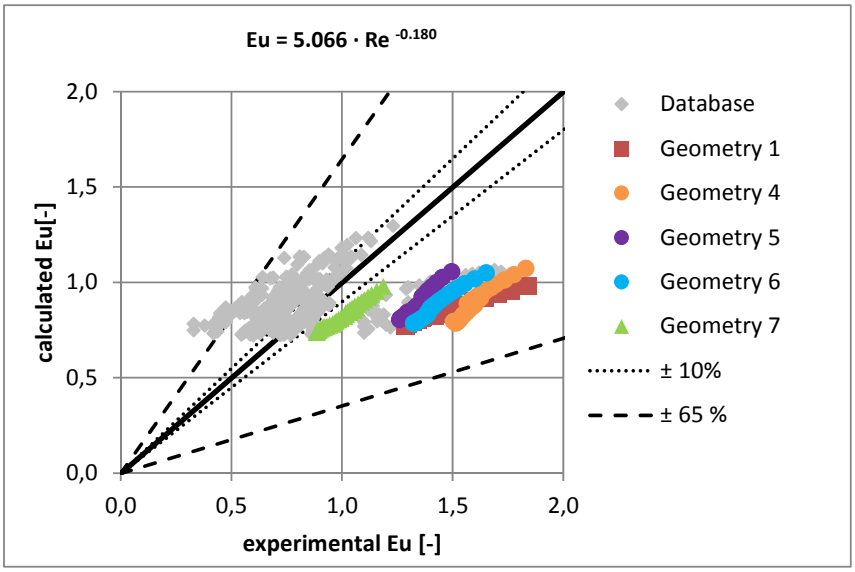

Figure 0-11: Fit of the serrated fin pressure drop data to Eq 6-9

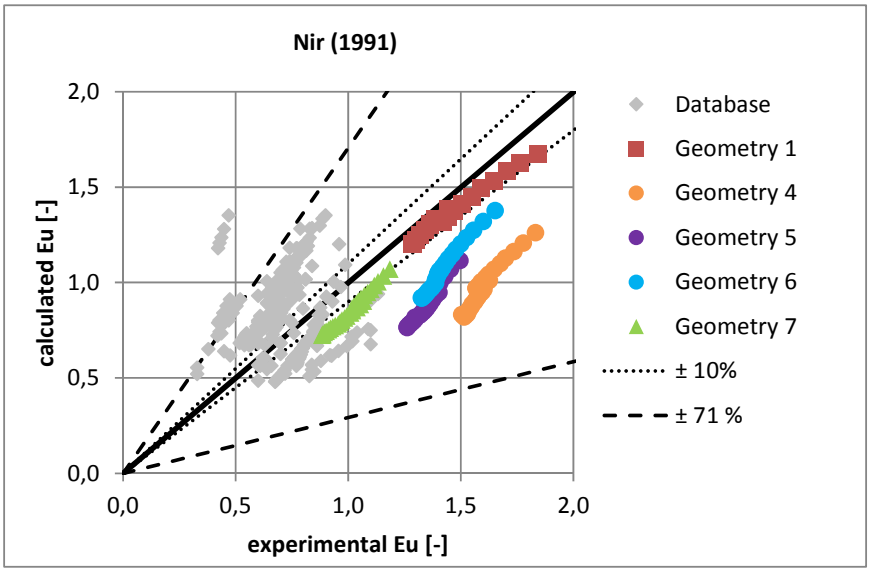

Figure 0-12: Fit of the serrated fin pressure drop data to Nir (1991)

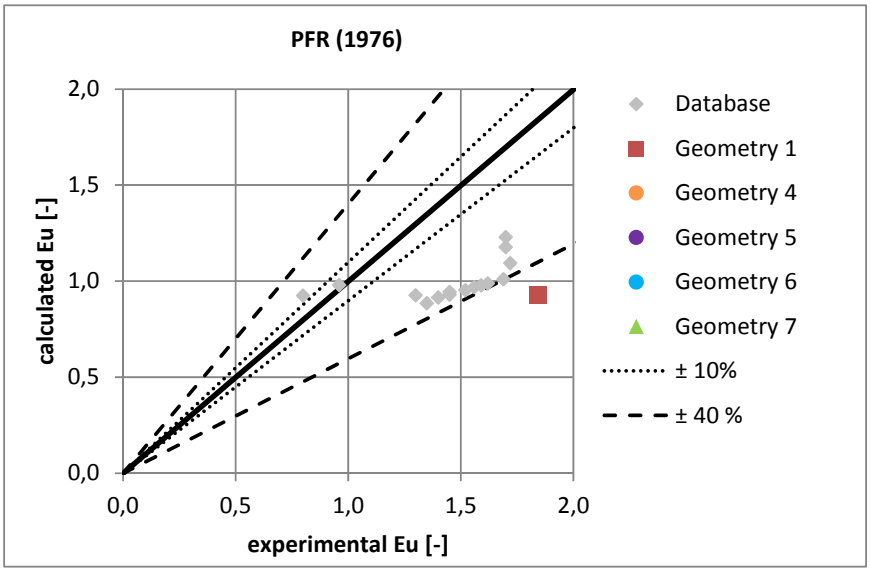

Figure 0-13: Fit of the serrated fin pressure drop data to PFR (1976)

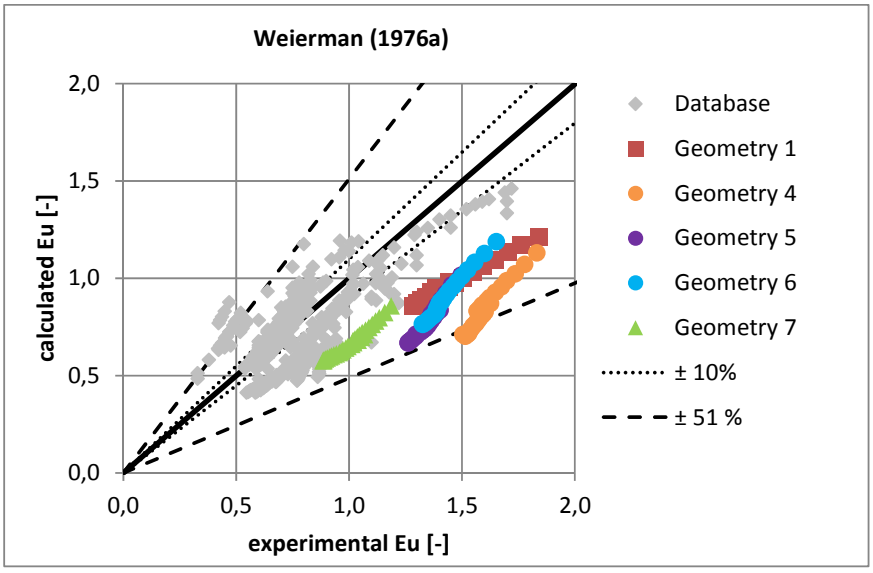

Figure 0-14: Fit of the serrated fin pressure drop data to Weierman (1976)

Solid fins

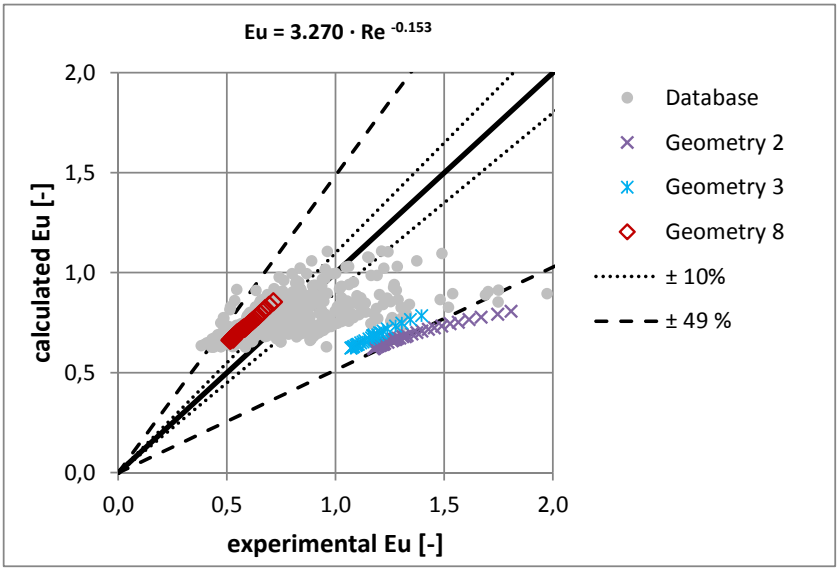

Figure 0-15: Fit of the solid fin pressure drop data to Eq 6-11

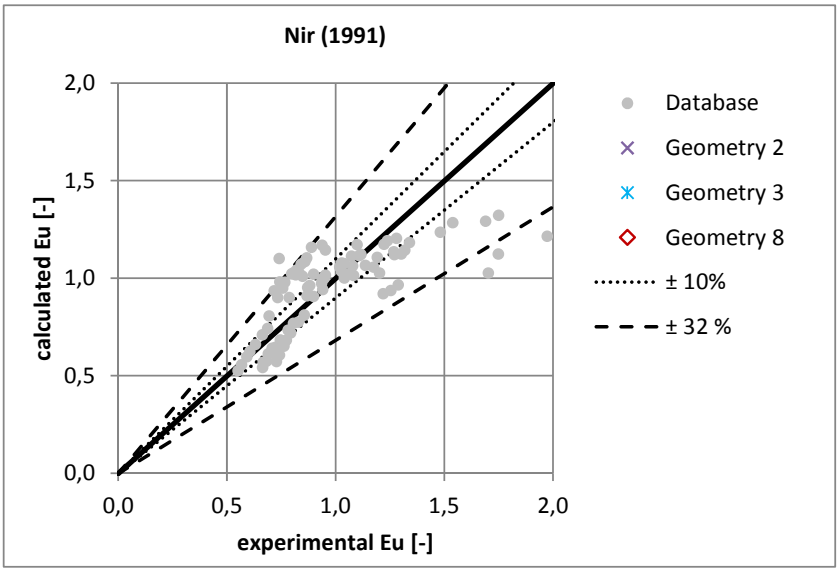

Figure 0-16: Fit of the solid fin pressure drop data to Nir (1991)

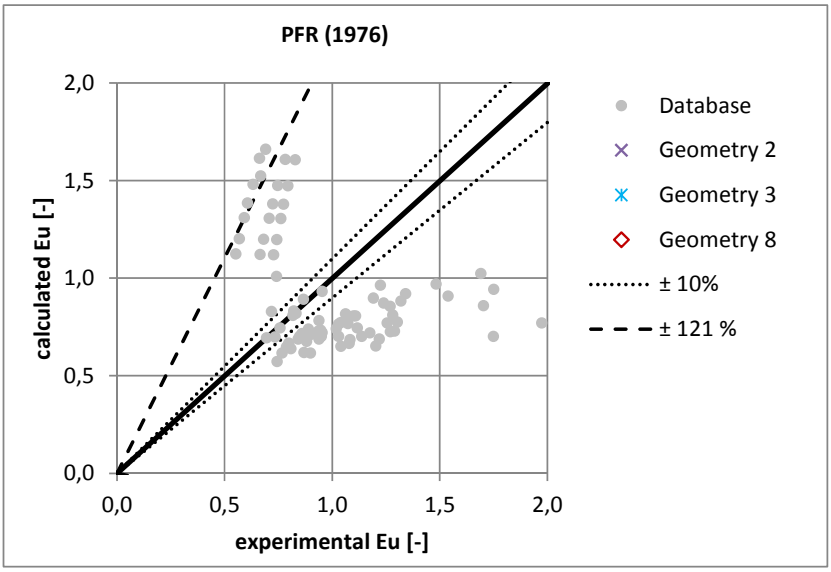

Figure 0-17: Fit of the solid fin pressure drop data to PFR (1976)

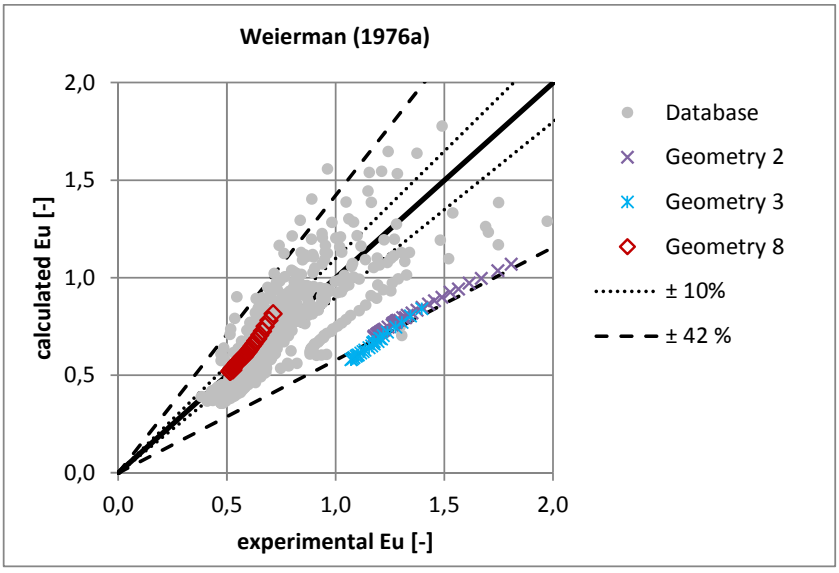

Figure 0-18: Fit of the solid fin pressure drop data to Weierman (1976)

Serrated and Solid fins

Table 0-3: Correlations for the pressure drop prediction of finned tubes

Equation	Data used	Correlation
Eq. 0-3	All DB and exp. data	$Eu = 3.270 \cdot Re^{-0.153}$
Eq. 0-4	All DB and exp. data	$Eu = 1.229 \cdot Re^{-0,118} \cdot \left(\frac{P_t}{P_l}\right)^{0.606} \cdot \left(\frac{A_{f,min}}{A_{f,fin}}\right)^{-0.510} \cdot Ar^{0.352}$

Table 0-4: Prediction accuracy of correlations for pressure drop of prediction of finned tubes

Equation	Points covered	Percentage of the data within ± 10%	95% of the data are within	R^2
Eq. 0-3	1169	19%	51%	0.092
Eq. 0-4	11057	27%	46%	0.590

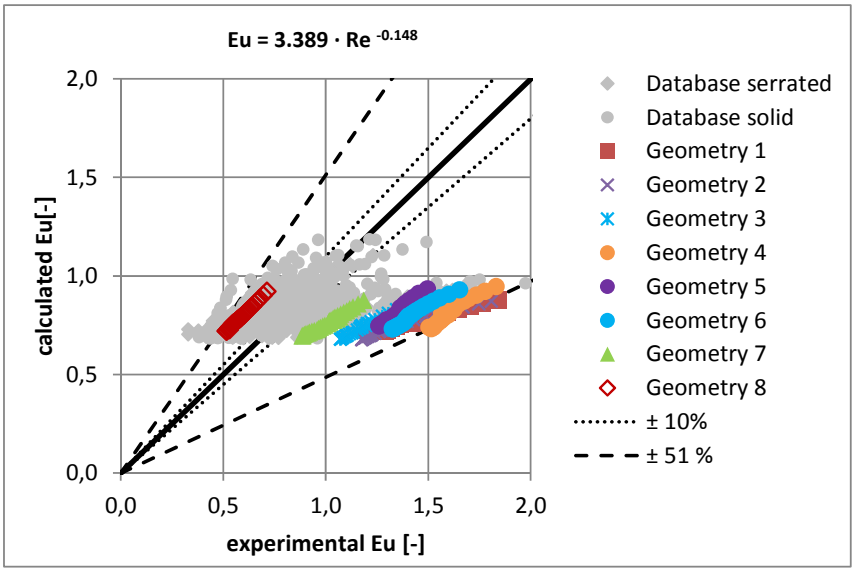

Figure 0-19: Fit of the pressure drop data to Eq. 0-3

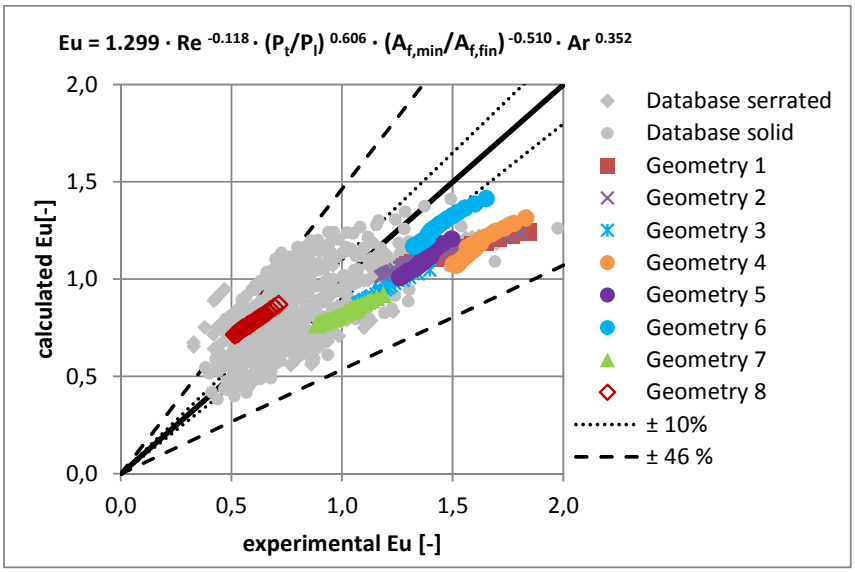

Figure 0-20: Fit of the pressure drop data to Eq. 0-4

IV. Publication

15th International Heat Transfer Conference – IHTC-15

10th-15th August 2014, Kyoto, Japan

Anna Holfeld, Erling Næss

"*Influence of the fin type and base tube diameter of serrated and solid-fin tubes on the heat transfer and pressure drop performance*"

Proceedings of the 15th International Heat Transfer Conference, IHTC-15
August 10-15, 2014, Kyoto, Japan

IHTC15-8718

INFLUENCE OF THE FIN TYPE AND BASE TUBE DIAMETER OF SERRATED AND SOLID-FIN TUBES ON THE HEAT TRANSFER AND PRESSURE DROP PERFORMANCE

Anna Holfeld[1*], Erling Næss[1]

[1]Norwegian University of Science and Technology, 7491 Trondheim, Norway

ABSTRACT

In heat recovery from gas turbine exhaust gases, finned tube bundles are frequently used. Especially in offshore applications compactness and light weight of components such as heat exchangers are important parameters. In order to optimize the size and weight of a gas turbine waste heat recovery unit an experimental investigation of the heat transfer and pressure drop performance of three finned tube bundles was carried out. Two tube bundles had an external tube diameter of 31.75 mm and were only varying in the fin type, having serrated and solid-fin tubes, respectively. The third bundle had an outer tube diameter of 19.05 mm and had serrated-fin tubes. All tube bundles had a fin height of 18 mm and 276 fins per meter tube length. The tube bundles were tested in a wind tunnel. They were arranged in a staggered, equilateral layout having eight tube rows in the direction of the flow.

The results show that serrated-fin tubes experience higher gas side heat transfer coefficients but also higher pressure drop coefficients than to solid-fin tubes. Secondly, the serrated-fin tubes having a large tube diameter experienced higher heat transfer coefficients and higher Euler numbers than smaller diameter tubes. A comparison of the heat duty per unit pressure drop showed that serrated-fin tubes having small-diameter tubes lead to higher heat duty per unit pressure drop and therefore will provide more compact tube bundles.

KEY WORDS: Heat transfer enhancement, Heat exchanger, Finned tubes, Heat recovery

1. INTRODUCTION

In order to increase the energy efficiency and reduce emissions in power production, waste heat is recovered from the exhaust gas from gas turbines. This is also the case for offshore power production in the oil and gas industry. A major challenge in offshore applications is to design compact and lightweight components.

Finned tubes are commonly used in heat exchangers for waste heat recovery due to the low gas-side heat transfer coefficient. They can vary in different geometric parameters, each influencing the heat transfer and pressure drop performance of the whole unit. In general it is desired to achieve high heat transfer rates in combination with a low pressure drop. The influence of geometric parameters on heat transfer and pressure drop has been investigated by various authors, for example Kawaguchi et al. [1], [2], [3], [4], Ma et al. [5] and Næss [6].

Staggered tube layouts generally lead to a more compact packing of the tube bundle. Brauer [7] carried out measurements on staggered and in-line tube arrangements and observed the flow patterns. He found that low heat transfer zones for a staggered layout were smaller than for an in-line layout. Measurements confirmed these observations. Weierman et al. [8] compared different serrated-fin tubes in both in-line and staggered layouts. The heat transfer coefficients for the measured staggered layout were higher than for the in-line

*Corresponding Author: anna.holfeld@ntnu.no

layout, but the friction factor was also higher. In accordance with the above investigations PFR [9] concluded that both the heat transfer coefficients and pressure drops for a staggered tube layout were higher than for an inline layout.

Næss [6] showed in his tests that the Nusselt number increased with increasing transversal to longitudinal tube pitch (P_t/P_l) up to ca. 2, equivalent to a tube bundle layout of about 45°. In this region the pressure loss coefficient was not affected by the tube pitch. For pitch ratios (P_t/P_l) above 2, both the Nusselt number and the Euler number decreased.

Figure 1 shows the differences in the fin type and the geometry parameter of the finned tubes. Kawaguchi et al. [1], [2] and Hofmann [10] published comparisons on serrated and solid-fin tubes. Kawaguchi et al. [1], [2] stated that for a large fin pitch (5.0 mm) the Nusselt and Euler numbers were higher for serrated-fin tubes. For a smaller fin pitch (3.3 mm) the Nusselt number was the same for serrated and solid-fin tubes and the Euler number was lower for serrated-fin tubes. Looking at the overall performance, no clear picture can be seen. On the one hand, for a small fin pitch, solid-fin tubes performed slightly better on an equal pressure drop basis; on the other hand, for a larger fin pitch, the result was vice versa, serrated-fin tubes showed higher heat transfer rate per unit pressure drop.

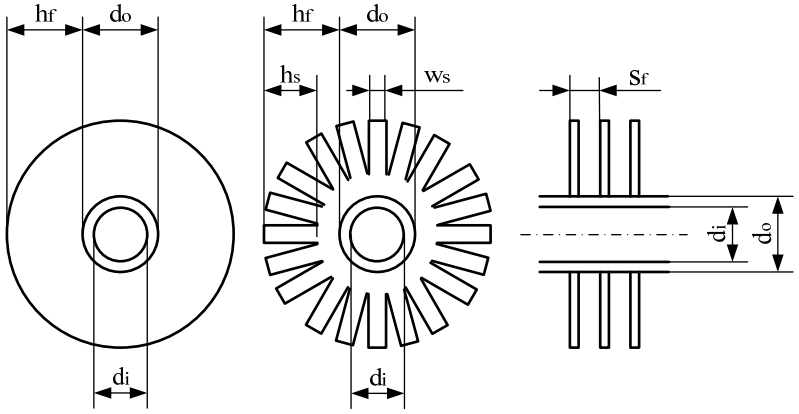

Fig. 1 Schematic overview of the fin types and geometry parameter; left: solid-fin tubes, middle: serrated-fin tubes, right: view from the side

Hofmann [10] found that solid-fin tubes experienced a 20% lower heat transfer coefficient compared to serrated-fin tubes, and the pressure drop was lower by the same order of magnitude. For constant pumping power and constant heat transfer rate Hofmann showed that solid-fin tubes perform marginally better with regards to minimization of the overall heat exchanger size.

Based on the above, no clear conclusion can be drawn. Hence, a set of experiments were carried out in order to investigate specifically the impact of fin type and base tube diameter on the heat exchanger performance.

2. EXPERIMENTAL SETUP AND DATA REDUCTION

2.1 Experimental setup

Figure 2 shows the schematic flow diagram of the test rig. Outside air is sucked by two fans, and is passed through an electric heater, where it is heated up to a pre-set temperature. After passing the orifice, where the flow rate is measured, it enters the diffusor and settling chamber. Here the velocity profile is straightened and the turbulence level controlled. Next, the contraction section passes the air to the test section.

Downstream the test section the air is sucked by means of an additional fan thus providing a nearly constant pressure in the test section.

In the cooling cycle, a 70/30% water-glycol mixture is used. The mixture is pumped through the test section. A plate heat exchanger cools the water-glycol mixture by means of city water. The circuit also contains a pump, expansion tank and instrumentation.

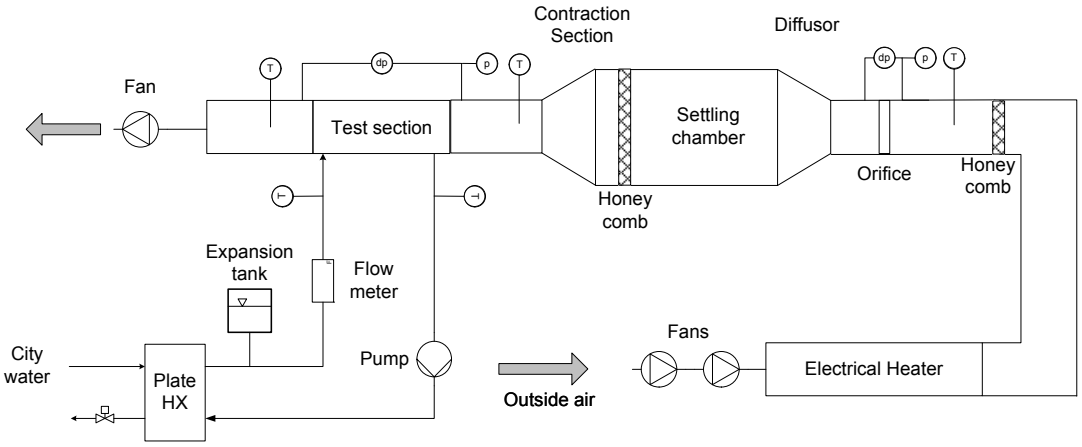

Fig. 2 Schematic overview of the test rig for heat transfer and pressure drop measurements

2.2 Data reduction

Heat transfer

From the measured heat duty, Q, the overall heat transfer coefficient U was calculated from

$$U = \frac{Q}{\left(A_f + A_t\right) \cdot LMTD} \tag{1}$$

where A_t is the tube outside surface area between the fins and LMTD the logarithmic mean driving temperature difference, given by

$$LMTD = \frac{\left(T_{air,in} - T_{w-gl,out}\right) - \left(T_{air,out} - T_{w-gl,in}\right)}{\ln\left(\frac{T_{air,in} - T_{w-gl,out}}{T_{air,out} - T_{w-gl,in}}\right)} \tag{2}$$

The external side heat transfer coefficient h_{air} was determined from

$$h_{air} = \left[\left(\eta_f \cdot A_f + A_t\right) \cdot \left(\frac{1}{U \cdot \left(A_f + A_t\right)} - \frac{1}{h_{w-gl} \cdot A_i} - \frac{\ln\left(\frac{d_o}{d_i}\right)}{k_t \cdot A_{bt}} \right) \right]^{-1} \tag{3}$$

The tube side heat transfer coefficient $h_{w\text{-}gl}$ was evaluated using the correlation from Gnielinski [11] for turbulent pipe flow.

The theoretical fin efficiency, assuming a uniform external heat transfer coefficient distribution, was calculated using Bessel functions as proposed by Gardner [12] for solid fins respectively according to Hashizume et al. [13] for serrated fins.

However, Krückels and Kottke [14] showed experimentally that the heat transfer coefficient is unevenly distributed over the fin surface and that the heat transfer coefficient was higher on the upstream surface of the fin than on the downstream surface. Also, higher heat transfer coefficients were observed on the fin tips. Weierman [15] and Hashizume et al. [13] presented empirically based correction factors, taking into account the uneven heat transfer distribution in the calculation of the fin efficiency. Weierman [15] introduced a rather simple correction for the fin efficiency, of the form:

$$\eta_f = \eta_{th} \cdot \left(A + B \cdot \eta_{th} \right) \tag{4}$$

where A and B are given in table 1.

Table 1 Factors for the Weierman [15] fin efficiency correction for an uneven heat transfer distribution

Fin type	A	B
Serrated	0.9	0.1
Solid	0.7	0.3

In contrast, the Hashizume et al. [13] correction also includes the Reynolds number as a parameter, but has a limited range of validity. However, there is no justification to select one correction method over the other. In the present work the correction of Weierman [15] was chosen to account for the uneven heat transfer distribution.

Pressure drop

The pressure drop over the tube bundle was measured at adiabatic conditions; hence, the acceleration part of the pressure drop due to temperature related density changes of the air could be disregarded. The pressure loss coefficient (Euler number, Eu), was calculated according to eq. (5), where $\dot{m}_{air}$ is the air mass flux in the narrowest flow passage.

$$Eu = \frac{2 \cdot \Delta p_{air} \cdot \rho_{air}}{\dot{m}_{air}^{\,2} \cdot N_L} \tag{5}$$

Uncertainty

The total uncertainty of the experimental results based on a 95 % confidence interval are estimated 2 % for the Reynolds number, 7% for the Nusselt number and 3% for the Euler number. The experimental uncertainty is mainly due to the temperature and mass flow measurements.

2.3 Test section and test geometries

The three tested geometries were arranged in an equilateral staggered layout. The test section contained four transversal and eight longitudinal active tube rows. In order to get a realistic flow distribution through the

bundle, dummy finned half tubes were added to the test section. The test section had a width of 500 mm and a height of 4.5 times the transversal tube pitch P_t (see figure 3).

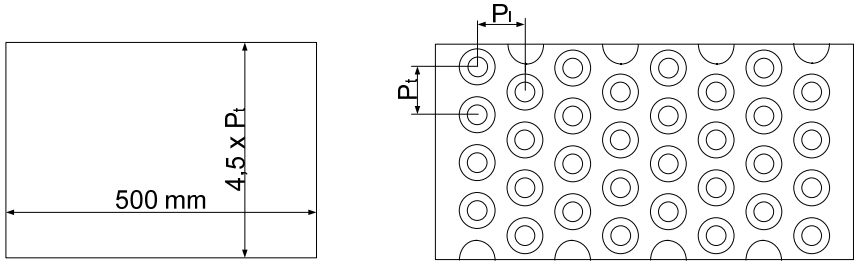

Fig. 3 Test section, left: view in flow direction, right: view from the side

Geometries 1 and 2 differed only in the fin type, whereas geometry 3 differed in the base tube diameter relative to geometry 1. The key geometric dimensions of all three geometries are given in table 2.

Table 2 Geometric dimensions of the test geometries

Geometry	Fin type	Base tube diameter d_o(mm)	Number of fins N_f (m^{-1})	Fin height h_f (mm)	Segment height h_s (mm)	Segment width w_s (mm)	Fin tip clearance c_f (mm)
1	Serrated	31.75	276	18	11	4.5	2
2	Solid	31.75	276	18	N.A.	N.A.	2
3	Serrated	19.05	276	18	11	4.5	5

3. RESULTS AND DISCUSSION

3.1 Comparison of the experimental data to published correlations

The measured heat transfer and pressure drop data were compared to published correlations. The experimental data of the serrated-fin tubes were compared to the heat transfer and pressure drop correlations of Ma et al. [5], Nir [16], Næss [6], PFR [9] and Weierman [15], whereas the experimental data for the solid-fin tube geometry was compared to the correlations published by Nir [16], PFR [9], Stasiulevičius et al. [17] and Weierman [15]. Solid lines in figures 4 and 5 indicate that the correlation predictions are within their validity range, whereas dashed lines indicate an extrapolation of the correlations outside their stated validity range.

Heat transfer

Figure 4 shows the experimentally obtained heat transfer coefficients. It can be seen (figure 4, left) that the measured heat transfer coefficients for geometry 2 (solid-fin tubes, large tube diameter) are 6 to 31 % higher than the estimation from all of the correlations. The measured results presented do not include the correction of Weierman [15] for uneven heat transfer distribution. This is due to the fact that most of the data used in the development of the correlations assumed uniform heat transfer distribution, hence a theoretical fin efficiency calculations (such as eq. 4) in the data reduction. Using the correction for the uneven heat transfer distribution is increasing the gap between the experimental results and the correlations up to 54%. The deviations between the correlations are in the range 14 to 26 %.

The measured heat transfer data of geometry 1 (serrated-fin tubes, large tube diameter) are underpredicted by the correlations by –22 - 44 % for low velocities and –14 - 46 % for higher velocities. The correction of Weierman [15] for the uneven heat transfer distribution for serrated-fin tubes is 3 to 7 %. It is observed from figure 4, middle, that the spread in the prediction span of the correlations is about twice that of the solid-fin tubes (39 - 60 %).

The measured heat transfer values of geometry 3 (serrated-fin tubes, small tube diameter) are well captured by the correlation of Næss [6] (figure 4, right). The correction of Weierman [15] for the uneven heat transfer distribution was also basis for the data used by Ma et al. [5] and Næss [6]. The discrepancy between correlations is the seen to be much higher for geometry 3, deviating between 63 and 77% to one another.

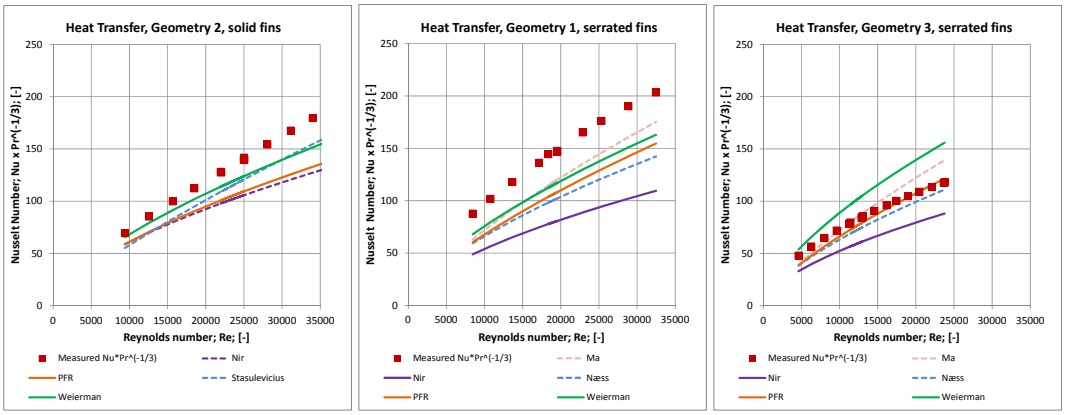

Fig. 4 Experimental heat transfer results and comparison to published correlations

Pressure drop

Figure 5 shows the experimental pressure drop coefficients (Euler number, Eu) and correlation predictions. The measurements for all three geometries are underestimated by all of the correlations.

The trend for the Euler number for geometry 2 (solid-fin tubes, large tube diameter; figure 5 left) is captured by all of the correlations. However, the data has an offset of ca. 0.16 compared to the correlation of Stasiulevičius et al. [17]. The spread between the correlations are much wider for the Euler numbers than for the Nusselt numbers, e.g. the Euler number predictions of Stasiulevičius et al. [17] are 136 to 160 % higher than the predictions of PFR [9].

The Euler number for geometry 1 (serrated-fin tubes, large tube diameter; figure 5 middle) is underpredicted by most of the correlations, but shows the best overall accordance with the correlation of Nir [16]. Especially the correlation of Ma et al. [5] predicts very low Euler numbers. This leads to a large deviation in the pressure drop predictions of the shown correlations; the highest predictions are 202 – 226 % higher than the lowest predictions.

Næss [6] captures the trend of the pressure drop for geometry 3 (serrated-fin tubes, small tube diameter; figure 5 right), but there is an offset in the Euler number of ca. 0.57 between the measured and calculated values. Again, the correlation of Ma et al. [5] predicts the lowest values. The spread between the predicted Euler numbers by the different correlations is 187-230 %

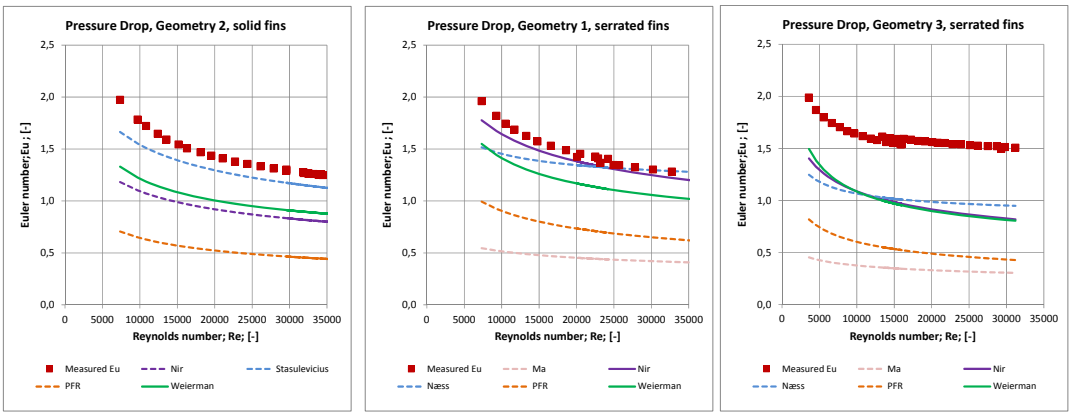

Fig. 5 Experimental pressure drop results and comparison to published correlations

3.2 Impact of fin type

The comparison between geometries 1 and 2, varying only in the fin type, showed that the heat transfer coefficient was higher for serrated-fin tubes than for solid-fin tubes (figure 6, left). This may be attributed to the frequent boundary layer break-up due to the serration of the fins. The advantage of serrated-fin tubes is observed to be higher for low flow rates than for high flow rates. The heat transfer coefficients are improved by 31 % at low flow rates, respectively 13 % at high flow rate when the theoretical fin efficiency is used in the data reduction assuming an even heat transfer coefficient distribution. Taking into account the correction for an uneven heat transfer distribution, according to eq. (4), the heat transfer coefficients of serrated-fin tubes compared to solid-fin tubes is 23 % higher at low flow rates and 8 % lower at higher flow rates.

The measured pressure drop for serrated-fin tubes were the same as for solid- finned tubes having the same overall configuration and geometry (figure 6, right).

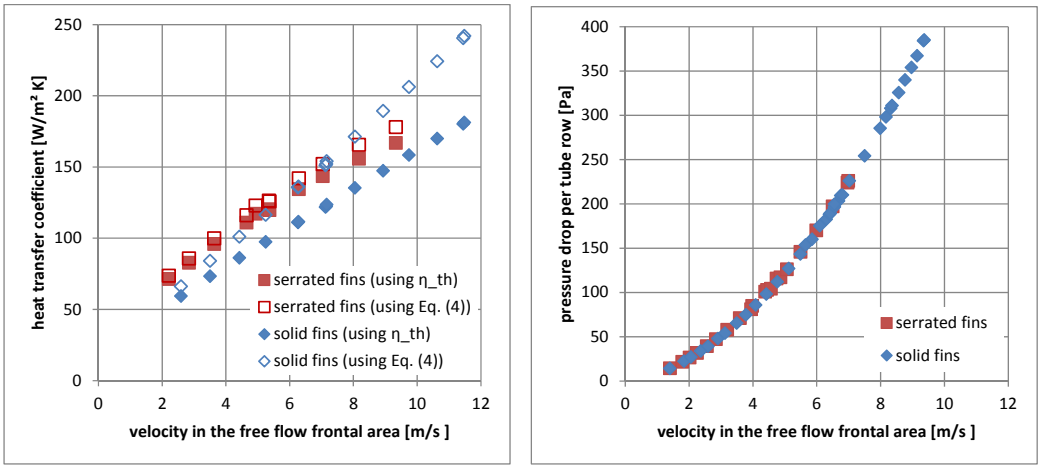

Fig. 6 Experimental results for heat transfer (left) and pressure drop (right) for serrated (geometry 1) and solid-fin tubes (geometry 2) as function of the Reynolds number

Based on the experimental results for geometries 1 and 2, the heat transfer rate per unit tube bundle volume ($W/m^3 \cdot K$) and weight ($W/kg \cdot K$) was calculated, based on a 1 m^3 tube bundle and is shown in figure 6. The serrated-fin tubes are shown to outperform the solid-fin tubes both with respect to volume and weight. The heat duty per unit volume is 15 to 42 % higher for the tested serrated-fin tubes than the solid-fin tubes, respectively 28 to 55 % higher per unit weight.

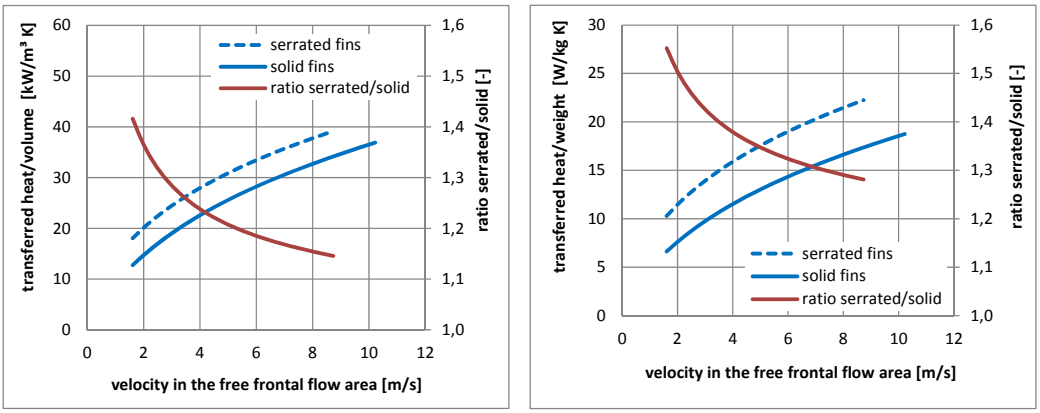

Fig. 7 Comparison between the heat transfer performance of serrated and solid-fin tubes with regards to the bundle volume (left) and bundle weight (right)

However, also on the comparison basis of heat duty per unit pressure drop, shown in figure 8, the advantage of serrated-fin tubes are apparent. Serrated-fin tubes experience a 15 to 37% higher heat transfer rate per unit pressure drop compared to solid finned tube bundles.

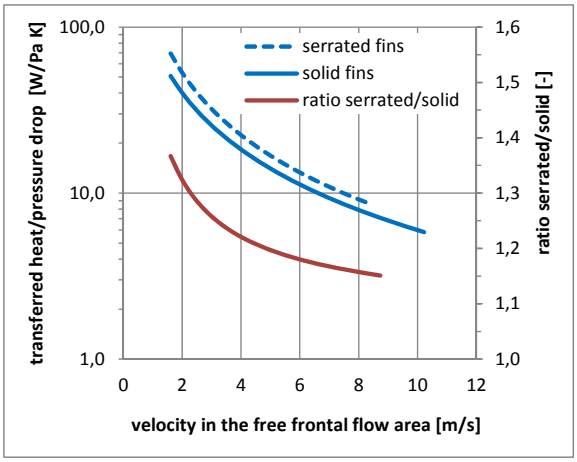

Fig 8 Comparison of the overall performance of serrated-fin and solid-fin tubes with transferred heat per unit pressure drop

3.3 Impact of base tube diameter

Figure 9 shows a comparison of the heat transfer and pressure drop performance of the two serrated-fin tube bundles (geometries 1 and 3). The left part of figure 9 shows that the heat transfer coefficient is significantly

higher for the tubes with the larger tube diameter (geometry 1) in comparison to the smaller tube diameter (geometry 3). The heat transfer coefficient is –21 - 26 % higher for the larger tube diameter compared on the basis of the superficial velocity in the free frontal flow area.

The measured pressure drop (figure 9 right) was also larger diameter for the larger tubes by 29 to 60 % compared on the basis the free frontal flow velocity.

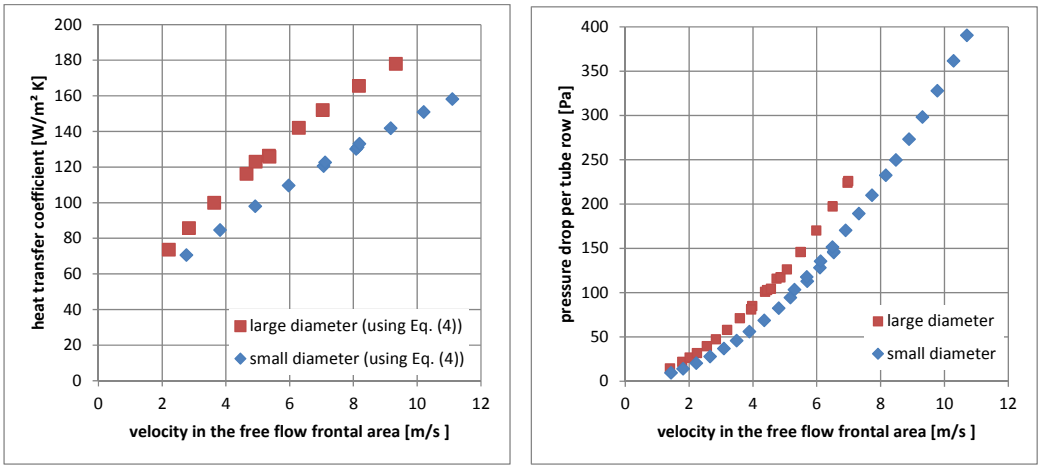

Fig. 9 Experimental results for tube diameters, 31.75 mm (geometry 1) and 19.05 mm (geometry 3); left: heat transfer coefficient; right: pressure drop per tube row

The comparison of the experimental data for a $1m^3$ tube bundle with tubes only differing in the tube diameter shows that the tubes with the larger tube diameter yield a 19 to 23% higher heat duty per unit volume and 6 to 10% higher performance per unit weight, see figure 10.

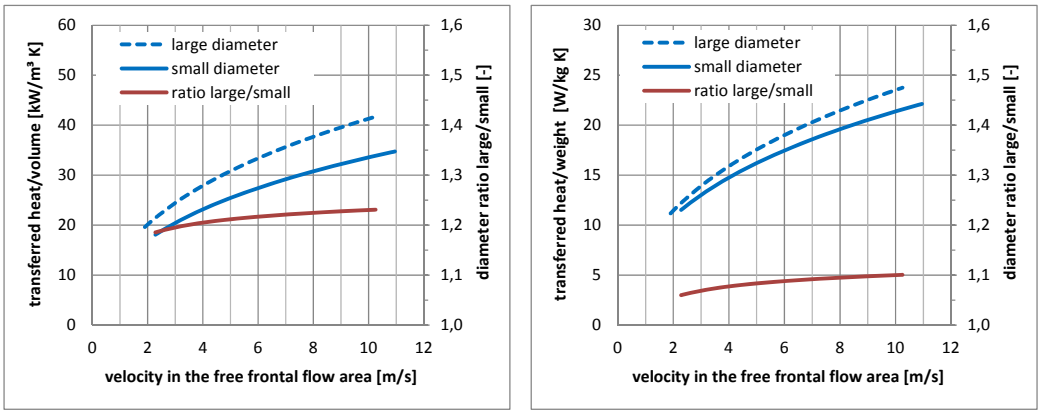

Fig. 10 Comparison of the heat transfer performance of serrated-fin tubes with different base tube diameter with regards to the bundle volume (left) and bundle weight (right)

A similar trend is also observed for the pressure drop. The pressure drop of the bundle with the larger tube diameter is 10 - 53 % higher than for the smaller tubes (figure 11). This is due to the larger friction surface and the higher velocities in the narrowest flow area of the larger tubes.

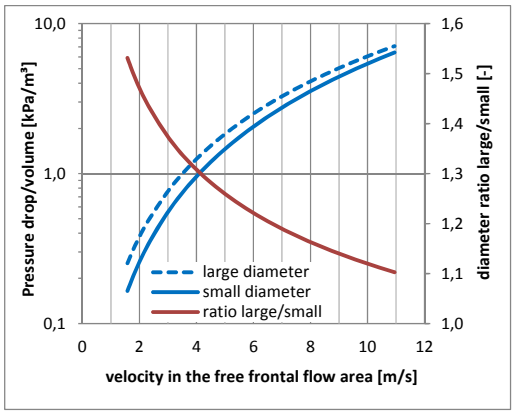

Fig. 11 Comparison of the pressure drop performance of serrated-fin tubes with different base tube diameter with regards to the bundle volume

The overall comparison of transferred heat per unit pressure drop (figure 12) shows that there is no clear recommendation as to whether small or large diameter tubes perform best with regards to compactness. The heat duty per unit pressure drop of small diameter tubes is 10 % higher at low flow rates and decreases to -18 % at high velocities. However, the comparison for 1 m^3 tube bundle took into account 16 % more longitudinal tube rows with a smaller diameter than for the large diameter tubes. If the number of longitudinal tube rows would be the same in both cases, the pressure drop for the small diameter tube rows would be even smaller and the overall performance of the heat duty per unit pressure drop would tend towards smaller tube diameters

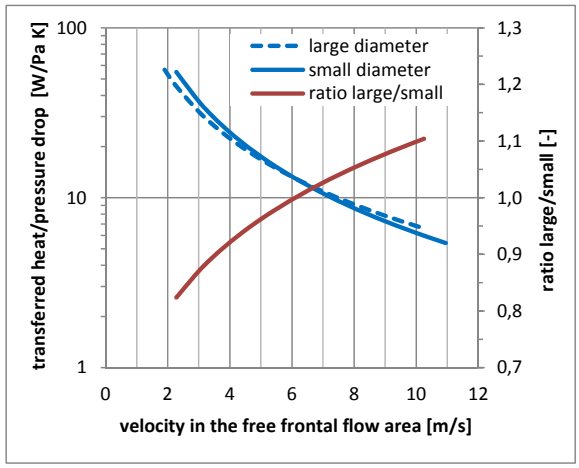

Fig 12 Comparison of the overall performance with transferred heat per unit pressure drop

4. CONCLUSIONS

The measurements showed that the heat transfer as well as the pressure drop coefficients are higher for serrated-fin tubes than for solid-fin tubes. Comparing both fin types with regards to compactness and weight of a tube bundle, serrated-fin tubes have higher heat duty per unit volume, weight and pressure drop than solid-fin tubes.

Comparing a 1 m^3 cube tube bundle with serrated-fin tubes having identical fins but different tube diameters, the large diameter tubes show slightly higher heat transfer rates per unit volume and weight. However, comparing the heat duty per unit pressure drop, no clear answer can be given. Changing shape of a 1m^3 tube bundle from a cube to a cuboid containing the same number of longitudinal tube rows, smaller tubes perform better than the larger diameter tubes.

All in all the results point towards serrated-fin tubes having small tube diameters when compactness is an important parameter of a waste heat recovery unit, such as in offshore applications.

ACKNOWLEDGMENT

This publication forms a part of the EFFORT project, performed under the strategic Norwegian research program PETROMAKS. The authors acknowledge the partners: Statoil, TOTAL E&P Norway, Shell Technology Norway, PETROBRAS, and the Research Council of Norway (203310/S60) for their support.

NOMENCLATURE

A	area	(m^2)
c_f	fin tip clearance	(m)
d	diameter	(m)
d_f	fin diameter ($d_f = d_o + 2 \cdot h_f$)	(m)
h	height	(m)
h	heat transfer coefficient	($W/m^2 K$)
k	thermal conductivity	(W/m K)
LMTD	log. mean temp. difference	(K)
m	characteristic value in Eq. (5) and (6)	(1/m)
$\dot{m}$	mass flux	($kg/m^2 s$)
N_l	no. of longitudinal tube rows	(--)
P	tube pitch	(m)
Δp	pressure drop	(Pa)
Q	heat duty	(W)
T	temperature	(K)
t	thickness	(m)
u	velocity	(m/s)
U	overall heat transfer coefficient	($W/m^2 K$)
w	width	(m)
η	fin efficiency	(--)
μ	dynamic viscosity	(kg/m s)
ρ	density	(kg/m^3)

dimensionless numbers

Eu Euler number $Eu = \dfrac{2 \cdot \Delta p}{\rho \cdot u_{max}^2 \cdot N_l}$

Nu Nusselt number $Nu = \dfrac{h \cdot d_o}{k}$

Re Reynolds number $Re = \dfrac{\rho \cdot u_{max} \cdot d_o}{\mu}$

subscript

air	air (hot side)
bt	bare tube
f	fin
l	longitudinal
max	maximum
i	inside
in	inlet
o	outside/base tube
out	outlet
s	segment
ser	serrated
sol	solid
t	tube
t	transversal
th	theoretical
w-gl	water-glycol mixture (cold side)

REFERENCES

[1] K. Kawaguchi, K. Okui and T. Kashi, "The heat transfer and pressure drop characteristics of finned tube banks in forced convection (comparison of the pressure drop characteristics of spiral fins and serrated fins)", *Heat Transfer—Asian Research*, 33(7), pp. 431-444, (2004)

[2] K. Kawaguchi, K. Okui and T. Kashi, "Heat transfer and pressure drop characteristics of finned tube banks in forced convection (comparison of the heat transfer characteristics between spiral fin and serrated fin)", *Heat Transfer—Asian Research*, 34(2), pp. 120-133, (2005)
[3] K. Kawaguchi, K. Okui, T. Asai and Y. Hasegawa, "The heat transfer and pressure drop characteristics of finned tube banks in forced convection (effects of fin height on pressure drop characteristics)", *Heat Transfer—Asian Research*, 35(3), pp. 179-193, (2006)
[4] K. Kawaguchi, K. Okui, T. Asai and Y. Hasegawa, "The heat transfer and pressure drop characteristics of the finned tube banks in forced convection (effects of fin height on heat transfer characteristics)", *Heat Transfer—Asian Research*, 35(3), pp. 194-208, (2006)
[5] Y. Ma, Y. Yuan, Y. Liu, X. Hu and Y. Huang, "Experimental investigation of heat transfer and pressure drop in serrated finned tube banks with staggered layouts", *Applied Thermal Engineering*, 37(pp. 314-323, (2012)
[6] E. Næss, "Experimental investigation of heat transfer and pressure drop in serrated-fin tube bundles with staggered tube layouts", *Applied Thermal Engineering*, 30(13), pp. 1531-1537, (2010)
[7] H. Brauer, "Compact heat exchangers", *Chem. Prog. Eng.*, 45(8), pp. 315-321, (1964)
[8] C. Weierman, J. Taborek and W. J. Marner, "Comparison of the performance of in-line and staggered banks of tubes with segmented fins", *AIChE Symposium Series*, 74(174), pp. 39-46, (1978)
[9] PFR, "Heat Transfer and Pressure Drop Data Characteristics of Dry Tower Extended Surfaces", PFR Report BNWL-PFR-7-100: PFR Engineering Systems Inc., (1976)
[10] R. Hofmann, *Experimental and Numerical Gas-Side Performance Evaluation of Finned-Tube Heat Exchangers*, Dr-Ing thesis, Technische Universität Wien, Wien, Austria, (2009)
[11] V. Gnielinski, "Neue Gleichungen für den Wärme-und den Stoffübergang in turbulent durchströmten Rohren und Kanälen", *Forschung im Ingenieurwesen*, 41(1), pp. 8-16, (1975)
[12] K. A. Gardner, "Efficiency of extended surfaces", *Trans. ASME*, 67(1), pp. (1945)
[13] K. Hashizume, R. Morikawa, T. Koyama and T. Matsue, "Fin Efficiency of Serrated Fins", *Heat Transfer Engineering*, 23(2), pp. 6-14, (2002)
[14] W. Krückels and V. Kottke, "Untersuchung über die Verteilung des Wärmeübergangs an Rippen und Rippenrohr-Modellen", *Chemie Ingenieur Technik*, 42(6), pp. 355-362, (1970)
[15] C. Weierman, "Correlations ease the selection of finned tubes", *Oil and Gas Journal*, 74(36), pp. 94-100, (1976)
[16] A. Nir, "Heat transfer and friction factor correlations for crossflow over staggered finned tube banks", *Heat Transfer Engineering*, 12(1), pp. 43-58, (1991)
[17] J. Stasiulevičius, A. Skrinska and A. Žukauskas, *Heat transfer of finned tube bundles in crossflow*, Hemisphere, Washington, (1988)